

Project Report
TST-72

Performance Comparison of Superresolution Array Processing Algorithms

A.J. Barabell
J. Capon
D.F. DeLong
J.R. Johnson
K.D. Senne

9 May 1984
Revised 15 June 1998

Lincoln Laboratory
MASSACHUSETTS INSTITUTE OF TECHNOLOGY
LEXINGTON, MASSACHUSETTS



**Prepared for the Department of the Air Force under
Contract F19628-95-C-0002.**

Approved for public release; distribution is unlimited.

19980623 085


This report is based on studies performed at Lincoln Laboratory, a center for research operated by Massachusetts Institute of Technology. The work was sponsored by the Department of the Air Force under Contract F19628-95-C-0002; in some cases, the work was supported under other contracts.

This report may be reproduced to satisfy needs of U.S. Government agencies.

The ESC Public Affairs Office has reviewed this report, and it is releasable to the National Technical Information Service, where it will be available to the general public, including foreign nationals.

This project report has been reviewed and is approved for publication.

FOR THE COMMANDER


Gary Nutungian
Administrative Contracting Officer
Contracted Support Management

MASSACHUSETTS INSTITUTE OF TECHNOLOGY
LINCOLN LABORATORY

**PERFORMANCE COMPARISON OF SUPERRESOLUTION
ARRAY PROCESSING ALGORITHMS**

*A.J. BARABELL
J. CAPON
D.F. DeLONG
K.D. SENNE
Group 44*

*J.R. JOHNSON
Group 96*

PROJECT REPORT TST-72

9 MAY 1984

REVISED 15 JUNE 1998

Approved for public release; distribution is unlimited.

LEXINGTON

MASSACHUSETTS

CONTENTS

I. INTRODUCTION	1
II. THEORETICAL PERFORMANCE BOUNDS	5
III. DESCRIPTION OF ALGORITHMS	15
IV. DESCRIPTION OF THE MONTE CARLO EXPERIMENTS	37
V. SUMMARY OF MAJOR FINDINGS	51
REFERENCES	61
APPENDIX A: CRAMER-RAO DIRECTION-FINDING BOUNDS FOR GAUSSIAN SIGNALS	65
APPENDIX B: LINEAR PREDICTION AND MAXIMUM ENTROPY SPECTRAL ANALYSIS	79
APPENDIX C: COMPARISON OF ALTERNATIVE LIKELIHOOD RATIO TESTS FOR ESTIMATING THE NUMBER OF SIGNAL PRESENT	93
APPENDIX D: COMPARISON OF TWO POWER ESTIMATION TECHNIQUES VIA COMPUTER SIMULATION	99
APPENDIX E: SAMPLING FROM THE WISHART DISTRIBUTION	111
APPENDIX F: DIRECTION FINDING EXPERIMENTS	119
APPENDIX G: ADAPTIVE LISTENING EXPERIMENTS	157

I. INTRODUCTION

A. Scope

This report summarizes the results of the initial phase of a comprehensive simulation study of alternative signal processing algorithms for data adaptive superresolution direction finding and spatial nulling to support signal copy in the presence of strong cochannel interference. The need for such a study arises because, although most of the techniques evaluated have been documented in the literature, no systematic comparison has heretofore been undertaken.

The general approach of the current study is to simulate a sequence of increasingly more general, i.e., realistic, signaling environments, and to expose each of the more promising algorithms to all of the "standardized" experiments, in turn. For the initial phase of the inquiry, we have selected an ideal environment characterized by a uniform, linear array of identical isotropic elements and perfect receivers. In addition, partial results are obtained for the case when the array steering vectors are in error by a small amount which might be caused by residual calibration errors, unmodeled multipath distortions, near-field emitters, etc.

B. Focus of the Initial Inquiry

Many of the techniques proposed for superresolution array processing have their origin in spectral estimation for time series. Since the sampling of a function in time is analogous to sampling a function in space, it is natural to make this association; estimating the frequency of sinusoids in noise can be seen to be equivalent to estimating the directions of planewaves in noise.

Although the superresolution problem involves finding plane waves in noise, most spectral estimation techniques make no use of any information about the underlying process. Indeed, such methods are only heuristically motivated, since the estimation of a completely unknown function based upon a finite number of samples is at best an underdefined process. Nevertheless,

since claims of success have been made for such techniques, we thought it best to start our investigation by reviewing these "classical" techniques. Representative of such techniques are the following:

- (1) Adapted Angular Response (AAR) [13]
- (2) Maximum Entropy Method (MEM) [9]
- (3) Maximum Likelihood Method (MLM) [12]
- (4) Thermal Noise Algorithm (TNA) [15]

By contrast with classical spectral methods, a technique which uses (requires) the fact that the number of plane waves is finite is the MUSIC algorithm [16]. MUSIC, which denotes MULTIpLe SIGnAL CLAsSiFiCaTiOn, is an extension of the method of Pisarenko [18]. MUSIC is but one member of a class of methods based upon the decomposition of covariance data into eigenvectors and eigenvalues. Such techniques, known as Singular Value Decompositions (SVD's), will be more completely reviewed in a subsequent phase of the study. In order to place SVD techniques relative to the classical methods, however, results for MUSIC are included in this report.

All of the techniques reviewed have application to arbitrary array geometries. When the array happens to be linear, however, it is possible to take advantage of the structure of the array to improve the resolving power of these techniques [2]. Each of the techniques involves the calculation of a quadratic form which, in the case of the linear array, becomes a complex, trigonometric polynomial which is being evaluated on the unit circle in the complex plane. The behavior of such functions is dominated by the polynomial roots which lie on or close to the unit circle. Thus, a rooting variant of each technique is possible which computes the arguments of the roots closest to the unit circle. The rooting variant of TNA is identical to that of AAR, so that only four rooting algorithms have been presented.

The adaptive listening or copy functions for closely-spaced signals requires the use of main-beam nulling. Since this is difficult to accomplish without accidentally nulling the desired signal [23], however, much attention must be placed upon the sensitivity introduced by only approximately knowing the direction of the desired signal. Two covariance modeling techniques for steering nulls in the direction of interferers are reviewed in this report.

The sensitivity to errors in the knowledge of the array response to plane waves will be the subject of a detailed study in a subsequent report. Only a brief introduction to this subject is included here to determine the consequences of such errors on the ability to place nulls for copy by the modeling techniques described above. A simple direction-independent gain and phase error, independent from receiver to receiver, has been utilized for this initial investigation.

C. Overview of the Report

The following section (II) describes the performance bounds for direction finding and copy. The bounds for estimation errors are the Cramer-Rao type for the assumed case of Gaussian signals in Gaussian noise; the limiting performance for ideal arrays and infinite data are given for copy performance bounds.

An expanded description of the algorithms considered during this study is given in Section III. The emphasis in this section is a comparative introduction to the techniques for direction finding, power estimation and adaptive copy weighting.

An overview of the simulation approach used for this study is given in Section IV and the results are summarized in Section V. Various appendices elaborating on some topics and a complete collection of the Monte Carlo simulation outputs are also included.

D. Major Findings

The principal conclusions based upon the initial experiments are as follows:

1. Although some of the spectral algorithms tested to date are more sensitive than MUSIC, the angle estimates provided by these algorithms are generally poor.
2. For the linear array problem, a root variant of MUSIC exists which is considerably more sensitive than the spectral version.
3. The direct solution for the power present in multiple directions can fail because of mutual dependencies among direction vectors whenever the array is irregular. This difficulty can be overcome by formulating the power estimation as a least-squares problem.
4. Modeling of interference vectors provides an effective means of avoiding signal cancellation as a result of direction-of-arrival errors for the desired signal. Unfortunately, the resulting performance is very sensitive to array calibration errors.

The implications of these observations are that Singular-Value Decomposition is a desirable prerequisite for superresolution of plane waves and the exploitation of special array structures leads to increased resolution sensitivity, but that sensitivity to array errors is the most serious obstacle to successful implementation. For these reasons, the emphasis for the next phase of the study will be in the following areas:

1. Singular-Value Decomposition techniques
2. Maximal exploitation of linear array structures
3. Robust algorithms to reduce array error sensitivities

In addition to these areas of emphasis, Monte Carlo experiments will be extended to explore the effects of larger numbers of signals, decreased SIR, and various forms of array errors.

II. THEORETICAL PERFORMANCE BOUNDS

A. Direction-Finding

A major portion of this report is concerned with direction-finding (DF) algorithms and their expected performance, as determined by extensive Monte Carlo simulations. Although these results can be studied on a stand-alone basis, suitable theoretical benchmarks serve to put the results in a better perspective.

Perhaps the most desirable benchmark would be the performance achieved by the quintessential "optimum" processor. Given such a benchmark, one could reasonably expect to make sound judgements as to whether or not a particular algorithm was "good enough". Unfortunately, optimum processors can be prohibitively expensive to simulate. Moreover, practical applications are often sufficiently complicated that a single criterion for "optimality" is virtually impossible to define.

As a relevant case in point, consider the problem of direction-finding in a multiple emitter environment. This problem is characterized by an unknown number of signals arriving from unknown directions. Thus, a good DF algorithm must determine the number of signals present as well as provide accurate direction estimates. In some instances, estimates of the signal power levels are also required. Finally, in order to be useful in unfriendly environments, all of these requirements must be met without detailed knowledge of the signal waveforms.

Taken in its entirety, the multiple emitter DF problem is too complex to admit a comprehensive theoretical analysis. One possible simplification is to specify the number of emitters. In this case, one can obtain theoretical bounds on the accuracy of the (DF) estimates by computing the relevant Fisher information matrix. Inverting this matrix yields the Cramer-Rao bound on the variance of any unbiased estimate.

For the purposes of direction-finding, the assumption is made that the signal sources are stationary (complex) Gaussian random processes. The received signals are sampled at a rate less than the receiver bandwidth. Under

the latter assumption, the signals obtained at two different instants of time are statistically uncorrelated. This model is extremely convenient for generating simulation data and leads to performance bounds that depend only on the signal directions and powers.

The Cramer-Rao (C-R) bound for locating Gaussian emitters is derived in Appendix A. Here, we merely state the underlying model and present the final form of the result. To check the tightness of the bound, F. White [1] has investigated the performance of two "optimum" DF processors. His results indicate that the C-R bound is achievable over an interesting and broad range of parameter values.

The samples obtained from the array elements at any given instant of time, called a snapshot, may be modelled as a vector

$$r = s + n \quad ,$$

where n denotes the contribution from thermal noise and other sources of error in the receiver(s) and s represents the received signal(s). When only one emitter is present, the signal vector may be written as

$$s = v(\alpha) p \quad ,$$

where p is the complex amplitude of the signal that would be observed at the phase center of the array, and $v(\alpha)$ is a vector constructed from the complex voltage gains of the individual array elements. The vector $v(\alpha)$ is often referred to as a "direction" or "steering" vector since it depends only upon the direction of arrival of the signal. For linear arrays, the most convenient measure of direction is the cosine of the angle between the array axis and the line-of-sight to the signal. The direction cosine is denoted by α .

When more than one emitter is present, the principle of superposition allows us to write the received signal as

$$s = Vp \quad ,$$

where the j th element of the vector p is the complex amplitude of the signal from the j th emitter as "seen" at the array phase center. Note that the j th column of the matrix V is the direction vector associated with the j th emitter, i.e.,

$$V = [v(\alpha_1) \mid \dots \mid v(\alpha_J)]$$

where J denotes the actual number of emitters.

Under our statistical assumptions, the "signal-in-space" vector p is completely described by its mean value, assumed to be zero, and its covariance

$$P = E\{pp^H\} \quad ,$$

where $E\{x\}$ generally denotes the expected value of x , and a superscript "H" indicates the conjugate (Hermitian) transpose operation. Naturally, the Gaussian model is extended to include the noise vector n , and we represent the noise covariance matrix as

$$N = E\{nn^H\} \quad .$$

Assuming the noise statistics are known, one could always normalize (or transform) the data in such a way that the components of the noise vector n are identically distributed and statistically independent (uncorrelated). Unless otherwise explicitly stated, we will proceed under the assumption that the noise covariance is the identity matrix I .

Consider the problem of estimating the directions of arrival when the signal-in-space covariance P is known. The Fisher information matrix for this problem can be stated in a reasonably compact form by first introducing the gramian matrix

$$W \triangleq V^H V$$

and solving

$$P-Q = PWQ$$

for Q . It can be shown that this equation always has a unique (Hermitian) solution. We next introduce the "derivative" of V

$$\dot{V} = [\dot{v}(\alpha_1) \mid \dots \mid \dot{v}(\alpha_J)] \quad ,$$

where

$$\dot{v} = dv/d\alpha$$

is the usual derivative of v with respect to α . It is also convenient to define

$$\dot{W} \triangleq \dot{V}^H \dot{V} \quad .$$

Under the conditions stated above, the Fisher matrix for the unknown directions α is given by

$$F_{\alpha\alpha} = 2K \operatorname{Re} \left\{ (P-Q)^T \square (\dot{V}^H \dot{V} - \dot{W}^H Q \dot{W}) + (Q \dot{W})^T \square (Q \dot{W}) \right\} \quad ,$$

where K is the number of available snapshots (observations). $\operatorname{Re}\{x\}$ denotes the real part of x , and a superscript "T" refers to the usual transpose operation. The element by element (Hadamard) product of two matrices A and B with the same dimensions is written as $A \square B$.

The main diagonal of the inverse of the Fisher matrix provides a lower bound on the accuracy (i.e., variance) of any unbiased DF estimate. However, when the signal-in-space covariance P is also unknown, the resulting bounds are not as tight as they might be.

If the signal-in-space covariance were completely unspecified, generating the required Fisher matrix would become extremely awkward. Fortunately, many applications of interest are adequately modelled by assuming uncorrelated emitters. In this important special case, P is a diagonal matrix, i.e.,

$$P_{ij} = 0 \quad ; \quad i \neq j \quad .$$

Thus, consider the vector β obtained by taking the logarithm of the emitter "powers" (i.e., the main diagonal elements of P). When the directions of arrival are known, the normalized Fisher matrix for estimating the emitter powers can be written as

$$F_{\beta\beta} = K (OW) \square (OW)^T .$$

When the directions and powers are both unknown, the "reduced" information matrix for the directions is generally of the form

$$F_{\alpha\alpha}^{(\beta)} = F_{\alpha\alpha} - F_{\beta\alpha}^T F_{\beta\beta}^{-1} F_{\beta\alpha} .$$

The amount of information lost depends upon the coupling matrix, which is given by

$$F_{\beta\alpha} = 2K \operatorname{Re} \{ (\dot{OW}) \square (OW)^T \}$$

for the problem considered here.

Inverting the reduced information matrix yields the C-R bound for (unbiased) DF estimates when the emitter powers are also unknown. While the exact expressions given above appear to be quite formidable, the asymptotic form of the DF bound is really quite simple. As the signal-to-noise ratios of all of the emitters become arbitrarily large, we may replace Q with the inverse of W (provided it exists, of course). Eventually, P completely dominates Q and the asymptotic approximation

$$F_{\alpha\alpha}^{(\beta)} \rightarrow F_{\alpha\alpha} \rightarrow 2K P \square A$$

emerges, where the array factor

$$A = \dot{V}^H \dot{V} - \dot{W}^H \dot{W}^{-1} \dot{W}$$

depends only on the directions of arrival. Since P is a diagonal matrix, inverting $P \square A$ is trivial and the asymptotic accuracy of any unbiased DF estimate is bounded by

$$\text{Var } \{\hat{\alpha}_j\} \rightarrow [2K P_{jj} A_{jj}(\alpha_1, \dots, \alpha_J)]^{-1},$$

where $\text{Var } \{x\}$ denotes the variance of a random variable x . Surprisingly, the asymptotic error predicted by the DF bound is independent of the relative strength of the emitters! However, as expected, the asymptotic DF variance is inversely proportional to the product of the signal-to-noise ratio and the number of snapshots.

Unfortunately, the array factor is generally a very complicated function of the directions of arrival and the array geometry. However, certain simplifications are possible under the assumption of identical elements in a linear array. In particular, the phase reference point may be chosen so that

$$\dot{V}^H \dot{V} = 0.$$

Consequently, the array factor for a single emitter is given by

$$\Xi = \frac{1}{2} \left| \mathbf{v} \right|^2,$$

and the array factor for two emitters may be written as

$$A_{jj}(\alpha_1, \alpha_2) = \Xi \eta(\alpha_2 - \alpha_1) \quad ; j = 1, 2$$

where $\eta(\alpha)$ is a symmetric function which approaches unity for sufficiently large α . Thus, η may be interpreted as an efficiency factor that only depends on the separation of the two emitters [2].

B. Adaptive Listening

A phased array receiver is assumed to be used to monitor, or listen, to a desired emitter by discriminating against the undesired emitters only on the basis of differences in angular directions of arrival. An adaptive array differs from a more conventional phased array in that the complex weights associated with the antenna elements are not determined by the designer a priori. Instead, these weights are optimized, according to some criterion, on the basis of measurements which are made on the signal environment.

Let \mathbf{x}_k denote vector sample of complex array data collected during the k th snapshot, where $k=1, \dots, K$. As in the above discussion, the data are representable as

$$\mathbf{x}_k = p_s \mathbf{v}(\alpha_s) + \mathbf{V}_I \mathbf{p}_k + \mathbf{n}_k$$

where it is assumed that the desired emitter arrives from direction α_s with complex amplitude p_s and the j th component of the vector \mathbf{p}_k is the complex amplitude of the j th interference wave source and

$$\mathbf{V}_I = [\mathbf{v}(\alpha_1) \quad \dots \quad \mathbf{v}(\alpha_{J-1})]$$

is the matrix of the interferer direction vectors. The objective of the adaptive listening array is to enhance the gain of the array toward the

desired signal while simultaneously nulling the signal energy due to the directional interference. This is accomplished by computing a set of complex-valued element weights which, when applied to the element outputs and linearly combined, results in a complex scalar array output of the form

$$y_k = w^H x_k$$

If the signals and noise are Gaussian, the weight vector which maximizes the probability of detection of the desired signal is given by

$$w_o = R_N^{-1} v(\alpha_s)$$

where R_N is the spatial covariance of the interference plus noise, viz.

$$\begin{aligned} R_N &= E\{[V_I p_k + \eta_k] [V_I p_k + \eta_k]^H\} \\ &= V_I P_I V_I^H + I \quad , \end{aligned}$$

where, as above, we have taken the noise to be isotropic with unit variance.

Moreover, this same weight vector maximizes the output signal power to average interference-plus-noise power ratio (SIR), given by

$$SIR = P_s \frac{|w^H v(\alpha)|^2}{w^H R_N w} \quad ,$$

Where P_s is the power of the desired signal, thus, the maximum output SIR is given by

$$SIR_{\max} = P_s v^H(\alpha_s) R_N^{-1} v(\alpha_s)$$

In the present application, it is important to separate the desired emitter from the interference and noise. In this case, we start by observing the covariance with all signals present

$$\hat{R} = \frac{1}{K} \sum_{k=1}^K x_k x_k^H$$

Of course, in the limit for large sample size, \hat{R} converges to R , where

$$R = R_N + P_S v(\alpha_s) v^H(\alpha_s),$$

so that

$$R^{-1} v(\alpha_s) = [1/(1 + T_o)] R_N^{-1} v(\alpha_s)$$

where $T_o = SIR_{\max}$.

Thus, if $v(\alpha_s)$ is correct, $w = \hat{R}^{-1} v(\alpha_s)$ will converge to the maximum SIR weight vector in the limit for large K . Unfortunately, as Miller [49] and Boroson [50] have noted, the convergence rate will be dependent upon T_o . Specifically, if we define a generalized SIR as

$$GIR(v_s, P, v) = P_S \left| v^H P^{-1} v_s \right|^2 / v^H P^{-1} R_N P^{-1} v,$$

then the convergence of the sampled data weight vector depends upon

$$\rho_1 \triangleq \frac{GIR(v_s, \hat{R}, v_s)}{T_o} = \rho / [1 + T_o (1 - \rho)],$$

where ρ is distributed according to the Beta density [49], [50]

$$f(\rho) = [1 / B(L - 1, K + 2 - 1)] \rho^{K-L+1} (1 - \rho)^{L-2} ,$$

$$0 \leq \rho \leq 1 ,$$

with $B(M, N) = (M-1)!(N-1)!/(M+N-1)!$

Therefore,

$$P[\rho_1 \leq 1 - \delta] = P\{\rho \leq (1 - \delta) (1 + T_0) / [1 + T_0 (1 - \delta)]\}$$

If the desired signal power in the covariance matrix were zero, the above expression predicts the familiar result of Reed, et al. [22] that $K \geq 2L - 3$ will result in $E[\rho_1] \geq 1/2$. On the other hand, with $T_0 = 20$ dB, as many as 50 times as many samples would be needed to achieve the same result [50, Fig. 3].

Throughout the preceding discussion, the steering constraint for the listening weight vector was taken to be correct. Actually, this constraint must be obtained from the direction-finding process described above in Section A. Thus, we have only an estimate $\hat{\alpha}_s$ of the signal direction. Since we need a direction vector to constrain the listening weights, however, we may choose to use $v_s = v(\hat{\alpha}_s)$, but this choice will lead to a well-known problem, termed "sensitivity to mismatch" by Cox [23]. Examples of this effect will be given in the next section.

For the present study, it is assumed that it is adequate to establish a set of adaptive weights for which the $GIR(v_s, \hat{R}, v(\alpha_s))$ exceeds some minimal operation level, such as (say) 10 dB. Because of the relatively rapid convergence of this performance with the number of array snapshots, a reasonable bound on the adaptive receiver operating characteristic, may be obtained by evaluating the GIR for infinite data. In the examples in this report, a single interferer is placed $\Delta\theta$ beamwidths from a desired signal and the locus of $GIR = 10$ dB for $\Delta\theta$ versus desired array signal-to-noise ratio is used to predict limiting performance.

III. DESCRIPTION OF ALGORITHMS

A. Direction-Finding

Many practical algorithms that simultaneously estimate the directions of several emitters generate a non-negative function called a DF spectrum from the available array data. The domain of this function is the set of all possible directions, and the locations of its maxima (peaks) correspond to the estimated directions of arrival. Most algorithms require a covariance estimate, which is obtained from the array data. The covariance estimate is then transformed to produce the spectral estimate.

For the purposes of this discussion, the covariance estimate may be taken to be the usual sample covariance matrix generated from K snapshots of data $\{x_k \mid k = 1, \dots, K\}$, i.e.,

$$\hat{R} = \frac{1}{K} \sum_{k=1}^K x_k x_k^H$$

This estimate is generally positive definite provided the number of snapshots is not less than the number of array elements.

Table 3.1 summarizes the type of transformation used by several of the currently most popular algorithms. In each case, the algorithm operates on the covariance estimate with the direction vector $v(\alpha)$ to generate the spectral estimate for the direction α . As can be seen, all of the DF spectra in Table 3.1 require the computation of at least one quadratic form.

For the case of a uniform linear array, any quadratic form

$$g(\alpha) = v^H(\alpha) G v(\alpha)$$

may be interpreted as a "trig" polynomial, provided G is a non-negative definite Hermitian matrix. The spectral factorization theorem allows us to represent $g(\alpha)$ by two ordinary polynomials, one with its roots inside the unit

TABLE 3.1

DIRECTION-FINDING SPECTRA

Adapted Angular Response

$$\frac{\mathbf{v}^H(\alpha) \hat{\mathbf{R}}^{-1} \mathbf{v}(\alpha)}{\mathbf{v}^H(\alpha) \hat{\mathbf{R}}^{-2} \mathbf{v}(\alpha)}$$

Beam-Scan Algorithm (BSA)

$$\mathbf{v}^H(\alpha) \hat{\mathbf{R}} \mathbf{v}(\alpha)$$

Maximum Entropy Method (MEM)

$$\frac{\text{constant}}{\left| \mathbf{v}^H(\alpha) \hat{\mathbf{R}}^{-1} \mathbf{u}_1 \right|^2}$$

; \mathbf{u}_1 is the first column of
the identity matrix

Maximum Likelihood Method (MLM)

$$\frac{1}{\mathbf{v}^H(\alpha) \hat{\mathbf{R}}^{-1} \mathbf{v}(\alpha)}$$

Multiple Signal Classification (MUSIC)

$$\frac{1}{\mathbf{v}^H(\alpha) \mathbf{E}_N \mathbf{E}_N^H \mathbf{v}(\alpha)}$$

; certain eigenvectors of $\hat{\mathbf{R}}$
are selected for the
columns of \mathbf{E}_N

Thermal Noise Algorithm (TNA)

$$\frac{1}{\mathbf{v}^H(\alpha) \hat{\mathbf{R}}^{-2} \mathbf{v}(\alpha)}$$

circle and the other with corresponding roots outside the unit circle. Moreover, if z is a root of one of these polynomials, then $1/z^*$ is a root of the other. Either of these two polynomials completely characterizes an "all-zero" or finite impulse response (FIR) filter that produces a random process with power spectrum $g(\alpha)$ when excited with white noise. A process generated in this manner is sometimes called a moving average process.

The beam scan algorithm (BSA) produces a spectral estimate consistent with a moving average process. All of the other DF spectra in Table III.A are characterized by a denominator polynomial except AAR, which has both a denominator and a numerator polynomial. The AAR spectrum is consistent with an autoregressive-moving average (ARMA) process. The linear filter required to synthesize an ARMA process has both poles and zeroes. Each of the remaining algorithms (MEM, MLM, TNA, and MUSIC) leads to a spectral estimate consistent with an autoregressive process. As one might expect, an autoregressive process is characterized by an "all-pole" filter.

The beam scan algorithm actually provides the best possible estimate of the direction of arrival of a single emitter received in the presence of (spatially) white noise. In practice, one can expect the beam scan method to perform adequately so long as the emitters are all well isolated. Unfortunately, this approach breaks down completely when two (or more) emitters are separated by less than an array beamwidth.

The beam scan algorithm is the DF equivalent of a standard technique used in classical time-series analysis. In many applications, a single record of data is Fourier transformed to obtain a rough spectral estimate called a periodogram. Averaging many periodograms yields a smoothed spectral estimate. The spectral resolution provided by this approach is limited by the length of the individual data records. Quite analogously, the resolution of the beam scan algorithm is determined by the length of the array.

The limitations of the traditional approach eventually led to fundamental investigations seeking spectral estimates with better resolution. Some of the more important results of these investigations are summarized as follows.

1. Maximum Entropy Method

In 1967, John Burg [3] shook the foundations of traditional time-series analysis with his assertion that conventional spectral estimation techniques were fundamentally unsound. Burg was upset by the fact that, at the time, all recognized methods for computing a power spectral density implicitly truncated the correlation lags. As an alternative, Burg proposed his now famous "maximum entropy" spectral estimate. Although it may not have been widely recognized at the time, Burg was actually advocating that spectral estimates be derived within the framework of an autoregressive (AR) model for the time series [4].

In the usual time-series setting, maximum entropy spectral estimates are derived from a linear prediction error filter. The leading coefficient of this filter is unity, and the remaining coefficients are chosen to minimize its expected output power, usually referred to as the prediction error. The theoretical basis for this procedure is discussed in detail in Appendix B and the references therein. The desired filter coefficients are obtained by solving the mixed system of linear equations

$$Rw = [e \ 0 \ \dots \ 0]^T \quad (3.1)$$

for the prediction error e and the unknown elements of

$$w = [1 \ ? \ \dots \ ?]^T \ ,$$

where R is the theoretical covariance (matrix) for an arbitrary snapshot. The spectral estimate obtained from the solution to (3.1) can be written as

$$\hat{S} = \frac{1}{|v^H(\alpha) R^{-1} u_1|^2}$$

where u_1 is the first column of the identity matrix. Strictly speaking, this expression can only be interpreted as a maximum entropy spectral density in the ideal case of uncorrelated emitters and a linear array with uniformly spaced, omni-directional elements. Much of the confusion in the literature concerning the maximum entropy approach (see, for example, [5]) can be attributed to the prevailing uncertainty regarding the proper choice of a covariance estimate. The elegance and efficiency of the well-known Levinson recursion [6] has prompted many researchers to force a Toeplitz structure on the covariance estimate. The standard Yule-Walker method [7] leads to an estimate that is positive definite but badly biased, at least for DF applications. The bias is easily removed, but only at the expense of destroying (with some non-zero probability) the desired positive definite property. Neither of these approaches is recommended when high resolution is important.

Fortunately, the intrinsic (temporal) smoothing provided by a sample covariance matrix is quite adequate for most direction-finding applications. Of course, sample covariance matrices are never Toeplitz (except by accident) and, if employed, one must then solve the linear prediction (3.1) without the help of a truly fast algorithm. However, in most DF applications, the data records (i.e., snapshots) are short and computational efficiency is relatively important. In the (rare) situations where the sample covariance approach is unsatisfactory, the problems encountered with the Yule-Walker approach can be circumvented by Burg's ingenious scheme for estimating reflection coefficients directly from the data.

The standard time-series implementation of Burg's technique [8] is quite efficient, and a Burg filter always has the minimum phase property. This property guarantees a stable inverse but is seldom crucial except perhaps when one wishes to synthesize the input process. Moreover, the extended Burg technique [9] for processing multiple snapshots is not significantly faster than standard (e.g., Cholesky type) algorithms for solving the prediction (3.1) via the sample covariance method [10].

2. Maximum Likelihood Method

In [11] Lacoss discusses the maximum entropy method (MEM) and another high-resolution spectral estimation algorithm attributed to J. Capon [12] called the maximum likelihood method (MLM). The basic idea behind the latter approach is simple. Weights for the array elements are chosen which insure unit gain in a given direction α while simultaneously minimizing the array output power. Under these conditions, the output of the adapted array provides an unbiased, minimum variance estimate of the (desired) signal arriving from the specified direction. When the interference is Gaussian, the power out of the adapted array is a maximum likelihood estimate of the power received from the direction α .

In mathematical terms, the power out of the array can be expressed as

$$P = \mathbf{w}^H \hat{\mathbf{R}} \mathbf{w} \quad (3.2)$$

where \mathbf{w} represents the array weights. Constraining the gain of the array to be unity in the direction α is achieved by demanding that \mathbf{w} satisfy

$$\mathbf{w}^H \mathbf{v}(\alpha) = 1 \quad (3.3)$$

Minimizing (3.2) subject to (3.3) is easily accomplished using the method of LaGrange multipliers. The optimum weights for this problem maximize the output signal-to-interference ratio (SIR) and are found by solving

$$\hat{\mathbf{R}} \mathbf{w}(\alpha) = \lambda \mathbf{v}(\alpha) \quad (3.4)$$

where the Lagrangian λ is chosen to satisfy (3.3). Pre-multiplying this equation by the Hermitian transpose of $\mathbf{w}(\alpha)$, we find that the MLM power estimate and the Lagrangian are numerically the same. Replacing λ with P in (3.4), solving for $\mathbf{w}(\alpha)$, and substituting the result in (3.2) leads to the MLM power estimate

$$\hat{P}_{MLM} = \frac{1}{\mathbf{v}^H(\alpha) \hat{\mathbf{R}}^{-1} \mathbf{v}(\alpha)}$$

3. Adapted Angular Response

The adapted array response (AAR) algorithm suggested by Borgiottia and Kaplan [13] can be interpreted as a variation on the MLM theme. As mentioned above, the MLM array weights maximize the output SIR. This fact remains true for any choice of the Lagrange multiplier. The AAR spectral estimate is generated by scaling the MLM weights so that the sum of their squared magnitudes is some fixed value, e.g.,

$$|\mathbf{w}(\alpha)|^2 = 1 \quad . \quad (3.5)$$

This modification leads to a DF method with the desirable property that the effect of white noise on the spectral estimate is (on the average) the same in every direction. Choosing the Lagrangian λ to satisfy (3.5) instead of (3.3) leads to the AAR power estimate

$$\hat{P}_{AAR} = \frac{\mathbf{v}^H(\alpha) \hat{\mathbf{R}}^{-1} \mathbf{v}(\alpha)}{\mathbf{v}^H(\alpha) \hat{\mathbf{R}}^{-2} \mathbf{v}(\alpha)} \quad .$$

4. Thermal Noise Algorithm

As was mentioned above, the AAR power estimate has the same mathematical structure as an ARMA power spectral density. Generally speaking, an ARMA process can be represented by the cascade of an all-zero (FIR) filter and an all-pole filter. In [14], the point was made that a signal consisting of sinusoids (i.e., plane waves) and additive white noise satisfies an ARMA-like

difference equation. However, the sinusoids in noise process is an extremely pathological case where the poles and zeroes lie on the unit circle and cancel exactly. Thus, the frequency response of the cascade is perfectly flat! The sinusoids arise from the transient response of the critically stable all-pole filter. This strongly suggests that the denominator (i.e., the AR part) of an ARMA spectral estimate suffices to determine the frequencies of the sinusoids. Although the underlying reasons that motivated Gabriel [15] were undoubtedly somewhat different, the thermal noise algorithm (TNA) uses only the denominator of the AAR spectrum, i.e.,

$$\hat{P}_{TNA} = \frac{1}{v^H(\alpha) \hat{R}^{-2} v(\alpha)}$$

5. Multiple Signal Classification

The Multiple Signal Classification (MUSIC) approach to direction-finding was first described in [16]. The theoretical framework behind the MUSIC algorithm [17] is quite general and substantially extends the pioneering harmonic retrieval method of Pisarenko [18].

The underlying assumption behind the MUSIC algorithm is that the number of emitters seen by the receiver is less than the number of antenna elements. Under this condition, the covariance matrix of the received signal

$$S = E\{ss^H\}$$

is singular. Referring to (3.1), we observe that the null vectors of S theoretically provide a perfect mechanism for spatially extrapolating (i.e., "predicting") the received signal. Thus, one intuitively expects that the emitter directions could somehow be extracted from the null space of S .

The space spanned by the columns of S is referred to as the signal space. Except in certain pathological cases (i.e., perfectly correlated signals), the direction vectors of the emitters will always lie in the signal space. On the other hand, an arbitrary direction vector will generally have a component in the (complementary) null space. Thus, a simple test based on the distance to the signal space determines whether or not an arbitrarily chosen direction is a possible emitter direction.

Given an orthonormal basis for the null space, the Euclidian distance from an arbitrary vector x to the signal space can be easily calculated. The projection of x into the null space can be written as

$$x_N = E_N E_N^H x$$

where the columns of E_N are the (orthonormal) basis vectors for the null space. Consequently, the distance from x to the signal space is

$$|x_N| = (x^H E_N E_N^H x)^{1/2},$$

since

$$E_N^H E_N = I$$

by construction.

The MUSIC (pseudo) spectrum is defined to be the inverse of the squared distance from an arbitrary direction vector to the signal space, i.e.,

$$\hat{P}_{\text{MUSIC}} = \frac{1}{v^H(\alpha) E_N E_N^H v(\alpha)}.$$

In theory, the MUSIC spectrum becomes infinite at the true directions. However, small errors in the null vectors or the direction vectors will almost surely prevent the denominator from vanishing entirely. Therefore, in practice, the direction vectors that lie closer to the signal space than their immediate neighbors determine the MUSIC direction estimates.

In an operational system, the MUSIC spectrum must be derived from a sample covariance matrix. The first step in the MUSIC algorithm is to determine the standard eigenvalue (spectral) decomposition [19] of the sample covariance matrix, i.e.,

$$\hat{R} = EDE^H$$

where E is a unitary matrix and D is a (positive) diagonal matrix. Post-multiplying by E , we immediately observe that the columns of E are eigenvectors of the sample covariance matrix, and the (diagonal) elements of D are the corresponding eigenvalues. Without loss of generality, we may assume that the eigenvalues have been arranged in descending numerical order.

The signal space is specified by a simple partition of E , i.e.,

$$E = [E_S \mid E_N] \quad .$$

At this point, the critical issue is the proper dimension of the signal space. If the number of emitters present is known apriori (never the case in practice), then the correct partition to employ is obvious. Given J emitters, E_S consists of the first J columns of E . However, when the number of emitters is unknown, a choice (for J) must be made based on the available data. Several methods for determining J from the eigenvalues have been examined. These algorithms perform a sequence of likelihood ratio (hypothesis) tests and select the smallest value of J that is statistically consistent with the empirical eigenvalue distribution. Simulations results and references for the various likelihood ratio tests studied thus far are presented in Appendix C.

6. Rooting Methods for Linear Arrays

The root-finding method discussed here applies to all-pole (autoregressive) spectra of the general form

$$S(\alpha) = \frac{1}{v^H(\alpha) P v(\alpha)}$$

where P is a non-negative definite $M \times M$ Hermitian matrix that generally depends on the sample covariance matrix in a nonlinear manner. For example, the MLM spectrum is obtained by choosing P to be the inverse of the (sample) covariance matrix. For the purposes of this report, we may restrict our attention to uniform linear arrays. In this special case, the direction vectors are specified in Section IV.A. However, the basic approach described here is easily extended to thinned (uniform) arrays with missing elements.

A direct calculation shows that the inverse of the (autoregressive) spectrum defined above can be written as

$$S^{-1} = \sum_{m=-M+1}^{M-1} p_m \exp \{-i 2\pi m \xi \alpha\},$$

where the m th coefficient is obtained by summing the elements on the m th diagonal of P , i.e.,

$$p_m = \frac{1}{M} \sum_{k-l=m} p_{kl} \quad (3.6)$$

By introducing the change of variables

$$z = \exp \{ i 2\pi \xi \alpha \} \quad (3.7)$$

the spectrum can be expressed in terms of the polynomial

$$P(z) = z^{M-1} \sum_{m=-M+1}^{M-1} p_m z^{-m} .$$

Specifically, we have

$$S = \left| P\{\exp \{-i2\pi\xi\alpha\}\} \right|^{-1} .$$

Clearly, the polynomial $P(z)$ contains all the information in the spectrum. In fact, spectral peaks are a natural consequence of polynomial roots that lie near the unit circle. Hence, we are led to explore rootfinding as an alternative to searching for spectral peaks.

The Hermitian property of P insures that the polynomial coefficients in (3.6) satisfy the (harmonic) relationship

$$p_{-m} = p_m^* .$$

Using this fact, it can be verified that:

If z_m is a root of $P(z)$, so is $1/z_m^*$.

In practice, exactly half the roots of $P(z)$ will lie inside the unit circle. Direction (cosine) estimates can be derived from the roots by referring to (3.7), i.e.,

$$\hat{\alpha}_m = \frac{\arg z_m}{2\pi\xi} .$$

When the separation between adjacent elements is less than $1/2$ wavelength, (i.e., $\xi < 1/2$), the magnitude of an estimated direction cosine may be larger than unity. In this case, the estimate lies outside "visible" space and should be discarded. Naturally, other criteria can also be used to eliminate spurious estimates. For example, roots that lie close to the origin are presumably of little interest, since they do not correspond to (significant) spectral peaks. In the case of the root version of the MUSIC algorithm, only the J roots closest to the unit circle are considered, where J is the (estimated) dimension of the signal space.

B. Power Estimation

It is well-known that sampling of a time function introduces ambiguities in the resulting spectrum. Similarly, sampling the received wavefront on an aperture produces ambiguities in the resulting estimates of angle of arrival. The most familiar example is that of grating lobes which are produced when the elements of an array are spaced farther than $\lambda/2$ apart. The ambiguity introduced by a grating lobe is fundamental; there is no way to determine from which of the two (or more) directions signals are arriving.

The existence of ambiguities is a consequence of the linear dependence of direction vectors. For example, suppose there exist direction vectors $\underline{v}_1, \underline{v}_2, \underline{v}_3$ such that

$$a\underline{v}_1 + b\underline{v}_2 + c\underline{v}_3 = 0$$

for some set of complex numbers (a,b,c) , and that the signal is composed of sources from directions $\underline{v}_1, \underline{v}_2$ with complex Gaussian amplitudes A, B . If the correct directions are selected, the resulting signal-in-space covariance matrix is

$$P_{12} = E \begin{bmatrix} A \\ B \end{bmatrix} (A^* \ B^*) = \begin{bmatrix} P_A & 0 \\ 0 & P_B \end{bmatrix}$$

The signal can be written equally well as

$$\underline{r} = (B - aA)\underline{v}_2 - bA\underline{v}_3$$

However, if directions \underline{v}_2 , \underline{v}_3 are selected, the resulting signal-in-space covariance is

$$P_{23} = E \begin{bmatrix} B-aA \\ -bA \end{bmatrix} [(B-aA)^* \quad (-bA)^*] = \begin{bmatrix} P_B + |a|^2 P_A & ab^* P_A \\ a^* b P_A & |b|^2 P_A \end{bmatrix}$$

which is not diagonal. The same is true if directions \underline{v}_1 , \underline{v}_3 , or \underline{v}_1 , \underline{v}_2 , \underline{v}_3 are chosen.

Adaptive algorithms for estimating the direction of arrival of incoherent signals all operate on the principle of adaptive cancellation. They select a set (or sets) of weights to apply to the array data so as to minimize the output power from the array. Some sort of constraint must be imposed on the weights to keep them from going to zero; the algorithms differ mainly in their choice of this constraint.

It is intuitively clear that the adapted array pattern (i.e., the array pattern using the adaptive weights) must have minimal gain in each of the source directions. These minima serve as estimates of the source directions. If \underline{v}_1 , \underline{v}_2 , \underline{v}_3 are linearly dependent directions, and sources are present in directions \underline{v}_1 , \underline{v}_2 , the adapted pattern will have minima in all three directions. To determine the true source distribution, a power estimation algorithm which can handle linearly dependent direction vectors is needed.

The usual method of power estimation requires that the candidate direction vectors be linearly independent. Then, knowing the noise power σ^2 , one can operate on the true covariance matrix

$$R = \sigma^2 I + VPV^H$$

and obtain

$$P = (V^H V)^{-1} V^H (R - \sigma^2 I) V (V^H V)^{-1} \quad (3.8)$$

Of course, R is not known, so that sample covariance matrix

$$S = \frac{1}{N} \sum \underline{r}_n \underline{r}_n^H \quad (3.9)$$

is used instead. If the direction vectors are linearly dependent, $(V^H V)^{-1}$ does not exist, and the method fails.

There are a variety of ways to avoid this problem. Several are described in a recent paper by d'Assumpcao [20]. The technique discussed here is called least squares power estimation.

The idea of least squares power estimation is to find positive numbers P_1, \dots, P_L (and σ^2 , if the noise power is not known) which minimize

$$E = \|S - \sigma^2 I - VPV^H\|_F^2 \quad (3.10)$$

$$= \text{Tr}(S - \sigma^2 I - VPV^H)^H (S - \sigma^2 I - VPV^H)$$

$$= \sum_{i,j} |(S - \sigma^2 I - VPV^H)_{ij}|^2$$

Assume first that σ^2 is known. Setting $\frac{\partial E}{\partial P_l} = 0$ for $l=1, L$, we obtain the set of equations¹

¹ Note that $\frac{\partial}{\partial P_l} (VPV^H) = \underline{v}_l \underline{v}_l^H$.

$$\underline{v}_l^H (S - \sigma^2 I) \underline{v}_l = \underline{v}_l^H V P V^H \underline{v}_l \quad l=1, L$$

$$= \sum_{m=1}^L P_m \left| \underline{v}_l^H \underline{v}_m \right|^2$$

These equations may be written in matrix form as

$$O \underline{P} = \underline{b} - \sigma^2 \underline{c} \quad (3.11)$$

where

$$b_l = \underline{v}_l^H S \underline{v}_l \quad (3.12)$$

$$c_l = \underline{v}_l^H \underline{v}_l \quad (3.13)$$

$$Q_{kl} = \left| \underline{v}_k^H \underline{v}_l \right|^2 \quad (3.14)$$

The matrix Q can be written as a Hadamard product. The Hadamard product of two matrices is defined to be

$$(A \square B)_{kl} = a_{kl} b_{kl} \quad (3.15)$$

With this notation we can write

$$Q = V^H V \square (V^H V)^* \quad (3.16)$$

where * denotes the complex conjugate.²

The solution of (3.11) is clearly

$$\underline{p} = \underline{0}^{-1}(\underline{b} - \sigma^2 \underline{c}) \quad (3.17)$$

In many cases, $\underline{0}^{-1}$ exists even when $(\underline{v}^H \underline{v})^{-1}$ does not.

When σ^2 is unknown, we first solve

$$\frac{\partial E}{\partial \sigma^2} = -2 \text{Tr} (S - \sigma^2 I - \underline{v} \underline{v}^H) = 0$$

with the result

$$\sigma^2 = \frac{1}{M} \text{Tr}(S - \underline{v} \underline{v}^H) \quad (3.18)$$

where M is the number of array elements (the dimension of S). Substitution into (3.10) gives

$$\begin{aligned} E &= \text{Tr}(S - \sigma^2 I - \underline{v} \underline{v}^H)^H (S - \underline{v} \underline{v}^H) \\ &= \text{Tr}(S - \underline{v} \underline{v}^H)^H (S - \underline{v} \underline{v}^H) - \frac{1}{M} \text{Tr}^2(S - \underline{v} \underline{v}^H) \end{aligned}$$

Setting the derivatives equal to zero yields

$$\sum_{k=1}^L p_k \left(\left| \frac{\underline{v}_k^H \underline{v}_\ell}{\underline{v}_k^H \underline{v}_k} \right|^2 - \frac{1}{M} \left(\frac{\underline{v}_k^H \underline{v}_k}{\underline{v}_k^H \underline{v}_k} \right) \left(\frac{\underline{v}_\ell^H \underline{v}_\ell}{\underline{v}_\ell^H \underline{v}_\ell} \right) \right) = \frac{\underline{v}_\ell^H}{\underline{v}_\ell^H \underline{v}_\ell} \left(S - \frac{\text{Tr} S}{M} I \right) \underline{v}_\ell \quad \ell = 1, L$$

²Since $\underline{v}^H \underline{v}$ is Hermitian, we could equally well write $\underline{0} = \underline{v}^H \underline{v} \times (\underline{v}^H \underline{v})^T$.

which can be written in the form

$$(Q - \frac{1}{M} \underline{c} \underline{c}^H) \underline{p} = \underline{b} - \frac{\text{Tr} S}{M} \underline{c} \quad (3.19)$$

The solution is, of course

$$\underline{p} = (Q - \frac{1}{M} \underline{c} \underline{c}^H)^{-1} (\underline{b} - \frac{\text{Tr} S}{M} \underline{c}) \quad (3.20)$$

If Q has an inverse, so does $Q - \frac{1}{M} \underline{c} \underline{c}^H$.

Unfortunately, (3.17), (3.18), and (3.20) do not guarantee positive estimates for the signal and noise powers. This reflects the fact that in the minimization, no constraint on the parameter values was imposed. If the minimization were done numerically by a nonlinear program, the constraints could easily be included. However, this would be computationally much more expensive than the simple unconstrained solution.

The least squares power estimation technique eliminates spurious spectral peaks by producing small (perhaps even negative) estimates of the power associated with them; they can then be eliminated by a simple threshold test. The results of a Monte Carlo computer simulation comparing the direct method ((3.8), retaining only the diagonal terms) and the least squares method (3.17) are presented in Appendix D.

C. Weight Design Procedures for Adaptive Listening

The problem of designing a set of optimal weights for an adaptive listening array has been considered. This problem has been treated extensively in the past [21-28]. In these previous analyses, it has been assumed that the covariance matrix of the interference, or noise, can be obtained, or is possibly known, in the absence of the desired signal. However, in the present work, it is assumed that the covariance matrix of the signal plus noise is the

quantity which can be obtained. This assumption leads to great complications, as has been observed by Cox [23]. In particular, if an attempt is made to use this covariance matrix to design a set of weights, using the procedure which maximizes the signal-to-interference ratio (SIR), then the resultant processor will be extremely sensitive to the mismatch problem, i.e., the assumption about the angle of arrival of the desired signal. This particular design procedure is termed the Measured Covariance Method, and the weights are designed as

$$W_A = R_x^{-1} V, \quad ,$$

where R_x is the covariance matrix for the desired signal plus interference, discussed in Section II.B., and V is a steering vector which points in the estimated direction of the desired signal.

A number of other design procedures were considered. The first method is termed the Model Covariance Method and the weights are computed as

$$W_C = \left(\sum_{j \neq k}^J p_j V_j V_j^H + \sigma^2 I \right)^{-1} V_k, \quad ,$$

where J is the number of emitters, V_k is a steering vector which points in the estimated direction of the k -th emitter, σ^2 is the incoherent noise power, I is the $L \times L$ identity matrix. It is assumed that the desired emitter corresponds to the k -th direction. In practice, the steering vectors would be obtained from a direction-finding algorithm.

An example of the problem of sensitivity to mismatch is shown in Figs. 3.1a-b. A linear array of 10 elements is considered with an inter-element spacing of 0.5 wavelengths. The power levels of the desired and undesired emitters, relative to the background incoherent noise, is 26 dB and 40 dB, respectively, per array element.

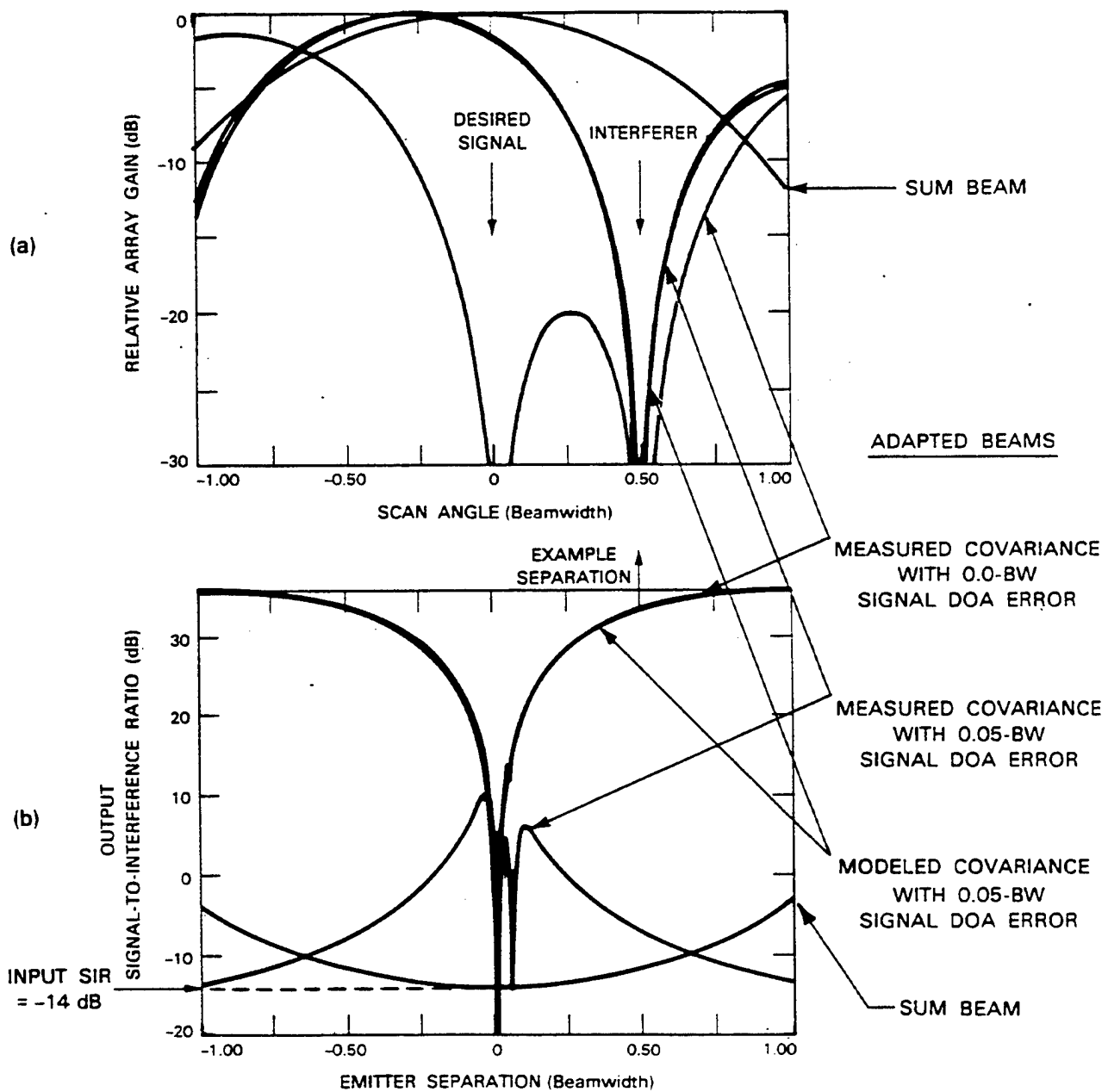


Fig. 3.1. Copy sensitivity to signal direction-of-arrival estimation errors.
 a) Typical beam patterns with emitter separation.
 b) Typical array output performance vs. emitter separation.

In Fig. 3.1a the beam patterns are depicted for the Measured Covariance Method and the Model Covariance method. The directions of arrival of the desired emitter, and interference, are assumed to be 0 and 0.5 beamwidths, respectively. The pattern for the sum beam, corresponding to a simple phase steering and then summing of the antenna element outputs, serves to define the natural beamwidth of the array as determined from the dimension of the array in wavelengths, which was discussed in Section II.B. The pattern for the Measured Covariance Method, when there is no error in the estimated direction of arrival of the desired emitter, produces a null in the direction of the interference, but has a relative array gain of about 0 dB for the desired signal. However, if an error of 0.05 beamwidths is made, the pattern for the Measured Covariance Method produces a null in the direction of the desired signal. The reason for this is that the design procedure treats the desired signal as interference, since its direction of arrival has not been specified precisely. The pattern for the Model Covariance Method under these conditions does not exhibit such behavior as seen in Fig. 3.1a. This pattern produces a null in the direction of the interference, but passes the desired signal. In essence, this behavior of the pattern occurs since the effect of the desired signal on the covariance matrix used in the design procedure has been eliminated. Thus, the Model Covariance Method is relatively insensitive to signal DOA errors.

The effect of emitter separation upon the sensitivity to mismatch problem is shown in Fig. 3.1b which depicts the output signal-to-interference ratio (SIR) in dB, vs. the emitter separation in beamwidths. The method for computing the SIR was discussed in Section II.B. The result for the sum beam shown in this figure indicates that the performance obtained with this method is not impressive when the magnitude of the emitter separation is less than 1 beamwidth. However, optimal performance is obtained for the Measured Covariance Method when there is no error made in estimating the direction of arrival of the desired signal. If the emitter separation is 0.5 beamwidths, for example, then it is possible to obtain a depth of null of about 45 dB.

That is, the desired signal level can be raised from 14 dB below the interference to about 31 dB above the interference. Unfortunately, if an error of 0.05 beamwidths is incurred, then the performance of this method deteriorates seriously, as shown in Fig. 3.1b. However, the impressive performance is maintained by the Model Covariance Method under these conditions, as depicted in Fig. 1b. These results indicate, once again, that the Model Covariance Method is not sensitive to the error made in estimating the direction of arrival of the desired signal.

Another weight design procedure which has been considered is the Projection Nulling Method. In this method the complex weights are computed as

$$W_P = (I - V(V^H V)^{-1} V^H) V_k$$

where

$$V = [V_1 \mid \cdots \mid V_{k-1} \mid V_{k+1} \mid \cdots \mid V_L] .$$

It has been shown ([8], p. 141) that if the signal-to-noise ratio is large, then the Projection Nulling Method is equivalent to the Model Covariance Method. This theoretical result has been confirmed by computer simulations in the present study. As a consequence, the Projection Nulling Method has not been discussed in detail. As a final comment, it should be noted that since the Projection Nulling Method is equivalent to the Model Covariance Method, the former method is also not sensitive to the error incurred in measuring the direction of arrival of the desired signal.

IV. DESCRIPTION OF THE MONTE CARLO EXPERIMENTS

A. Direction-Finding Comparison

A primary motivating factor behind this report is the desire to communicate the results of an extensive simulation of a number of potentially interesting direction-finding algorithms. These quantitative performance comparisons are presented, in their entirety, in Appendix F. A conceptual flow diagram of the simulation experiments is shown in Fig. 4.1.

The basic scenario for all of the experiments consisted of two independent emitters and a uniform linear array with ten omni-directional elements. Adjacent elements were separated by $1/2$ wavelength. The only source of error was additive thermal noise at each of the array elements. The signals and noise were modelled as complex Gaussian variables as discussed in Section II.A. Sample covariance matrices were generated using the Wishart technique described in Appendix E. Since our antenna model exhibits perfect symmetry with respect to its geometric (phase) center, the sample covariance matrix was first processed using the forward/backward averaging technique described below. Based on the resulting covariance estimate, tentative direction of arrival estimates were generated using one of the algorithms discussed in Section III.A. The array signal-to-noise ratio (SNR) associated with each candidate direction was estimated using the direct method discussed in Section III.B. All candidate directions with an SNR estimate less than 0 dB were discarded. The remaining direction estimates were compared with the true directions. Those direction estimates resulting in the smallest total (absolute) direction error were assigned to the true directions subject to the following provisions:

1. A single estimate could not be assigned to both emitters.
2. Assignments with an absolute direction error larger than a beamwidth were not permitted.
3. An assignment was disallowed if the power estimate was 10 dB larger than the true power.

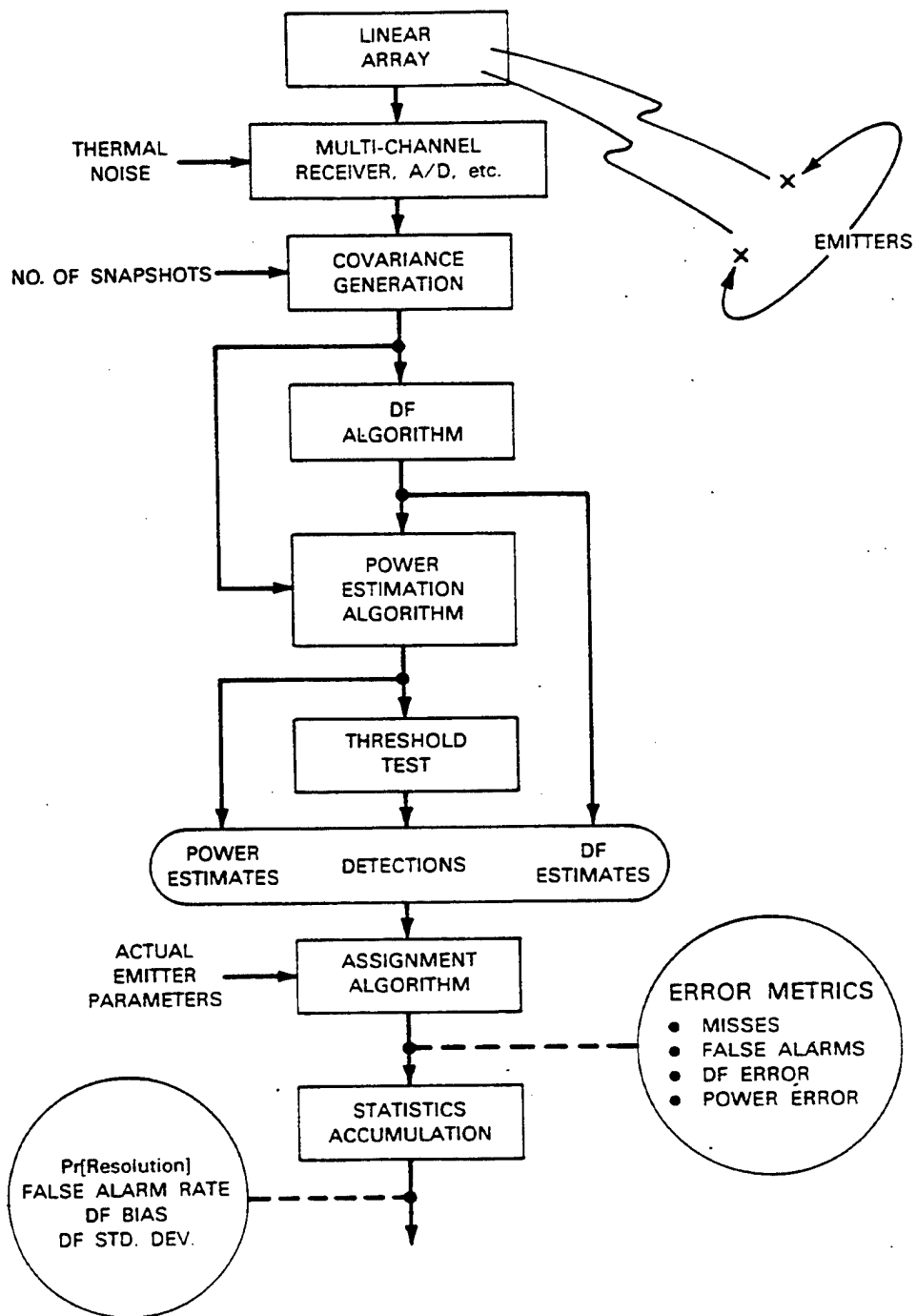


Fig. 4.1. Process for simulating superresolution.

All unassigned estimates were counted as false alarms. An unassigned emitter was declared to be a miss. The emitters were said to be resolved if neither was missed. The probability of resolution and the false alarm rate were calculated based on 100 Monte Carlo trials. Second order statistics on the DF errors were also accumulated, conditioned upon successfully resolving the two emitters.

During the course of the simulation study, the fundamental parameters of the system were varied in order to provide a better perspective on the relative performance of the algorithms. The sensitivity of the algorithms to thermal noise was tested by changing the number of snapshots used to construct the sample covariance. Three cases were considered, namely 10, 100, and 1000 snapshots (looks). To assess the resolution limits of the DF algorithms, emitter separations of 0.1, 0.2, and 0.4 beamwidths were considered. Initially, the relative power of the two emitters was 0 dB. Subsequently, an identical series of experiments was conducted with the relative power set at -10 dB. In both cases, the array SNR of the desired (weaker) signal was varied from 10 to 50 dB in 5 dB steps. These parameter variations are summarized in Table 4.1.

Table 4.1
PARAMETER VARIATIONS

SIR	: 0, -10 dB
Emitter Separation	: 0.1, 0.2, 0.4 beamwidths
Number of Looks	: 10, 100, 1000
Array SNR	: 10, 15, ..., 45, 50 dB

The relative power of the desired signal to the interfering signal is called the signal-to-interference ratio (SIR). The emitter separation is specified in terms of the available beamwidth of the array, defined to be the inverse of the length of the array expressed in wavelengths. The desired signal was always located broadside to the array (i.e., $\alpha = 0$), and the beamwidth was 0.2 radians or 11.5 degrees. The number of independent (uncorrelated) snapshots used to construct the sample covariance matrix, denoted by K , is referred to as the number of "looks". If the receiver IF bandwidth is B and the data collection interval is T , then the number of looks is limited by the (time-bandwidth) product BT , i.e.,

$$K \leq BT \quad .$$

The array SNR is the total energy (in joules) received from an emitter in a single snapshot divided by the thermal noise level (in watts/Hz = joules). Note that the array SNR includes the signal gain available from the antenna. For the ideal ten element array considered here, the array SNR is 10 dB greater than the SNR on a single antenna element.

Calculations of the array SNR are facilitated by scaling the direction vector $\mathbf{v}(\alpha)$ to have unit norm. Moreover, it is usually convenient to choose the phase reference (center) to be at the geometric center of the array. Thus, the m th element of the normalized direction vector for an ideal array is

$$\mathbf{v}_m(\alpha) = \frac{1}{M^{1/2}} \exp \{j 2\pi(m - M/2) \xi \alpha\} \quad ; m = 0, 1, \dots, M-1 \quad (4.1)$$

where M is the number of array elements and $\xi (= d/\lambda)$ is the element separation in wavelengths. One may easily verify that the direction vector constructed from (4.1) has the properties

$$|\mathbf{v}(\alpha)|^2 = 1$$

and

$$v(\alpha) = Jv^*(\alpha) \quad , \quad (4.2)$$

where J is the (usual) exchange matrix that reverses the order of the elements of a vector (see Appendix B).

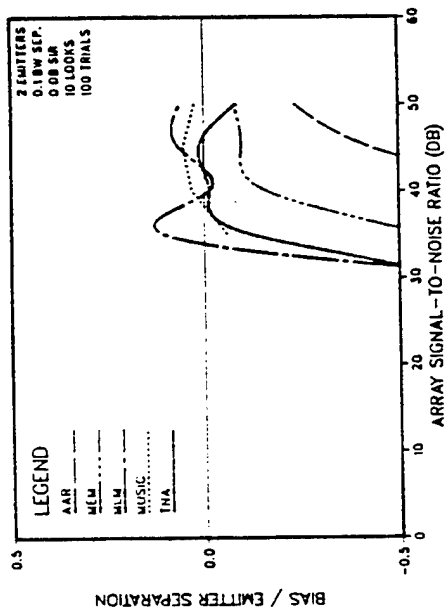
A vector that satisfies the relationship in (4.2) is said to be harmonic. A simple calculation reveals that every symmetric array with isotropic (i.e., identical) elements has harmonic direction vectors. In turn, the covariance matrix of the received signal, $s = Vp$ (see Section II.A), satisfies a similar harmonic property, e.g.,

$$\begin{aligned} S &= E\{ss^H\} \\ &= VPV^H \\ &= JV^*PV^TJ \\ &= JS^*J \end{aligned}$$

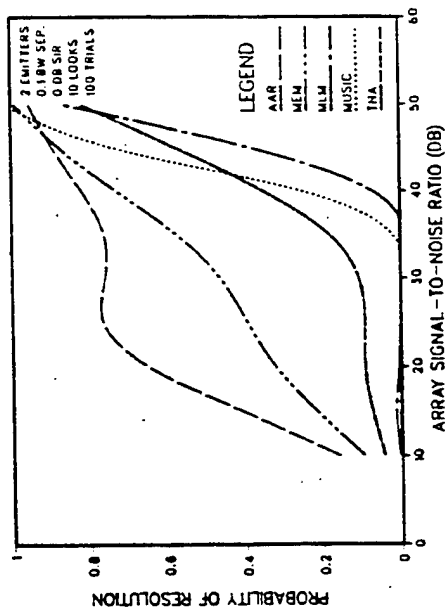
where P is a real diagonal matrix consisting of the emitter powers that would be measured at the array phase center. When a Gaussian signal with a harmonic (persymmetric) covariance matrix is received in Gaussian white noise, it can be shown [29] that the forward/backward averaged sample covariance matrix, i.e.,

$$\hat{R}_{F/B} = \frac{1}{2} [\hat{R} + J\hat{R}^*J] \quad , \quad (4.3)$$

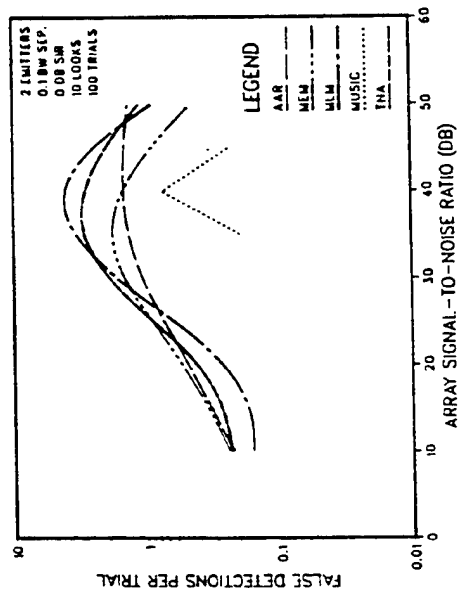
DIRECTION-FINDING BIAS



MULTIPLE SIGNAL DETECTION PERFORMANCE



FALSE ALARM PERFORMANCE



DIRECTION-FINDING ACCURACY

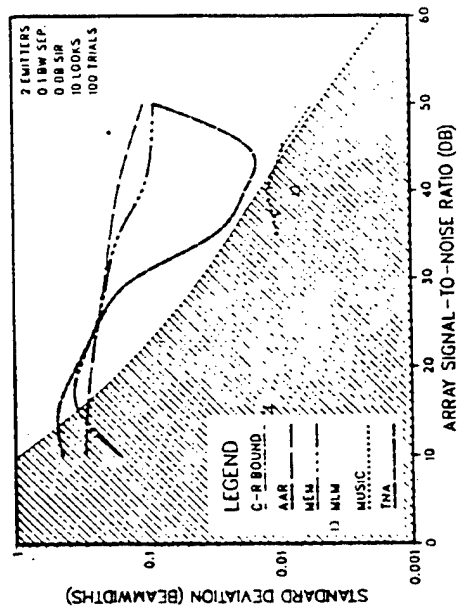


Fig. 4.2. Typical output from a superresolution experiment.

is a sufficient statistic for estimating any parameter of the (true) covariance matrix. Note that this (harmonic) covariance estimate is obtained by taking the arithmetic average of the usual sample covariance matrix and the (sample) covariance matrix constructed from reversed and conjugated data. All of the algorithms compared in this report derived their DF estimates from the covariance estimate in (4.3).

Examples of the statistical data produced by the simulation are shown in Fig. 4.2. Each data point was calculated on the basis of 100 Monte Carlo trials. Smooth curves were fitted to the simulation data with a standard algorithm provided in the software package used to plot the results. For purely aesthetic reasons, the actual data points are normally suppressed.

Perhaps the most important DF statistic is the probability of resolving two emitters. Generally speaking, most DF algorithms cannot reliably resolve closely spaced emitters at very low signal-to-noise ratios. However, as indicated by the example in Fig. 4.2, an algorithm's ability to resolve emitters improves rapidly once the SNR exceeds some critical threshold level. Below threshold, most algorithms erroneously report the presence of a single emitter at the "centroid" of the two emitters. At the two extremes, relatively few spurious estimates are generated. However, the transition from low to high probability of resolution is usually characterized by an increase in the false alarm rate. Since an inordinately large number of spurious direction estimates would be undesirable, the average number of false alarms (per trial) for each of the algorithms tested has been plotted.

Above threshold, the precision of the direction estimates is the primary measure of DF performance. In the statistical literature, an estimate is said to be efficient if its variance agrees with the Cramer-Rao bound. The example in Fig. 4.2 indicates that the DF algorithms are asymptotically unbiased (consistent) and efficient as the SNR increases. In fact, most of the algorithms become unbiased within a few dB of the resolution threshold. Thus, the remaining issue is how quickly the direction error approaches the Cramer-Rao bound. The simulation data in Appendix F address these issues over the range of parameter values specified in Table 4.1.

The algorithms tested (see Section III.A) were AAR, MEM, MLM, MUSIC, and TNA. Data was obtained for both spectral and root versions of these algorithms. Since the root version of TNA is the same as the root version of AAR, only the results for the latter are presented. In several instances, the false alarm data for some of the algorithms (especially MUSIC) may appear to be missing. In these case, no false alarms were observed.

Occasionally, the standard deviation curve for an algorithm drops below the C-R bound. Strictly speaking, the C-R bound plotted in the performance comparisons is valid only for unbiased and unexpurgated estimates. The latter requirement means that, in every instance, direction estimates for both emitters must be generated in order to interpret the bound rigorously. As stated previously, the DF statistics presented in this report are conditioned on the emitters being resolved. Near (or below) threshold, practical algorithms often fail to find both emitters and are usually biased. Consequently, the C-R bounds are not strictly applicable except at high SNR. Moreover, because of the conditioning, the statistical significance of the average performance decreases as the probability of resolution drops.

B. Adaptive Nulling to Support Signal Copy

1. Overview

The primary function of adaptive nulling of interference is to improve the signal-to-noise interference ratio (SIR) of the emitter selected for copy. For the case of multiple emitters separated by less than one beamwidth in azimuth angle, the adaptive nulling system must be able to place deep nulls, within the "main beam", on the interferers while maintaining sufficient gain on the desired signal to permit classification and/or monitoring. In order to properly support signal copy, the nulling system must increase the (presumably negative) SIR in each of the receiver channels to an output SIR of at least (say) +10 dB by a linear weighting of the receiver outputs.

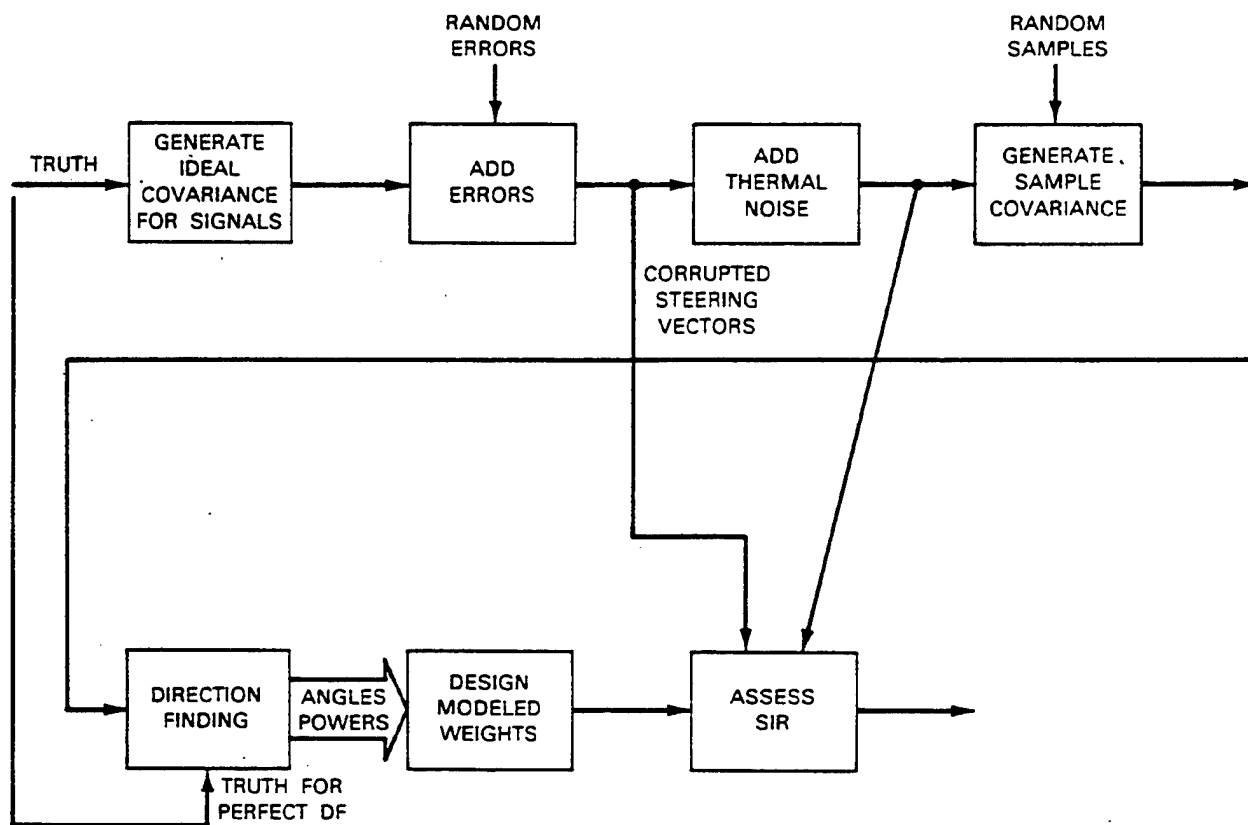
As discussed in Section III.5, the two initial candidate nulling methods under investigation base their nulling weights solely upon the estimated directions and powers of all the emitters present. Therefore, either of these nulling techniques is potentially compatible with any of the techniques for super-resolution direction-finding. Since there are several performance measures which are appropriate to the evaluation of direction-finding algorithms and since the relative performance ranking of the various algorithms depended upon the specific performance measure selected, it was not obvious at the outset which combinations of DF methods vs. nulling algorithms would be most successful on the average. Thus, an initial standardized experiment was formulated to investigate the compatibility issue.

The standard experiment which was used for the initial review of nulling alternatives was based upon the same 10-element, half-wavelength spaced array which was used for the initial direction-finding algorithm assessment (see Fig. 4.3 for a conceptual block diagram). Two emitters were modelled with the desired signal -10 dB in power relative to the interferer. For each of the candidate pairings of the DF and nulling algorithms, two basic parametric variations were explored: (1) the effects of sample-size and (2) the effects of residual calibration errors. For all experiments, the criterion used to evaluate the relative performance was the same: "what array signal-to-noise ratio (SNR) is required to achieve +10 dB output SIR as a function of emitter separation?" As before, array SNR is measured relative to the weaker, or in this case desired, signal.

2. Description of Simulation Output

A typical summary plot, illustrating the comparison of several algorithms for a particular setting of the experimental parameters, is shown in Fig. 4.4². The shaded region in the corner of the plot indicates those combinations of array SNR and signal separation for which the indicated nulling technique (in this case the Model Covariance Method) would be unable to provide +10 dB output SIR, even if given perfect knowledge of all emitter

²The ARM, or Auto Regressive Root Method, algorithm shown in Fig. 4.4 is from [2]. Its performance is identical with the root variant of MEM when forward-backward averaging of the covariance matrix is employed.



131922-11

Fig. 4.3. Processing for simulating adaptive copy.

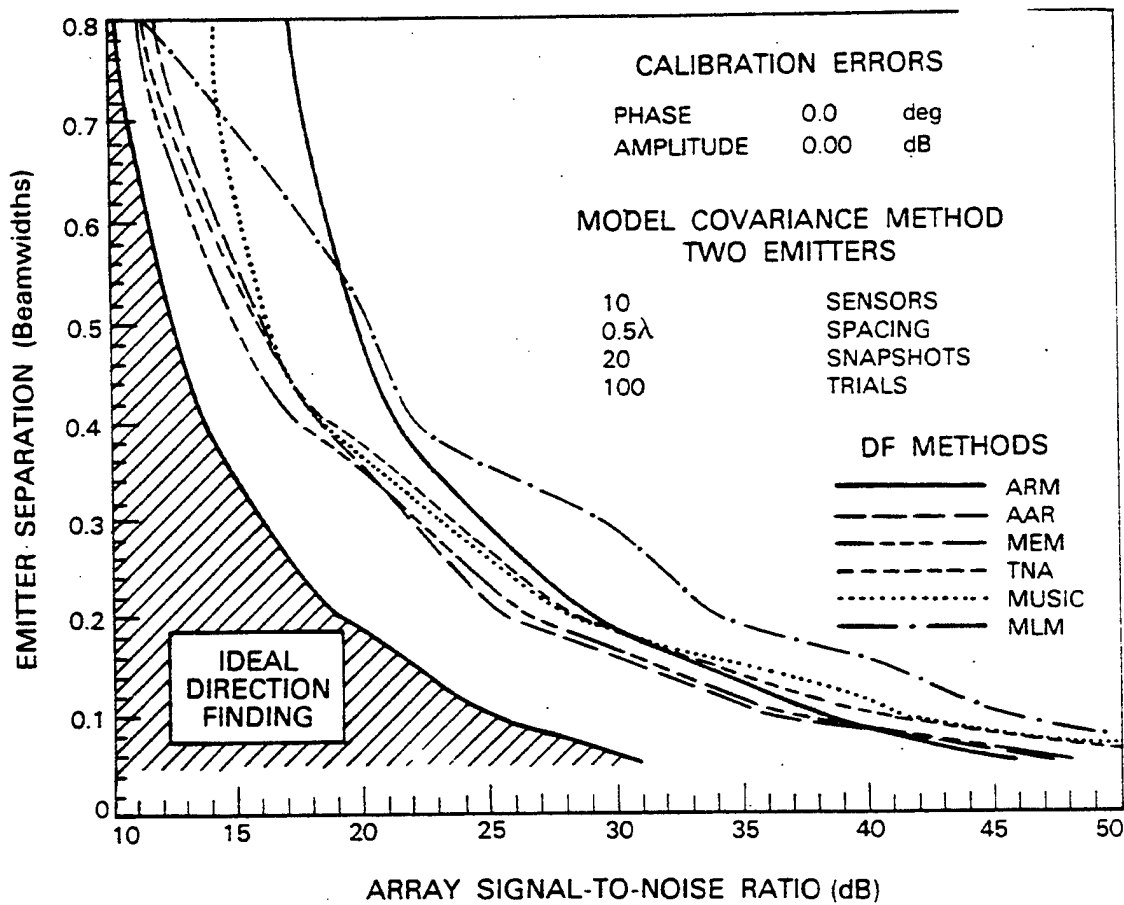


Fig. 4.4. Typical output from adaptive copy experiment.

directions-of-arrival and received powers. Thus, for example, at 0.1 beamwidth emitter separation, at least 24 dB array SNR of the target emitter is required to support copy, according to this criterion.

The curves in Fig. 4.4 correspond to different super-resolution algorithms. In each case, the DF outputs were used by the nulling system to set up the weights for copy. The interpretation of the results is the same as for the "ideal direction-finding" bound: below and to the left of each curve it is not possible, on the average, for the indicated DF method to provide +10 dB output SIR when combined with the Model Covariance Nulling method.

Using Fig. 4.4 as a reference then, we conclude that about 40 dB array SNR is required in order for MUSIC (with 20 snapshots of array data) to provide sufficiently accurate angle data on emitters to permit copy at 0.1 beamwidth emitter separation, as compared with 24 dB for ideal direction finding, as described above.

3. Details of the Experiment

In order to evaluate the proposed performance criterion, separate Monte Carlo simulation experiments were performed for 45 pairs of emitter separations (0.05, 0.1, 0.2, 0.4, 0.8 beamwidths) and array SNR's (10, 15, 20, 25, 30, 35, 40, 45, 50 dB). The theoretically evaluated output power in the true signal "direction," including residual calibration errors, if any, were tabulated. The desired locus of +10 dB output SIR was obtained from a contour plotting program, based upon the rectangular array of output power data.

For each setting of emitter separation and array SNR, a composite DF/copy experiment was performed as illustrated in the block diagram of Fig. 4.3. This diagram depicts the flow of data during each of the 100 Monte Carlo trials over which the output SIR was accumulated.

Given the positions and powers of the interferer and signal, the ideal signal covariance (uncorrupted by calibration errors) is first computed as

$$R_s = P_s V(\theta_s) V^H(\theta_s) + P_I V(\theta_I) V^H(\theta_I)$$

Next, using a random error vector, V_E , having Gaussian phase and log-normal amplitude with the assumed standard deviations, the steering vectors are corrupted to reflect residual calibration effects, such as unmodelled near-field multipath, etc. This transformation is obtained by premultiplying the direction vectors with a diagonal matrix of the form

$$R_E = \begin{bmatrix} a_1 e^{j\phi_1} & & 0 \\ & \ddots & \\ 0 & & a_n e^{j\phi_n} \end{bmatrix}$$

where a_i , ϕ_i are the n pairs of amplitude and phase errors as selected above. Since the same calibration errors are assumed for both signal and interferer, the corrupted signal covariance is directly obtained by premultiplying by R_E and post-multiplying by R_E^H . Thermal noise of the required intensity is next added to the corrupted signal covariance to yield the true covariance of the signals in space, as observed through the system with residual calibration errors.

Since the signal and the thermal noise are assumed gaussian conditioned on the steering vector errors, the Wishart density is appropriate for generating samples, given the assumed number of array snapshots. Note that this assumes that the measurement errors, although unknown, are constant during the sampling process. The sampled covariance matrix is then introduced to the chosen direction-finding algorithm, which yields angles-of-arrival and received powers for all of the emitters detected. Because the desired signal was always given a direction cosine algebraically lower than that of the interferer, the lowest detected direction cosine from the direction-finding algorithm was used by the copy algorithm as the estimated direction cosine of the signal.

Note that neither the DF algorithm nor the nulling algorithm is given knowledge of the corrupted steering vectors, so that both use ideal, linear-phase, constant-amplitude steering vectors. In order to determine the best nulling weights that can be obtained with the modelling errors present, therefore, the nulling algorithm is given the correct signal DOA's and powers, but again is not told of the direction vector errors. The "ideal direction-finding" curve in the Monte Carlo results represent a (generally unachievable) performance limit for nulling methods which model the received signals with erroneous steering vectors. Only in the limits of zero modelling errors and infinite array snapshots is this ideal performance bound achievable.

The assessment of the output SIR is done with full knowledge of the corrupted signal steering vector, $V_c(\theta_s)$, and the theoretical interference plus noise covariance matrix, Q_c , with the corruptions present. Thus, if the candidate nulling algorithm yields the weight vector, W , then the output SIR in the true signal direction is computed as follows:

$$SIR = \frac{P_s |W^H V_c(\theta_s)|^2}{W^H Q_c W}$$

The above quantity is linearly averaged for the 100 Monte Carlo trials to obtain the performance statistics for the overall DF/copy experiment. This measure may be interpreted as the average performance achievable by the calculated nulling vector when it is used with array data that are statistically identical to those used to determine the nulling weights.

V. SUMMARY OF MAJOR FINDINGS

A. Direction-Finding

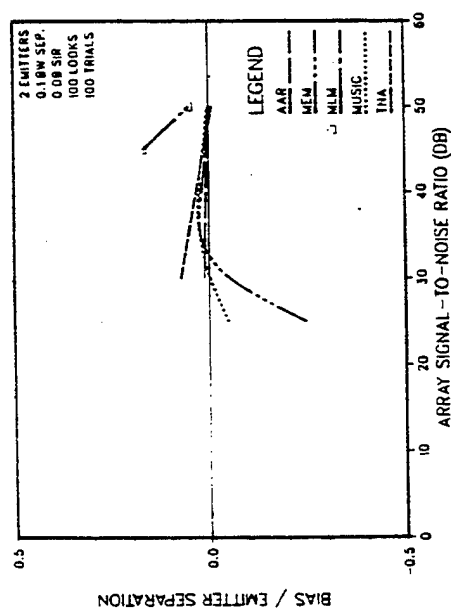
One of the goals of the DF investigation was to determine what combination of algorithms and system parameters are needed to achieve superresolution, somewhat arbitrarily defined here as the ability to resolve emitters separated by only 0.1 beamwidth. In theory, superresolution is possible but, in practice, may require extremely high signal-to-noise ratios and/or large numbers of looks (snapshots). The simulation results presented in Appendix F serve to quantify these requirements for a number of interesting algorithms.

For example, an examination of the data in Fig. 5.1 indicates that superresolution is difficult to achieve with spectral-type algorithms given only a modest amount of data (i.e., 10 looks). However, with more data, the situation is not nearly so bleak. Given 100 snapshots, the performance data in Fig. 5.2 show considerable improvement in most of the algorithms, particularly MUSIC. Increasing the number of looks by yet another order of magnitude, the results in Fig. 5.3 clearly indicate that MUSIC is asymptotically much more sensitive than any of the other algorithms tested.

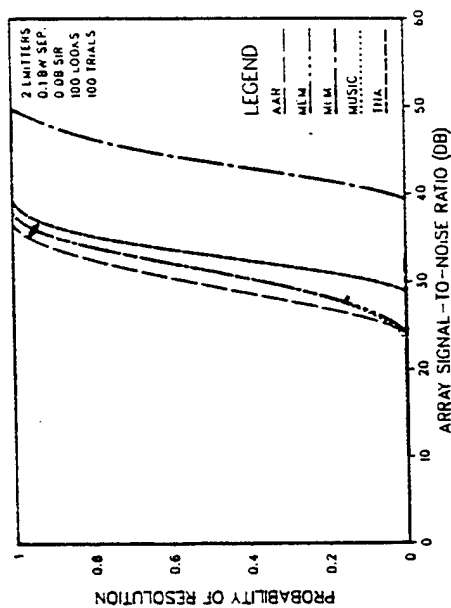
The general trend of the data suggests that the error in the MUSIC direction estimate approaches the Cramer-Rao bound as either the SNR or the number of looks becomes sufficiently large. In other words, MUSIC appears to be asymptotically efficient. However, the relatively poor sensitivity of MUSIC in the data-limited (10 snapshots) case is somewhat disappointing.

In Fig. 5.4, the 10 look experiment has been repeated with the emitter separation increased by a factor of two (i.e., 0.2 beamwidth separation). We again see that spectral MUSIC is noticeably less sensitive than some of the other algorithms (esp., MEM and AAR) in terms of its ability to detect the presence of both emitters at low SNR. This trend continues to exist even at 0.4 beamwidth separation (see Fig. 5.5). However, in spite of its relatively poor sensitivity, MUSIC is generally superior in terms of producing more accurate estimates than any of the other spectral algorithms. Of course, the SNR must be sufficiently large to allow MUSIC to resolve the two emitters.

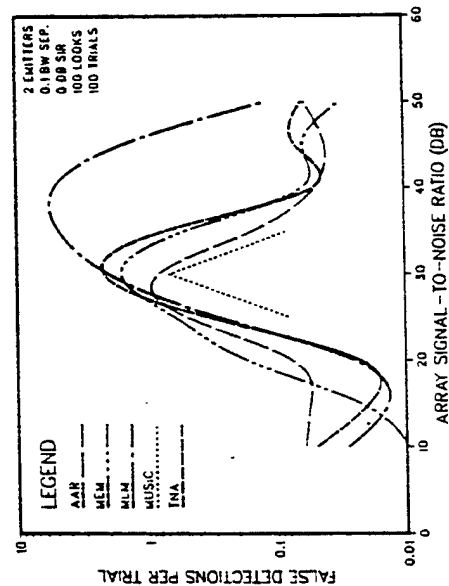
DIRECTION-FINDING BIAS



MULTIPLE SIGNAL DETECTION PERFORMANCE



FALSE ALARM PERFORMANCE



DIRECTION-FINDING ACCURACY

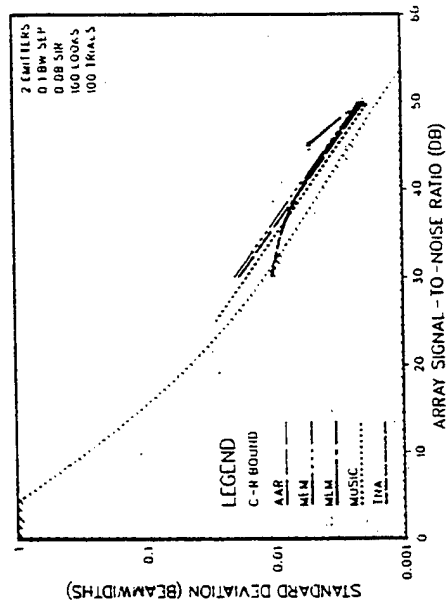


Fig. 5.2. Spectral algorithms at 0.1 beamwidths with 100 looks.

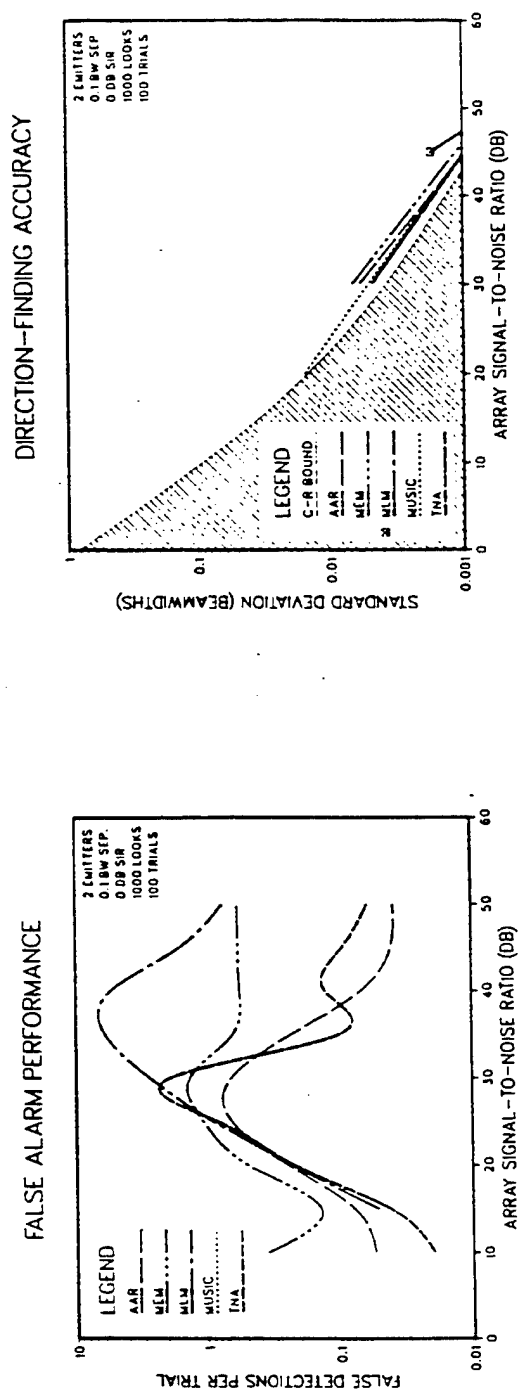
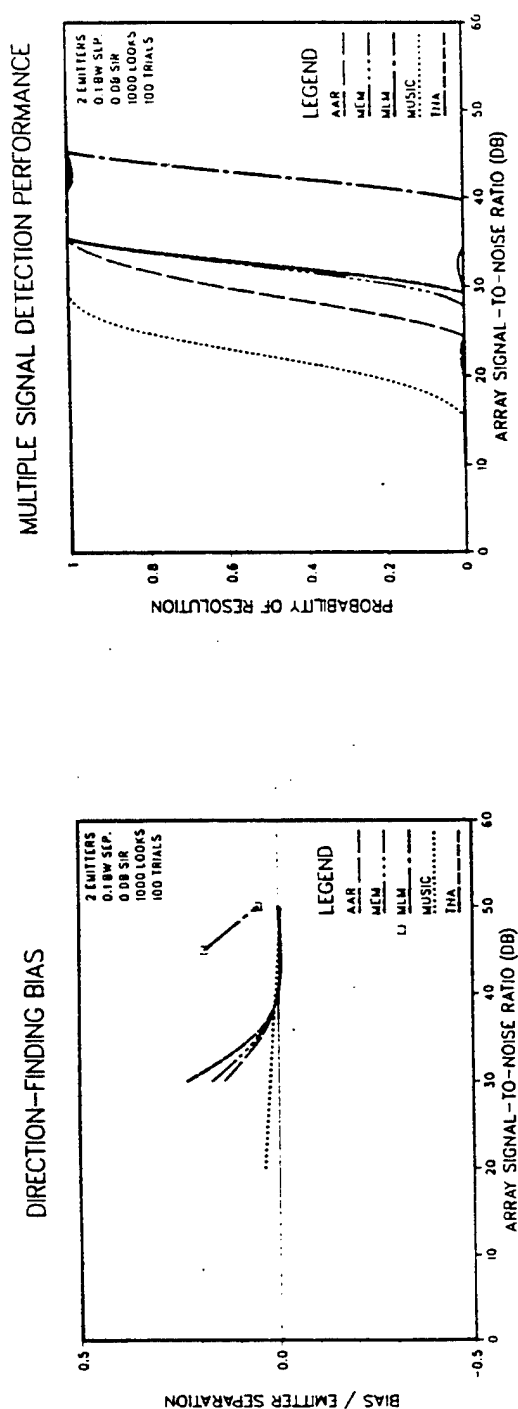


Fig. 5.3. Spectral algorithms at 0.1 beamwidths with 1000 looks.

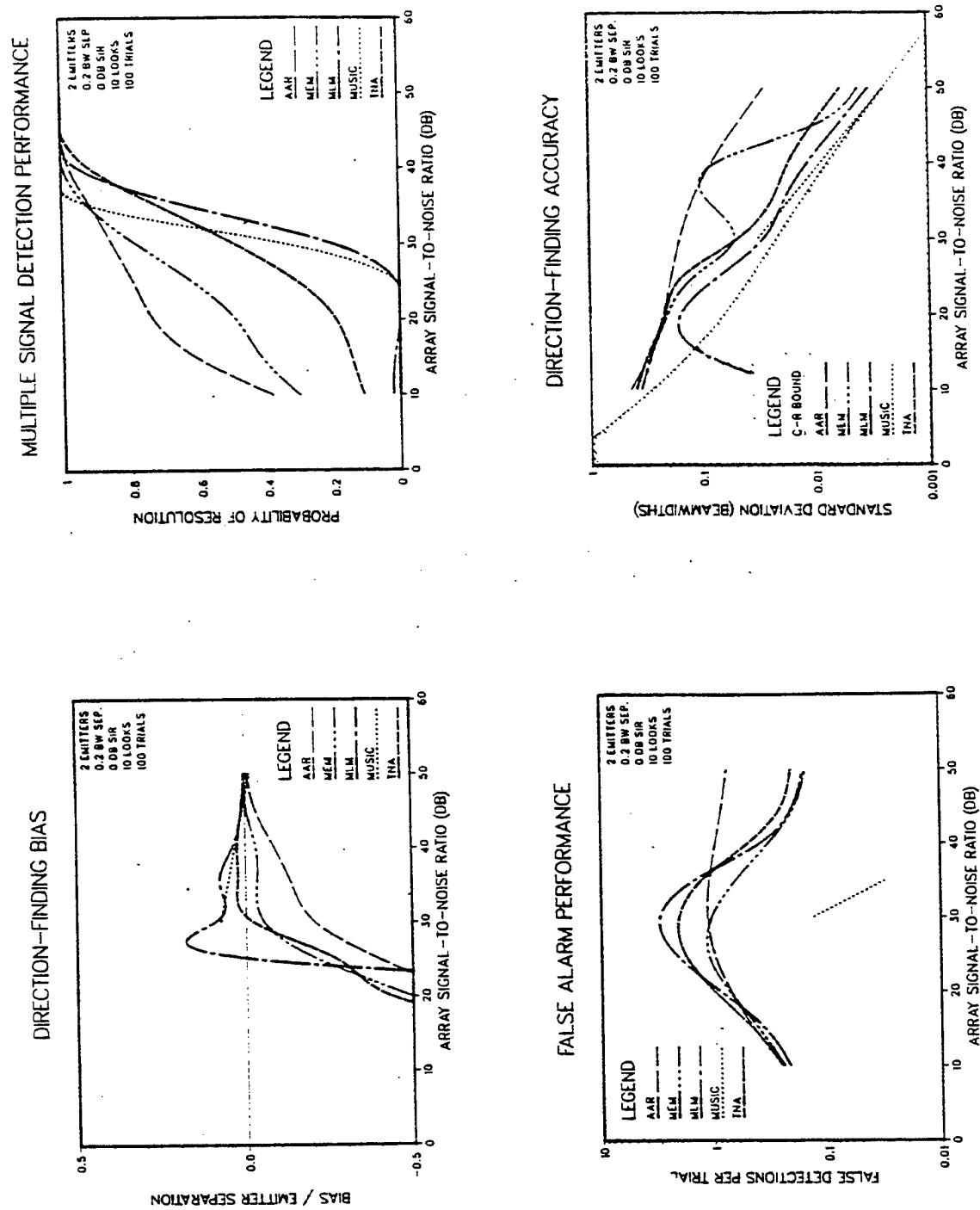


Fig. 5.4. Spectral algorithms at 0.2 beamwidths with 10 looks.

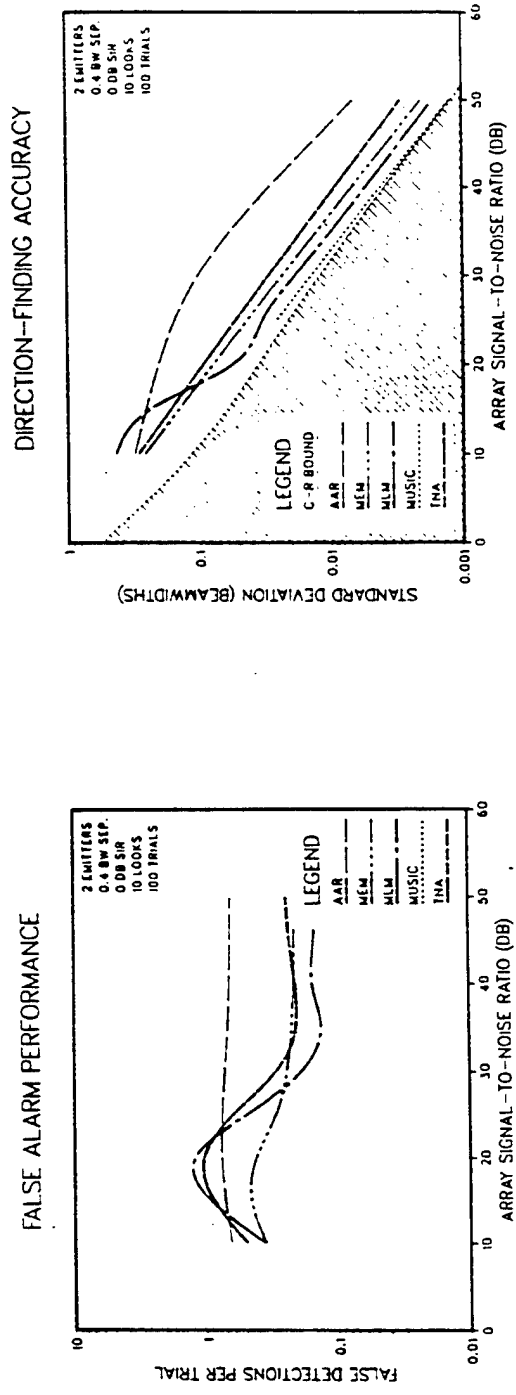
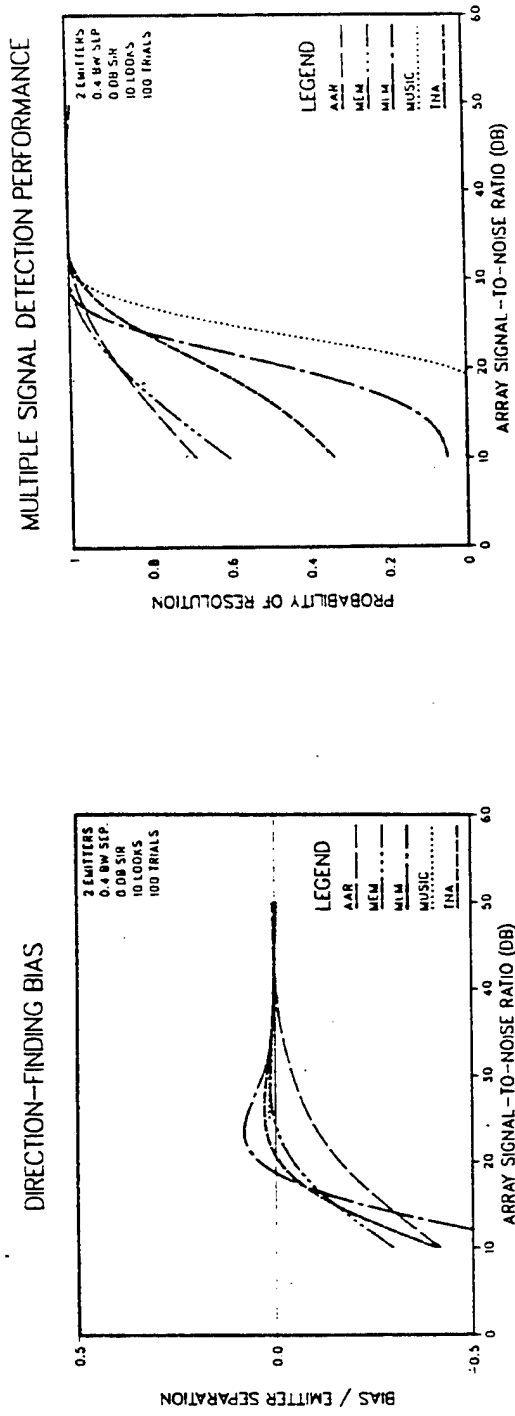


Fig. 5.5. Spectral algorithms at 0.4 beamwidths with 10 looks.

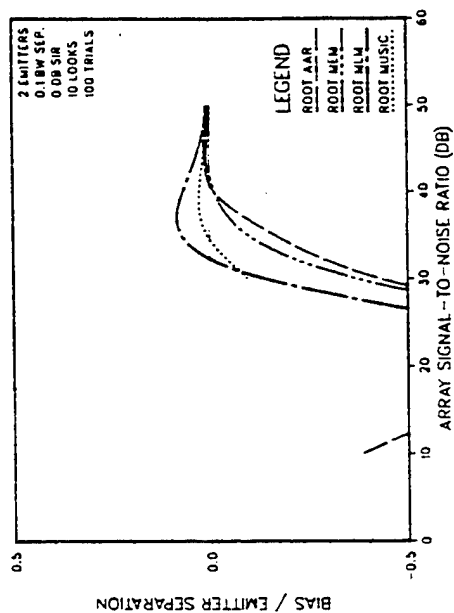
The sensitivity of MUSIC and, in fact, all of the algorithms tested, is improved considerably by adopting the root-finding approach discussed in Section III.A. Even when limited to only 10 looks, all of the root-type algorithms are capable of resolving two emitters separated by 0.1 beamwidth at reasonable signal-to-noise ratios (see Fig. 5.6). Although MUSIC again appears to be less sensitive than its competitors, this slight disadvantage is relatively insignificant in view of the bias results. As the number of available snapshots is increased, the difference among the root versions of the DF algorithms become even less important. At 100 looks, the sensitivity of all the algorithms is comparable (see Fig. 5.7). However, MUSIC retains a discernible advantage in terms of accuracy. Also significant is the smaller bias and lower false alarm rate exhibited by MUSIC.

B. Adaptive Copy

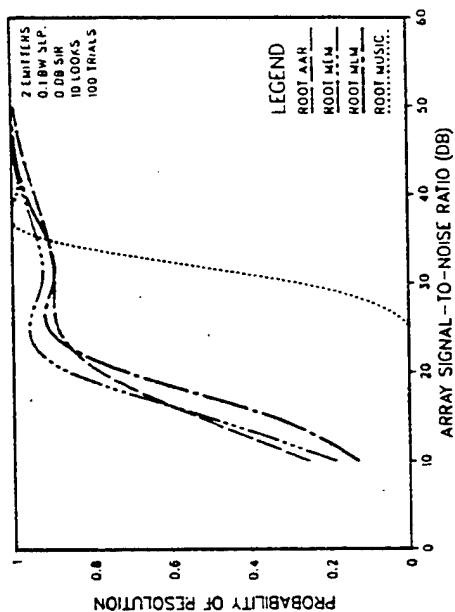
Since it was not known in advance what the tradeoffs were in combining the proposed Model Covariance Method or the Projection Nulling Method with the various direction-finding techniques, all combinations were tried. For the adaptive copy experiment defined in Section IV.B, the copy algorithm assumed that the lowest detected direction cosine was that of the desired signal. Thus, the assumed direction-of-arrival could be far removed from the actual direction-of-arrival whenever the direction-finding algorithm failed to resolve the two emitters. For this reason, one might expect the direction-finding algorithms having the best probability of resolution to give the best copy performance. This was found to generally be the case for both spectral and rooting algorithms, as can be seen by comparing Fig. 5.8 to Fig. F-19, Fig. 5.9 to Fig. F-21, and Fig. 5.10 to Fig. F-20. For the rooting algorithms, this observation tends to hold only for those values of array SNR above that value where the roots cross in angle (a dip in the resolution probability often occurs at that SNR, as can be seen in Fig. F.20).

By comparing Figure 5.10 to Figure 5.8 and Figure 5.11 to Figure 5.9, we see that the rooting variants of the direction-finding

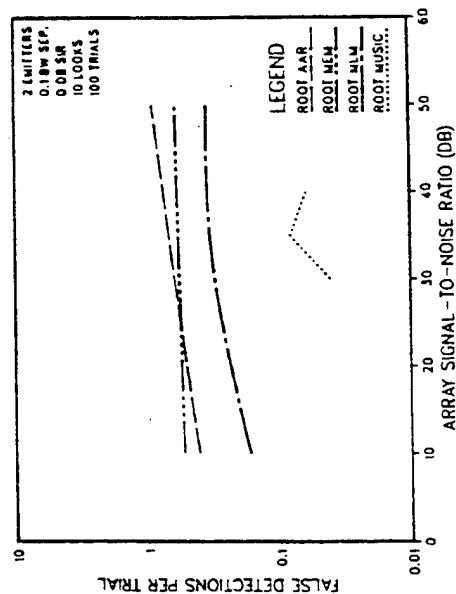
DIRECTION-FINDING BIAS



MULTIPLE SIGNAL DETECTION PERFORMANCE



FALSE ALARM PERFORMANCE



DIRECTION-FINDING ACCURACY

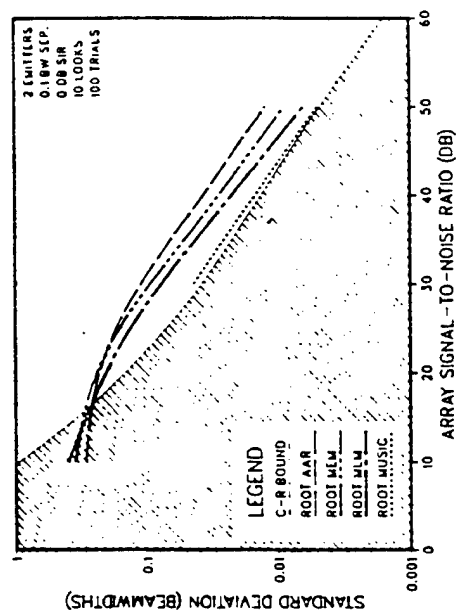


Fig. 5.6. Root algorithms at 0.1 beamwidths with 100 looks.

algorithms again offer significantly superior performance. This again implies that exploitation of the array structure is desired in order to achieve the best results.

The above results indicate that the modeling techniques which steer nulls to perform copy offer nearly optimal performance in the case that the array is perfectly calibrated for plane wave direction finding. On the other hand, if small gain and phase errors are introduced randomly into each receiver channel, independent of direction-of-arrival, there results a significant loss of superresolution copy performance, as seen in Fig. 5.12. This result implies that null steering is an unacceptable approach for obtaining superresolution copy. Techniques which exploit the signal space decomposition employed in SVD-type direction-finding algorithms to overcome this deficiency are being studied as alternatives and will be reported in a future phase of this study.

C. Conclusions

Noise cancellation by singular-valued decomposition is a necessary prerequisite to superresolution (e.g., less than $1/10$ beamwidth). Exploitation of regular array structures (e.g., linear arrays) is necessary to optimize resolution sensitivity and accuracy of estimates with small amounts of data. Array errors due to, for example, calibration residuals, cause significant degradation of superresolution performance and copy. Methods based upon open-loop null steering cannot provide superresolution performance based upon array information which is only slightly in error (e.g., 5° phase and/or 0.5 dB amplitude errors per element).

Because of the above conclusions for the initial phase of the study, focus for subsequent phases has been directed toward SVD-type algorithms, both for direction-finding and copy, and robust extensions to desensitize performance to array errors.

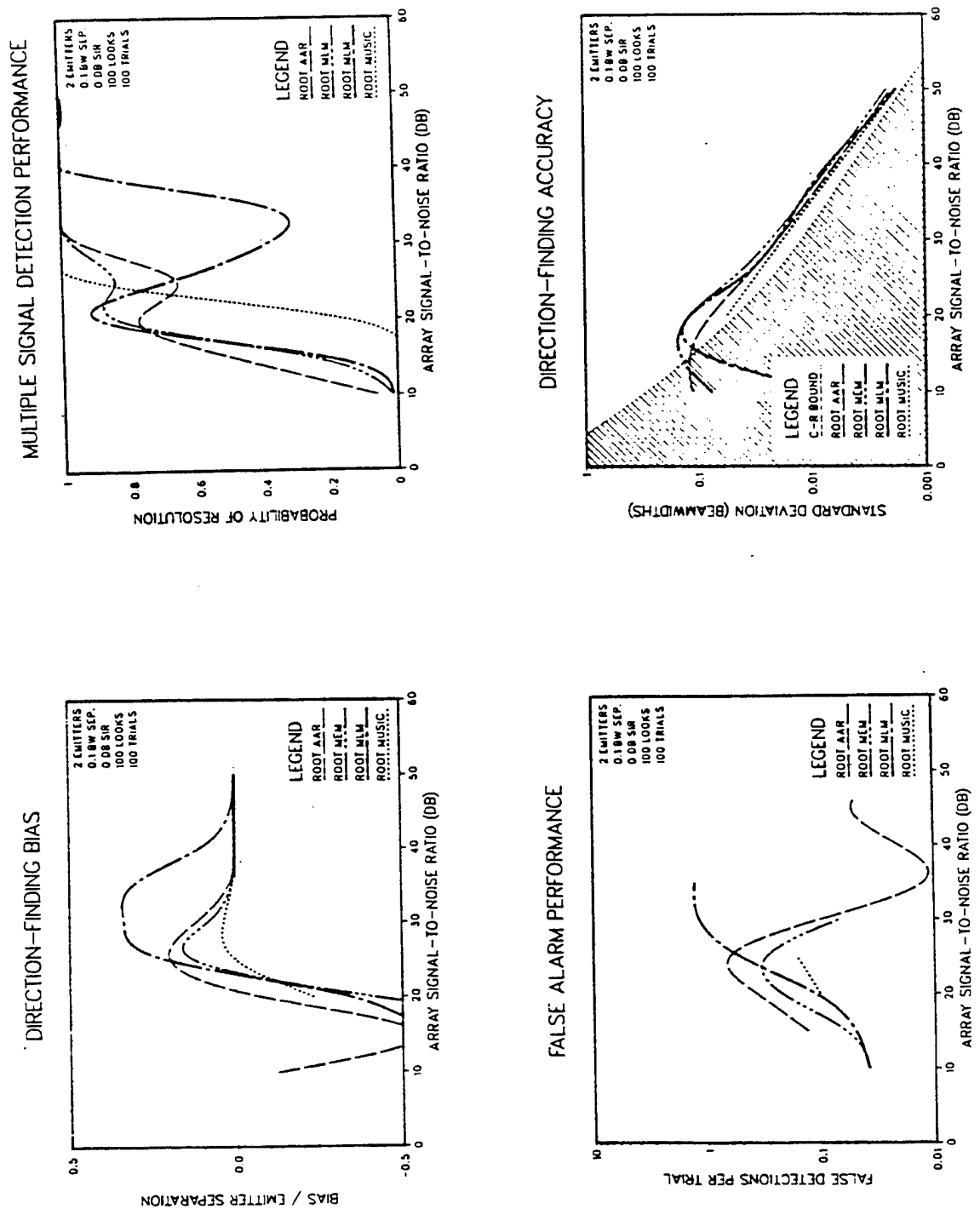


Fig. 5.7. Root algorithms at 0.1 beamwidths with 100 looks.

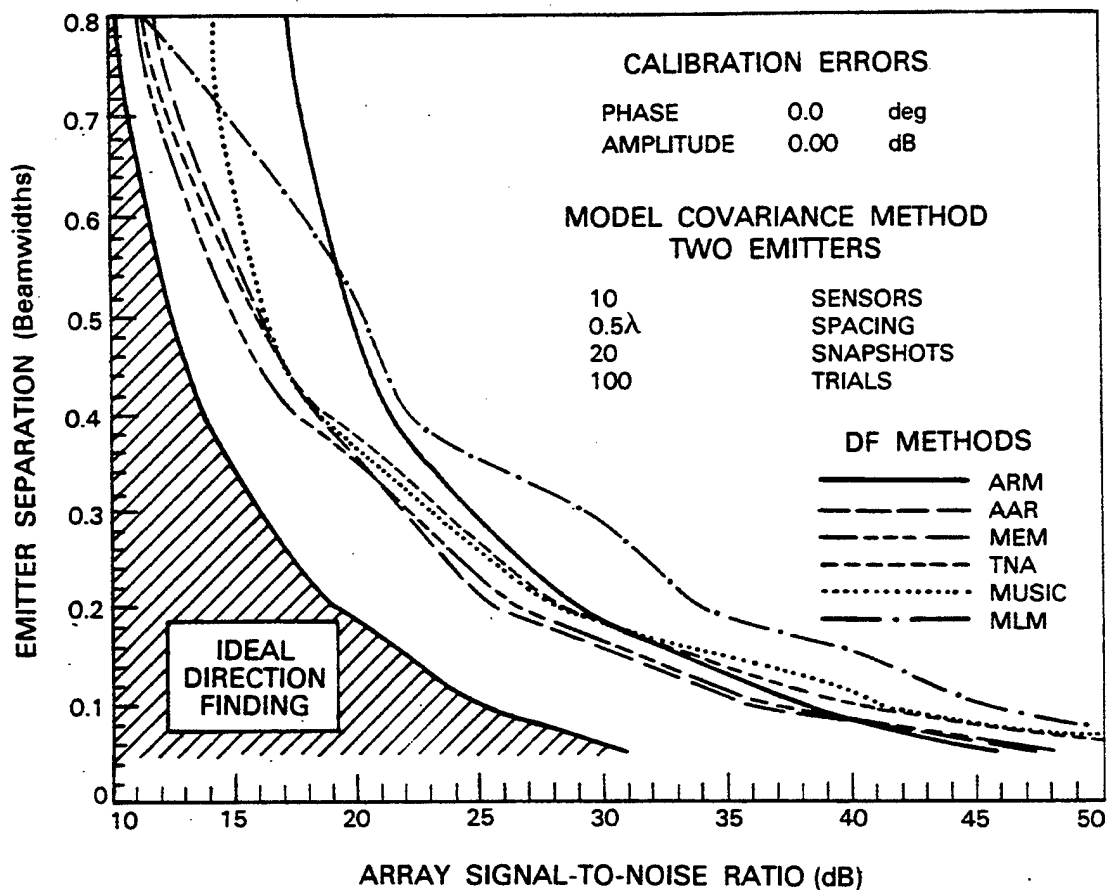
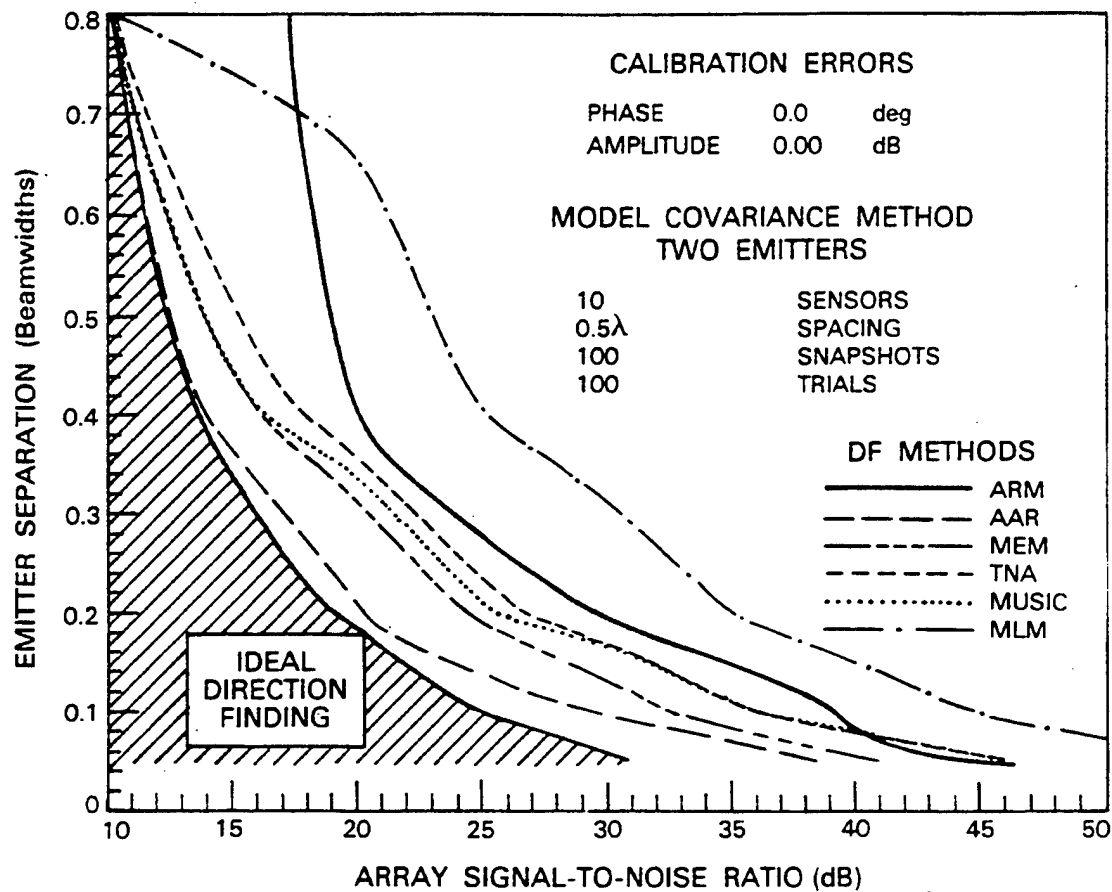


Fig. 8. Adaptive listening with spectral superresolution algorithms and 20 array snapshots (contours of 10 dB output SIR with -10 dB input SIR).



133981-R

Fig. 5.9. Adaptive listening with spectral superresolution algorithms and 100 array snapshots (contours of 10 dB output SIR with -10 dB input SIR).

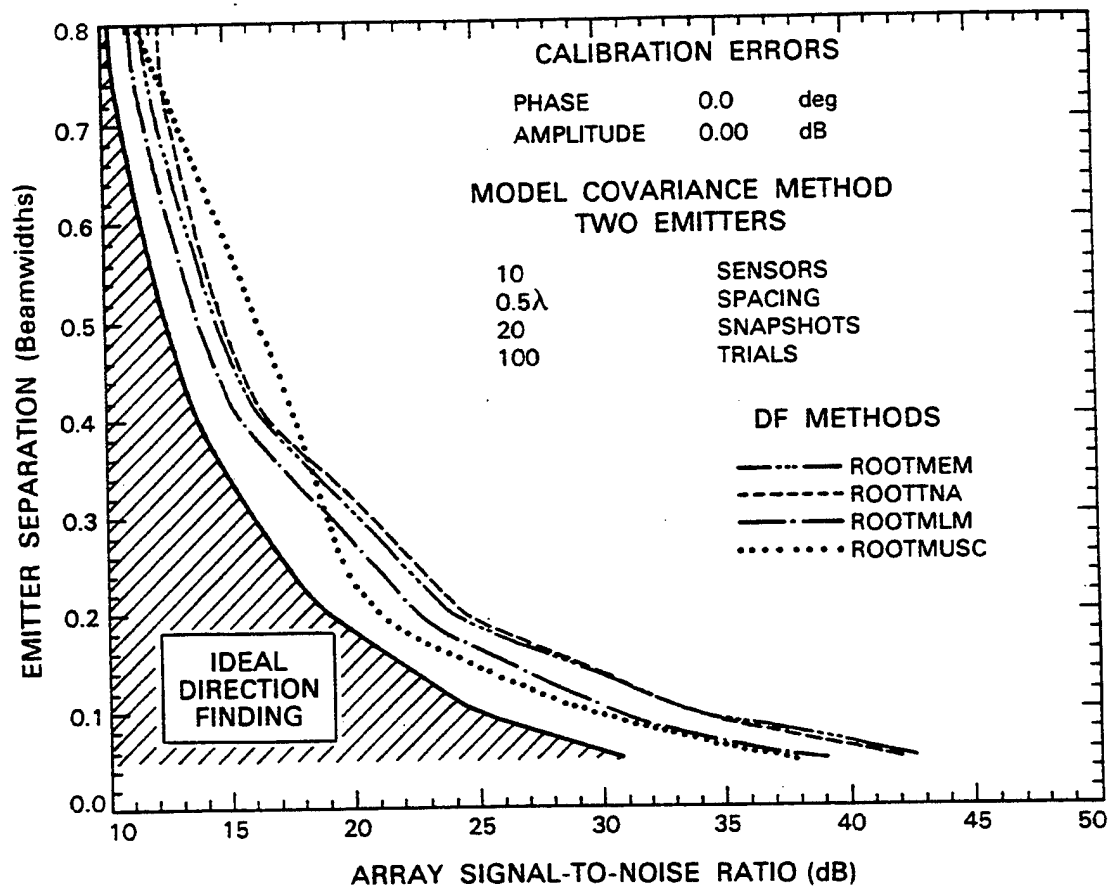


Fig. 5.10. Adaptive listening with rooting algorithms and 20 array snapshots (contours of 10 dB output SIR with -10 dB input SIR).

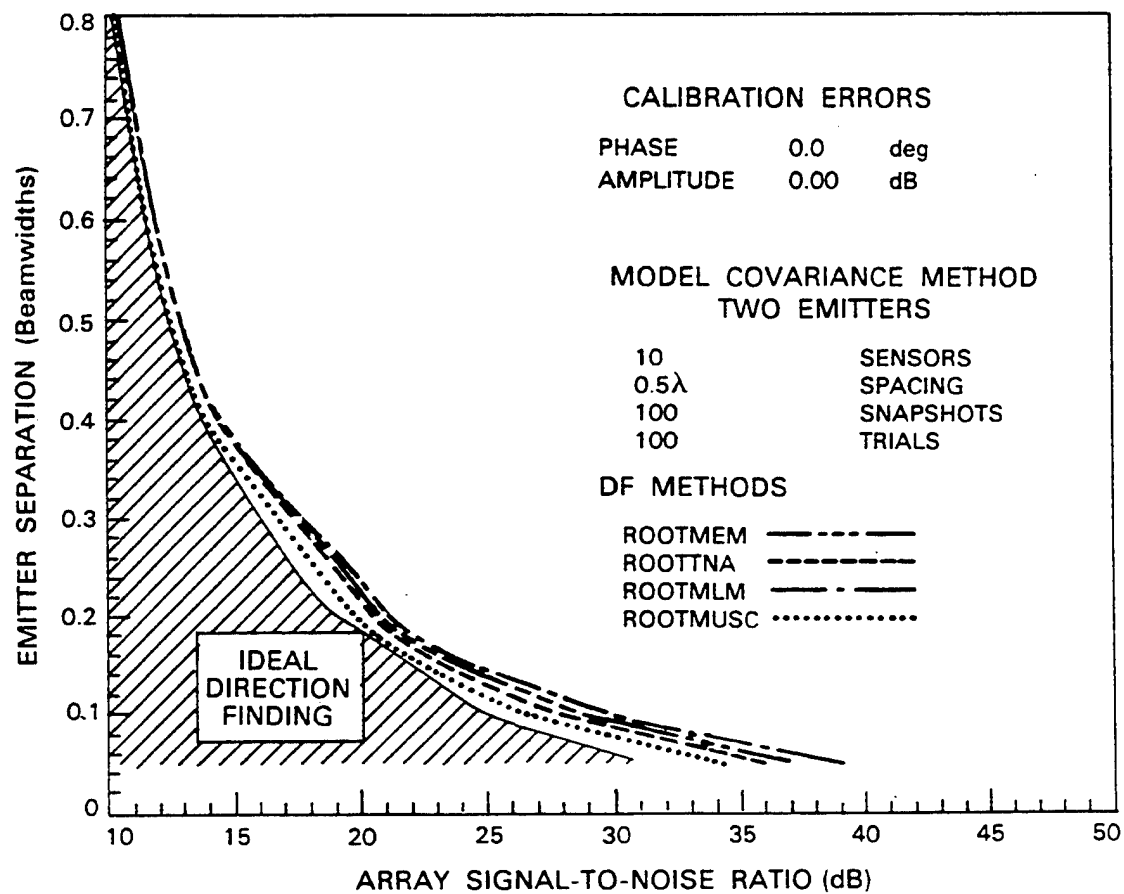
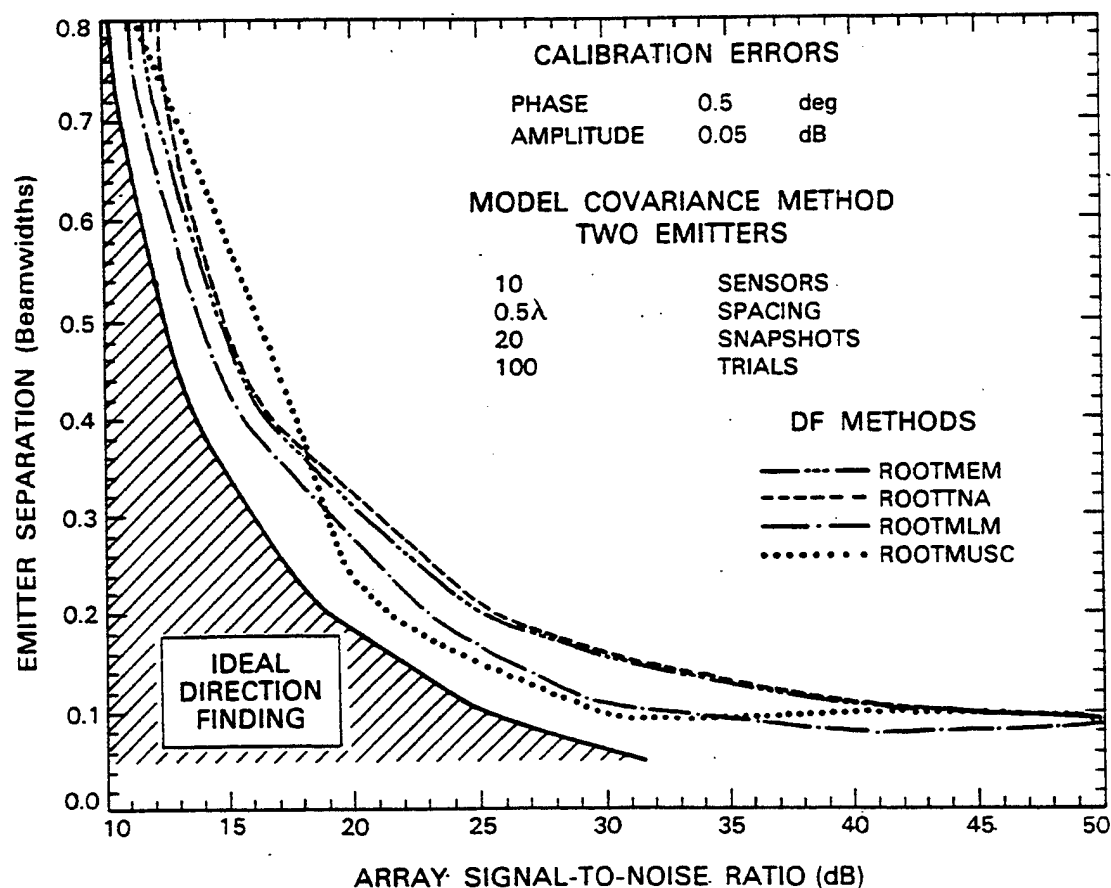


Fig. 5.11. Adaptive listening with rooting algorithms and 100 array snapshots (contours of 10 dB output SIR with -10 dB input SIR).

133907-R



113905-R

Fig. 5.12. Effects of small calibration errors on adaptive listening performance (contours of 10 dB output SIR with -10 dB input SIR).

REFERENCES

1. F. M. White, "Performance of Bayes-Optimal Angle-of-Arrival Estimators," Project Report TR-654, Lincoln Laboratory, M.I.T. (to be published).
2. J.E. Evans, J.R. Johnson, and D.F. Sun, "Application of Advanced Signal Processing Techniques to Angle of Arrival Estimation in ATC Navigation and Surveillance Systems", Technical Report 582, Lincoln Laboratory, M.I.T. (23 June 1982).
3. J.P. Burg, "Maximum Entropy Spectral Analysis," Proc. 37th Annual Meeting of the Society of Exploration Geophysicists, Oklahoma City, Oct. 31, 1967.
4. A. Van den Bos, "An Alternative Interpretation of Maximum Entropy Spectral Analysis," IEEE Trans. Inf. Theory IT-17, 493 (1971).
5. R.H. Wilkinson, "Will the Real MEM Please Stand Up?," Proc. ASSP Workshop Spectral Estimation, Atlanta, GA., 1982.
6. N. Wiener, Extrapolation, Interpolation, and Smoothing of Stationary Time Series (Wiley, N.Y., 1950).
7. G.E. Box and G.M. Jenkins, Time Series Analysis Forecasting and Control (Holden-Day, San Francisco, CA, 1970).
8. N.O. Anderson, "On the Calculation of Filter Coefficients for Maximum Entropy Spectral Analysis," Geophysics, 39, 69 (1974).
9. J.P. Burg, "Maximum Entropy Spectral Analysis," PhD Thesis, Stanford Univ., May 1975.
10. J. Makhoul, "Linear Prediction: A Tutorial Review," Proc. IEEE, 63, 561 (1975).
11. R.T. Lacoss, "Data Adaptive Spectral Analysis Methods," Geophysics, 36, 661 (1971).
12. J. Capon, "High-Resolution Frequency-Wavenumber Spectrum Analysis," Proc. IEEE, 57, 1408 (1969).
13. G.V. Borgiotti and L.J. Kaplan, "Superresolution of Uncorrelated Interference Sources by Using Adaptive Array Techniques," Trans. Antennas Propag., AP-27, 842 (1979).
14. S. Haykin and J. Reilly, "Mixed Autoregressive-Moving Average Modeling of the Response of a Linear Array Antenna to Incident Plane Waves," Proc. IEEE, 68, 622 (1980).

15. W. Gabriel, "Spectral Analysis and Adaptive Array Superresolution Techniques," Proc. IEEE, 68, 654 (1980).
16. R. Schmidt, "Multiple Emitter Location and Signal Parameter Estimation," Proc. RADC Spectrum Estimation Workshop, Rome, NY, 1979.
17. R.O. Schmidt, "A Signal Subspace Approach to Multiple Emitter Location and Spectral Estimation," PhD Thesis, Stanford Univ., November 1981.
18. V.F. Pisarenko, "The Retrieval of Harmonics from a Covariance Function," Geophys. R. Astr. Soc., 33, 347 (1973).
19. Y. Bard, Nonlinear Parameter Estimation, (Academic Press, NY, 1974).
20. H.A. d'Assumpcao, "Some New Signal Processors for Arrays of Sensors," IEEE Trans. Inf. Theory, IT-26, 4, 441 (1980).
21. L. E. Brennan and I. S. Reed, "Theory of Adaptive Radar," IEEE Trans. Aerospace Electron. Systems, AES-9, 237 (1973).
22. I. S. Reed, J. D. Mallet, and L. E. Brennan, "Rapid Convergence Rate in Adaptive Arrays," IEEE Trans. Aerospace Electron. Systems, AES-10, 853 (1974).
23. H. Cox, "Resolving Power and Sensitivity to Mismatch of Optimum Array Processors", J. Acoust. Soc. Am., 54, 3, 771 (1973).
24. O. L. Frost, "An Algorithm for Linearly Constrained Adaptive Array Processing," Proc. IEEE, 60, 926 (1972).
25. S. P. Applebaum and D. J. Chapman, "Adaptive Arrays with Mainbeam Constraints." IEEE Trans. Antennas Propag., AP-24, 650 (1976).
26. A. M. Vural, "Effects of Perturbations on the Performance of Optimum/Adaptive Arrays," IEEE Trans. Aerospace Electron. Systems, AES-15, 767 (1979).
27. R. A. Monzingo and T. W. Miller, "Introduction to Adaptive Arrays", (Wiley and Sons, N.Y., 1980).
28. J. E. Hudson, "Adaptive Array Principles," (Peter Peregrinus Limited, N.Y., 1981).
29. R. Nitzberg, "Application of Maximum Likelihood Estimation of Persymmetric Covariance Matrices to Adaptive Processing," IEEE Trans. Aerospace Electron. Systems, AES-16, 124 (1980).

30. H.L. Van Trees, Detection, Estimation, and Modulation Theory, Part I, (Wiley, N.Y., 1968).
31. N.R. Goodman, "Statistical Analysis Based on a Certain Multivariate Complex Gaussian Distribution," Ann. Math. Stat., 34, 152 (1963).
32. M. Athans and F.C. Schweppe, "Gradient Matrices and Matrix Calculations," Tech. Note 1965-13, Lincoln Laboratory, M.I.T. (17 Nov. 1965).
33. A. Vieira and T. Kailath, "On Another Approach to the Schur-Cohn Criterion," IEEE Trans. Circuits and Systems, CAS-24, 218 (1977).
34. A. Arcese and A.J. Goldberg, "Stable Recursive Filters Using Gradient Techniques," IEEE Trans. Inf. Theory, IT-22, 15 (1976).
35. J.P. Burg, "The Relationship Between Maximum Entropy Spectra and Maximum Likelihood Spectra," Geophysics, 37, 2, 375 (1972).
36. R. Bartle, The Elements of Real Analysis, (Wiley, N.Y., 1964).
37. U. Grenander and G. Szego, Toeplitz Forms and Their Application, (U. of Calif. Press, Berkely, 1958).
38. A. Papoulis, Probability, Random Variables, and Stochastic Processes, (McGraw-Hill, N.Y., 1965).
39. R.B. Blackman and J.W. Tukey, The Measurement of Power Spectra, (Dover, N.Y., 1958).
40. M.S. Bartlett, "A Note on Multiplying Factors for Various Chi-Squared Approximations," J. Royal Statist. Soc. B, Vol 16, pp 296-298, 1954.
41. D.N. Lawley, "Tests of Significance for the Latent Roots of Covariance and Correlation Matrices", Biometrika, 43, 128 (1956).
42. T.W. Anderson, "Asymptotic Theory for Principal Component Analysis," Ann. Math. Statist., 34, 122 (1963).
43. K.V. Mardia, J.T. Kent, and J.M. Bibby, Multivariate Analysis (Academic Press, London, 1979).

44. D.N. Simkins, "Multichannel Angle-of-Arrival Estimation", Ph.D. Dissertation, Stanford University, Stanford, CA, Nov. 1980.
45. Abramowitz and Stegun (eds), Handbook of Mathematical Functions, (U.S. Government Printing Office, Washington, D.C., 1964).
46. P.L. Meyer, Introductory Probability and Statistical Applications, (Addison-Wesley, Reading, MA, 1965).
47. International Mathematics and Scientific Program Library (1978).
48. H. Kahn, "Applications of Monte Carlo," Rand Corp. Research Memorandum RM-1237-AEC (April, 1956).
49. D. M. Boroson, "Sample Size Considerations for Adaptive Arrays," IEEE Trans. Aerospace Electron. Systems, AES-16, 4, (1980).
50. T. W. Miller, "The Transient Response of Adaptive Arrays in TDMA Systems," Ohio State University Electroscience Lab, Report RADC-TR-76-390, Dec. 1976.

Appendix A

CRAMER-RAO DIRECTION-FINDING BOUNDS FOR GAUSSIAN SIGNALS

1. GENERAL DISCUSSION

Detailed treatments of the multiparameter Cramer-Rao bound are readily available in the engineering literature (e.g., see [30]). For our purposes, the fundamental theoretical result may be stated as follows:

Consider a probability density function $p(r| \theta)$ that governs a probabilistic mapping from a parameter space into an observation space r . The basic problem is to estimate the (vector) parameter θ from the (vector) observation r . The Cramer-Rao bound asserts that the covariance matrix of any unbiased estimate of θ must satisfy

$$\text{Cov}(\hat{\theta}) \geq F^{-1},$$

where F is the Fisher information matrix with elements

$$\begin{aligned} F_{mn} &= E \left\{ \frac{\partial \ln p}{\partial \theta_m} \frac{\partial \ln p}{\partial \theta_n} \right\} \\ &= -E \left\{ \frac{\partial^2 \ln p}{\partial \theta_m \partial \theta_n} \right\}. \end{aligned} \quad (A.1)$$

Of course, the expected value operation is defined in terms of the given probability density function (pdf), i.e.,

$$E \{x\} = \int x(r) p(r| \theta) dr.$$

Situations frequently arise where one is primarily interested in a subset of the unknown parameters. The remaining "nuisance" parameters are only important to the extent that they adversely affect estimates of the "desired" parameters. By simply partitioning θ , i.e.,

$$\theta = \begin{bmatrix} \alpha & \beta \end{bmatrix},$$

the Fisher matrix may be written as

$$F = \begin{bmatrix} F_{\alpha\alpha} & F_{\alpha\beta} \\ F_{\beta\alpha} & F_{\beta\beta} \end{bmatrix}.$$

If the Fisher matrix has an inverse, it may be written as

$$F^{-1} = \begin{bmatrix} [F_{\alpha\alpha} - F_{\alpha\beta} F_{\beta\beta}^{-1} F_{\beta\alpha}]^{-1} & *^T \\ * & [F_{\beta\beta} - F_{\beta\alpha} F_{\alpha\alpha}^{-1} F_{\alpha\beta}]^{-1} \end{bmatrix}. \quad (A.2)$$

The remaining (off-diagonal) terms can be easily obtained but are not needed here.

If the nuisance parameters (e.g., β) were known, the Cramer-Rao bound for an unbiased estimate of the desired parameters (i.e., α) would be

$$\text{Cov}(\hat{\alpha}) \geq F_{\alpha\alpha}^{-1}.$$

This inequality is always valid but the bound obtained from (A.2) is tighter, i.e.,

$$\text{Cov}(\hat{\alpha}) \geq [F_{\alpha\alpha}^{(\beta)}]^{-1} \geq F_{\alpha\alpha}^{-1},$$

where the "reduced" information matrix is

$$F_{\alpha\alpha}^{(\beta)} = F_{\alpha\alpha} - F_{\alpha\beta} F_{\beta\beta}^{-1} F_{\beta\alpha}.$$

In the following sections, it will be convenient to use the notation

$$F_{a b_{m n}} = (F_{ab})_{mn}$$

to refer to an arbitrary element of a Fisher submatrix.

2. STATISTICAL INFERENCE BASED ON COMPLEX GAUSSIAN OBSERVATIONS

Consider a complex Gaussian vector r with zero mean, i.e.,

$$E \{r\} = 0 \quad ,$$

and circular components, i.e.,

$$E \{rr^T\} = 0 \quad ,$$

and covariance R , i.e.,

$$E \{rr^H\} = R \quad .$$

Note that a superscript T indicates the usual (real) transpose operation, whereas an H represents the complex conjugate (Hermitian) transpose operation. The unknown parameters θ are imbedded in the covariance, i.e.,

$$R = R(\theta) \quad .$$

Assuming the covariance matrix R is positive definite, the complex multivariate Gaussian pdf [31] is given by

$$p(r|\theta) = \frac{1}{\pi^L |R|} \exp \{ -r^H R^{-1} r \} \quad ,$$

where L is the dimension of r and $|R|$ denotes the determinant of R . By introducing the sample covariance matrix

$$\hat{R} = \frac{1}{K} \sum_{k=1}^K r(k)r^H(k) \quad ,$$

the logarithm of the pdf for K statistically independent observations can be written as

$$\ln p(\{r(k)|k=1,\dots,K\}|\theta) = -K [\text{Tr}\{R^{-1} \hat{R}\} + \ln |R| + L \ln \pi] \quad ,$$

where $\text{Tr}\{ \}$ is the standard trace operator. In arriving at this result, use has been made of the identity

$$\text{Tr}\{AB\} = \text{Tr}\{BA\} \quad . \quad (A.3)$$

In the next section, we will also have occasion to use

$$\text{Tr}\{A^H\} = \text{Tr}^*\{A\} \quad , \quad (A.4)$$

where a superscript asterisk (*) denotes the complex conjugate operation.

As indicated by (A.1), an arbitrary element of the Fisher information matrix can be determined by calculating

$$F_{\theta_m \theta_n} = -E \left\{ \frac{\partial^2 \ln p}{\partial \theta_m \partial \theta_n} \right\} \quad .$$

Invoking the differential rules [32]

$$d R^{-1} = -R^{-1} dR R^{-1} \quad (A.5)$$

and the less familiar

$$d \ln |R| = \text{Tr} \{ R^{-1} dR \} ,$$

we first obtain

$$\frac{\partial \ln p}{\partial \theta_m} = K \text{Tr} \left\{ R^{-1} \frac{\partial R}{\partial \theta_m} (R^{-1} \hat{R} - I) \right\} .$$

Since the sample covariance matrix is always an unbiased estimate of the actual covariance, i.e.,

$$E \{ \hat{R} \} = R ,$$

it follows that

$$\begin{aligned} E \left\{ \frac{\partial^2 \ln p}{\partial \theta_m \partial \theta_n} \right\} &= K \text{Tr} \left\{ R^{-1} \frac{\partial R}{\partial \theta_m} \frac{\partial R^{-1}}{\partial \theta_n} R \right\} \\ &= K \text{Tr} \left\{ \frac{\partial R}{\partial \theta_m} \frac{\partial R^{-1}}{\partial \theta_n} \right\} . \end{aligned}$$

Thus, the number of observations enters the result only as a multiplicative constant. Since no loss of generality is incurred, the simplifying assumption $K=1$ is imposed at this point. Applying (A.5) once more and ignoring K , we finally obtain the desired result in a suitable form for subsequent calculations.

$$F_{\theta_m \theta_n} = \text{Tr} \left\{ \frac{\partial R}{\partial \theta_m} R^{-1} \frac{\partial R}{\partial \theta_n} R^{-1} \right\} . \quad (\text{A.6})$$

3. APPLICATION TO DIRECTION-FINDING

For the direction-finding (DF) problem posed in Section II.A of this report, the covariance matrix of the observed vector (snapshot) r can be written as

$$R = APA^H + N \quad ,$$

where the unknown directions

$$\alpha = [\alpha_1 \ \alpha_2 \ \dots \ \alpha_J]^T$$

enter the problem through the direction matrix

$$A = [a(\alpha_1) \mid \dots \mid a(\alpha_J)] \quad .$$

The only requirement imposed on the (vector) array gain $a(\alpha)$ is that it possess a derivative in the usual sense, i.e.,

$$\dot{a} = \frac{da}{d\alpha}$$

is assumed to exist at every direction α . The matrix constructed from the derivatives of the array gain at each of the unknown directions is written as

$$\dot{A} = [\dot{a}(\alpha_1) \mid \dots \mid \dot{a}(\alpha_J)] \quad .$$

The "signal-in-space" covariance matrix P may be interpreted in terms of the pairwise correlations that would exist among the J signals at some convenient reference point on (or near) the array. Unfortunately, the general problem where P is totally unknown soon becomes overwhelming as the number of signal

directions increases. Thus, we first consider the ideal case of known P . We then treat the important case where P is an unknown diagonal matrix. Since the signals transmitted by two emitters are normally uncorrelated, the latter assumption is quite reasonable for a large class of DF problems.

The noise covariance matrix N is assumed to be non-singular and known. Under these conditions, the general problem is easily converted via a linear transformation to the special case where N is the identity matrix, i.e.,

$$N \rightarrow I \quad .$$

Under this transformation, the direction matrix becomes

$$A \rightarrow V = N^{-1/2} A \quad ,$$

and similarly,

$$\dot{A} \rightarrow \dot{V} = N^{-1/2} \dot{A} \quad .$$

The covariance matrix for the transformed problem is

$$R = VPV^H + I$$

Our results are somewhat easier to interpret if the inverse covariance matrix is expressed in the form

$$R^{-1} = I - VOV^H \quad . \quad (A.7)$$

A direct calculation shows that Q is the (Hermitian) solution to

$$P - Q = PQQ = OWP \quad (A.8)$$

where we have introduced the Gramian matrix

$$W = V^H V \quad . \quad (A.9)$$

The uniqueness of the representation in (A.7) follows from the fact that $I + PW$ is a non-singular matrix. The proof is by contradiction, i.e., suppose there exists a non-zero x such that

$$(I + PW)x = 0 \quad .$$

Premultiplying this equation by V , it follows that

$$(I + VPV^H)Vx = 0 \quad .$$

Since R is obviously non-singular, it follows that $Vx = 0$. In turn, $Wx = 0$ and hence the contradiction ($x = 0$).

Thus, Q may be written explicitly as

$$Q = (I + PW)^{-1}P = P(I + WP)^{-1} \quad .$$

If P is positive definite, we also have

$$Q = (P^{-1} + W)^{-1} \quad .$$

In the ensuing development, we make extensive use of the notational device

$$\dot{V}_j = \frac{\partial V}{\partial \alpha_j} \quad (A.10)$$

for the partial derivative of the direction matrix V with respect to an unknown direction. This derivative can be extracted from the matrix of derivatives defined previously, i.e.,

$$\dot{V}_j = \dot{V} e_j e_j^T, \quad (A.11)$$

where the unit vector e_j is the j th column of the $J \times J$ identity matrix.

Using (A.10), we first write the partial derivative of the covariance matrix with respect to the j th direction as

$$\frac{\partial R}{\partial \alpha_j} = \dot{V}_j P V^H + V P \dot{V}_j^H.$$

Substituting this expression in (A.6) and expanding terms, we get

$$\begin{aligned} F_{\alpha_m \alpha_n} = & \text{Tr} \{ \dot{V}_m P V^H R^{-1} \dot{V}_n P V^H R^{-1} \} + \text{Tr} \{ \dot{V}_m P V^H R^{-1} V P \dot{V}_n^H R^{-1} \} \\ & + \text{Tr} \{ V P \dot{V}_m^H R^{-1} \dot{V}_n P V^H R^{-1} \} + \text{Tr} \{ V P \dot{V}_m^H R^{-1} V P \dot{V}_n^H R^{-1} \}. \end{aligned} \quad (A.12)$$

Since R and P are Hermitian, it follows from the identities (A.3) and (A.4) that the last term on the right-hand side of (A.12) is the complex conjugate of the first term. Similarly, the second and third terms form a conjugate pair. Further simplifications result from substituting (A.11) and arranging terms, with the help of (A.3), to obtain scalar expressions within the braces. In this manner, we eventually arrive at

$$F_{\alpha_m \alpha_n} = 2 \text{Re} \{ e_n^T P V^H R^{-1} \dot{V}_m e_m^T P V^H R^{-1} \dot{V}_n + e_n^T P V^H R^{-1} V P e_m^T \dot{V}_m^H R^{-1} \dot{V}_n \}, \quad (A.13)$$

where $\text{Re} \{x\}$ denotes the real part of x .

At this point, it is convenient to introduce the Hadamard product $A \square B$ of two matrices, defined by

$$(A \square B)_{mn} = A_{mn} B_{mn}$$

for any two matrices with the same dimensions. Unlike the usual matrix product, the Hadamard product is commutative, i.e., $A \square B = B \square A$. Since

$$(A^T \square B)_{mn} = A_{nm} B_{mn},$$

the Fisher (sub)matrix with elements specified by (A.13) can be written as

$$F_{\alpha\alpha} = 2 \operatorname{Re} \{ (PV_R^{H-1} \dot{\hat{V}})^T \square (PV_R^{H-1} \dot{\hat{V}}) + (PV_R^{H-1} VP)^T \square (\dot{\hat{V}}^H R^{-1} \dot{\hat{V}}) \} \quad (A.14)$$

The matrix expressions that appear in this result can be simplified considerably by using (A.7), (A.8), and (A.9), e.g.,

$$\begin{aligned} PV_R^{H-1} VP &= PV^H (I - VOV^H) VP \\ &= (P - PWO) WP \\ &= OWP \\ &= P - Q \end{aligned} \quad (A.15)$$

Similarly,

$$\begin{aligned} PV_R^{H-1} \dot{\hat{V}} &= PV^H (I - VOV^H) \dot{\hat{V}} \\ &= (P - PWO) \dot{\hat{V}}^H \dot{\hat{V}} \end{aligned}$$

$$= Q\dot{W} \quad (A.16)$$

where, in the last step, we have introduced

$$\dot{W} = V^H \dot{V}$$

despite the apparent abuse of notation. Consequently, we may also write

$$\begin{aligned} V^H R^{-1} V &= V^H (I - V Q V^H) V \\ &= V^H V - W^H Q W \end{aligned}$$

Substituting these identities in (A.14), the final form of the Fisher matrix for the unknown directions α emerges as

$$F_{\alpha\alpha} = 2 \operatorname{Re} \{ (P-O)^T \square (V^H \dot{V} - W^H Q \dot{W}) + (Q \dot{W})^T \square (Q \dot{W}) \}$$

In order to proceed without undue difficulty, we now assume that the signal-in-space covariance P is a positive (definite) diagonal matrix and, accordingly, introduce the nuisance parameters

$$\beta_j = \ln P_{jj}$$

The partial derivatives of the covariance matrix R with respect to the nuisance parameters are given by

$$\begin{aligned} \frac{\partial R}{\partial \beta_j} &= V \frac{\partial P}{\partial \beta_j} V^H \\ &= P_{jj} V e_j e_j^T V^H \end{aligned}$$

It follows easily from (A.6) that

$$\begin{aligned} F_{\beta_m \beta_n} &= \text{Tr} \left\{ P_{mm} V e_m e_m^T V^H R^{-1} P_{nn} V e_n e_n^T V^H R^{-1} \right\} \\ &= P_{mm} e_m^T V^H R^{-1} V e_n P_{nn} e_n^T V^H R^{-1} V e_m \end{aligned}$$

Since

$$(DA)_{mn} = D_{mm} A_{mn}$$

for any diagonal matrix D , we may write the submatrix for the nuisance parameters as

$$F_{\beta\beta} = (P V^H R^{-1} V) \square (P V^H R^{-1} V)^T .$$

From the development in (A.15), we deduce the identity

$$P V^H R^{-1} V = OW \quad , \quad (A.17)$$

which yields

$$F_{\beta\beta} = (OW) \square (OW)^T .$$

The calculation of the coupling matrix proceeds along similar lines, e.g.,

$$F_{\beta_m \alpha_n} = \text{Tr} \left\{ R^{-1} \frac{\partial R}{\partial \beta_m} R^{-1} \frac{\partial R}{\partial \alpha_n} \right\}$$

$$\begin{aligned}
&= \text{Tr} \left\{ P_{mm} R^{-1} V e_m e_m^T V^H R^{-1} (\dot{V}_n P V^H + V P \dot{V}_n^H) \right\} \\
&= 2 \text{Re} \left\{ P_{mm} e_m^T V^H R^{-1} \dot{V}_n e_n^T P V^H R^{-1} V e_m \right\} .
\end{aligned}$$

Consequently, the information coupling between the directions and the nuisance parameters is determined by

$$F_{\beta\alpha} = 2 \text{Re} \left\{ (P V^H R^{-1} \dot{V}) \square (P V^H R^{-1} V)^T \right\} .$$

Simplifying with (A.16) and (A.17) yields

$$F_{\beta\alpha} = 2 \text{Re} \left\{ (O \dot{W}) \square (O W)^T \right\} .$$

Finally, since a Fisher information matrix is symmetric, it follows that

$$F_{\alpha\beta} = F_{\beta\alpha}^T .$$

Appendix B

LINEAR PREDICTION AND MAXIMUM ENTROPY SPECTRAL ANALYSIS

Maximum entropy spectral analysis is closely linked to one of the more fascinating questions in time series analysis — given a record of the past, how well can one predict the future? Differences of opinion concerning such matters are what horseracing is all about; however, within the relatively orderly realm of stationary random processes, the theory of linear prediction offers a fairly complete answer. The discussion in this appendix covers most of the salient points of this theory for complex-valued processes.

1. LINEAR PREDICTION

Let $e(n)$ denote the minimum mean square error that can be achieved by linearly combining the n most recent observations of a zero-mean, stationary complex random process in order to predict its next value. Intuitively, one would expect the prediction error to decrease as the number of available observations increases. Indeed, it is a well-known fact that the prediction error satisfies a recursive relationship of the form

$$e(n) = [1 - |k(n)|^2] e(n-1) \quad (\text{B.1})$$

where $k(n)$ is the n th (complex) reflection coefficient of the process. Since the prediction error is always non-negative, the magnitude of a reflection coefficient can never exceed unity. Unless otherwise explicitly stated, perfectly predictable (i.e., degenerate) processes are excluded from consideration in order to obtain the strict inequality

$$|k(n)| < 1 \quad (\text{B.2})$$

Makhoul [10] has emphasized the equivalence between the reflection coefficients of a process and its correlation coefficients. Unless a process is

degenerate, the first n correlation coefficients uniquely determine the first n reflection coefficients and vice versa. This statement also holds for degenerate processes provided $e(n-1) > 0$.

Reflection coefficients provide an extremely convenient way to generate prediction filters recursively. Let the vector $w(n)$ denote the weights of the n th order prediction error filter based on the n most recent observations. As shown in Fig. B.1, a prediction error filter is constructed by subtracting the output of the corresponding prediction filter from its input. Given the filter weights obtained at the $(n-1)$ st stage of the recursion, the n th order weights are completely determined by the n th reflection coefficient. This relationship may be stated as

$$w(n) = w_+(n-1) - k(n) J w_+^*(n-1) \quad (B.3)$$

where the subscript "+" denotes a vector which has been extended by appending a trailing zero, e.g.,

$$[a \ b]_+ = [a \ b \ 0] \quad ,$$

and J is the appropriate exchange matrix that simply reverses the order of the elements within a vector. For example, the 3×3 exchange matrix is

$$J = \begin{vmatrix} 0 & 0 & 1 \\ 0 & 1 & 0 \\ 1 & 0 & 0 \end{vmatrix}$$

and

$$[a \ b \ c] J = [c \ b \ a] \quad .$$

The self-inverting property of exchange matrices, i.e.,

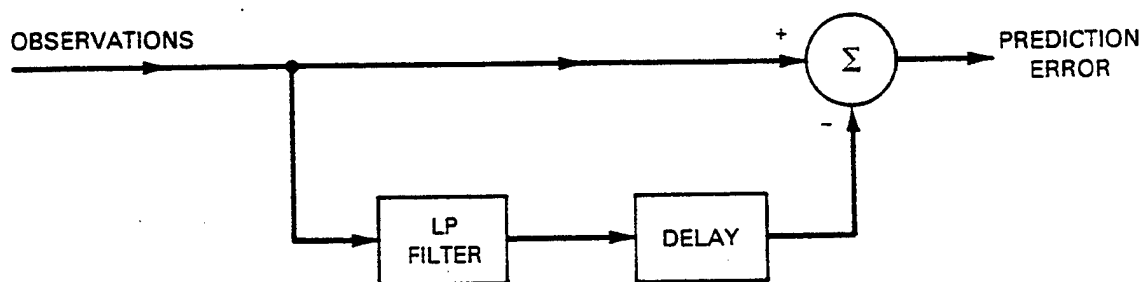


Fig. B.1. Prediction error filter.

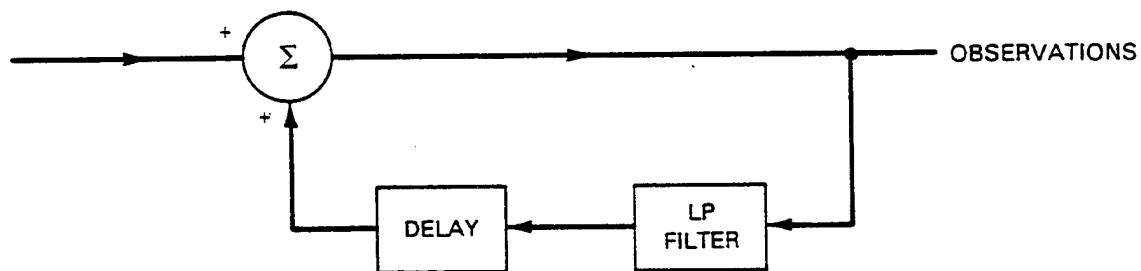


Fig. B.2. Autoregressive model.

$$J^2 = I \quad ,$$

is often useful.

The prediction error filter of order zero has no memory, and the recursion in (B.3) begins with $w(0) = 1$. Actually, the leading element of $w(n)$ is always unity — a consequence of the direct signal path in the block diagram defining the prediction error filter (see Fig. B.1). A more noteworthy observation is that the last coefficient of the n th order prediction filter is the n th reflection coefficient. This interesting property enables one to reconstruct the first n reflection coefficients from the n th order linear prediction (LP) filter. The procedure for accomplishing this task is essentially the same as the famous Schur stability test [33]. The key here is to realize that $w(n-1)$ can be obtained directly from $w(n)$, e.g.,

$$w_{+}(n-1) = (1 - |k(n)|^2)^{-1} [w(n) + k(n)Jw^*(n)]$$

follows easily from (B.3)

Of course, the coefficients for a prediction error filter may be obtained directly by minimizing its expected output power. In order to pursue this (equivalent) approach, let the vector r represent an arbitrary segment of the observed process. The covariance (correlation) matrix of r is usually written as

$$R = E\{rr^H\} \quad .$$

where a superscript H denotes the complex conjugate (Hermitian) transpose operation. The response of a finite impulse response (FIR) filter to a segment of the process can be written as

$$y = w^T J r \quad ,$$

where w represents the coefficients (impulse response) of the filter, and the superscript T denotes the usual (real) transpose operation.

The minimum mean square prediction error is

$$\begin{aligned} e &= \min E\{|y|^2\} \\ &= \min w^T J R J w^* \end{aligned} \quad , \quad (B.5)$$

where the minimization is over all w with a leading coefficient of unity.

When the observed process is statistically stationary, R is a Toeplitz matrix of (complex) correlation coefficients, i.e.,

$$\begin{aligned} R_{mn} &= E\{r_m r_n^*\} \\ &= c_{m-n} \end{aligned} \quad . \quad (B.6)$$

Since a covariance matrix is always Hermitian, the correlation coefficients (lags) must also satisfy

$$c_{-n} = c_n^* \quad . \quad (B.7)$$

Finally, without suffering any significant loss of generality, we may restrict our attention to normalized processes with unit variance, i.e.,

$$c_0 = 1 \quad .$$

Given (B.6) and (B.7), it is a relatively trivial exercise to show that R has the (harmonic) property

$$JRJ = R^* \quad . \quad (B.8)$$

Substituting (B.8) in (B.5), the linear prediction problem may be stated as follows. Find the filter weights which achieve the minimum mean square error

$$e = \min_w w^H R w \quad ,$$

subject to the constraint

$$[1 \ 0 \ \dots \ 0] w = 1 \quad .$$

This constrained minimization problem is easily solved using the method of Lagrangian multipliers. A complete solution is obtained by solving the (mixed) linear system of equations

$$Rw = e [1 \ 0 \ \dots \ 0]^T \quad . \quad (B.9)$$

Thus, the first n lags of a stationary process determine the n th order prediction filter. The following argument establishes the converse.

Using the method of bordering, it can be shown [34] that (B.1) and (B.3) solve (B.9) recursively. For non-degenerate processes, the n th reflection coefficient is

$$k(n) = c^T(n) J w_+(n-1) / e(n-1) \quad (B.10)$$

where the vector

$$c(n) = [1 \ c_1 \ \dots \ c_n]^T$$

is constructed from the first n lags.

Given a prediction error filter w , we may (now) invoke (B.4) to generate all the lower order prediction error filters. Following Burg [35], we construct a lower triangular matrix L , column by column, from the weights for the error filters of order n through 0. Since the first n reflection coefficients can be extracted from L , e.g.,

$$[0 \dots 0 \ 1] L = [-k(n) \dots -k(1) \ 1] \quad ,$$

we may compute the corresponding prediction errors from (B.1), starting with $e(0) = 1$. The prediction errors are placed along the main diagonal of a (diagonal) matrix D in order of increasing value.

By taking advantage of the Toeplitz structure of the correlation matrix R , the prediction error filter Eq. (B.9) can be generalized to

$$RL = UD \tag{B.11}$$

where U is an upper triangular matrix (to be determined). By construction, the main diagonals of L and U consist of all "1"s. Pre-multiplying (B.11) by the Hermitian transpose of L , we obtain

$$\begin{aligned} L^H RL &= L^H UD \\ &= DU^H L \end{aligned} \tag{B.12}$$

Since the product of two lower (upper) triangular matrices is also a lower (upper) triangular matrix, the left-hand side of (B.12) is both an upper and a lower triangular (Hermitian) matrix, i.e., a real diagonal matrix. It follows that

$$L^H U = U^H L$$

is a real diagonal matrix with "1"s along the main diagonal (i.e., an identity matrix). Therefore, U is the inverse of the Hermitian transpose of L , and consequently, the correlation matrix R is given by

$$R = L^{-H} D L^{-1} = UDU^H \quad . \quad (B.13)$$

Since L and D were constructed from the prediction error filter w , we may conclude that the n th order LP filter for a stationary process uniquely specifies the first n lags of the process.

If the determinant of the $n \times n$ correlation matrix R is written as $d(n)$, it follows from (B.13) that

$$d(n+1) = \prod_{k=0}^n e(k)$$

or equivalently,

$$e(n) = d(n+1)/d(n) \quad . \quad (B.14)$$

2. MAXIMUM ENTROPY SPECTRAL ANALYSIS

The "ratio of determinants" formula ultimately enables us to relate the error in predicting a process, given its entire past, to the entropy of the process. Taking the limit of (B.14) for arbitrarily large n and applying a well-known theorem from real analysis [36] yields

$$\begin{aligned} e(\infty) &= \lim e(n) \\ &= \lim d(n+1)/d(n) \\ &= \lim [n d(n)]^{1/n} \quad . \end{aligned}$$

Taking the logarithm of both sides leads to

$$\ln e(\infty) = \lim (1/n) \ln d(n) \quad . \quad (B.15)$$

Although it is not essential for this discussion, the right-hand side of this result can be expressed in closed form, e.g., see [37],

$$\lim (1/n) \ln d(n) = (1/2\pi) \int_{-\pi}^{\pi} \ln S(\omega) d\omega \quad . \quad (B.16)$$

where

$$S(\omega) = 1 + 2 \sum_{n=1}^{\infty} \frac{c_n}{n} \cos n\omega$$

is the true power spectral density of the process (i.e., the Fourier series of the correlation coefficients). The absolute integrability of $\ln S(\omega)$ is known in the literature as the Paley-Wiener condition. The right-hand side of (B.16) is sometimes referred to as the entropy (rate) of the power spectral density $S(\omega)$.

The entropy of a random vector r with probability density function $p(r)$ is defined to be

$$h = E \{ -\ln p(r) \} \quad .$$

In particular, the entropy of an n -dimensional circular (complex) Gaussian vector with covariance R is given by [see Appendix A, section 2].

$$h(n) = n (1 + \ln \pi) + \ln |R| \quad . \quad (B.17)$$

Thus, the average entropy per observation of a stationary complex Gaussian process is

$$\langle h \rangle = \lim (1/n) h(n)$$

$$= 1 + \ln \pi + \lim (1/n) \ln d(n) \quad (B.18)$$

Setting $n = 1$ in (B.17), we note that the entropy of a circular Gaussian random variable with unit variance is

$$h = h(1)$$

$$= 1 + \ln \pi \quad . \quad (B.19)$$

Substituting (B.15) and (B.19) in (B.18), the relationship between the entropy (rate) of a complex stationary Gaussian process and its optimum prediction error emerges as

$$\langle h \rangle = h + \ln e(\infty) \quad . \quad (B.20)$$

Thus, the greater its entropy (i.e., disorder), the more difficult a process is to predict.

At this point, we are to consider the class of processes that share the same given set of N initial lag values. Of course, every process in this class has the same prediction error based on the N most recent observations. Given additional (older) observations, the worst conceivable situation is for the prediction error to remain constant. The implication of this rather pessimistic assumption is that the additional observations are absolutely useless.

Pessimistic or not, the situation described above is a legitimate model and corresponds to choosing the (unknown) reflection coefficients to be identically zero for $n > N$. For this model, we have

$$e(\infty) = e(N)$$

and, in light of (B.20), the average entropy is clearly maximized. Moreover, (B.3) shows that the Nth order maximum entropy model has the property that its optimum prediction filter, based on the infinite past, is the same as its Nth order prediction filter.

One of the most important consequences of the orthogonality principle [38] is that the output of an optimum prediction error filter is a white noise process. Consequently, a statistically equivalent input process can be generated by driving the inverse of the optimum error filter with white noise. Referring to Fig. B.1, elementary linear systems analysis shows that the required inverse can be constructed using the simple feedback arrangement depicted in Fig. B.2. Since the maximum entropy error filter has a finite memory (impulse response), its inverse is an all-pole filter. Thus, the critical assumption behind the maximum entropy method is that the observed time series is an autoregressive process.

The validity of the autoregressive assumption is an issue far beyond the scope of this report. Ultimately, a preference for one model over another should be based on empirical considerations. Deliberations about such matters could perhaps be made more meaningful by the intelligent application of statistical hypothesis testing techniques [30].

The point to be made here is that the maximum entropy method (MEM) always leads to legitimate spectral estimates. An MEM spectral estimate takes the form

$$\hat{S}_{\text{MEM}}(\omega) = \frac{e}{\left| 1 + \sum_{n=1}^N w_n \exp(-in\omega) \right|^2} \quad (\text{B.21})$$

where the coefficients are obtained from the underlying LP filter

$$w = [1 \ w_1 \ \dots \ w_n]^T \quad ,$$

and e is the corresponding prediction error. In the traditional Blackman-Tukey approach, a spectral estimate is derived from N lag estimates by computing the (truncated) Fourier series

$$S(\omega) = 1 + 2 \sum_{n=1}^N c_n \cos n\omega \quad . \quad (B.22)$$

Unfortunately, this estimate is not generally guaranteed to be positive!

The difficulty with the latter approach can be attributed to the fact that the calculation in (B.22) implicitly assumes that the (unknown) lags for $n > N$ are zero. The standard "fix" for this problem is to pre-multiply the lags by a window function that is zero for $n > N$ and has a positive Fourier series (transform). This class of functions has been studied extensively [39], and a window can usually be found that yields a positive spectral estimate. However, a spectrum computed from "windowed" lags is never entirely consistent with the original information (lag values).

Burg was disturbed by the distortion introduced by a more or less arbitrarily selected window function, and he argued that the given set of correlation coefficients should be extended to produce the spectral estimate. Of all possible extensions, Burg preferred the extension with maximum entropy. As we have already seen, this choice amounts to truncating the reflection coefficients rather than the lags. One may certainly question whether maximizing entropy is the "correct" approach, but the fact remains that the maximum entropy method always yields a positive spectral estimate (B.21) consistent with the original lags.

3. A NOTE ON DEGENERATE PROCESSES

If the process is perfectly predictable (i.e., degenerate) after M observations, the LP filters are no longer uniquely specified for $n > M$. Faced with this situation, one may prefer the filter with minimum norm. The coefficients for this filter are easily computed by simply choosing the n th reflection coefficient to minimize

$$|w(n)|^2 = |w_+(n-1) - k(n) J w_+^*(n-1)|^2$$

for $n > M$. The reflection coefficient that minimizes this expression is

$$k_{\min}(n) = \frac{w_+^T(n-1) J w_+(n-1)}{|w_+(n-1)|^2} .$$

In this case, the Schwartz inequality guarantees that the magnitude of the reflection coefficient is less than unity. Filter weights calculated via the minimum norm criterion obey the (now) familiar recursive relationship

$$|w(n)|^2 = [1 - |k_{\min}(n)|^2] |w(n-1)|^2 .$$

Appendix C

COMPARISON OF ALTERNATIVE LIKELIHOOD RATIO TESTS
FOR ESTIMATING THE NUMBER OF SIGNALS PRESENT

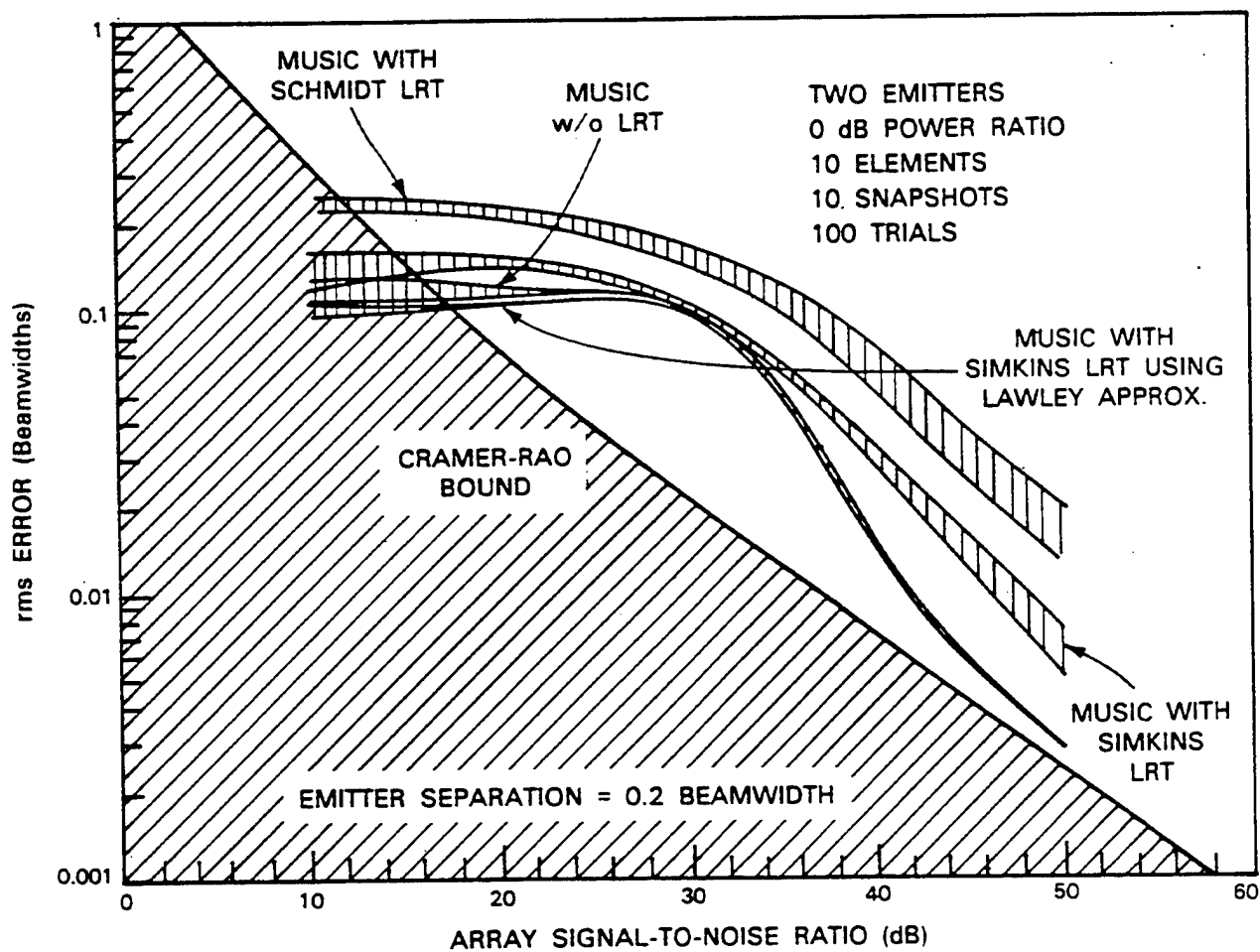
As was discussed earlier, the MUSIC algorithm needs an estimate for the number of emitters in order to form the direction finding spectrum. In this appendix, we present the results of a comparative study of several candidate likelihood ratio tests (LRT's) which have origins in the multivariate statistics literature [42-45]. Simkins [46] and Schmidt [47] have proposed the use of an LRT for driving the MUSIC algorithm. The number of signals is estimated as follows: A sequence of likelihood ratios is formed using the eigenvalues of the sample covariance matrix for the hypotheses of zero signals, one signal, etc. Their values are compared to a user-selected confidence level of the appropriate χ^2 distributions, and the first hypothesis whose likelihood ratio passes the test is accepted.

1. Candidate LRT's for use with MUSIC

Figure C.1 illustrates the direction-finding accuracy achieved by MUSIC when driven by various LRT's.¹ As a benchmark, the performance of MUSIC when the number of signals is assumed to be two is also shown (as "MUSIC w/o LRT"). The best performance was achieved by MUSIC driven by the Simkins LRT using the Lawley approximation [42-44]² - it was able to achieve the benchmark standard. All the LRT's studied asymptotically approach a χ^2 distribution [42-46]; the Lawley approximation helps to match the LRT to the

¹For Figs. C.1 and C.3, the statistics were accumulated based on the condition that at least one signal was detected. For assessment purposes, when only one signal was resolved, the angle estimate of the second, undetected signal was set equal to that of the first. At low SNR's the MUSIC spectrum exhibits one peak located at the centroid of the two emitters. As a result, the RMS error tends to equal half the emitter separation for the case of equal-powered emitters.

²The form for the extra approximation term given by Simkins [44] is incorrect, and should be replaced by the form given by Lawley [41].



136515-H

Fig. C.1. Comparison of MUSIC accuracies obtained with various likelihood ratio tests.

assumed distribution for small numbers of snapshots [43, 46]. Without the Lawley approximation, the LRT overestimates the number of signals. As a result, "MUSIC with the Simkins LRT" performs poorer than "MUSIC with the Simkins LRT using the Lawley approximation". Finally, "MUSIC with the Schmidt LRT" is not at all matched well to the problem. The Schmidt LRT [47] exhibits poor performance because the χ^2 distribution being used has the wrong number of degrees of freedom for the complex valued sample covariance matrices under consideration.

2. Candidate LRT's for use with ROOT MUSIC

Because of their poor performance in the MUSIC LRT comparison, the Schmidt LRT and the Simkins LRT (without the Lawley approximation) were automatically ruled out for use with ROOT MUSIC. A comparison of ROOT MUSIC driven by the Simkins LRT with the Lawley approximation versus ROOT MUSIC assuming two emitters (i.e., "w/o LRT"), as seen in Figs C.2 and C.3, demonstrated a need for a more sensitive LRT.

All of the previously considered LRT's make no assumption regarding the noise power. For the problem at hand, we decided that it was reasonable to assume a known noise level, so we tested an LRT which takes advantage of this knowledge -- what we refer to as the "Lawley LRT (known noise power)" [43]. As seen in Fig. C.4, the Lawley LRT detects the presence of two emitters approximately 4 dB earlier than the Simkins LRT with the Lawley approximation, resulting in improved performance in the ROOT MUSIC algorithm (Figs. C.2 and C.3). Note that in Fig. C.2 it is apparent that perhaps an additional 5 dB of sensitivity might be obtainable, but that its impact (Fig. C.3) upon estimation performance would not be significant. Thus, the Lawley LRT with the Lawley approximation was used for ROOT MUSIC Monte Carlo experiments described in Section IV.

3. Summary

The Simkins LRT with the Lawley approximation was judged adequately sensitive to drive the MUSIC algorithm, regardless of the number of snapshots available. The Lawley LRT for known noise power provides needed additional sensitivity to drive ROOT MUSIC and, of course, could also be used with MUSIC. There remains a study of the sensitivity of the performance of the Lawley LRT to errors in estimating the noise power.

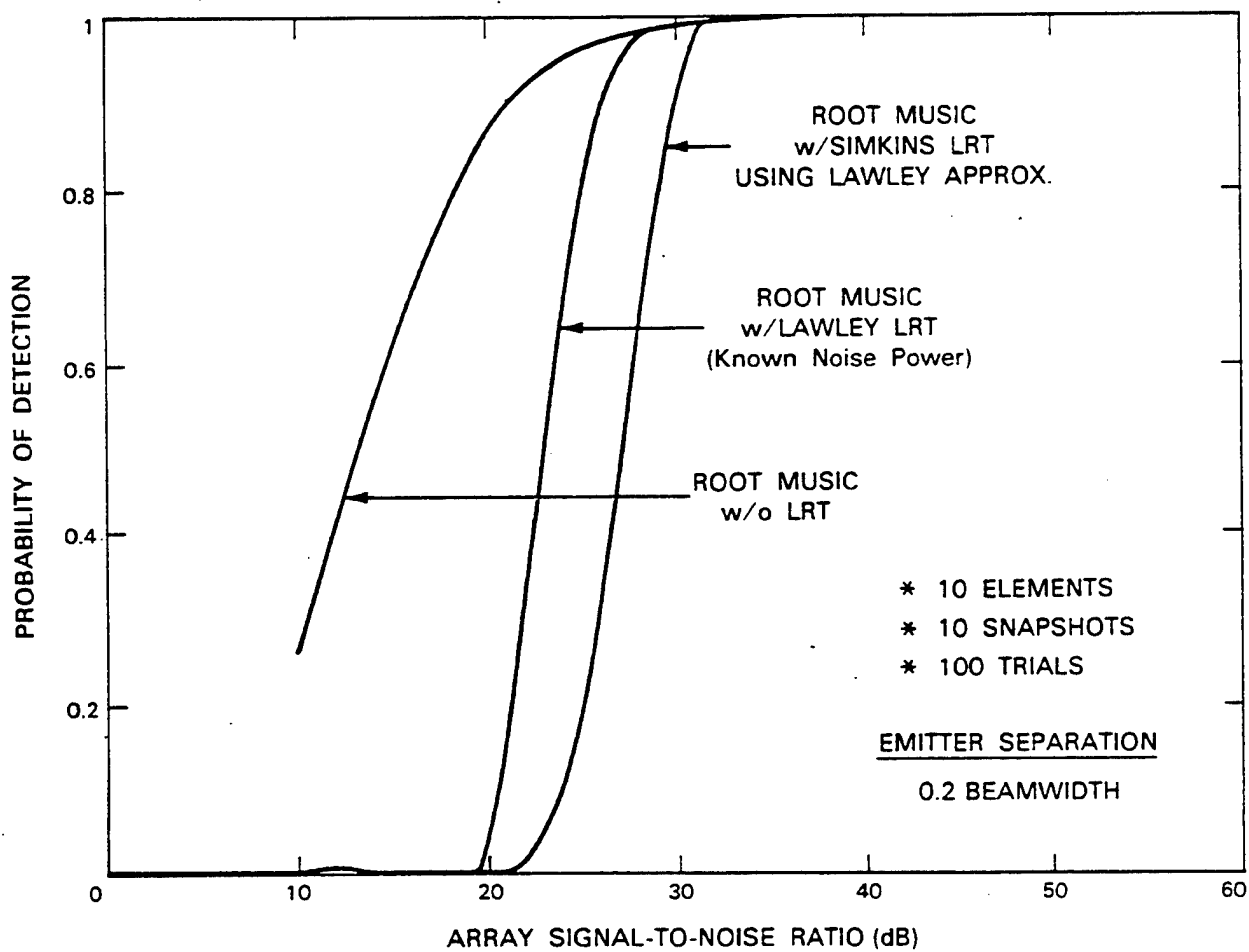


Fig. C.2. Comparison of ROOT-MUSIC resolution performance with various likelihood ratio tests.

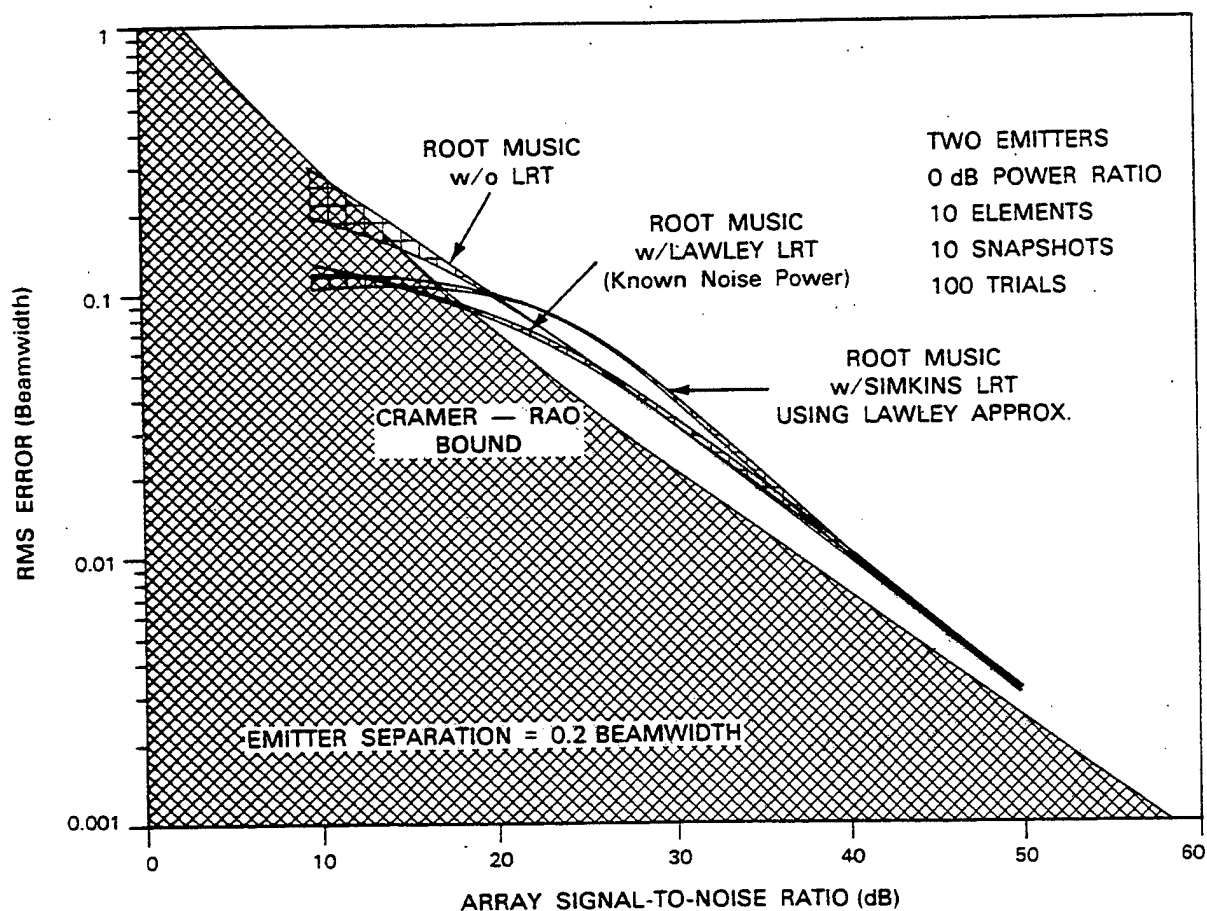


Fig. C.3. Comparison of ROOT-MUSIC accuracies obtained with various likelihood ratio tests.

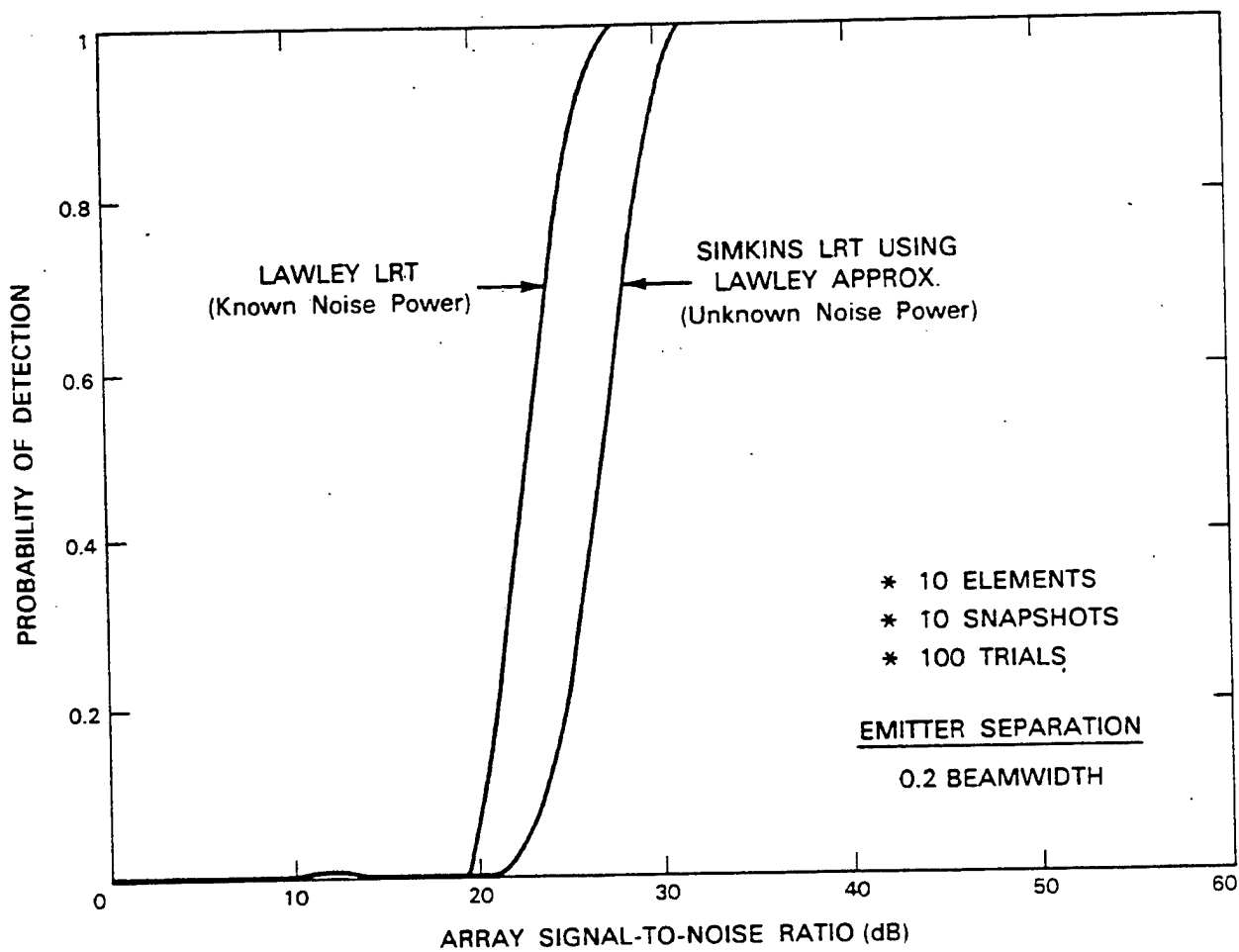


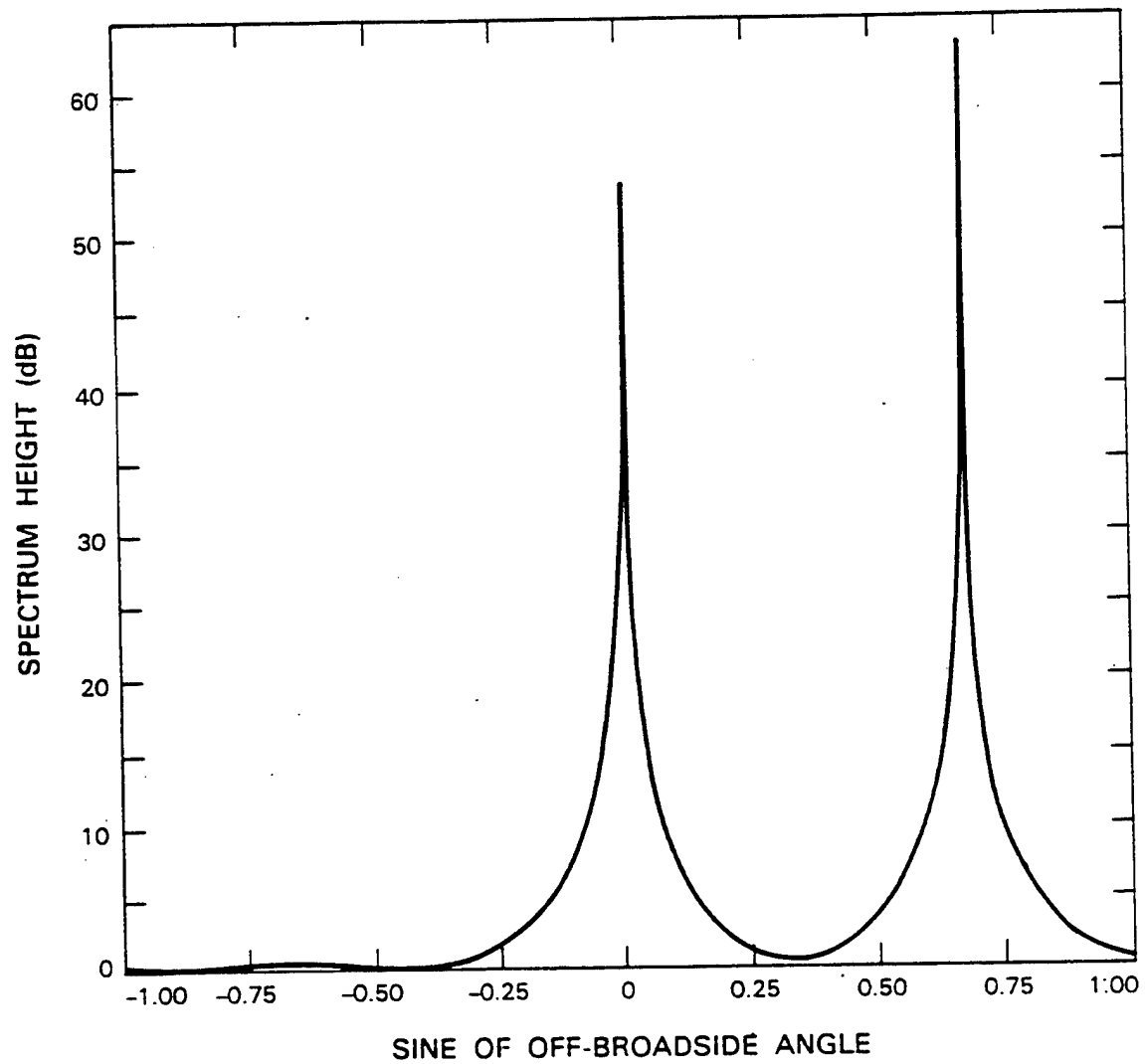
Fig. C.4. Detector output comparisons for two likelihood ratio tests.

Appendix D
COMPARISON OF TWO POWER ESTIMATION TECHNIQUES
VIA COMPUTER SIMULATION

An angle estimation algorithm produces a set of candidate signal directions and tests them for authenticity by computing a power estimate for each one. To obtain a set of direction estimates, a vector of weights must be computed which minimizes the total power output of the array under various constraints which serve to prevent the weighting vector from being the zero vector. Many such constraints are possible, leading to many different direction finding algorithms. With total power minimized, the gain in each of the true signal directions must also be minimized. Therefore, the locations of nulls in the weighted array pattern (or peaks in the reciprocal pattern) provide the desired set of candidate directions. An example of a plot of the reciprocal array pattern produced by the MUSIC algorithm is shown in Fig. D.1 for a uniform linear array of five elements spaced $\lambda/2$ apart. There are two signals located at 0 and $2/3$ ($\sin\theta$ coordinates), and since there are no ambiguities in this array, the two peaks accurately reflect the directions of the signals. Notice that these are the only two peaks appearing in the reciprocal pattern.

Unfortunately, many angle estimation algorithms produce more candidate directions than the number of actual signals present, with the true signal directions scattered among spurious candidate directions. This is especially true for thinned linear arrays due to the existence of ambiguities. An ambiguity occurs when the direction vectors associated with a set of directions are linearly dependent. True signals located in these linearly dependent directions will cause false signal indications in other directions which are linearly dependent upon the directions of the actual signals.

To more clearly illustrate this concept of linearly dependent directions, refer to Fig. D.2. This shows how ambiguous, linearly dependent angles are created when the center element of the aforementioned five-element uniform array is removed. For emitters at the angles of $\pm 41.8^\circ$ ($\sin 41.8^\circ = 2/3$) to the thinned array, the phase at each element is shifted $\pm 120^\circ$,



1339 16-8

Fig. D.1. MUSIC spectrum with infinite looks for a uniform five-element array.

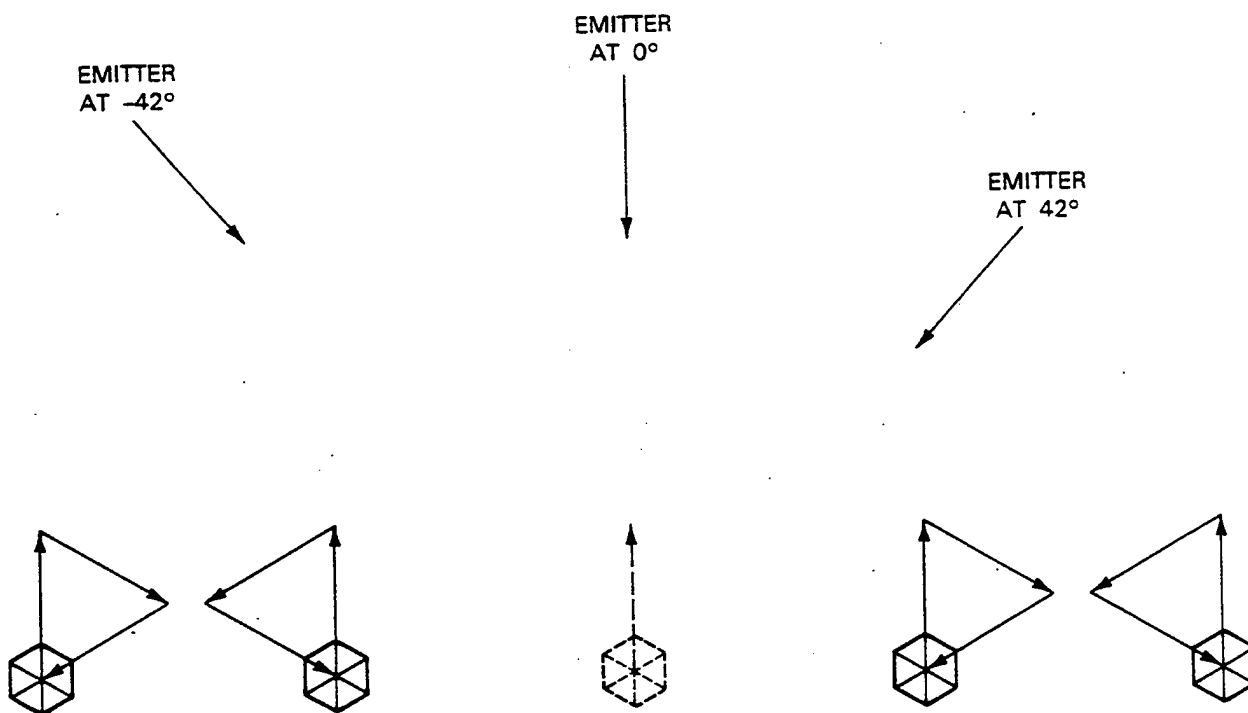


Fig. D.2. Example of linearly dependent direction vectors for thinned five-element array.

combined with an emitter at 0° , the total signal at each element adds to zero. The signal does not add to zero at the center element, but since that element has been removed, this information is not available. Due to the linear dependence of the direction vectors, signals located at 0° and 42° would be indistinguishable from a pair located at $\pm 42^\circ$, or 0° and -42° . Furthermore, this ambiguity is amplitude independent and occurs for any set of three angles which satisfy

$$\sin\theta_3 - \sin\theta_2 = \sin\theta_2 - \sin\theta_1 = 2/3$$

Figure D.3 is the reciprocal pattern plot from the four-element thinned array mentioned above. The true signals are still located at 0 and $2/3$ as in the other pattern, but notice how removing the center antenna element causes the angle estimation algorithm to show a third spurious peak at $-2/3$.

The purpose of the power estimation algorithm is now clear. Hopefully, if a signal power estimate is computed for each candidate signal direction, then the powers in the spurious directions will be at the noise level or significantly below those of the true signal directions. A simple threshold test can then identify and reject the "false alarms" while retaining the true signal directions.

The most straightforward way to estimate the power of each signal is via a direct mathematical solution. First, assume that the sampled covariance matrix, S , is equal to the true covariance matrix, R , which is unknown. It may be shown that any true covariance matrix can be written in the form

$$R = \sigma^2 I + VPV^H$$

where the columns of V are the direction vectors and P is a diagonal matrix¹ whose entries correspond to the power for each direction vector \underline{v} . Solving the above equation for P with S substituted for R yields

¹i.e., the signals are incoherent.

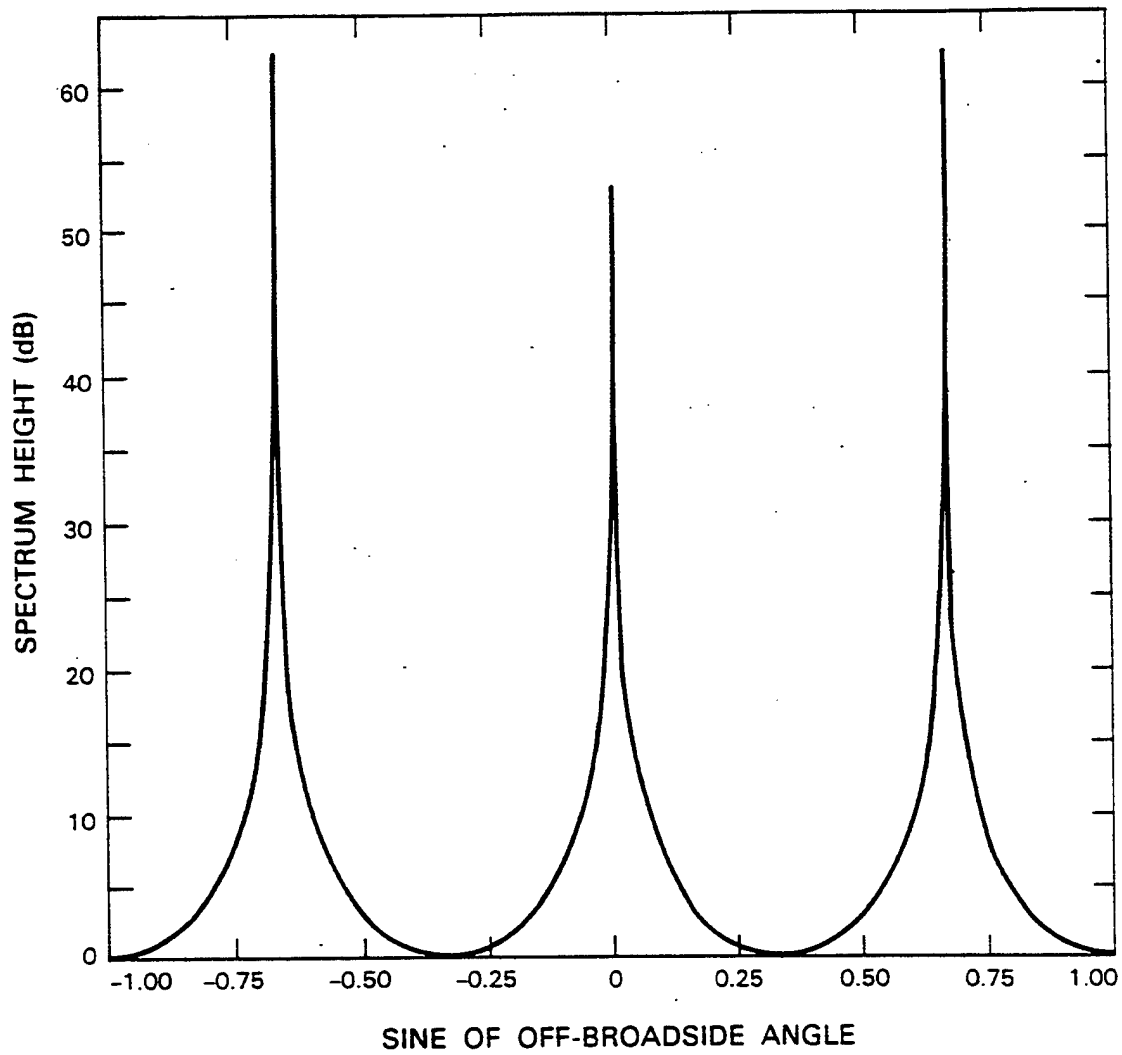


Fig. D.3. MUSIC spectrum with infinite looks for a thinned linear array.

$$P = (V^H V)^{-1} V^H (S - \sigma^2 I) V (V^H V)^{-1} .$$

When P is determined in this manner, it will not be exactly diagonal, since $S = R$ was only an approximation. The diagonal elements of P are nonetheless a very reasonable approximation of the signal powers, so the non-diagonal elements may be ignored.

The direct solution method will work unless $(V^H V)$ is singular. This occurs when the columns of V are dependent. A singular $(V^H V)$ is not a problem for uniform linear arrays with interelement spacing $\leq \lambda/2$ because no direction vectors are dependent, but it is a problem for thinned arrays.

To avoid this problem a least-squares solution is sought in which the powers P_1, P_2, \dots, P_N are selected so as to minimize the squared error between S and R . The squared error may be expressed

$$E = \|S - R\|_R \quad (\text{Frobenius norm})$$

$$= \sum_m \sum_n \left| S_{mn} - R_{mn} \right|^2 .$$

Since the inverse of $V^H V$ is not required to solve this problem, this method has a chance of exhibiting reasonable performance when signals are located ambiguously. In an ambiguous case, the actual signals should have normal power estimates and the spurious signal indications should have power estimates at the noise level.

In order to compare the theoretical performance of the direct solution and the least-squares solution in an ambiguous situation, a computer simulation was set up using the four-element thinned array as the receiving antenna (Fig. D.4) and two emitters of equal power. One emitter was held fixed at 0° or directly broadside to the antenna. The other emitter was moved step by step closer to 41.8° ($\text{Arcsin } 2/3$) which is an ambiguous situation. The beamwidth of this antenna is 23° and the simulation began

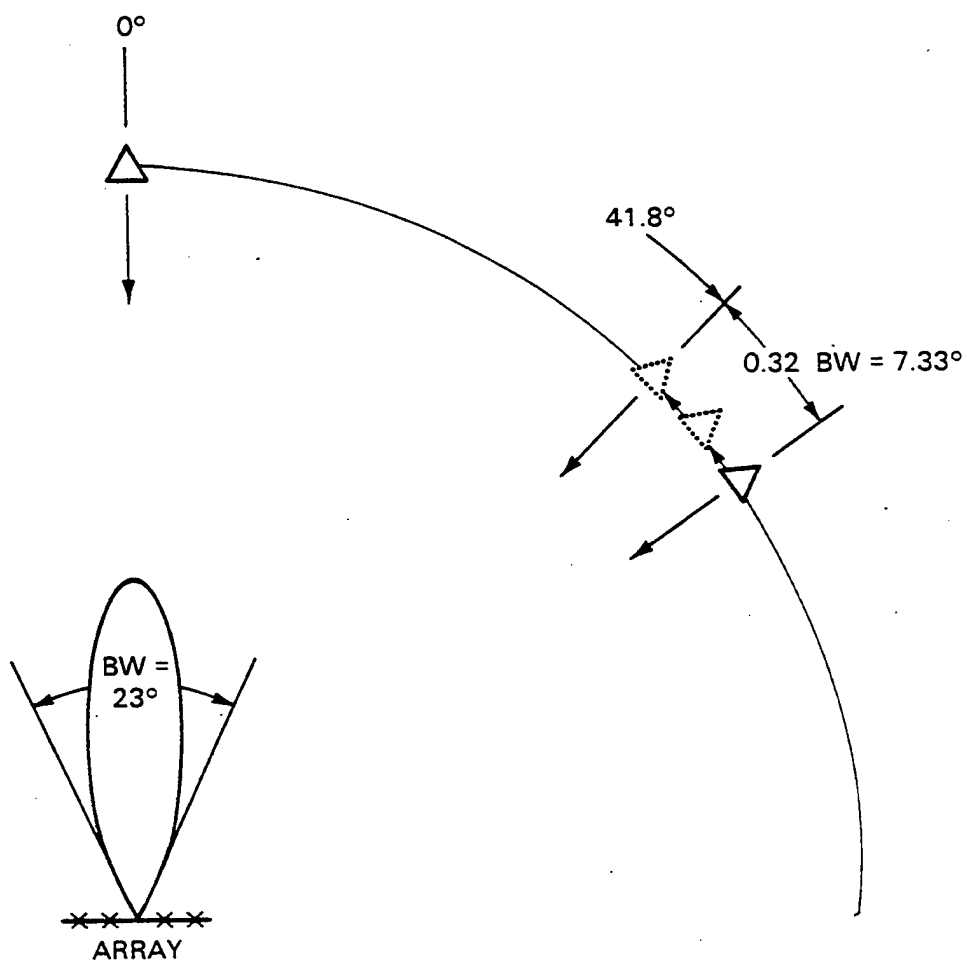


Fig. D.4. Variation of two-emitter geometry to simulate the effect of linear dependence for thinned linear array.

with the unfixed signal 0.32 beamwidths or 7.33° away from the ambiguous angle. The separation was reduced in 3 dB steps beamwidth separation and then to a zero beamwidth separation (exact coincidence with the ambiguous angle). The second input variable was the signal-to-noise ratio. A trial consisted of 100 "looks" at the array output, that is, 100 data vectors which were processed to form a single covariance matrix. After the angle estimation algorithm produced a set of direction estimates for the signals, the power estimation algorithm generated a power estimate for direction. For each signal-to-noise ratio (0 to 50 dB in 10 dB steps) at each separation angle, 100 trials were conducted in order to compile power error statistics for each solution method.

The results of the simulation may be seen in Figs. D.5 and D.6. There are two curves for each separation, one for each signal, and the area between them is shaded. In Fig. D.5, the bottom curve (brown) represents the best performance of the direct solution method. For separations greater than .32 BW, this curve approximately represents the lower error bound. When the separation decreases, however, representative curves break away from the lower bound at progressively higher signal-to-noise ratios. Finally the direct method breaks down completely at zero separation.

Now, the least-squares performance curves in Fig. D.6 may be compared with the direct solution. The thick curve includes all of the separations of Fig. D.5, including zero separation. The curves in Fig. D.6 are all almost exactly coincident with the lower error bound for the direct solution, regardless of the separation from the ambiguity.

In summary, theory and experiments show that the direct solution power estimator can fail for non-uniform arrays. Whereas the traditional direction finding problem has been resolving closely-spaced signals, it has been shown that wide angles are also a problem when non-uniform arrays are used. The least-squares power estimator is able to identify and reject spurious signals in situations where the direct solution breaks down due to ambiguities. Experimental data shows that least-squares performance remains constant independent of the signal separation from an ambiguity. Therefore,

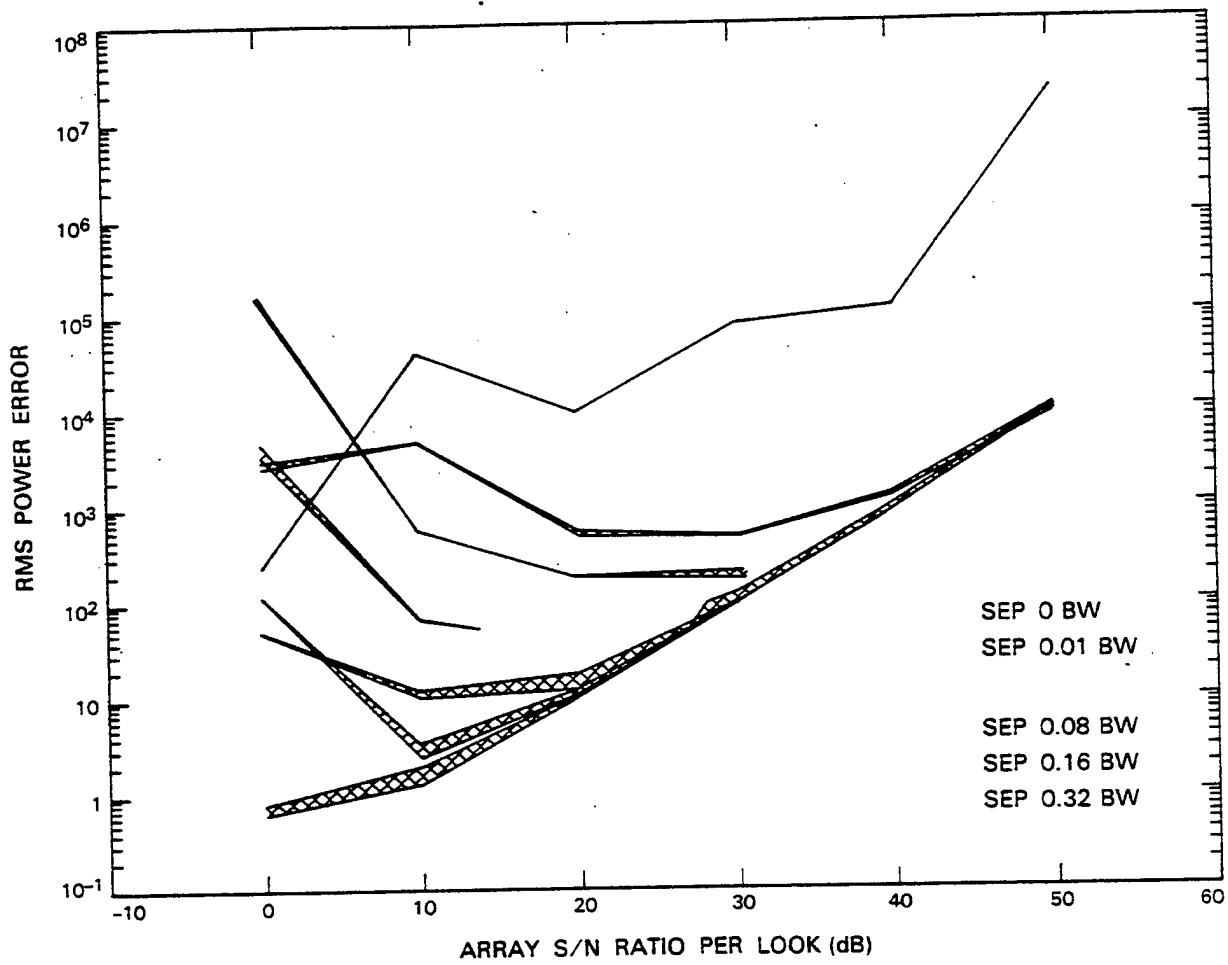


Fig. D.5. Comparison of direct solution power estimation error as emitters approach linear dependence.

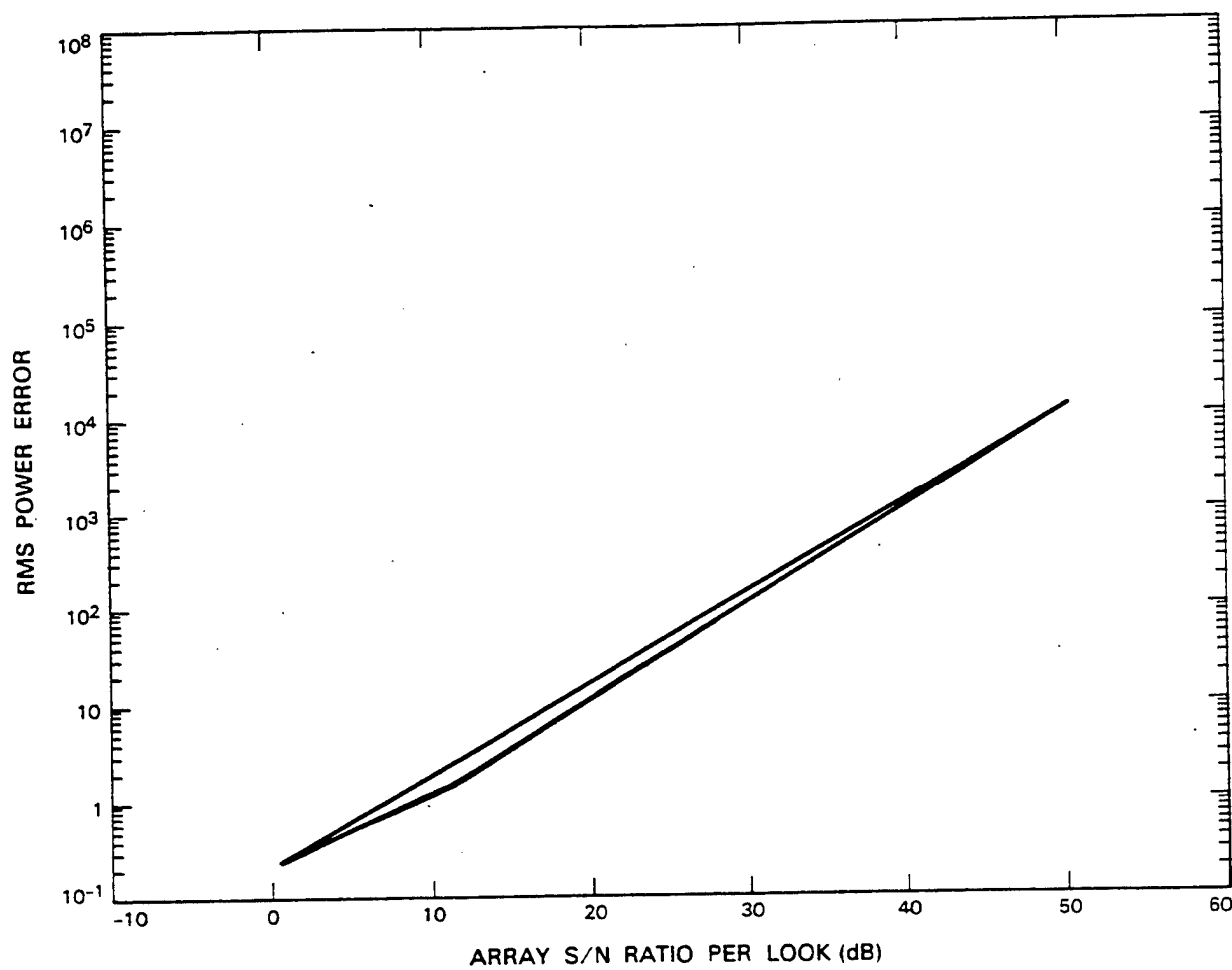


Fig. D.6. Comparison of least-squares power estimation errors as emitters approach linear dependence.

a processing system using this power estimation technique will be able to overcome the ambiguity problem of thinned arrays while allowing accuracy comparable to uniform arrays.

Appendix E SAMPLING FROM THE WISHART DISTRIBUTION

1. THE COMPLEX WISHART DISTRIBUTION

Let r be an M -dimensional, complex (circular) Gaussian vector with zero mean and covariance R . Given K observations $\{r(k) | k=1, \dots, K\}$, the sample covariance matrix

$$\hat{R} = \frac{1}{K} \sum_{k=1}^K r(k)r^H(k)$$

is a sufficient statistic for inferring parameters of R . However, when K is less than M , the sample covariance matrix has less than full rank and is therefore singular. To avoid unnecessary complications, the analysis presented here is based on the simplifying assumption

$$K \geq M \quad .$$

Under the above conditions, the probability distribution of the elements of a sample covariance matrix is completely specified by the complex Wishart distribution [31]. In particular, the joint probability density function of the elements of

$$A = K \hat{R} \tag{E.1}$$

may be written as

$$p(A) = \frac{|A|^{K-M} |R|^{-K}}{c(K,M)} \exp \{ -\text{Tr} (R^{-1}A) \} \quad . \tag{E.2}$$

The normalization constant $c(K,M)$ is given by

$$c(K,M) = \pi^{M(M-1)/2} \Gamma(K) \dots \Gamma(K-M+1) \quad ,$$

where $\Gamma(v)$ is the gamma function [45]

$$\Gamma(v) = \int_0^{\infty} x^{v-1} e^{-x} dx \quad ; \quad v \geq 1 \quad .$$

Since $\Gamma(1) = 1$, the recursive property of the gamma function

$$\Gamma(v+1) = v \Gamma(v) \tag{E.3}$$

establishes the familiar factorial formula

$$\Gamma(n) = (n-1)!$$

for any positive integer n .

The probability density function (pdf) in (E.2) is defined over the domain of non-negative definite Hermitian matrices. While theoretically quite elegant, this formula is awkward to use in many practical calculations. The fundamental problem is that the elements of a sample covariance matrix are not statistically independent. Even in the special case where R is the identity and $K=M$, the restriction of (E.2) to a semi-definite domain complicates matters considerably.

Fortunately, the Cholesky decomposition of A leads to a much more useful representation. Thus, consider the class of $(M \times M)$ upper triangular complex matrices with (real) positive elements along the main diagonal. The elements above the main diagonal are unrestricted, whereas the elements below the main diagonal are identically zero. For every positive definite Hermitian matrix A defined by (E.1) there exists a unique upper triangular matrix U such that

$$A = U^H U \quad .$$

Goodman [31] has shown that the joint pdf of the elements of U is generally of the form

$$p(U) = \frac{2^M}{c(K,M)} |R|^{-K} U_{11}^{2K-1} U_{22}^{2K-3} \dots U_{MM}^{2K-(2M-1)} \exp\{-\text{Tr}(R^{-1} U^H U)\} \quad (E.4)$$

However, when R is the identity matrix I , the joint pdf of the elements of U may be expressed as the product of the marginal densities of the individual elements. This observation stems from the fact that

$$\text{Tr}(U^H U) = \sum_{m,n} |U_{mn}|^2 \quad .$$

The implication is that in the special case $R=I$ the elements of U are statistically independent! In order to establish this important result, we first recognize that

$$p_{U_{mn}}(z) = (1/\pi) \exp\{-|z|^2\} \quad ; \quad \text{complex } z, m < n \quad (E.5)$$

is the pdf of a (complex) circular Gaussian random variable with zero mean and unit variance. Setting $R=I$ in (E.4) and integrating out the $M(M-1)/2$ complex Gaussian terms leaves the pdf of the main diagonal of U , i.e.,

$$p(U_{11}, \dots, U_{MM}) = \prod_{m=1}^M \frac{2}{\Gamma(K-m+1)} U_{mm}^{2K-(2m-1)} \exp\{-U_{mm}^2\} \quad .$$

Evidently, the m th diagonal element has the marginal density

$$p_{U_{mm}}(x) = \frac{2}{\Gamma(K-m+1)} x^{2(K-m+1)-1} \exp\{-x^2\}, \quad x > 0 \quad . \quad (E.6)$$

This pdf is closely related to the chi-square distribution with $2(K-m+1)$ degrees of freedom. Thus, consider the random variable

$$\gamma_n = (1/2) x_{2n}^2 \quad (E.7)$$

obtained by simply scaling a chi-square random variable with $2n$ degrees of freedom. It can be shown that the pdf of (E.7) is a gamma density, i.e.,

$$p_{\gamma_n}(x) = \frac{1}{\Gamma(n)} x^{n-1} \exp\{-x\}, \quad x > 0 \quad .$$

The general form of the gamma density [46] is obtained by replacing n with a real number $v \geq 1$ and introducing a positive scale factor a , i.e.,

$$\begin{aligned} p_{a\gamma_v}(x) &= a p_{\gamma_v}(ax) \\ &= \frac{a^v}{\Gamma(v)} x^{v-1} \exp\{-ax\}, \quad x > 0 \quad . \end{aligned} \quad (E.8)$$

The gamma variate (i.e., random variable) obtained by setting $a=1$ in (E.8) is referred to here as the v th order gamma variate. It follows from the recursive property of the gamma function (E.3) that the expected value of the v th order gamma variate is v .

The pdf of the square root of the v th order gamma variate is

$$p_{\gamma_v}^{1/2}(x) = 2 x p_{\gamma_v}(x^2)$$

$$= \frac{2}{\Gamma(v)} x^{2v-1} \exp \{ -x^2 \} \quad , x > 0 \quad .$$

Comparing this pdf with (E.6), we conclude that the diagonal elements of U are square roots of integer order gamma variates. Specifically, we have

$$U_{mm} = \gamma_{K-m+1}^{1/2} \quad .$$

2. APPLICATION TO MONTE CARLO SIMULATIONS

Sample covariance matrices can be generated directly from the Wishart distribution as follows. Given an arbitrary covariance matrix R, consider any convenient "square-root" decomposition

$$R = LL^H \quad .$$

The observed vector r may be interpreted as the linear transformation

$$r = Lw$$

of a normalized vector w with covariance

$$E \{ ww^H \} = I \quad .$$

It follows that any sample (covariance matrix) of r is statistically equivalent to a linear transformation of a corresponding sample (covariance matrix) of w, i.e.,

$$\hat{R} = L\hat{W}L^H \quad .$$

Since

$$E \{ \hat{W} \} = I \quad ,$$

the argument presented in the previous section applies, and hence we may construct

$$K \hat{W} = U^H U$$

from the upper triangular matrix U with statistically independent elements described by (E.5) and (E.6). If L is the (lower) Cholesky factor of R , then

$$\begin{aligned} K \hat{R} &= L U^H U L^H \\ &= (L U^H) (L U^H)^H \end{aligned}$$

is obtained as the product of its Cholesky factors.

The complex Gaussian elements of U (above the main diagonal) can be generated using any one of a number of well-known techniques. Perhaps the most elegant approach is to compute

$$z = (-\ln u)^{1/2} \exp \{ i 2 \pi v \}$$

where u and v are statistically independent random variables uniformly distributed over the semi-open interval $(0,1]$. This method is based on the fact that $-\ln u$ is an exponential random variable with unit mean (i.e., a first order gamma variate). Moreover, n th order gamma variates can be generated by summing n jointly independent exponential variates. Thus, the remaining elements of U (on the main diagonal) could be obtained from expressions of the form

$$x = \sum_{k=m+1}^{K-m+1} [-\ln u(k)]^{1/2}$$

where the $\{u(k)\}$ are uniformly distributed over $(0,1]$ and jointly independent. However, a Fortran subroutine is widely available [47] that calculates gamma variates much more efficiently, particularly for large values of K . This algorithm is based on the method of acceptance/rejection testing [48].

APPENDIX F DIRECTION FINDING EXPERIMENTS

The results of the Monte Carlo experiments described in Section IV.A are included in their entirety. Four different parameter variations are explored:

(1) Signal-to-Interference Ratio Group

A. 0 dB B. -10 dB

(2) Emitter Separation Group

A. 0.1 Beamwidths B. 0.2 Beamwidths C. 0.4 Beamwidths

(3) Number of Looks Group

A. 10 B. 100 C. 1000

(4) DF Method Group

A. Spectral B. Root

AAR	ROOT AAR
MEM	ROOT MEM
MLM	ROOT MLM
MUSIC	ROOT MUSIC
TNA	

Using these group designations, the 36 summary plots for the direction finding experiments can be indexed as follows:

<u>SIR GROUP</u>	<u>SEPARATION GROUP</u>	<u>LOOKS GROUP</u>	<u>DF METHOD GROUP</u>	<u>FIGURE</u>
A	A	A	A	F-1
			B	F-2
		B	A	F-3
			B	F-4

<u>SIR GROUP</u>	<u>SEPARATION GROUP</u>	<u>LOOKS GROUP</u>	<u>DF METHOD GROUP</u>	<u>FIGURE</u>
B	B	C	A	F-5
			B	F-6
		A	A	F-7
			B	F-8
		B	A	F-9
			B	F-10
		C	A	F-11
			B	F-12
	C	A	A	F-13
			B	F-14
		B	A	F-15
			B	F-16
		C	A	F-17
			B	F-18
	A	A	A	F-19
			B	F-20
		B	A	F-21
			B	F-22
		C	A	F-23
			B	F-24
	B	A	A	F-25
			B	F-26
		B	A	F-27
			B	F-28
		C	A	F-29
			B	F-30
	C	A	A	F-31
			B	F-32
		B	A	F-33
			B	F-34
		C	A	F-35
			B	F-36

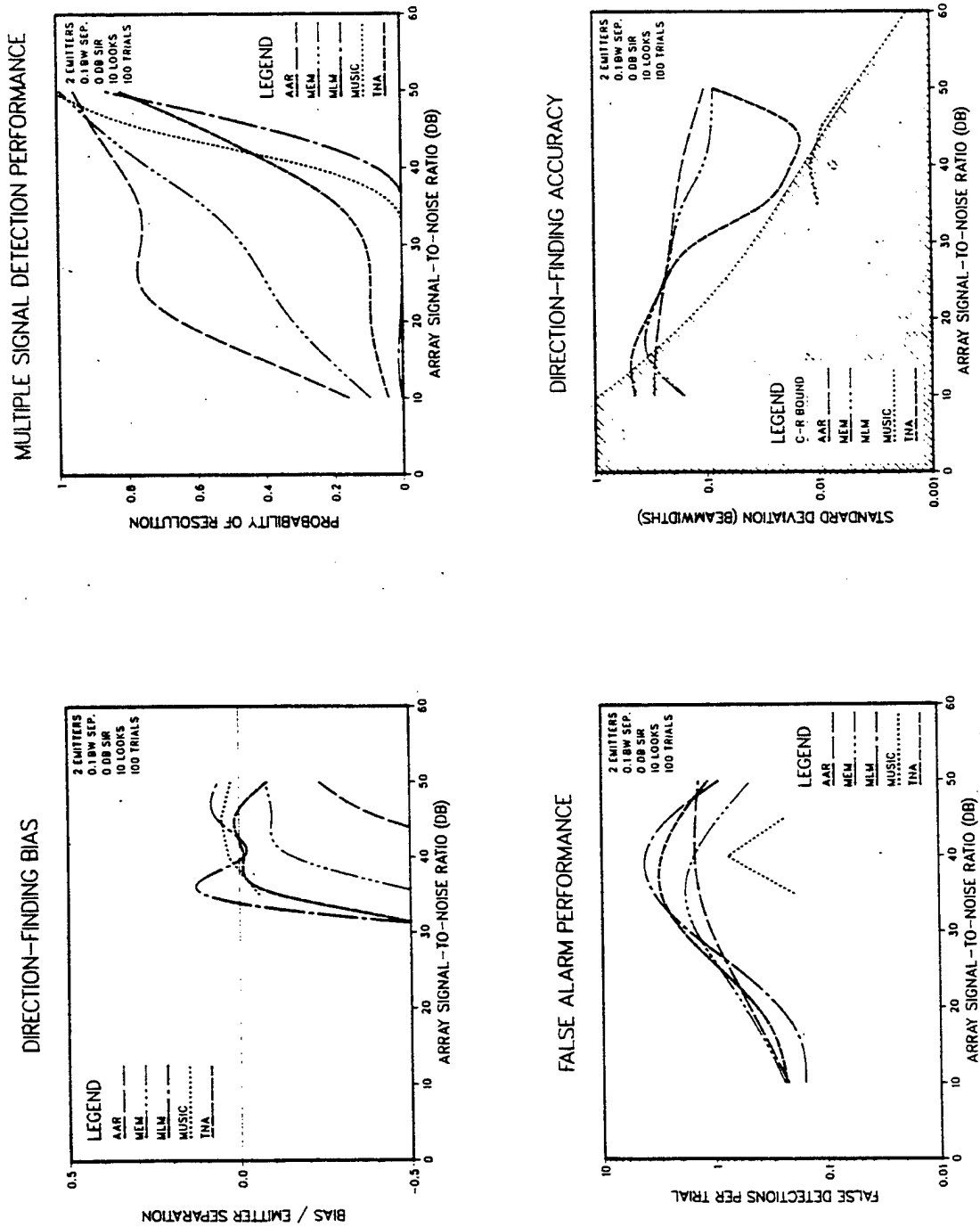


Fig. F.1.

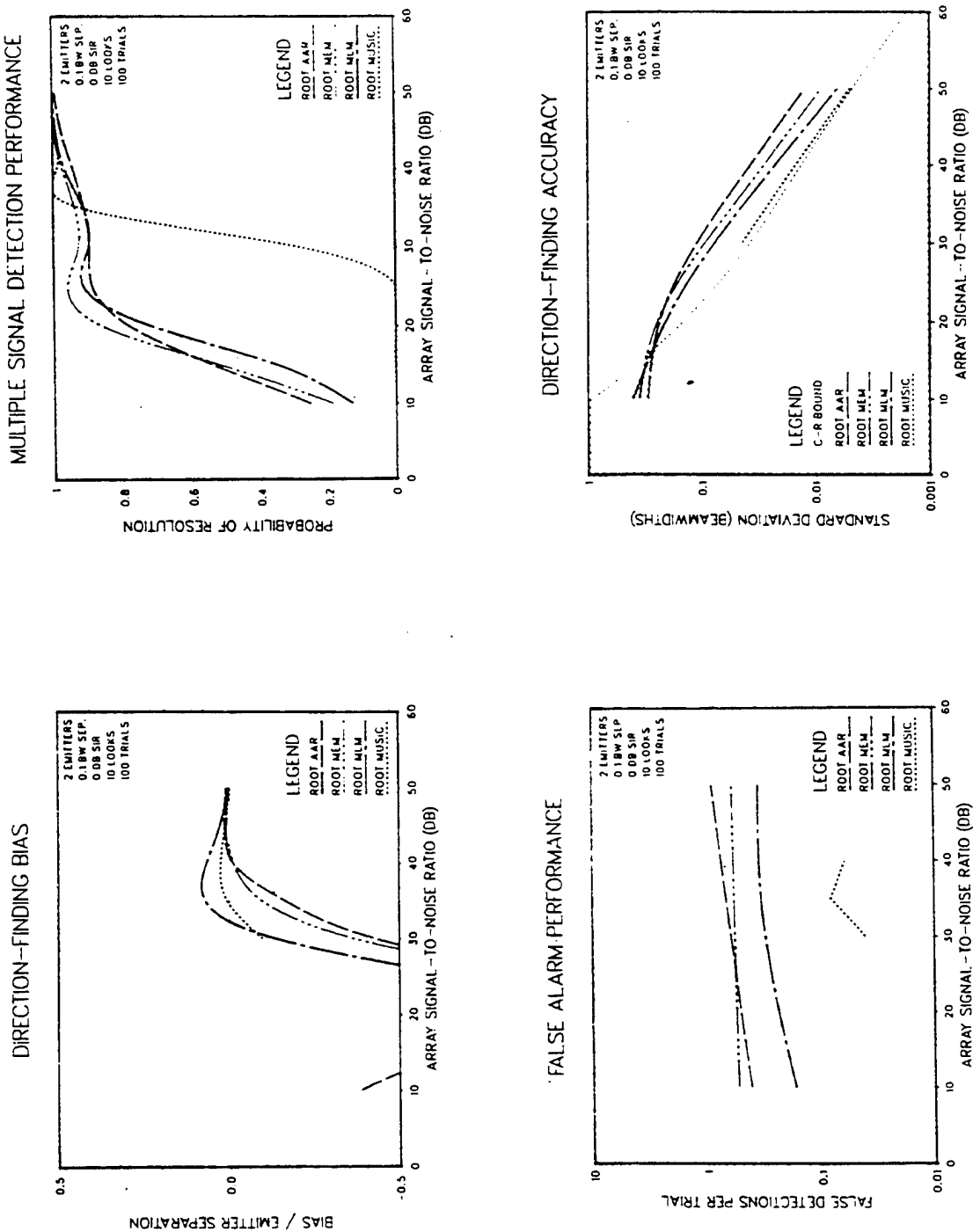


Fig. F.2

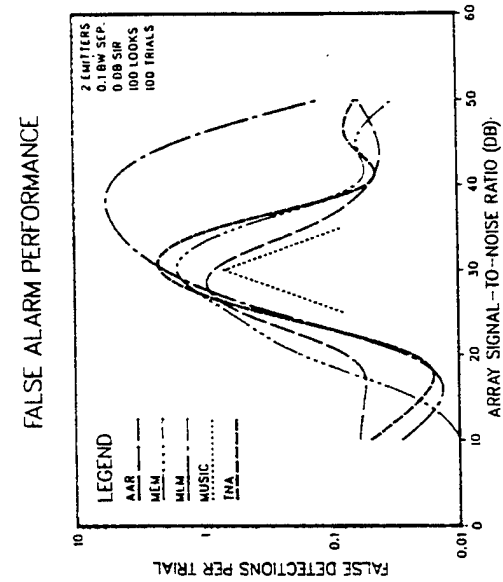
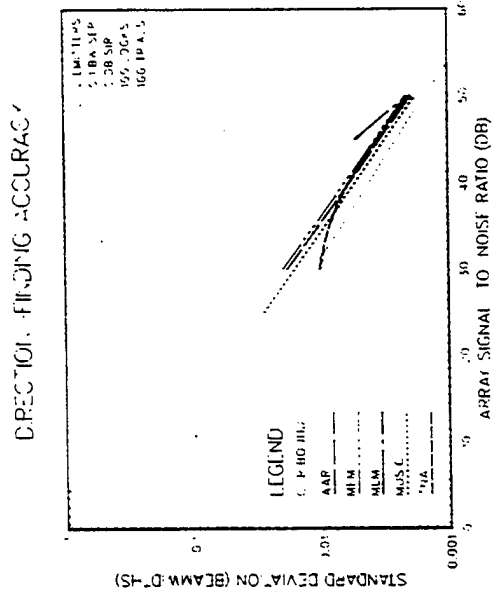
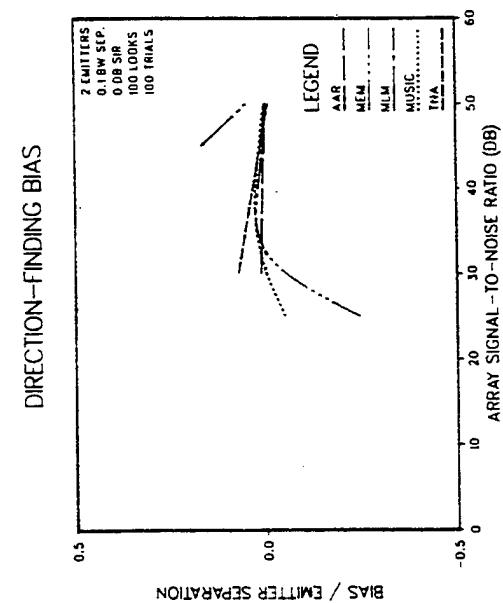
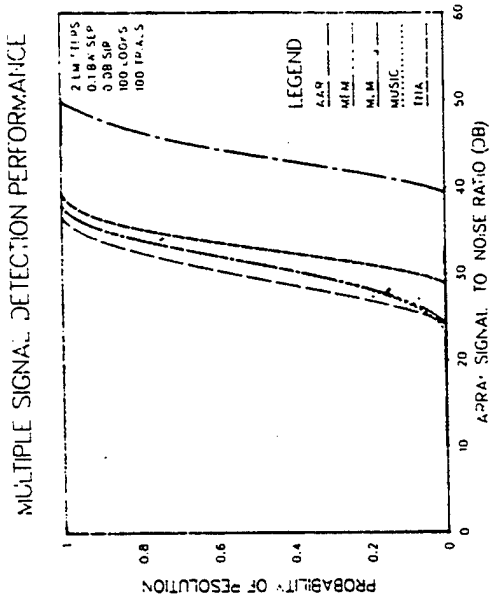
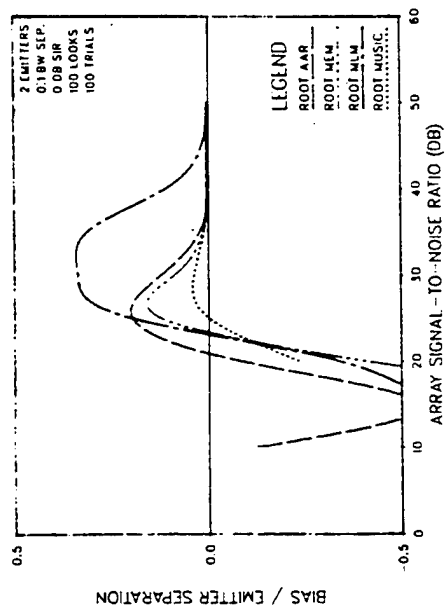
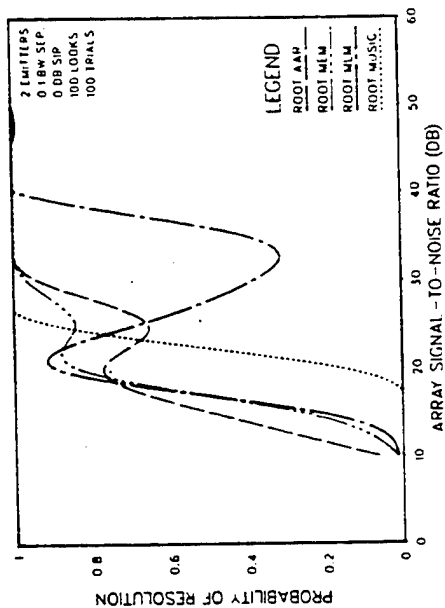


Fig. F.3

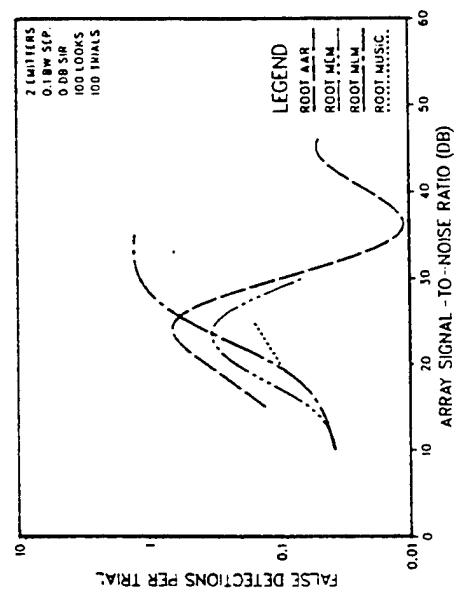
DIRECTION-FINDING BIAS



MULTIPLE SIGNAL DETECTION PERFORMANCE



FALSE ALARM PERFORMANCE



DIRECTION-FINDING ACCURACY

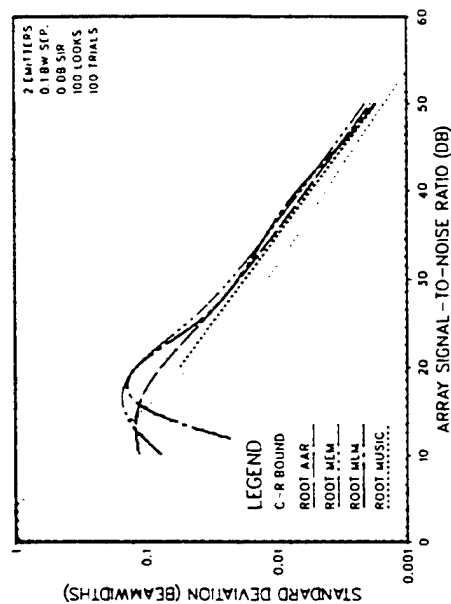


Fig. F.4

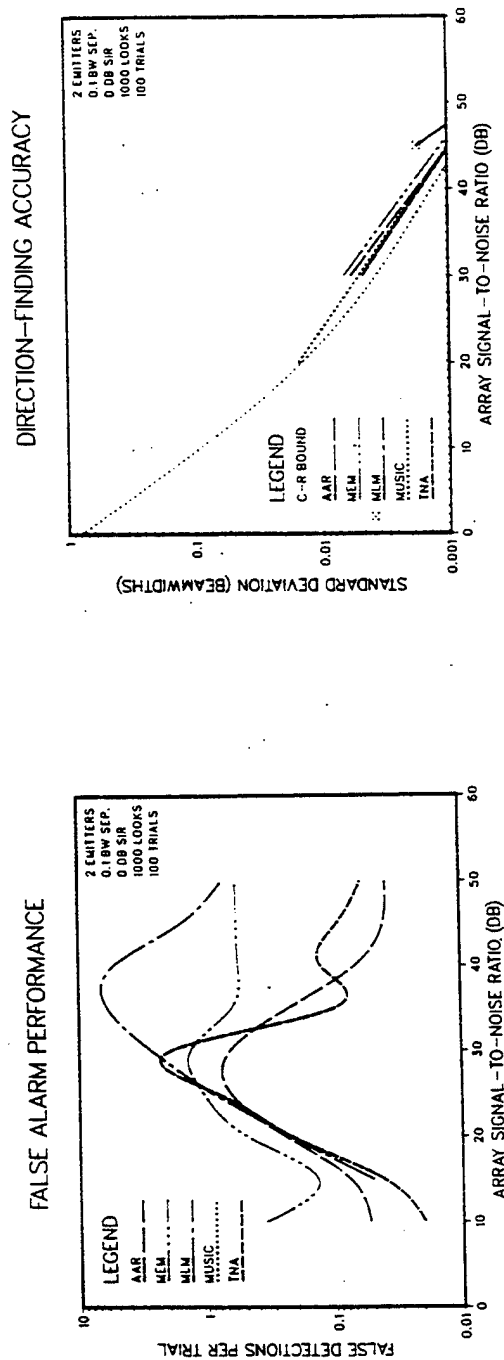
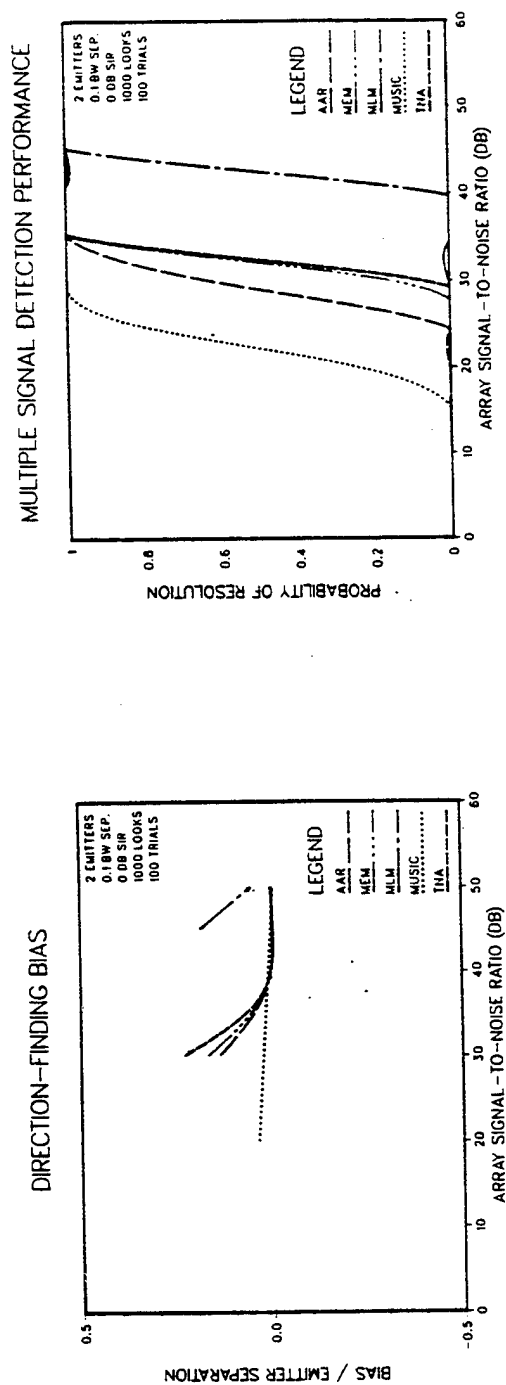


Fig. F.5

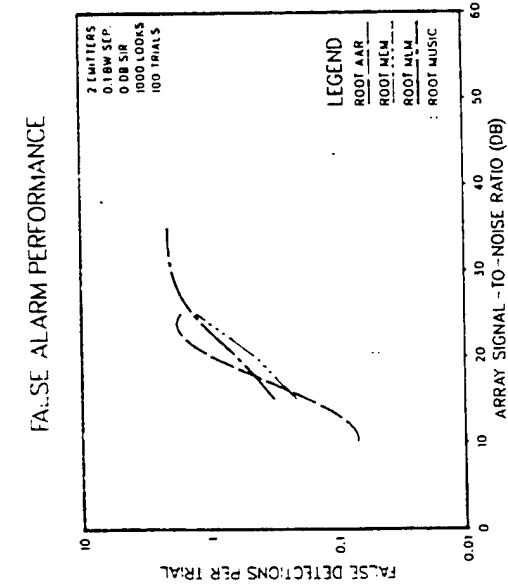
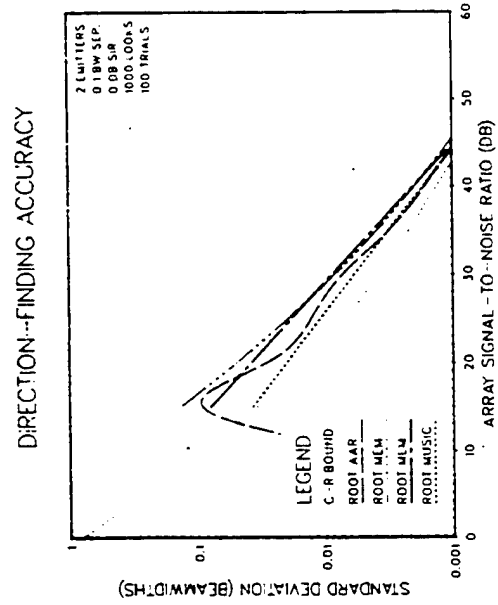
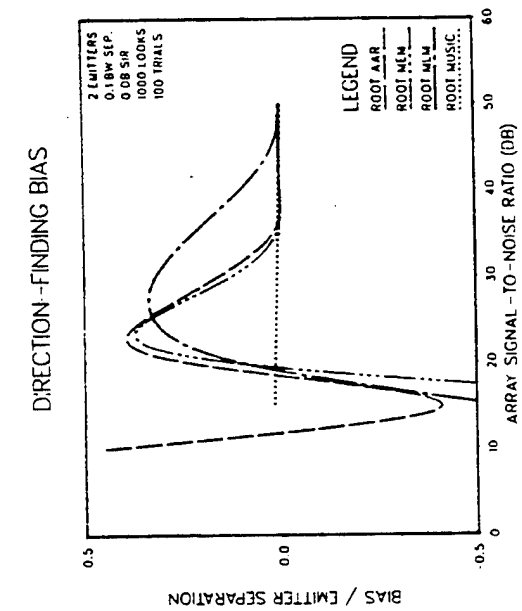
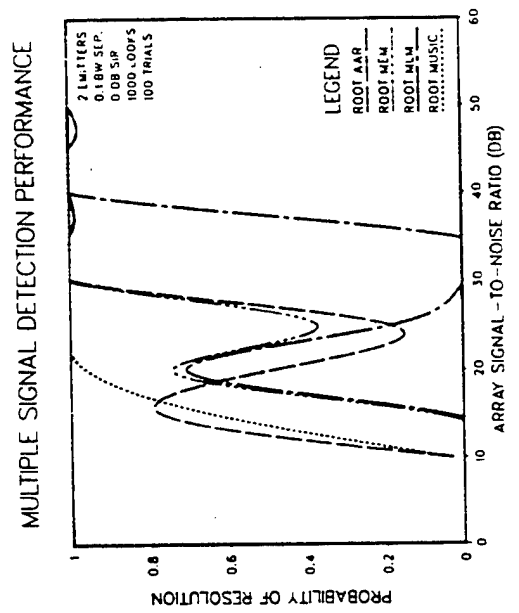


Fig. F.6

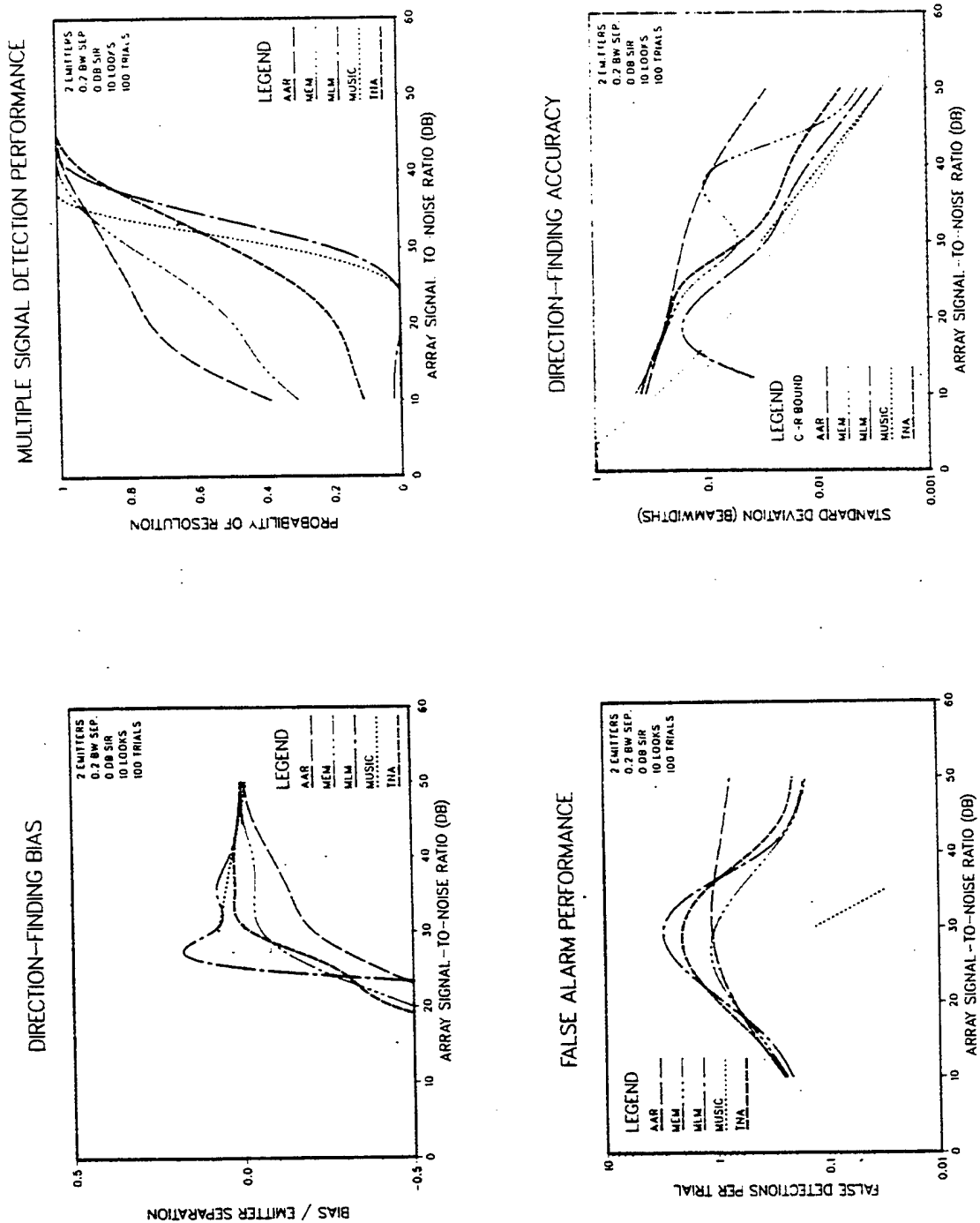


Fig. F.7

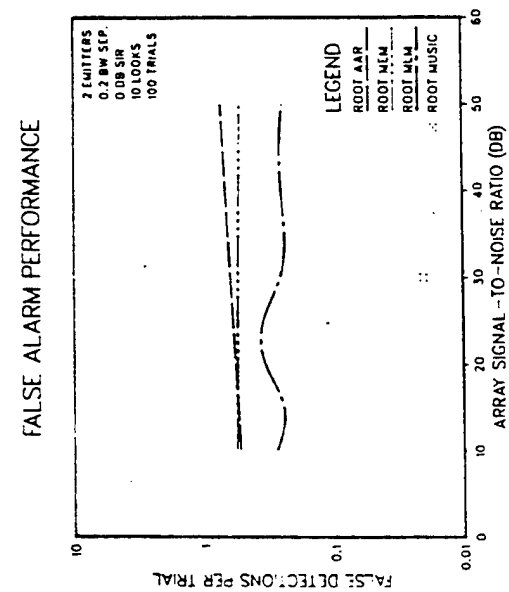
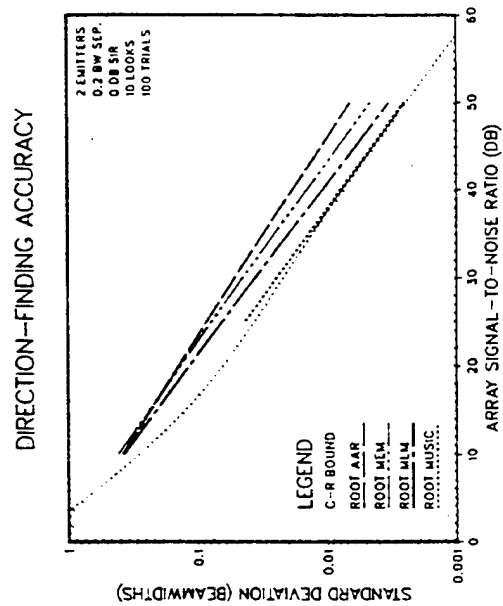
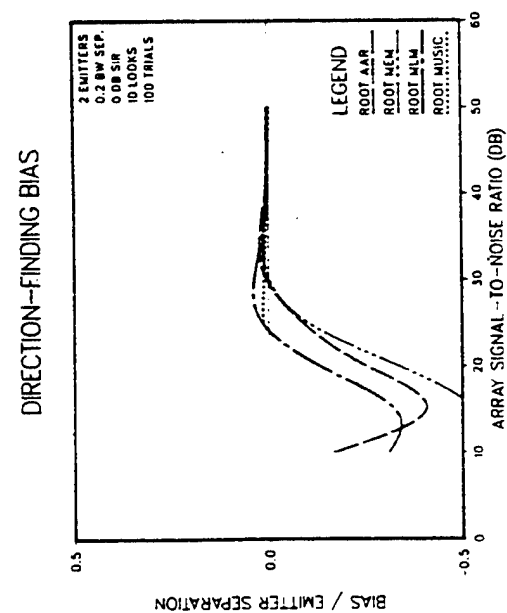
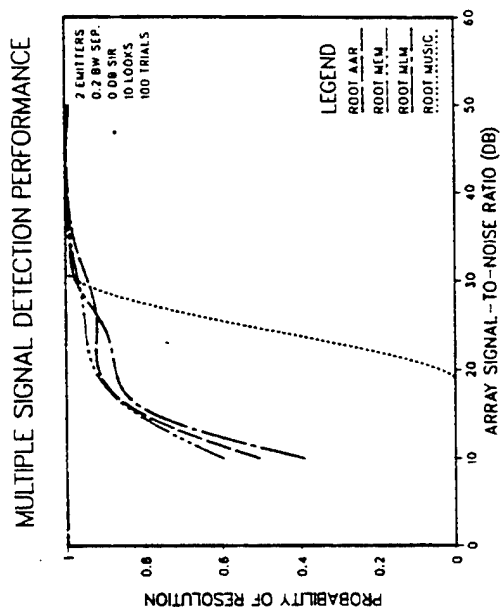
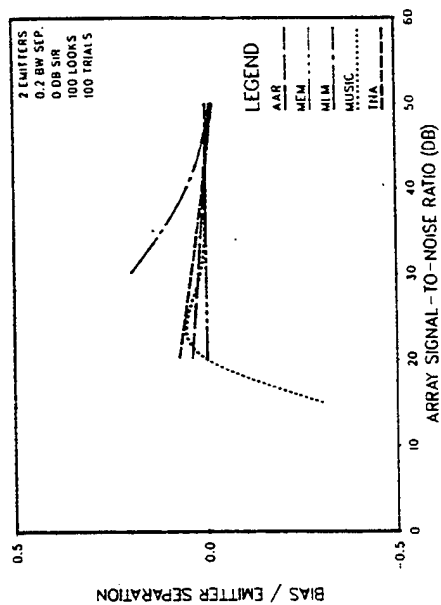
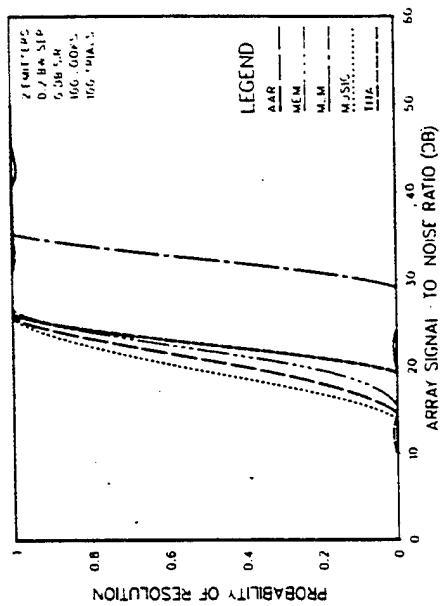


Fig. F.8.

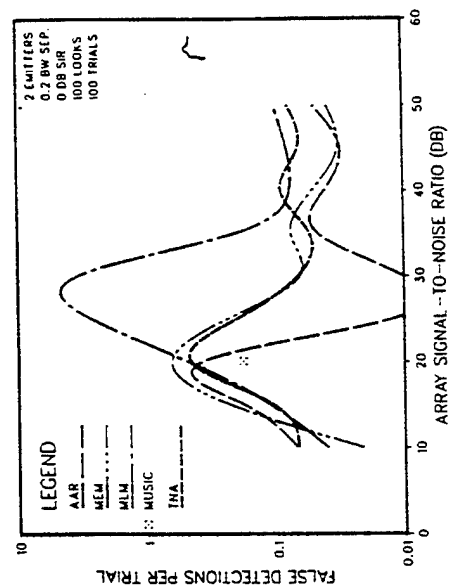
DIRECTION-FINDING BIAS



MULTIPLE SIGNAL DETECTION PERFORMANCE



FALSE ALARM PERFORMANCE



DIRECTION-FINDING ACCURACY

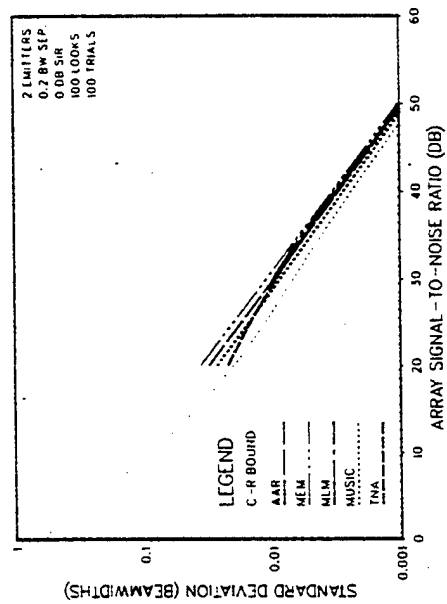


Fig. F.9.

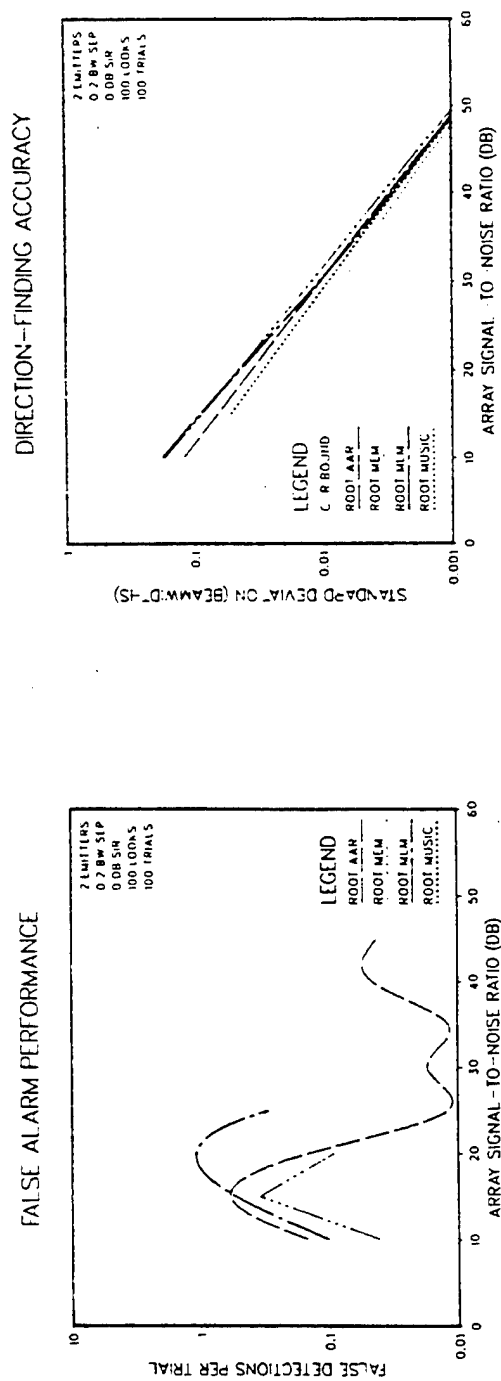
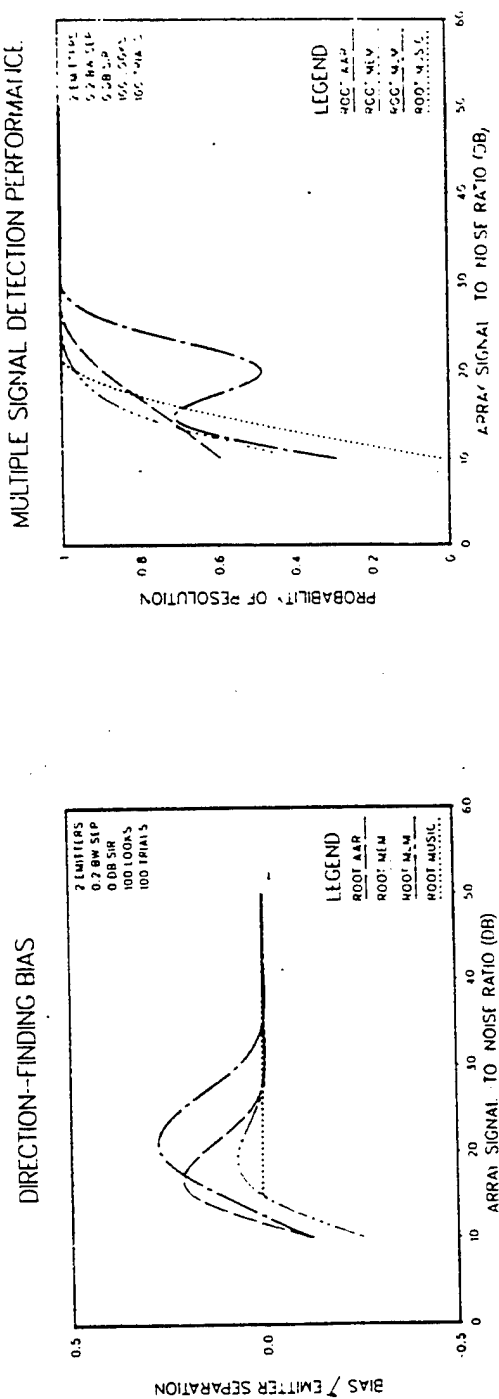


Fig. F.10.

113951-5

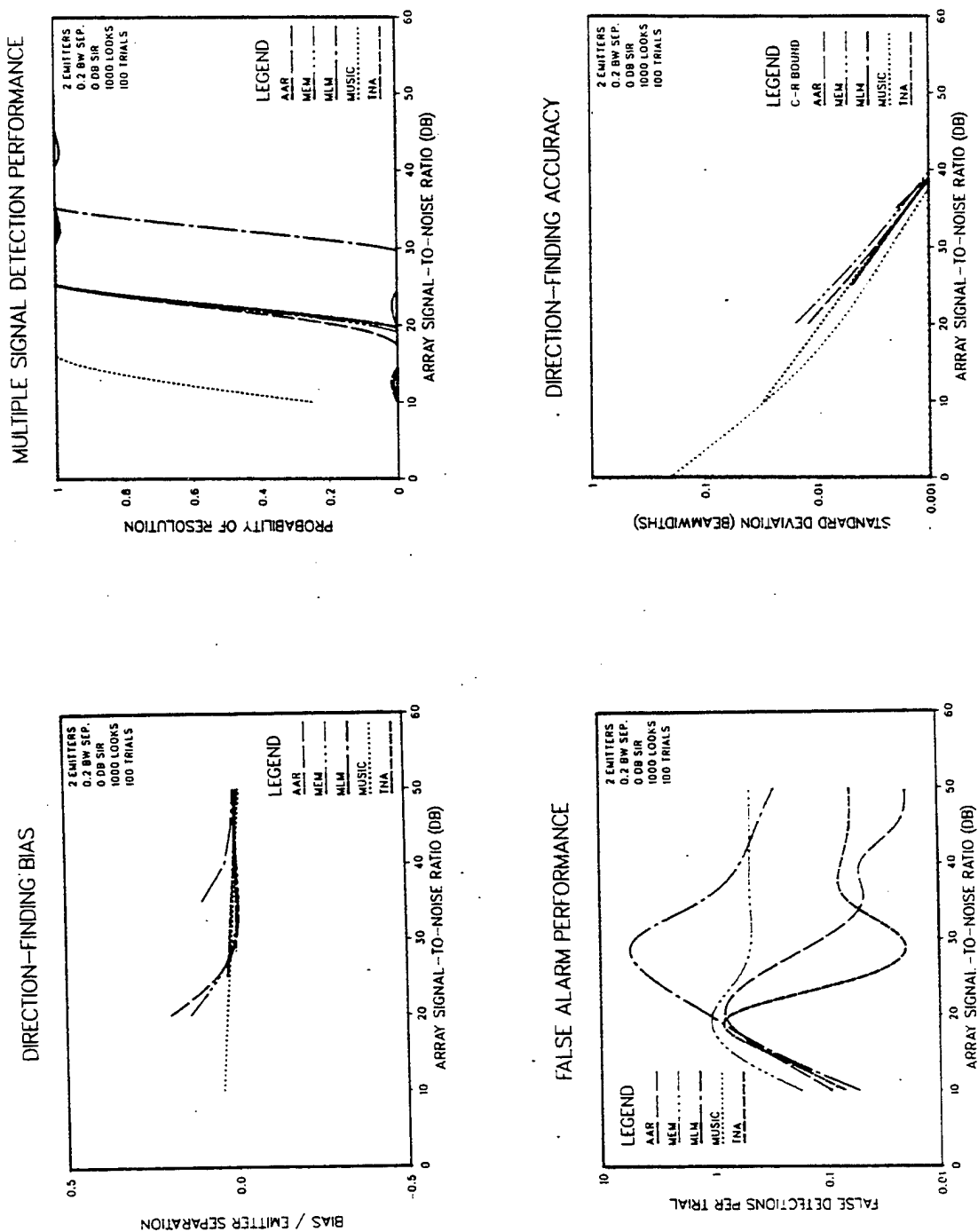


Fig. F.11.

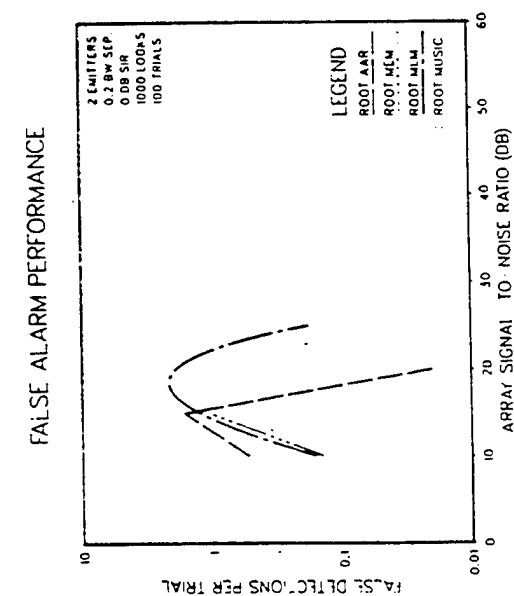
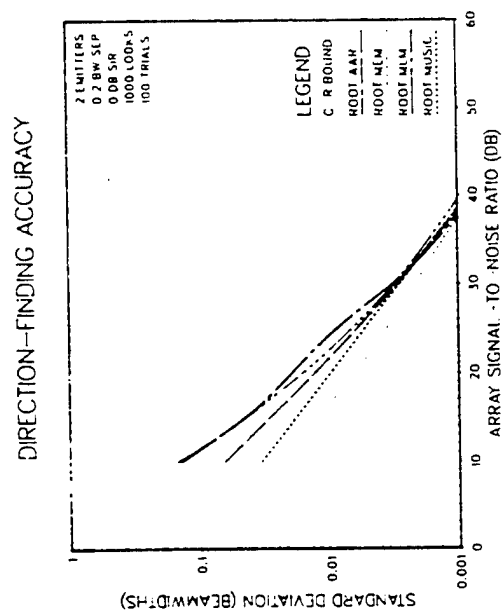
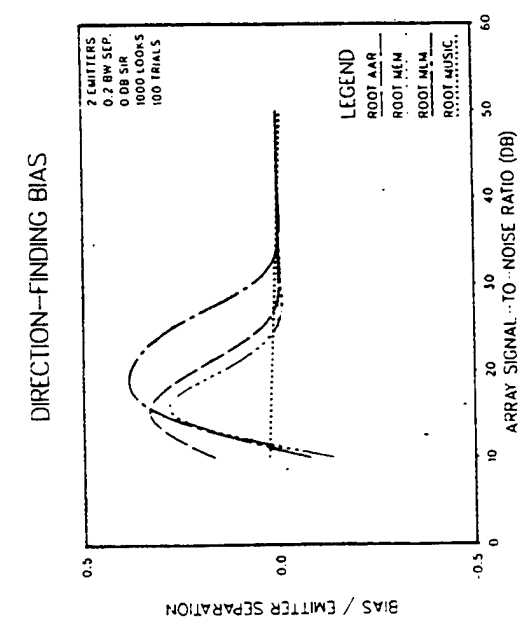
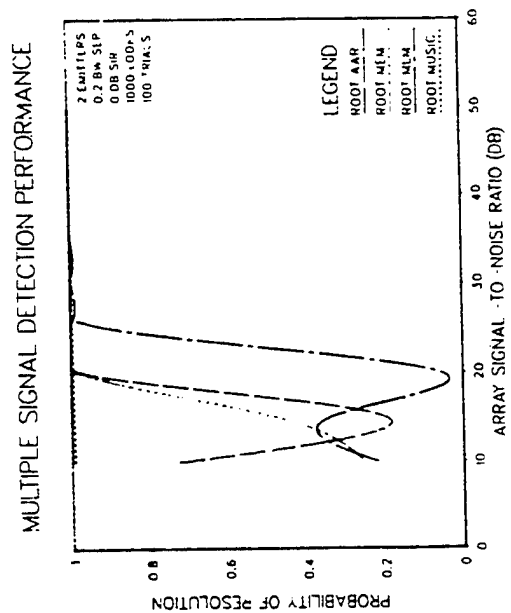


Fig. F.12.

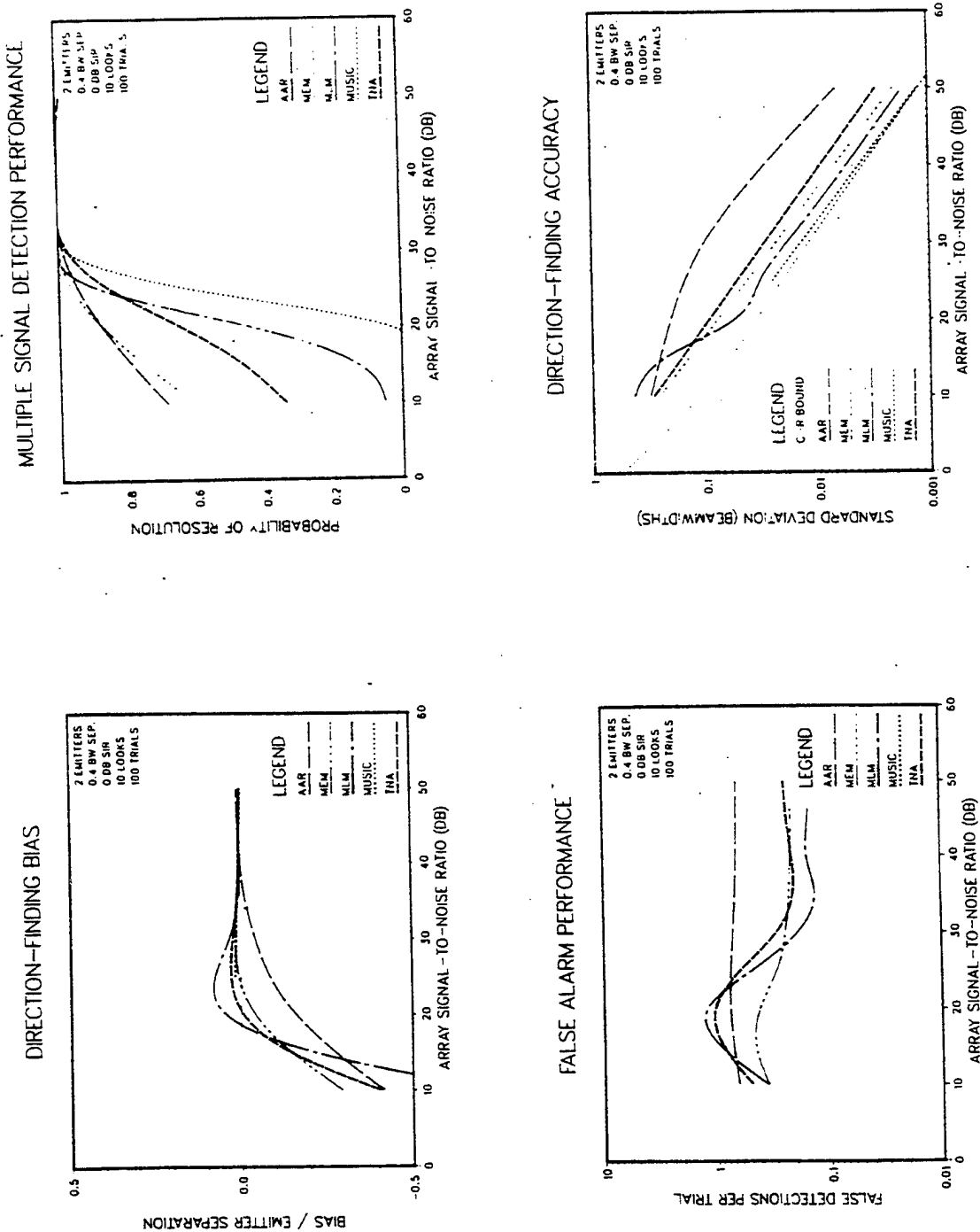


Fig. F.13.

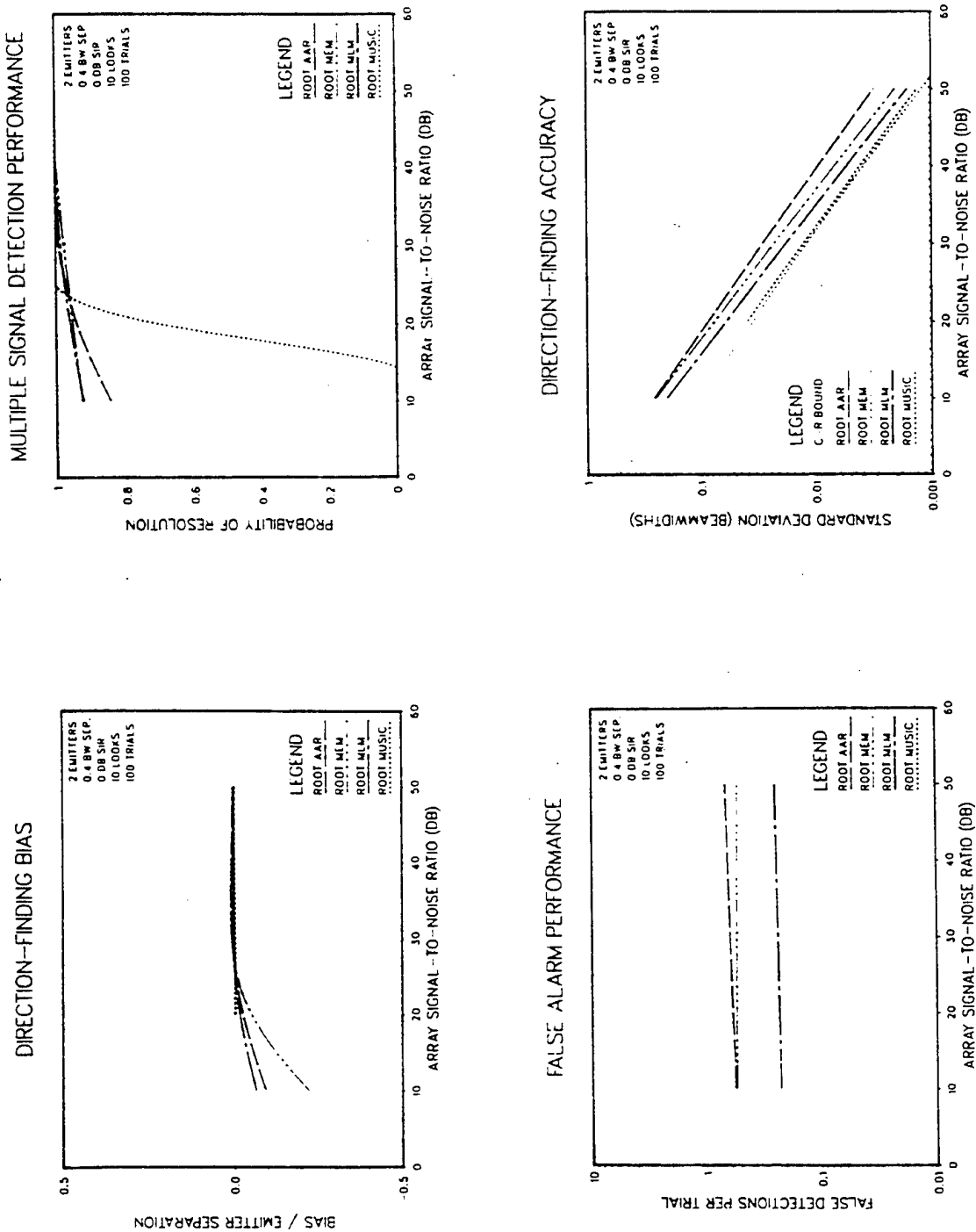


Fig. F.14.

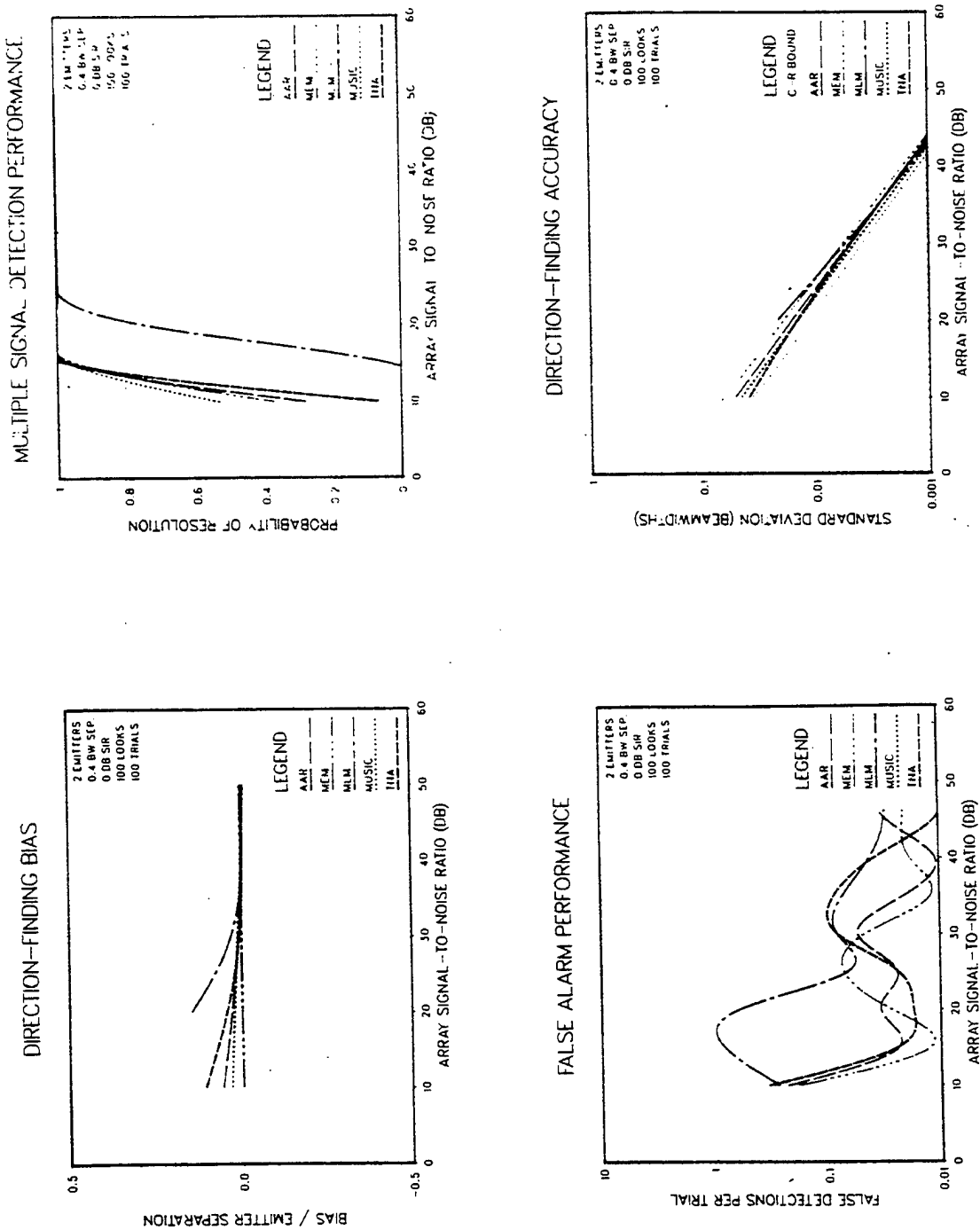


Fig. F.15.

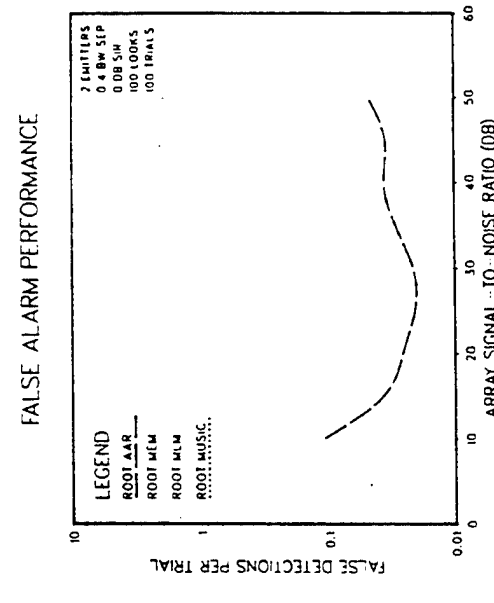
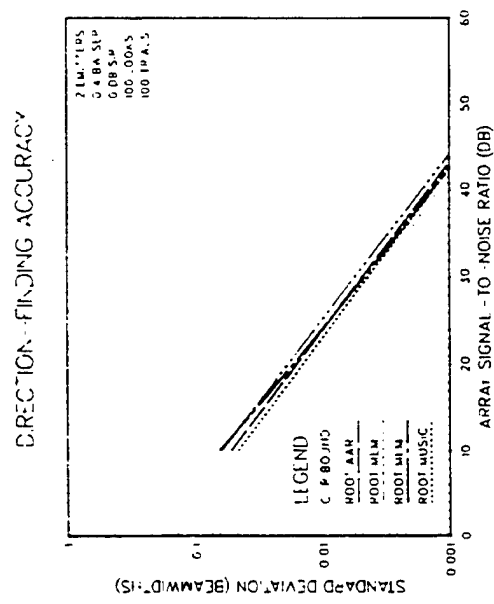
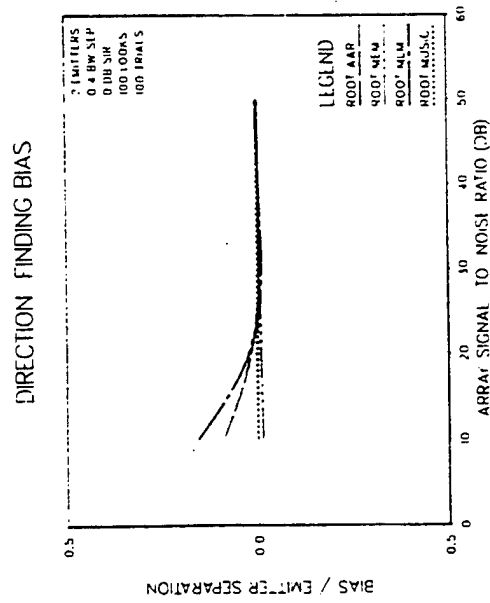
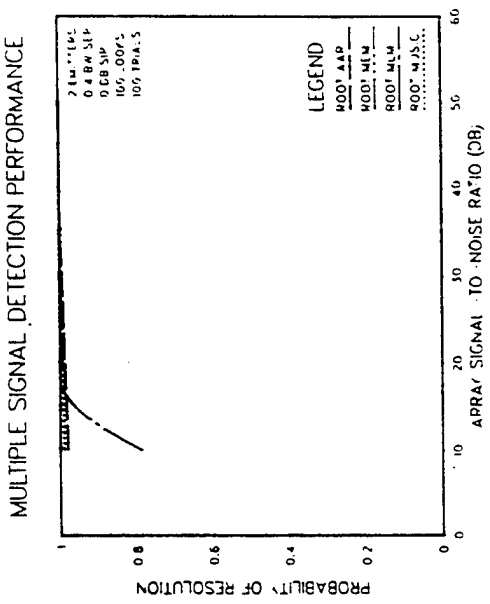


Fig. F.16.

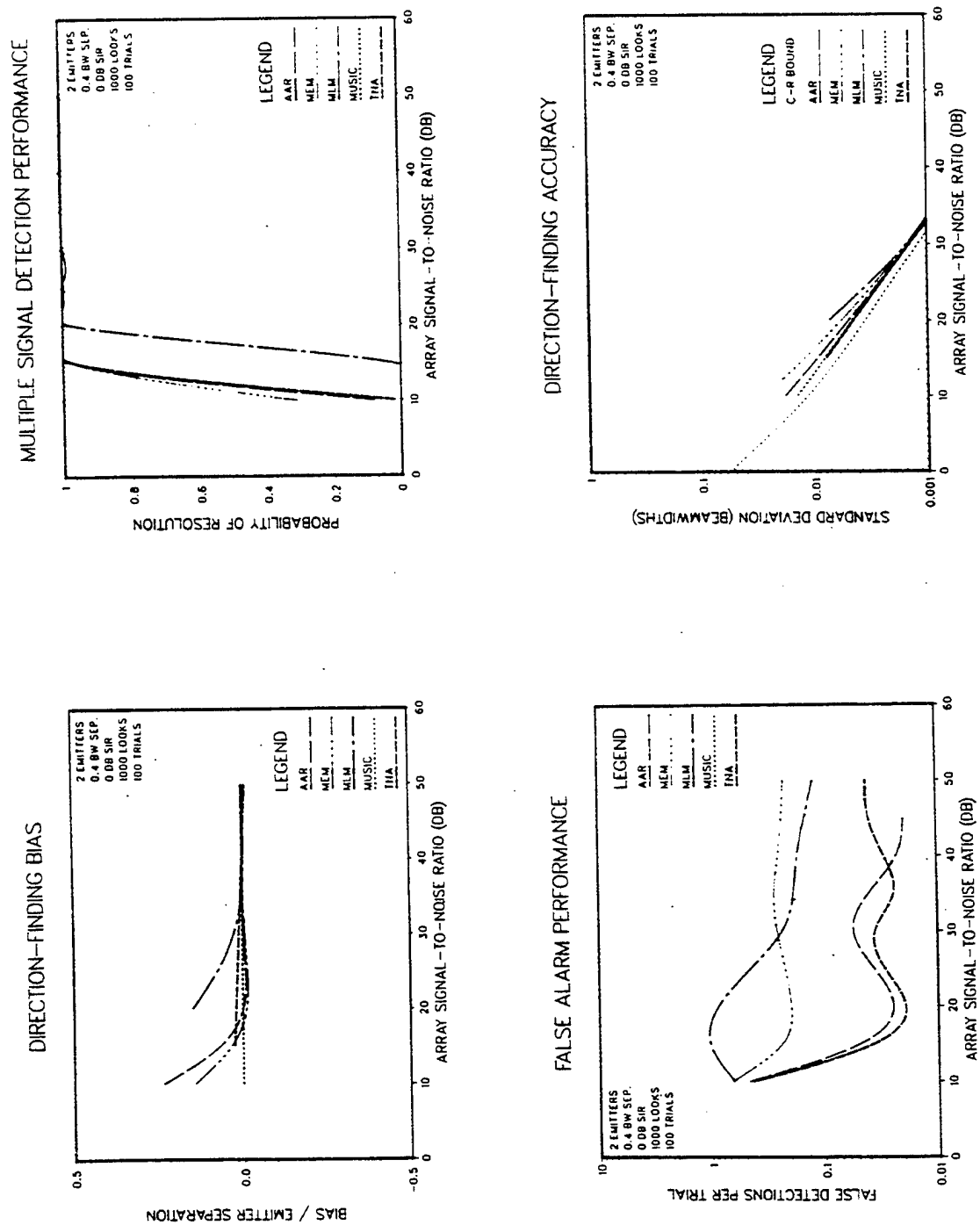


Fig. F.17.

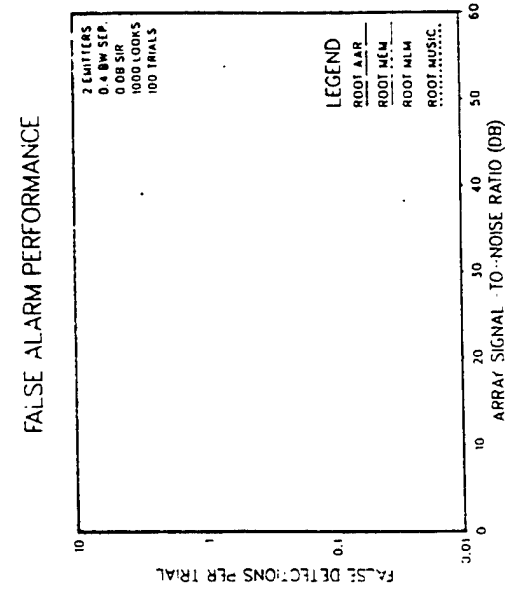
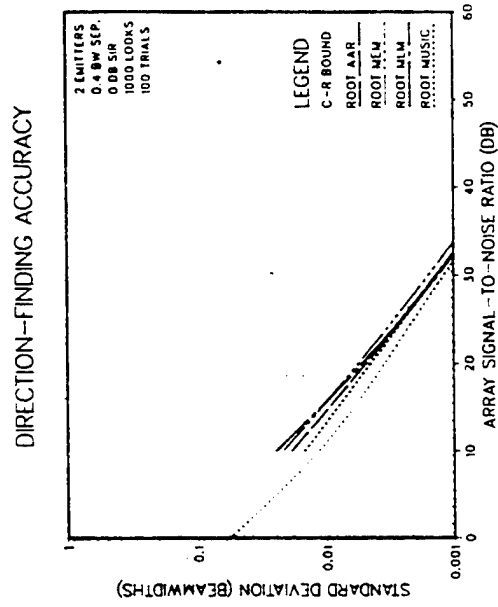
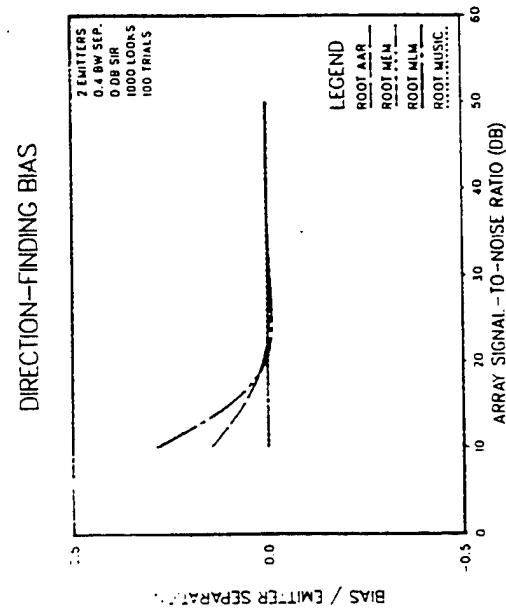
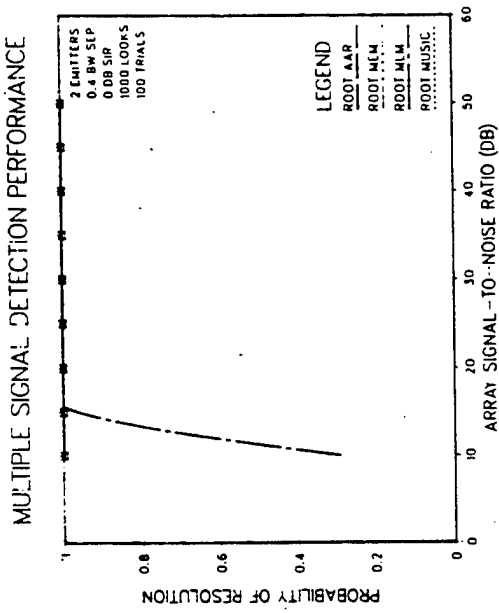


Fig. F.18.

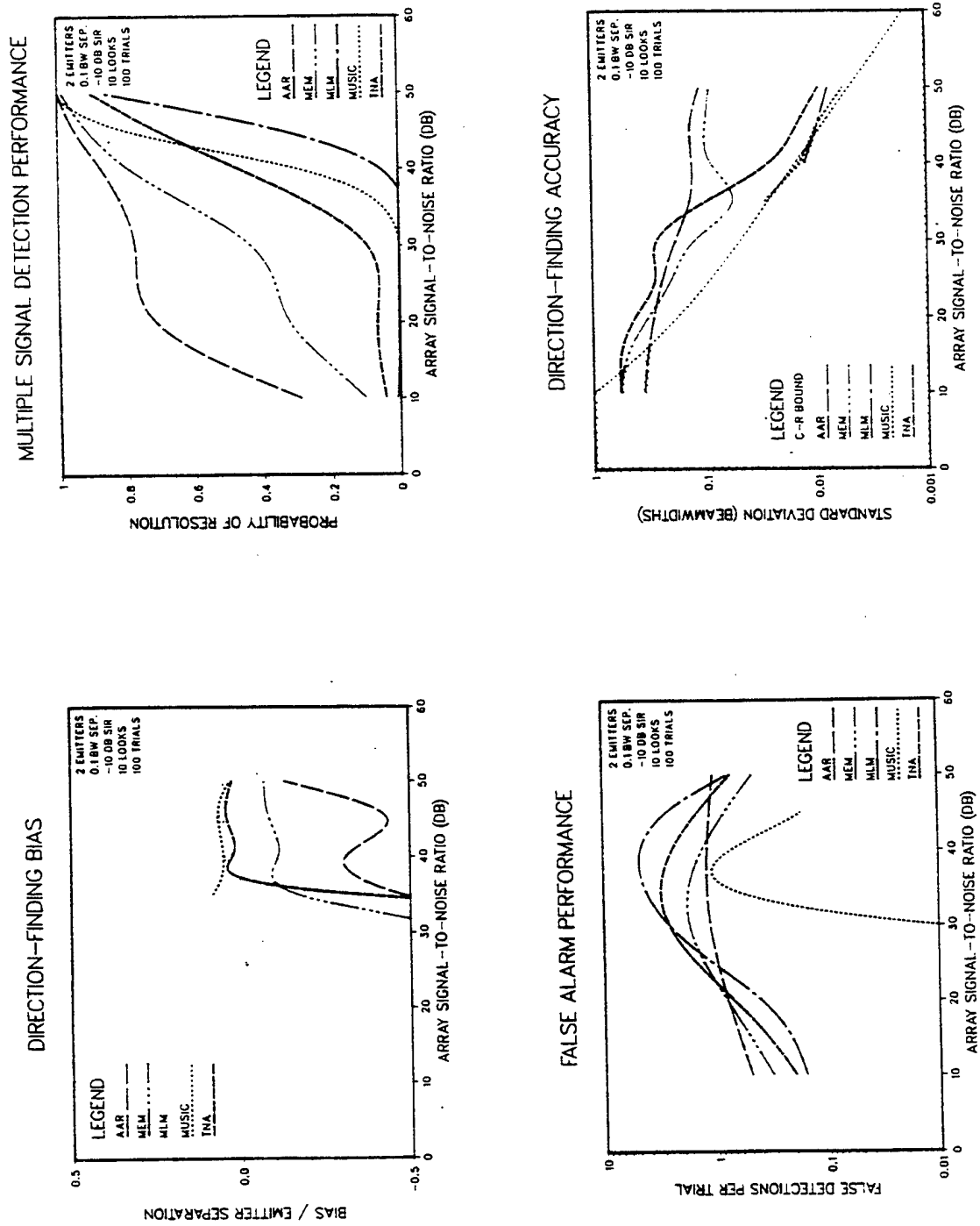


Fig. F.19.

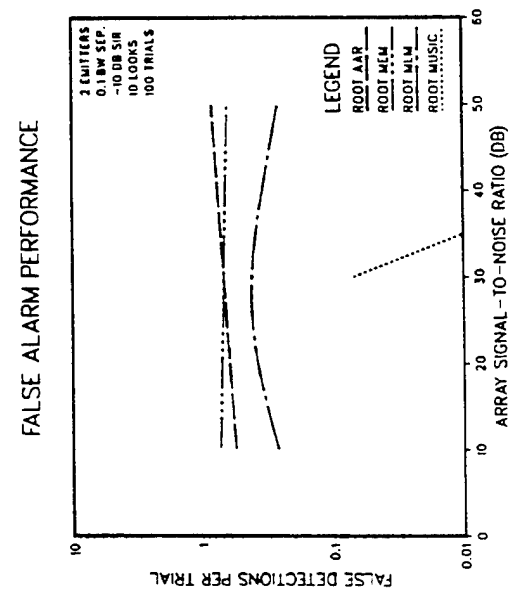
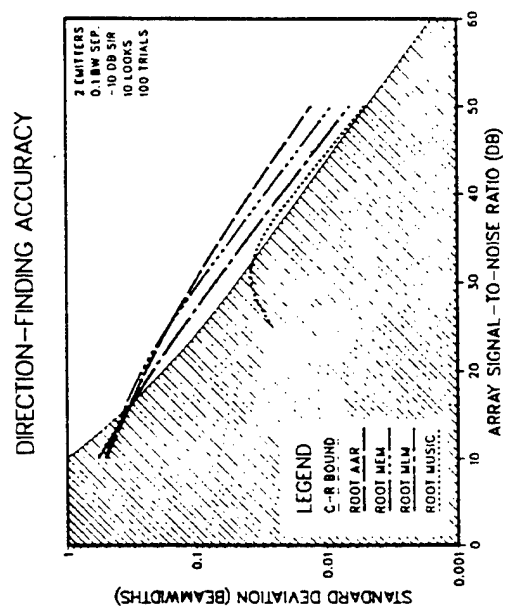
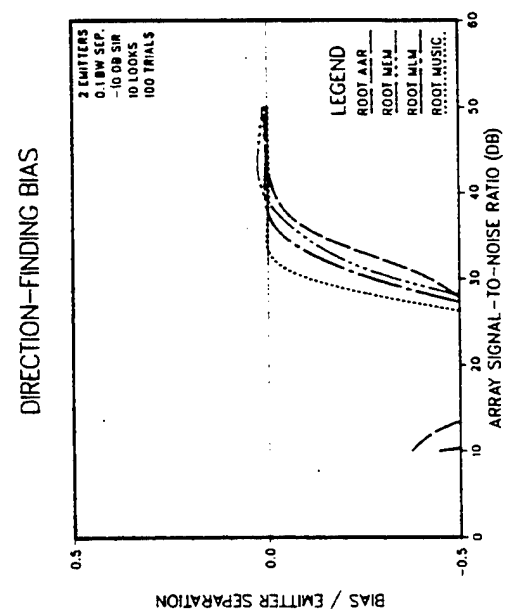
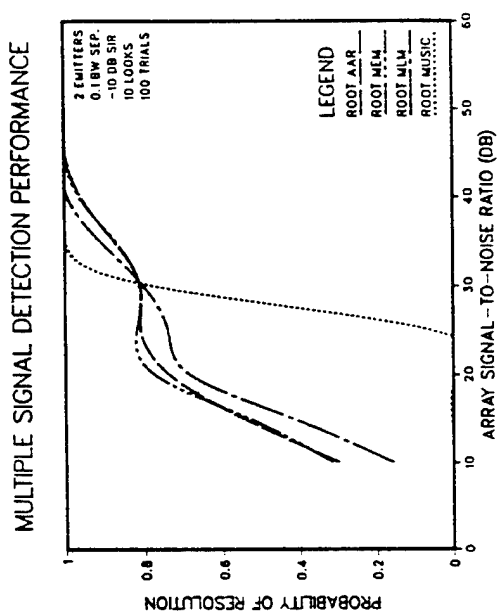


Fig. F.20.

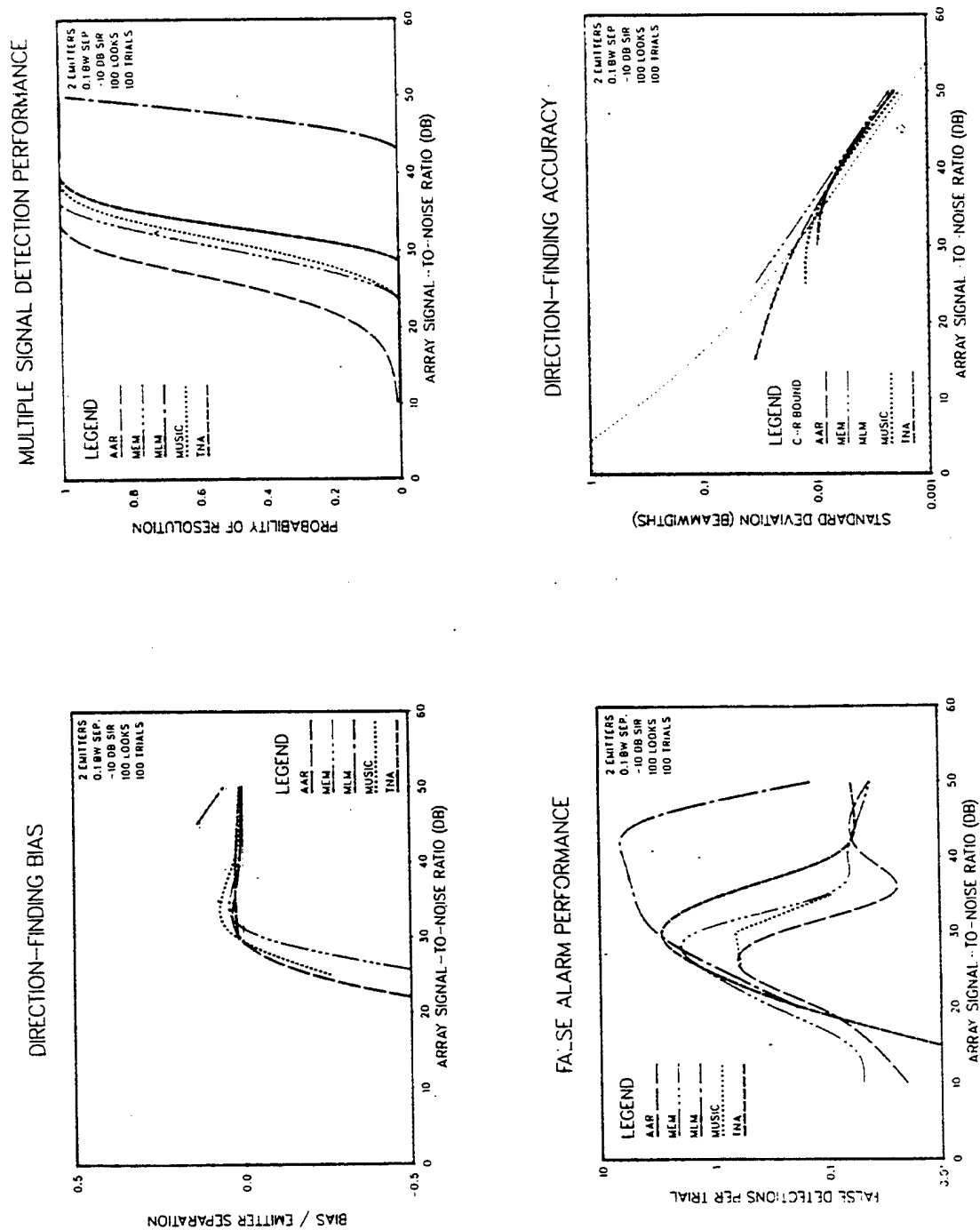
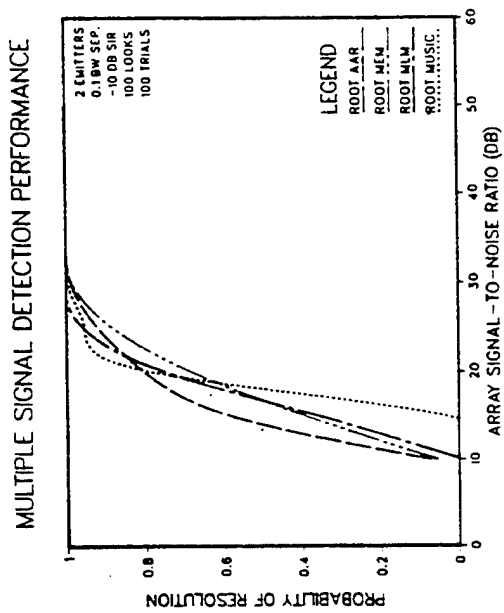
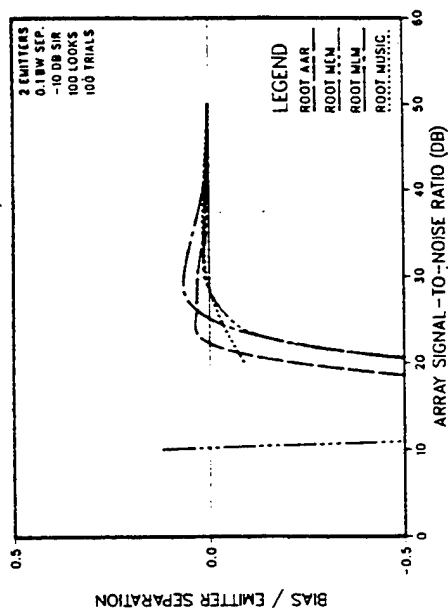


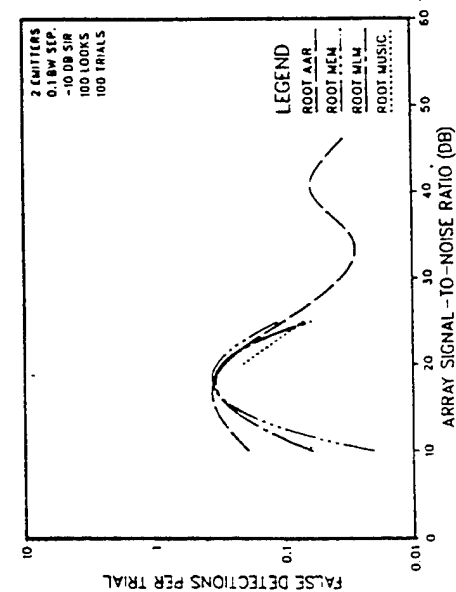
Fig. F.21.



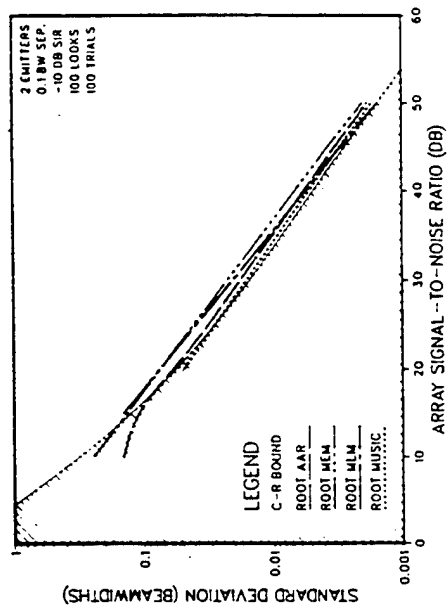
DIRECTION-FINDING BIAS



FALSE ALARM PERFORMANCE



DIRECTION-FINDING ACCURACY



MULTIPLE SIGNAL DETECTION PERFORMANCE

Fig. F.22.

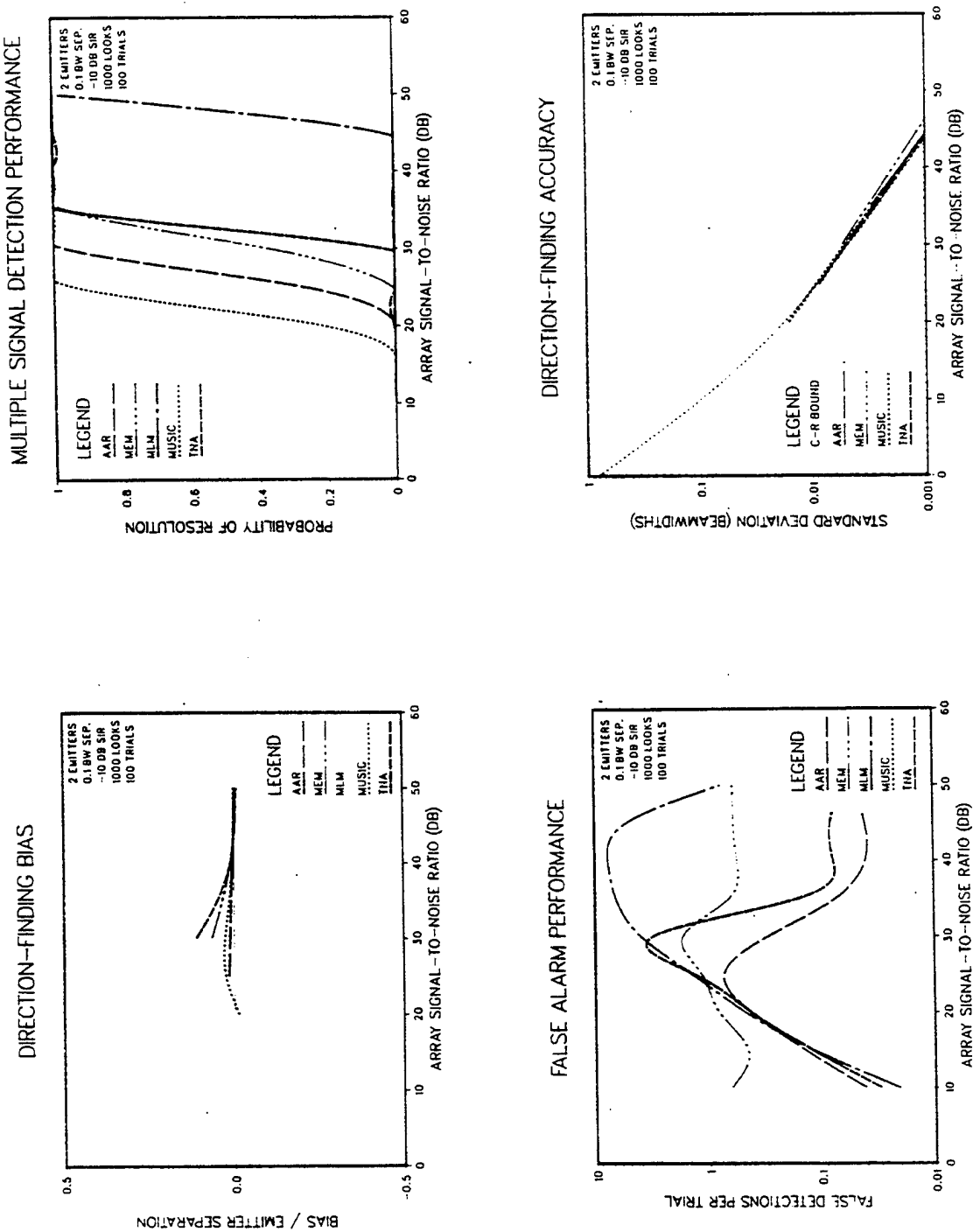


Fig. F.23.

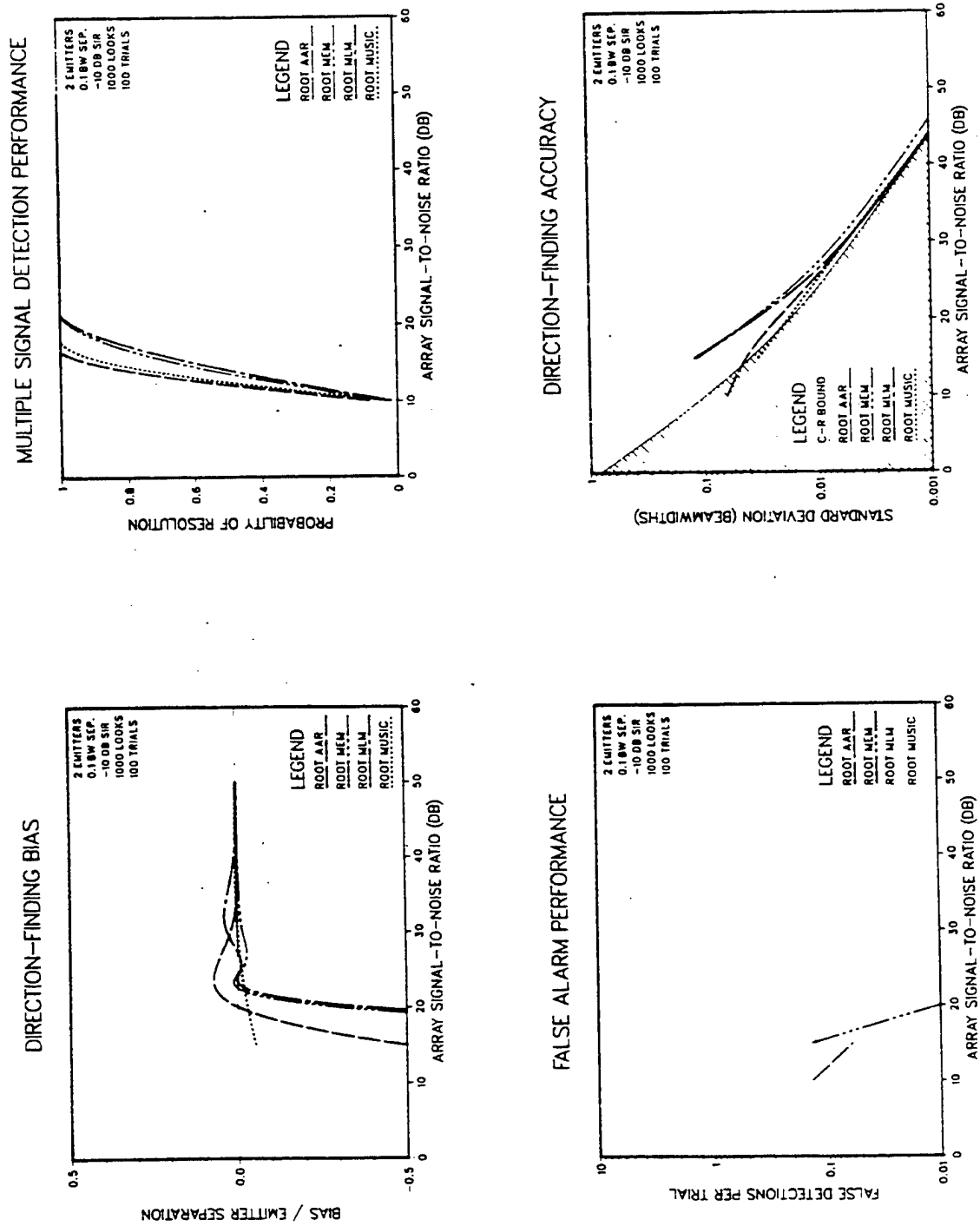
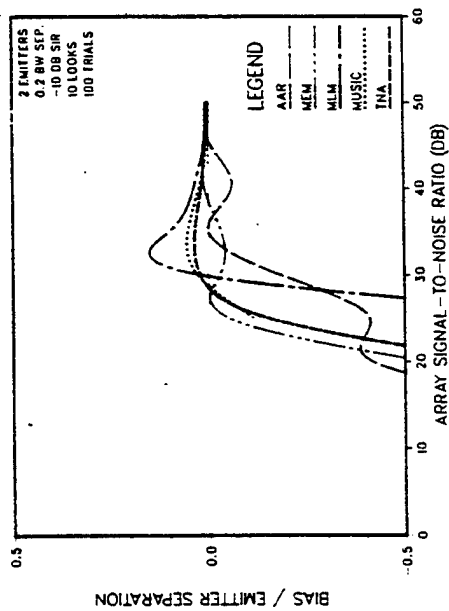
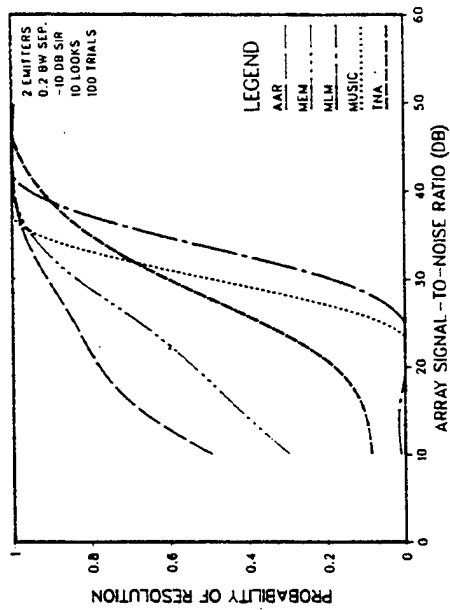


Fig. F.24.

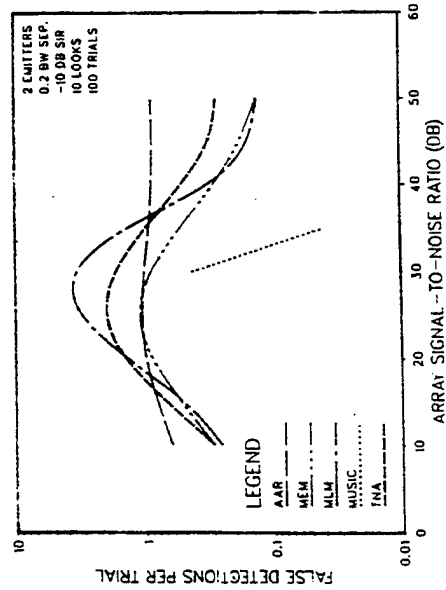
DIRECTION-FINDING BIAS



MULTIPLE SIGNAL DETECTION PERFORMANCE



FALSE ALARM PERFORMANCE



DIRECTION-FINDING ACCURACY

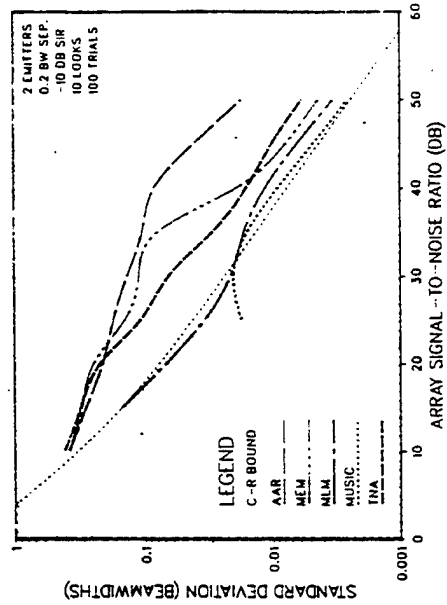


Fig. F.25.

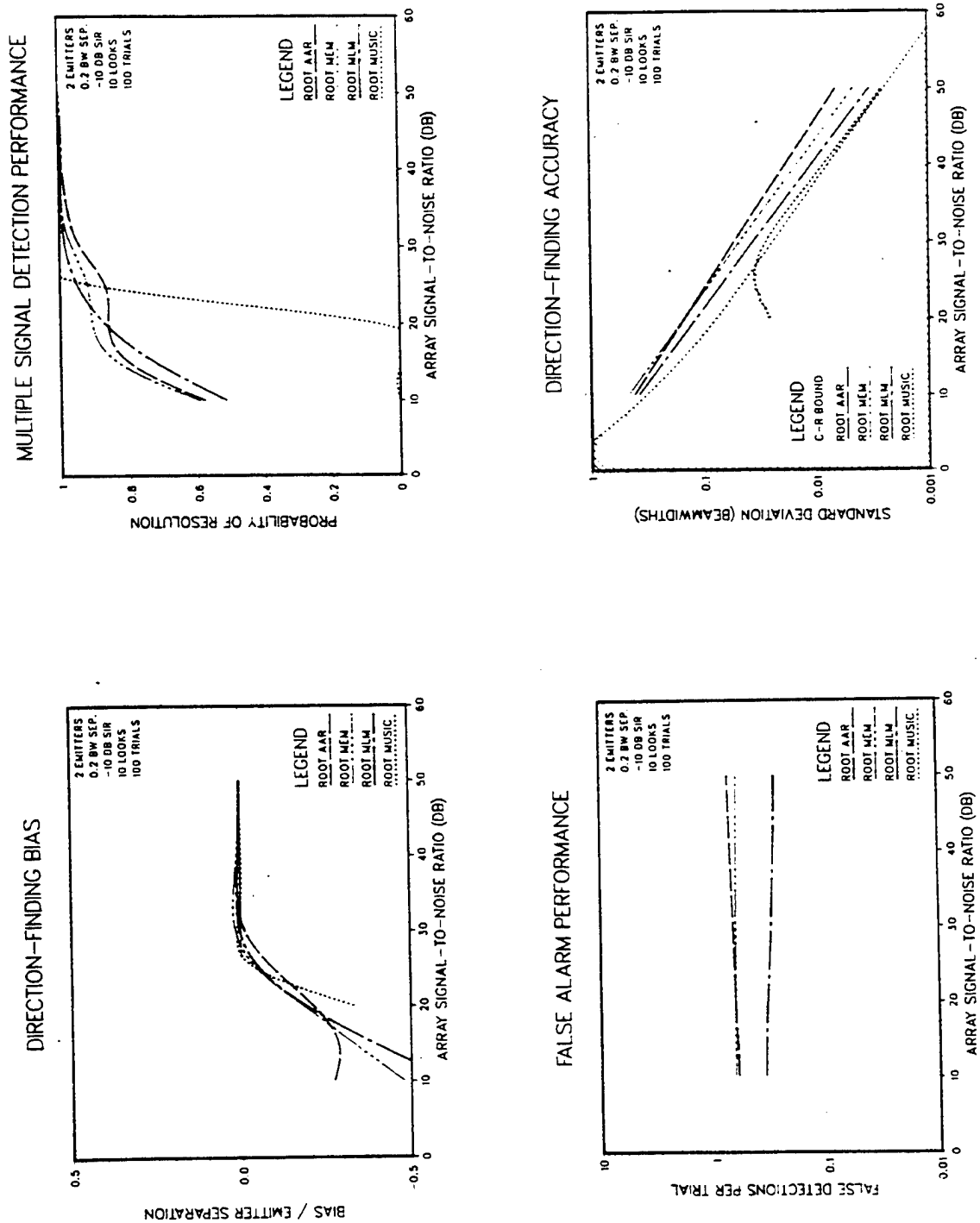


Fig. F.26.

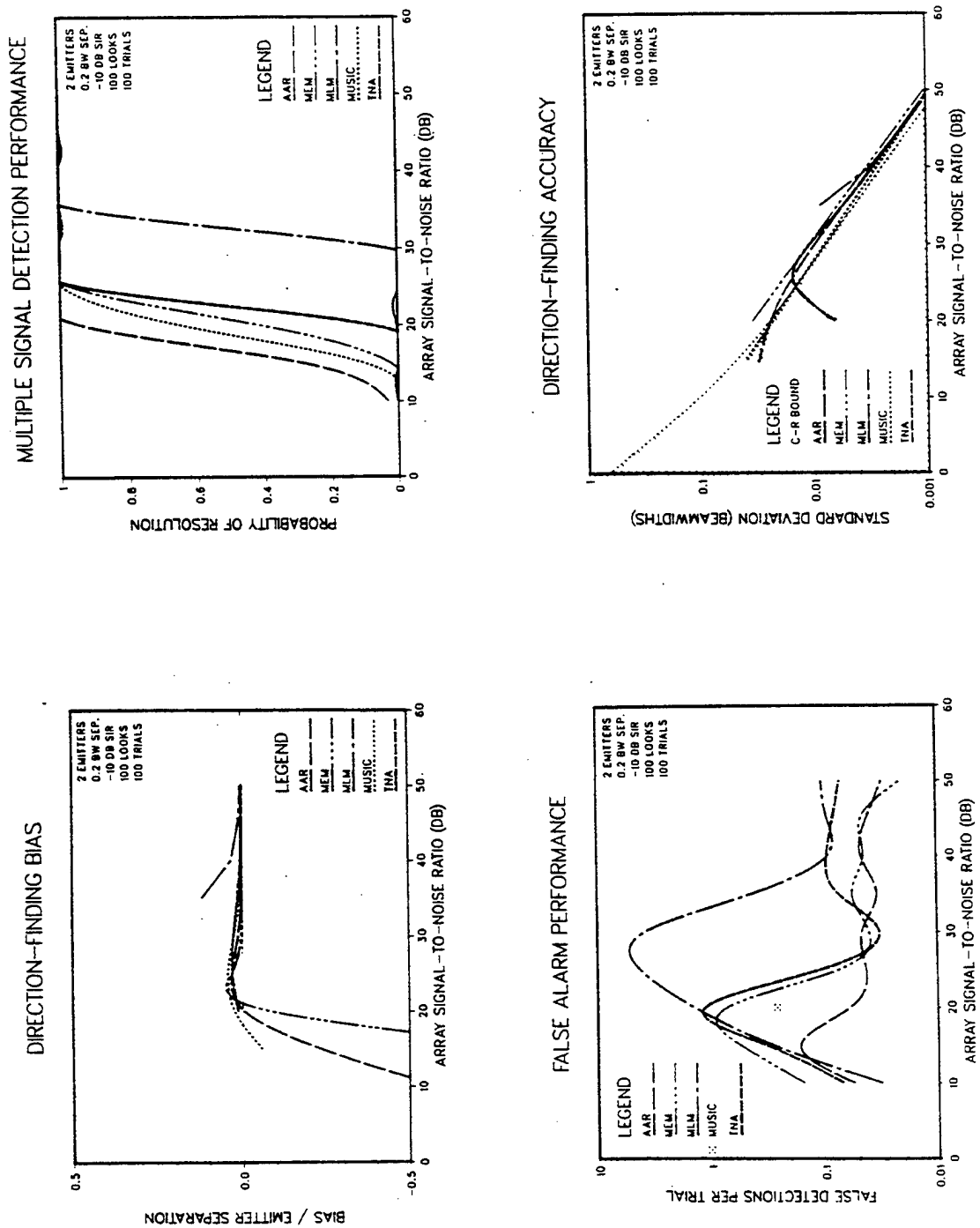


Fig. F.27.

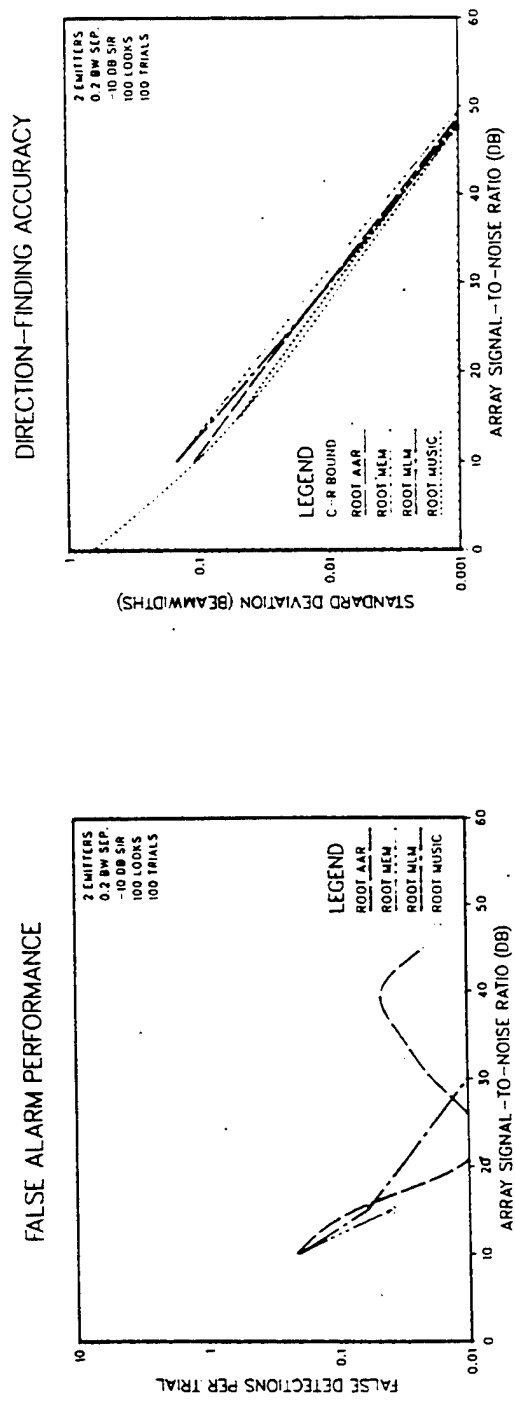
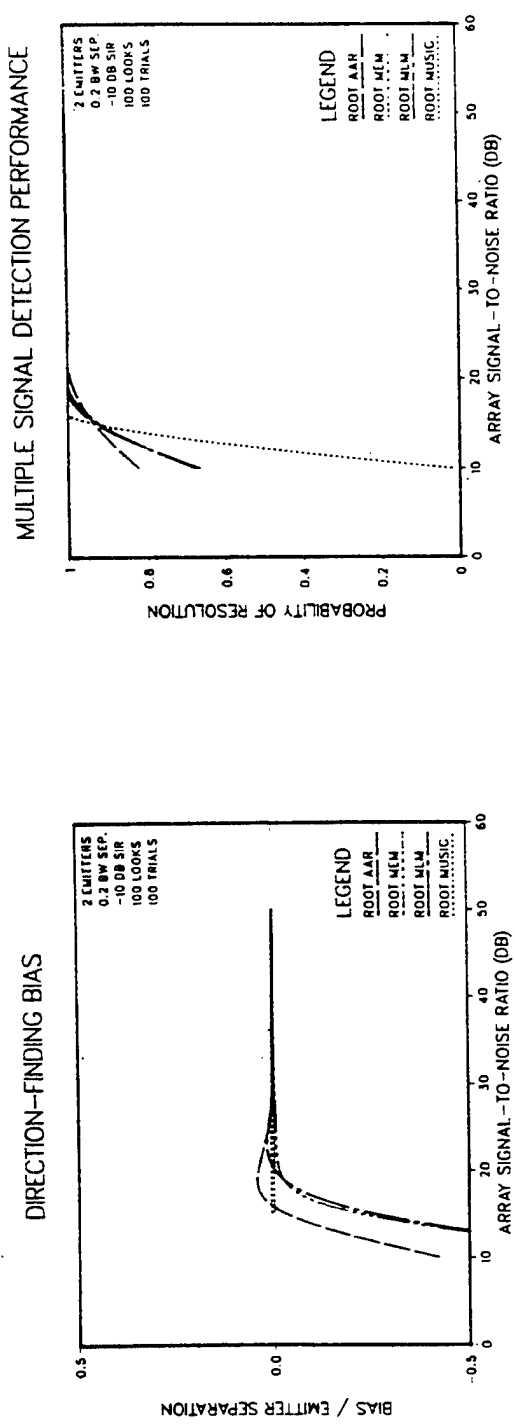


Fig. F.28.

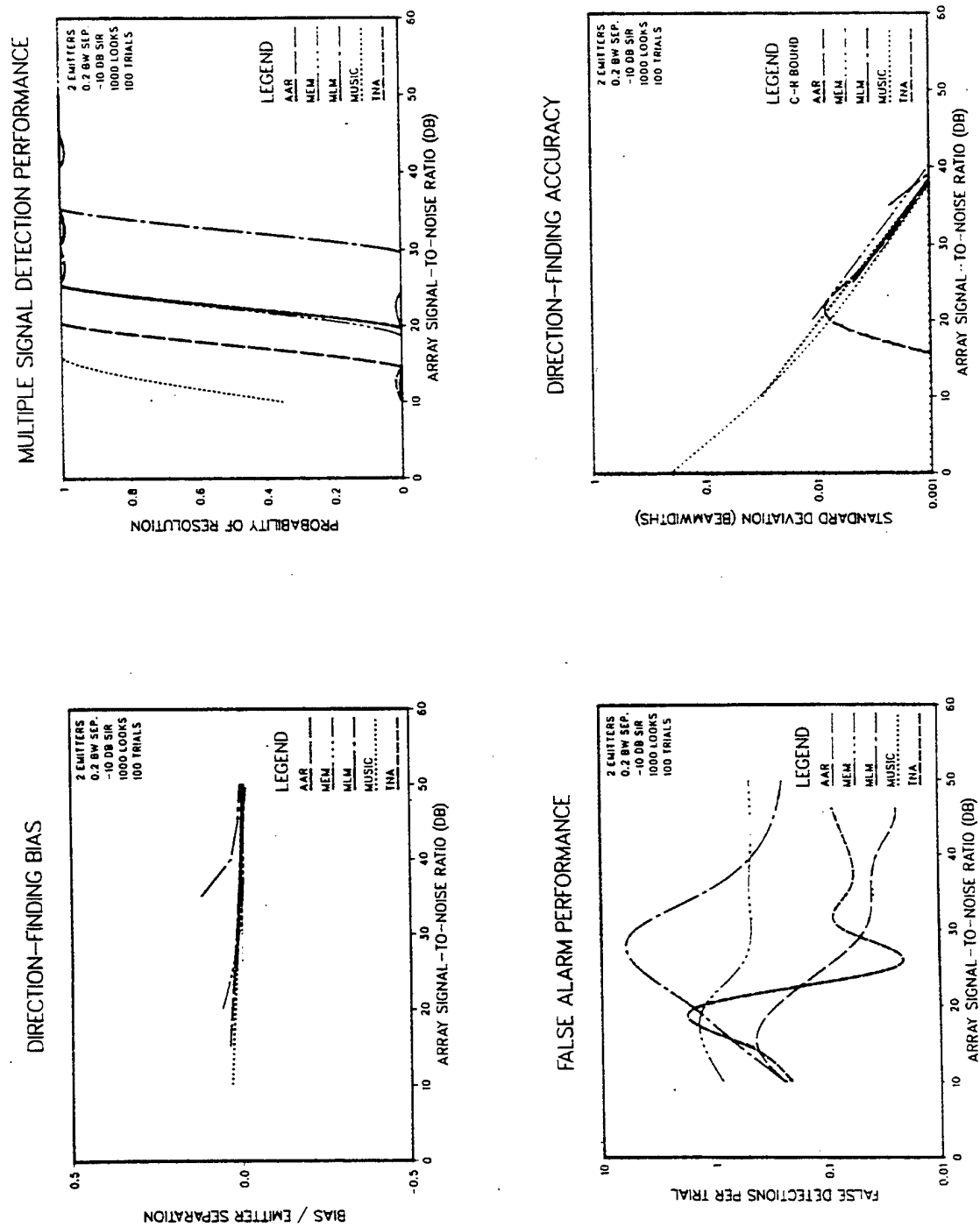


Fig. F.29.

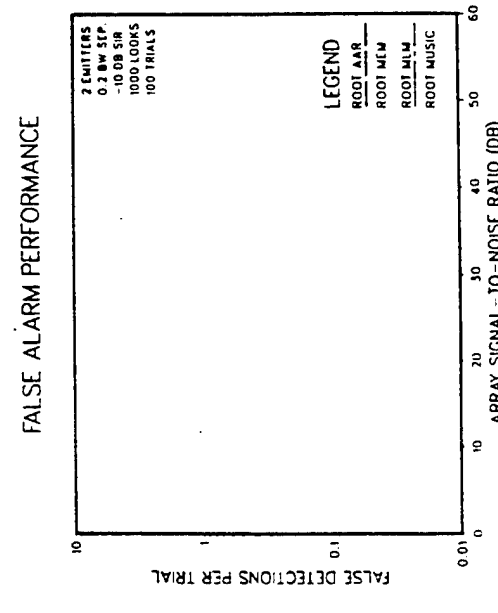
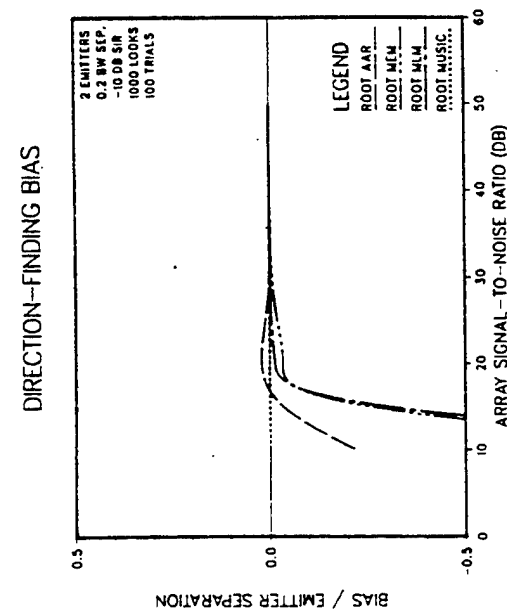
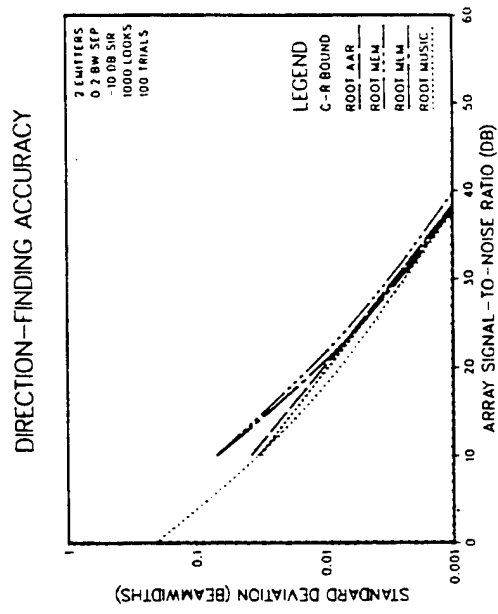
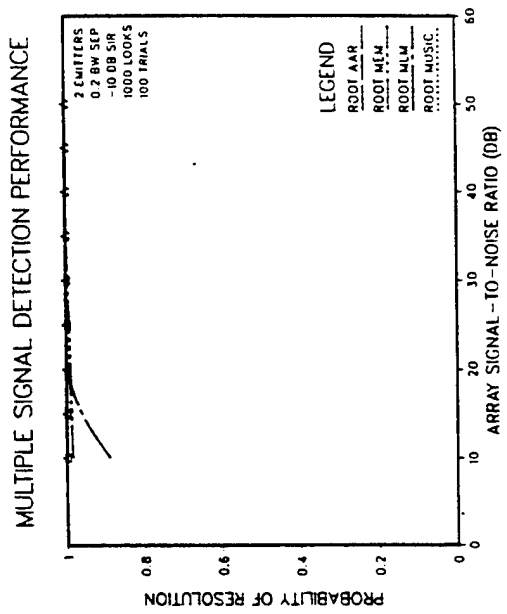
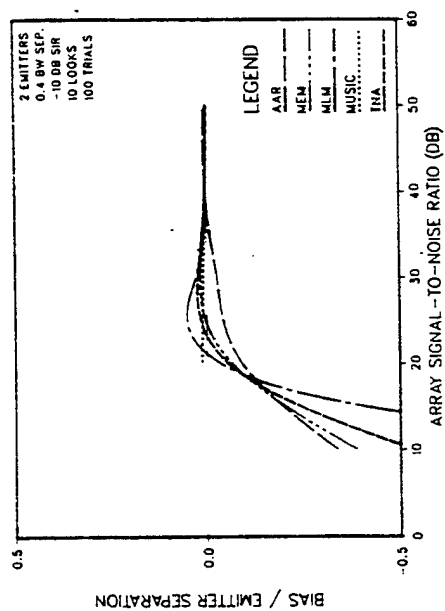
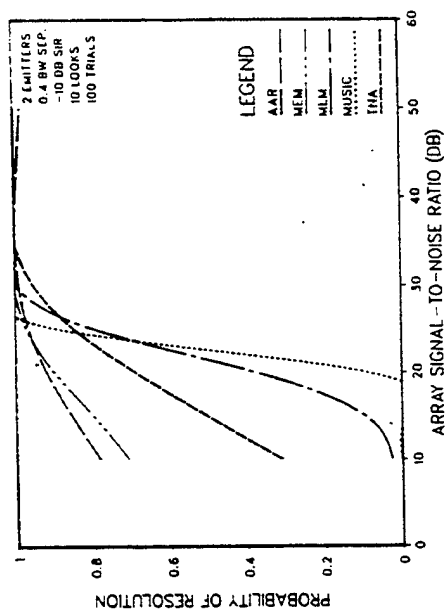


Fig. F.30.

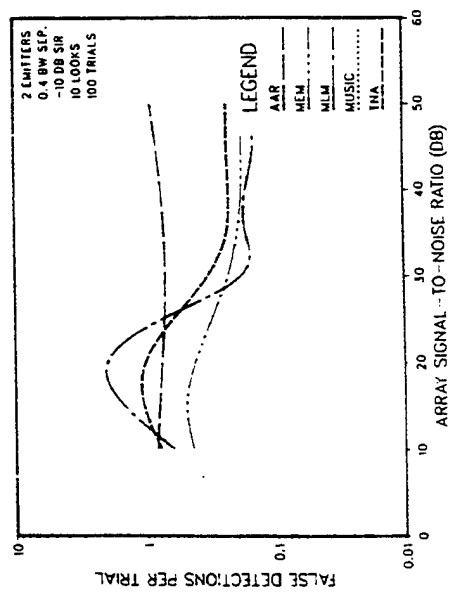
DIRECTION-FINDING BIAS



MULTIPLE SIGNAL DETECTION PERFORMANCE



FALSE ALARM PERFORMANCE



DIRECTION-FINDING ACCURACY

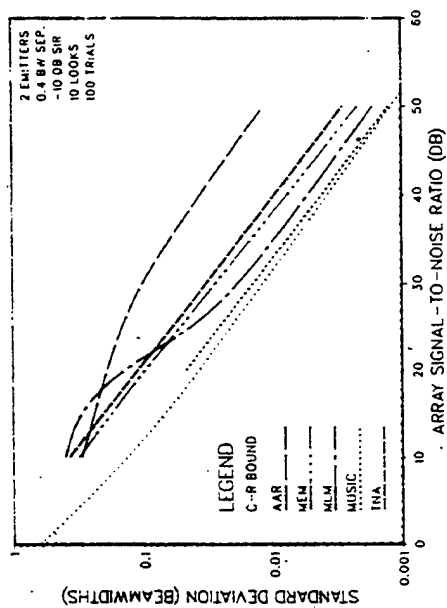


Fig. F.31.

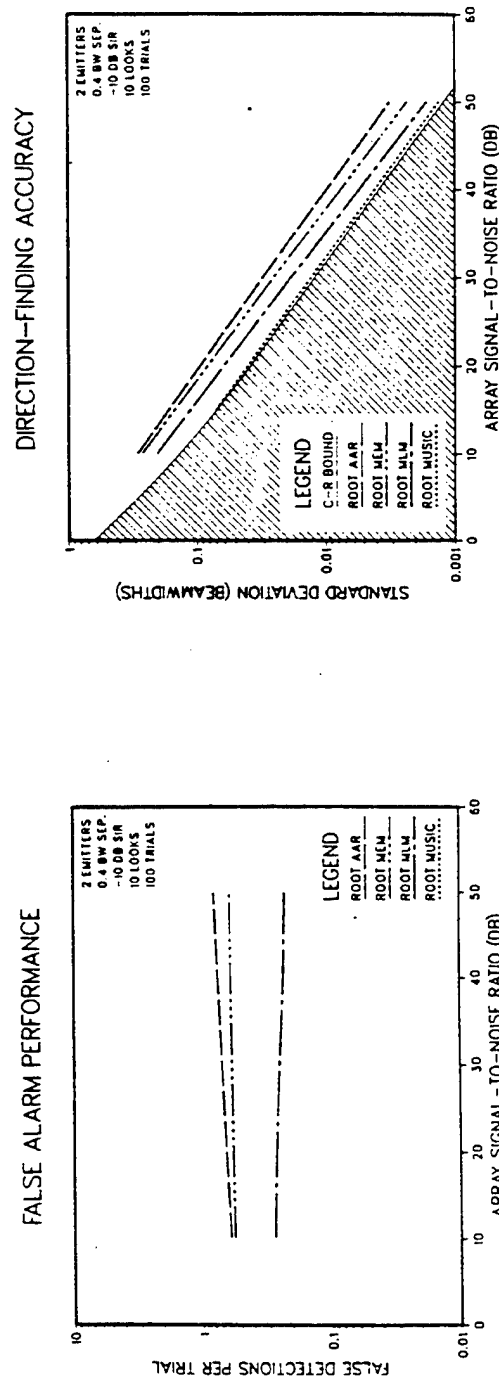
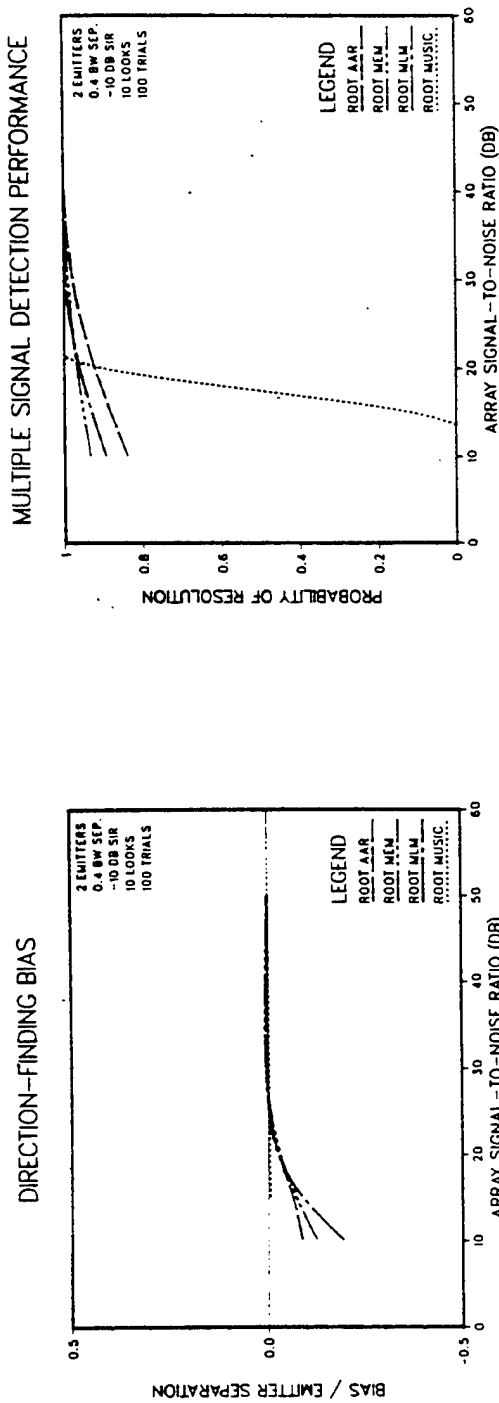


Fig. F.32.

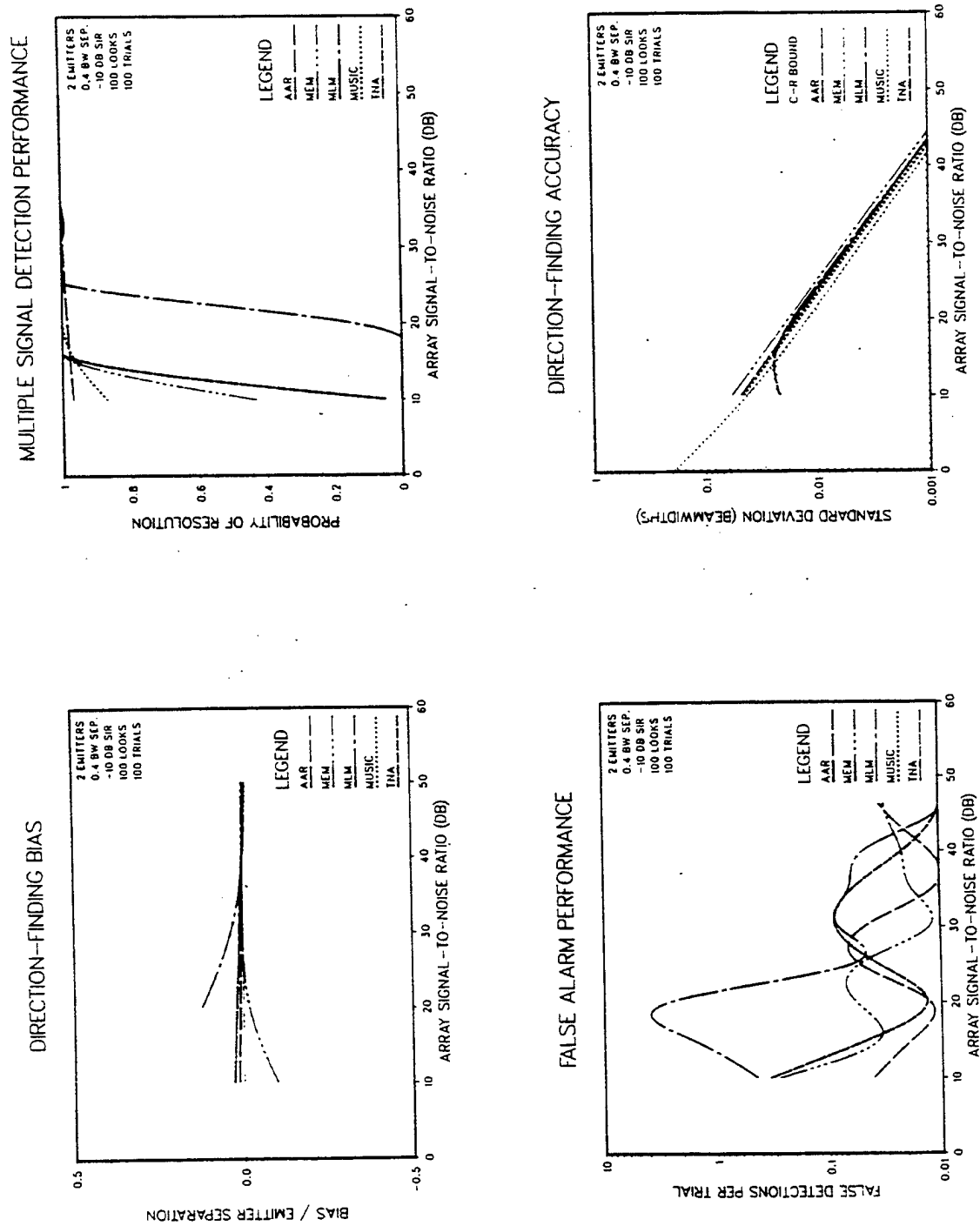


Fig. F.33.

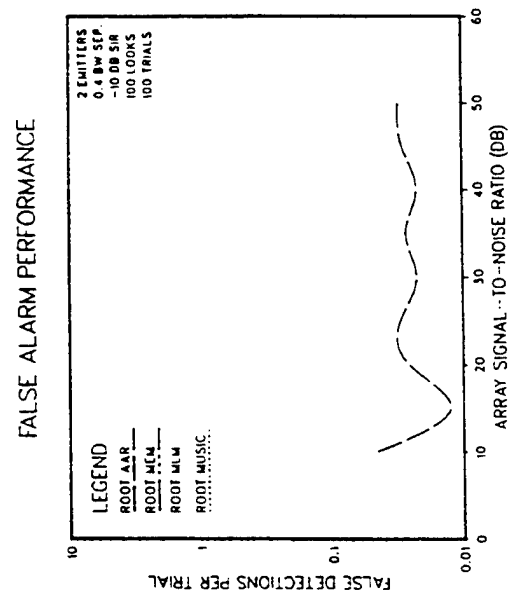
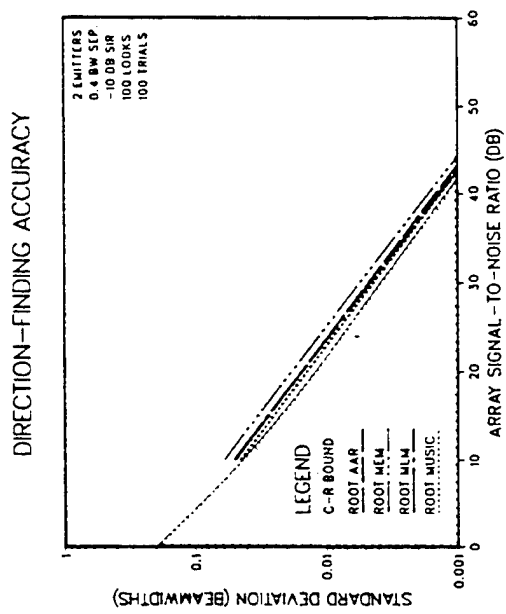
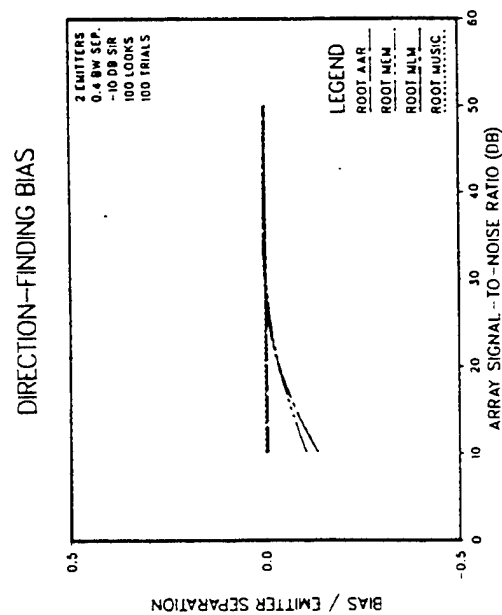
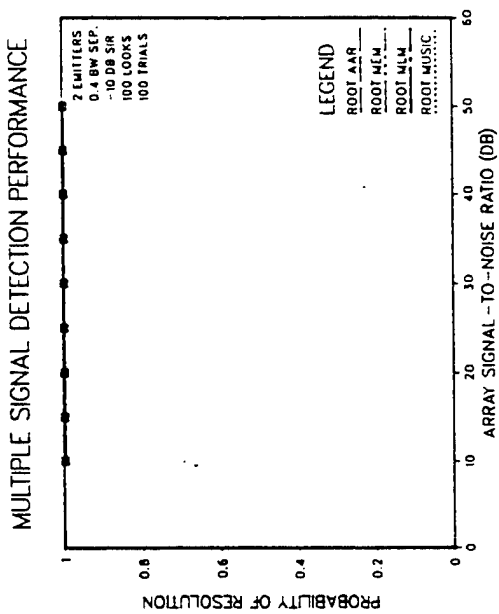
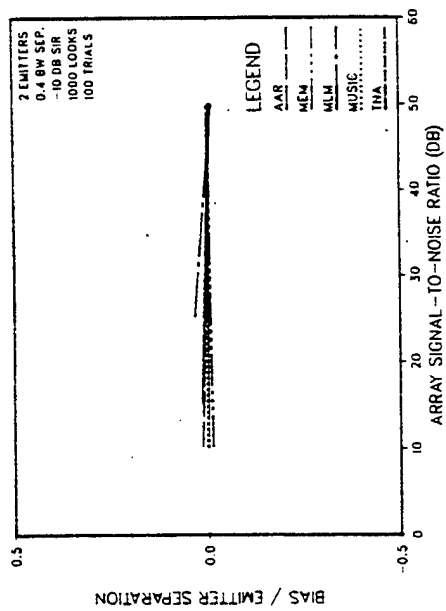
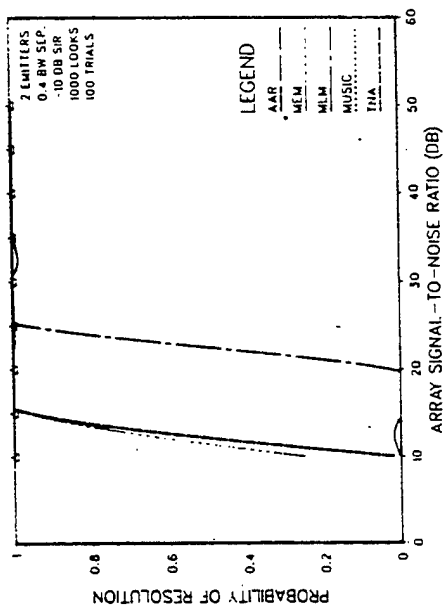


Fig. F.34.

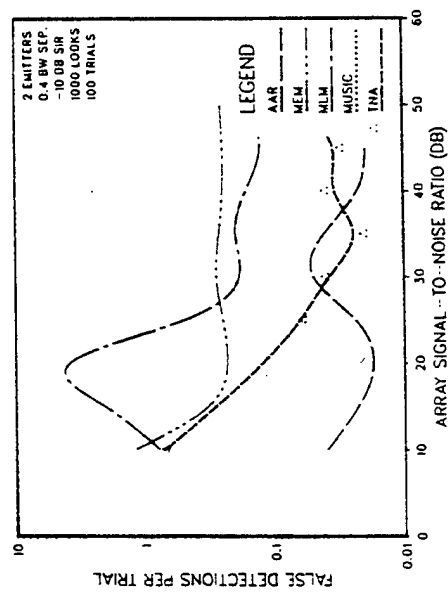
DIRECTION-FINDING BIAS



MULTIPLE SIGNAL DETECTION PERFORMANCE



FALSE ALARM PERFORMANCE



DIRECTION-FINDING ACCURACY

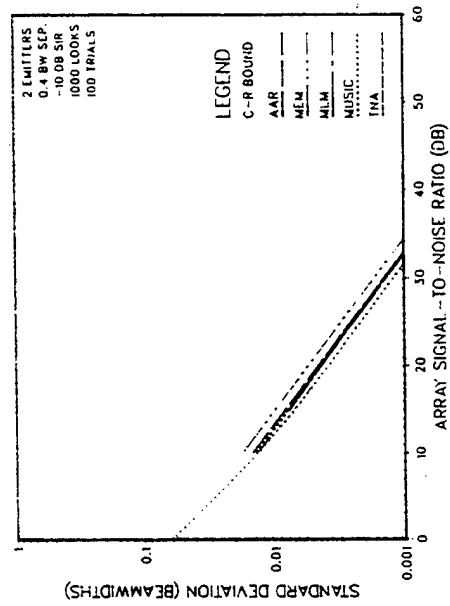


Fig. F.35.

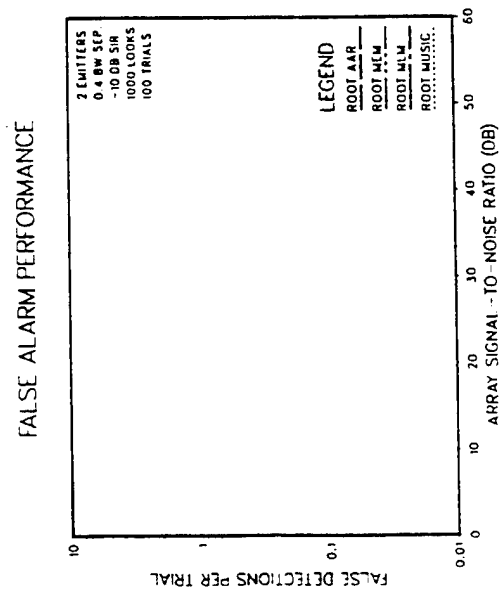
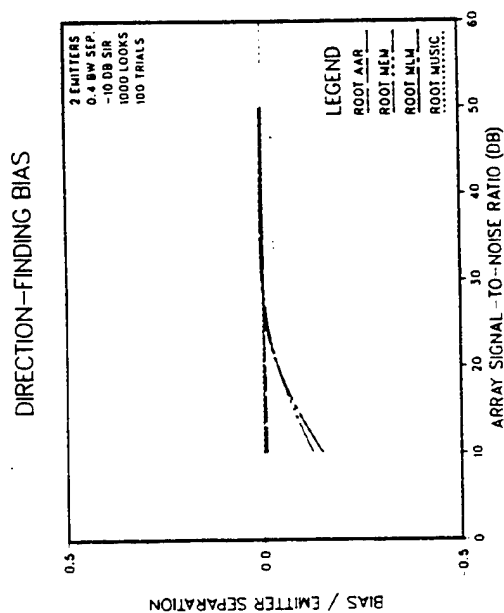
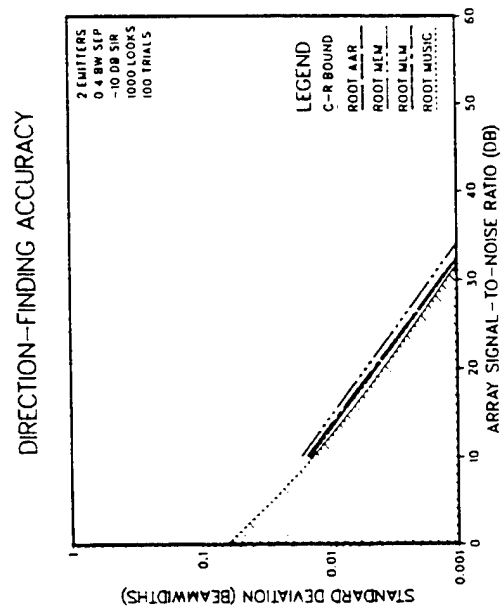
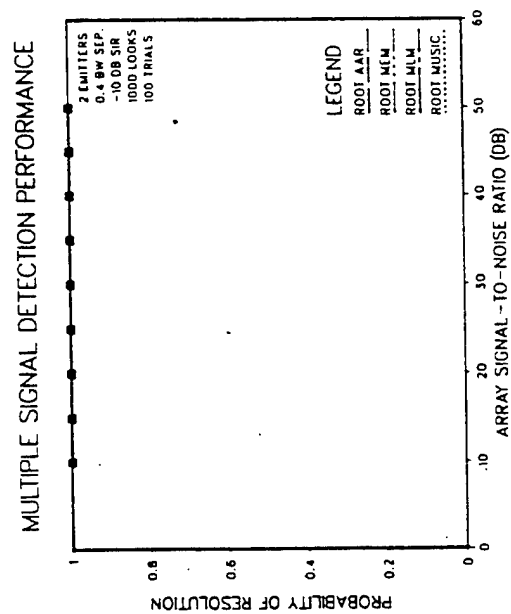


Fig. F.36.

Appendix G
ADAPTIVE LISTENING EXPERIMENTS

The results of the Monte Carlo experiments described in Section IV.B. are included here in their entirety. The curves in these figures all represent loci of 10 dB output signal-to-interference-plus-noise ratio for a two-emitter problem with the desired signal 10 dB weaker than the interferer. The results are divided into three sections: (1) Model Covariance Method Experiments (pp. G-3 - G-14); (2) Projection Method Experiments (pp. G-15 - G-26); and (3) Effects of Likelihood Ratio Test for MUSIC (pp. G-27 - G-30).

In the first two sections, three different parameter variations are explored:

(1) DF Method Group

A.	ARM*	B.	ROOTMEM
	AAR		ROOTTNA
	MEM		ROOTMLM*
	TNA		ROOTMUSIC*
	MUSIC*		
	MLM		

(2) Snapshot Group

A.	20	B.	100
----	----	----	-----

(3) Calibration Error Group

A.	0 dB Amplitude	B.	0.05 dB	C.	0.5 dB
	0° Phase		0.5°		5.0°

Using these group designations, the 24 summary plots for the Model Covariance Method and Projection Nulling Method can be indexed as follows:

*Note that in the projection method evaluation only the algorithms indicated were compared, since the results tended to be identical with those obtained for the model covariance method.

DF METHOD GROUP	SNAPSHOT GROUP	CALIBRATION ERROR GROUP	MODEL COVARIANCE METHOD FIGURE	PROJECTION NULLING FIGURE
A	A	A	G-1	G-13
		B	-2	-14
		C	-3	-15
	B	A	-4	-16
		B	-5	-17
		C	-6	-18
B	A	A	-7	-19
		B	-8	-20
		C	-9	-21
	B	A	-10	-22
		B	-11	-23
		C	-12	-24

The remaining four plots (G-25 to -28) illustrate the impact of the alternative likelihood ratio tests for driving MUSIC and Root MUSIC, as described in Section III.A and Appendix C. It can be seen from these results that, even for only 20 array snapshots, the choice of LRT is not important for signals separated by less than 0.4 beamwidths with spectral MUSIC or less than 0.2 beamwidths for Root MUSIC. Moreover, even in the worst case, the impact of the choice of LRT is only seen to be at most a couple of dB in required array SNR. Thus, we conclude that the choice of LRT is more important as a factor in direction-finding performance than it is for adaptive listening.

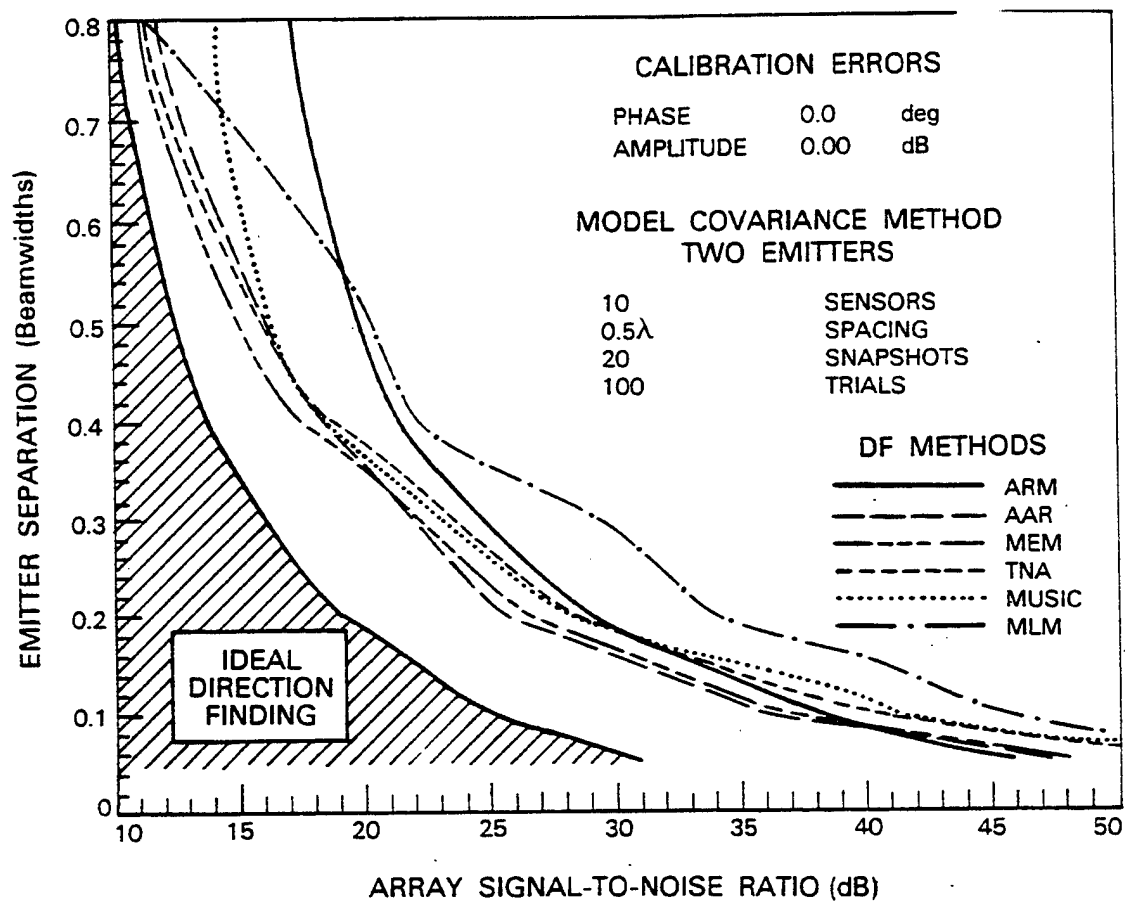


Fig. G.1.

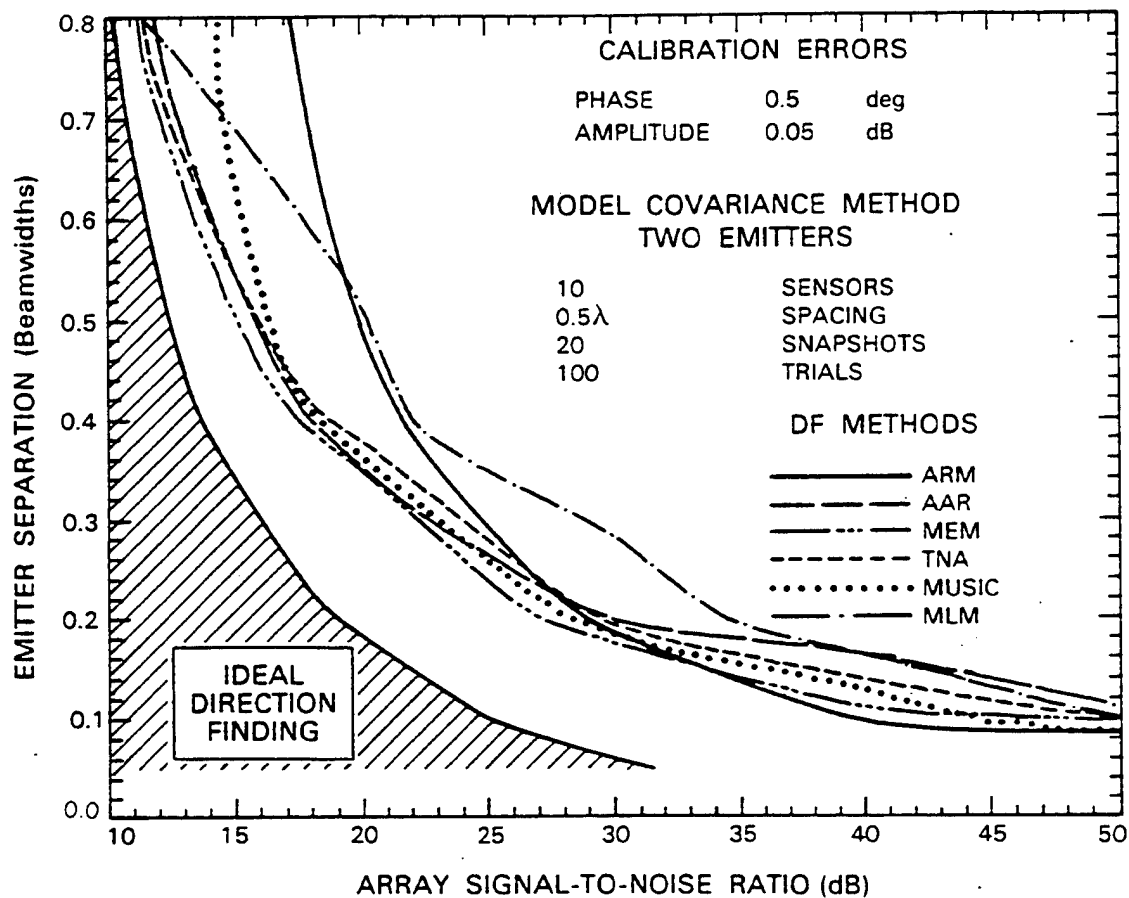


Fig. G.2.

CALIBRATION ERRORS

PHASE 5.0 deg
 AMPLITUDE 0.50 dB

MODEL COVARIANCE METHOD TWO EMITTERS

10 SENSORS
 0.5λ SPACING
 20 SNAPSHOT
 100 TRIALS

DF METHODS

ARM —————
 AAR ————
 MEM ————
 TNA ————
 MUSIC
 MLM ————

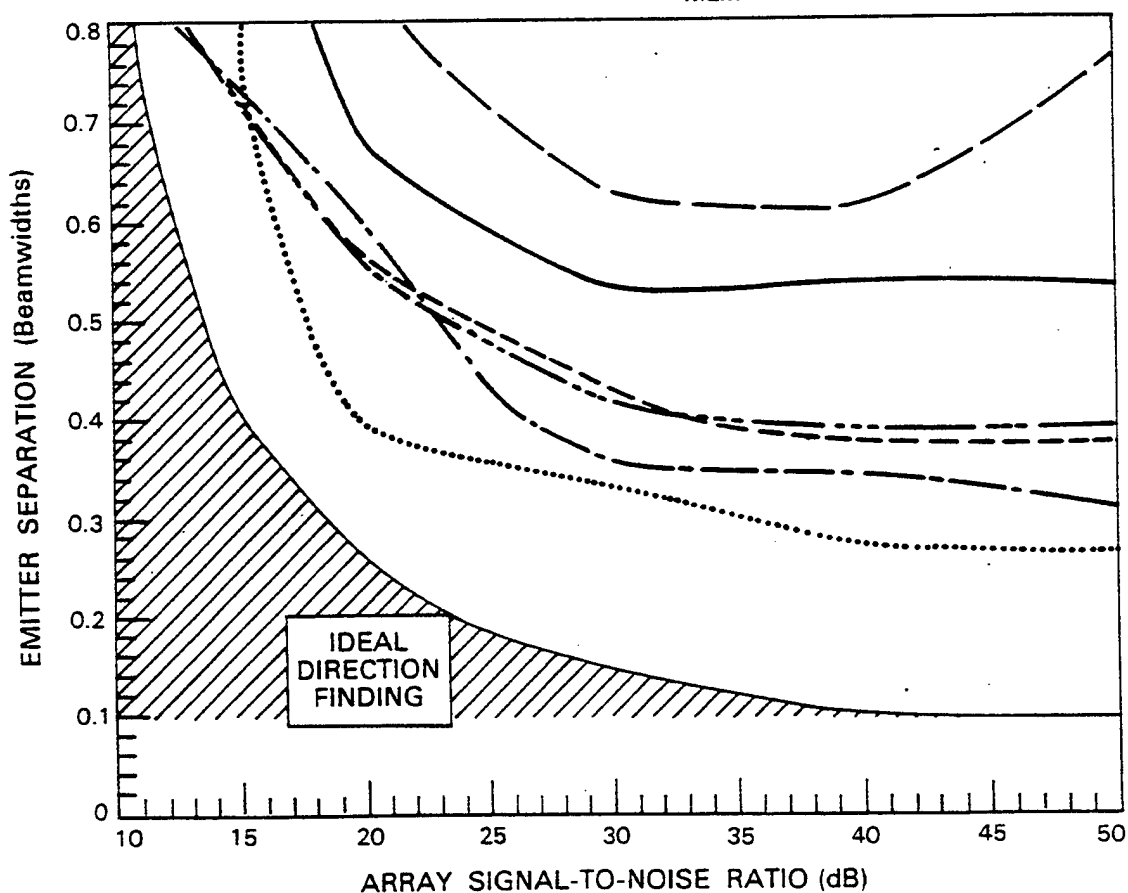


Fig. G.3.

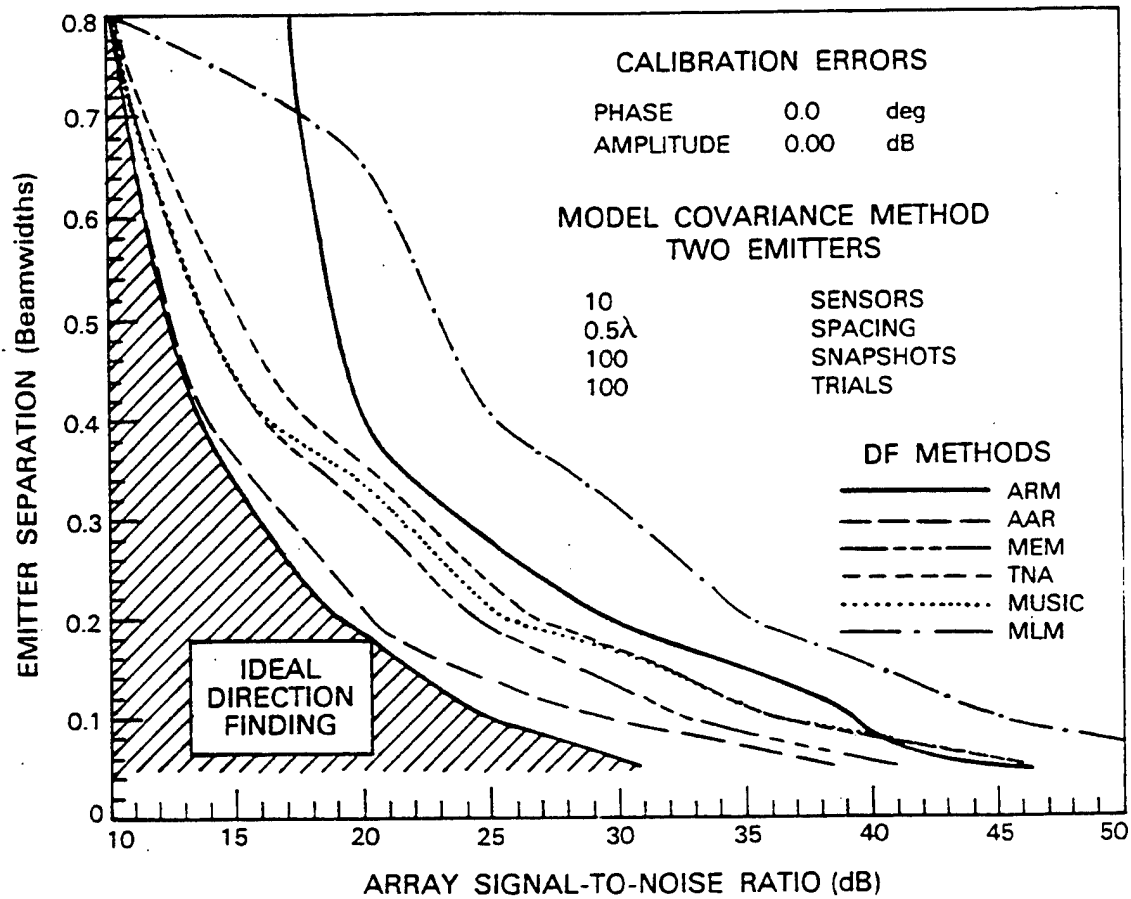


Fig. G.4.

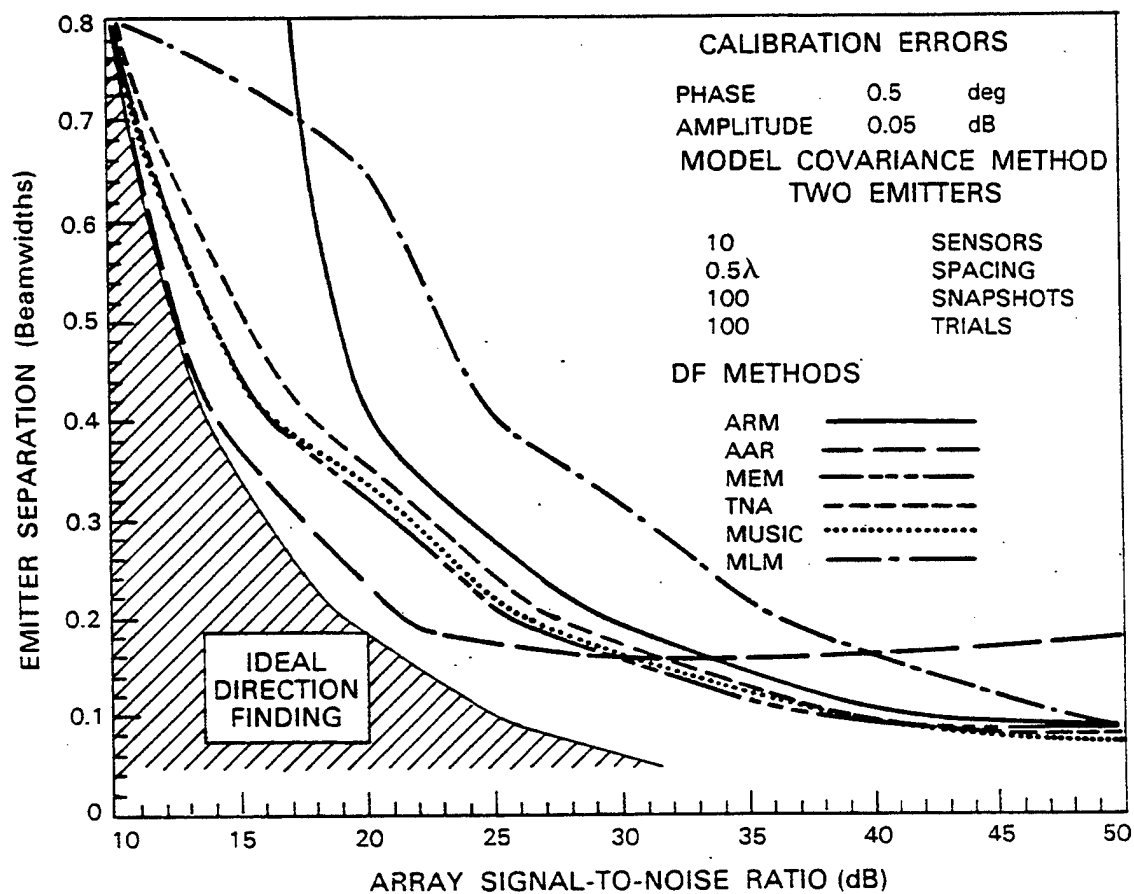


Fig. G.5.

CALIBRATION ERRORS

PHASE 5.0 deg
 AMPLITUDE 0.50 dB

MODEL COVARIANCE METHOD TWO EMITTERS

10 SENSORS
 0.5λ SPACING
 100 SNAPSHOTS
 100 TRIALS

DF METHODS

ARM —————
 AAR —————
 MEM —————
 TNA —————
 MUSIC
 MLM — — — — —

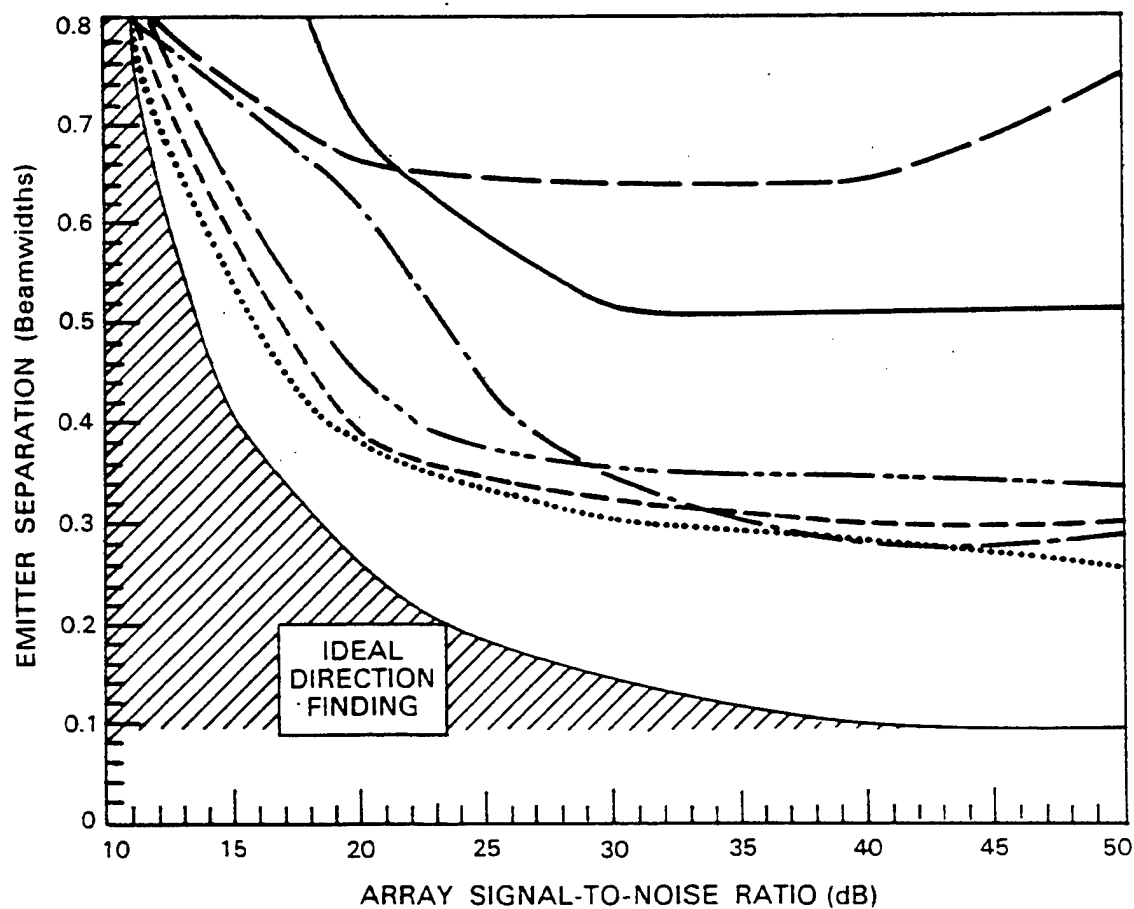


Fig. G.6.

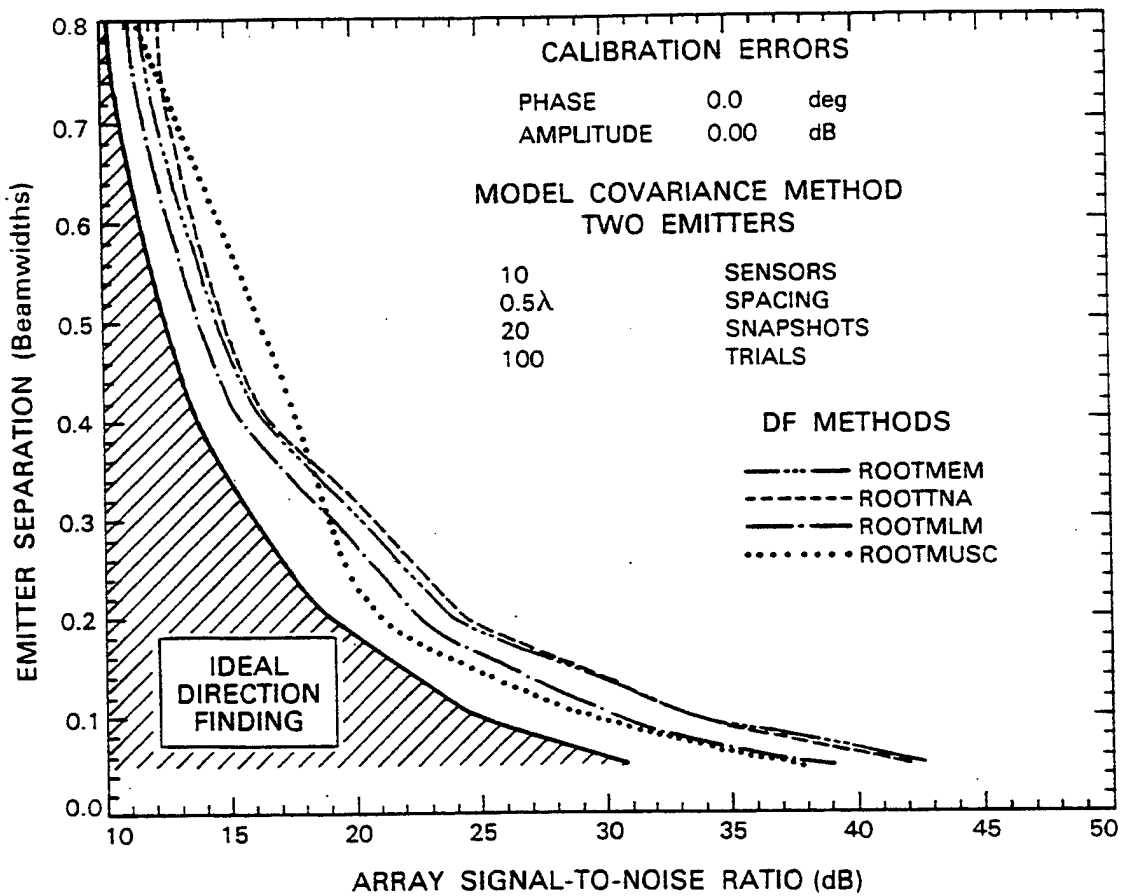


Fig. G.7.

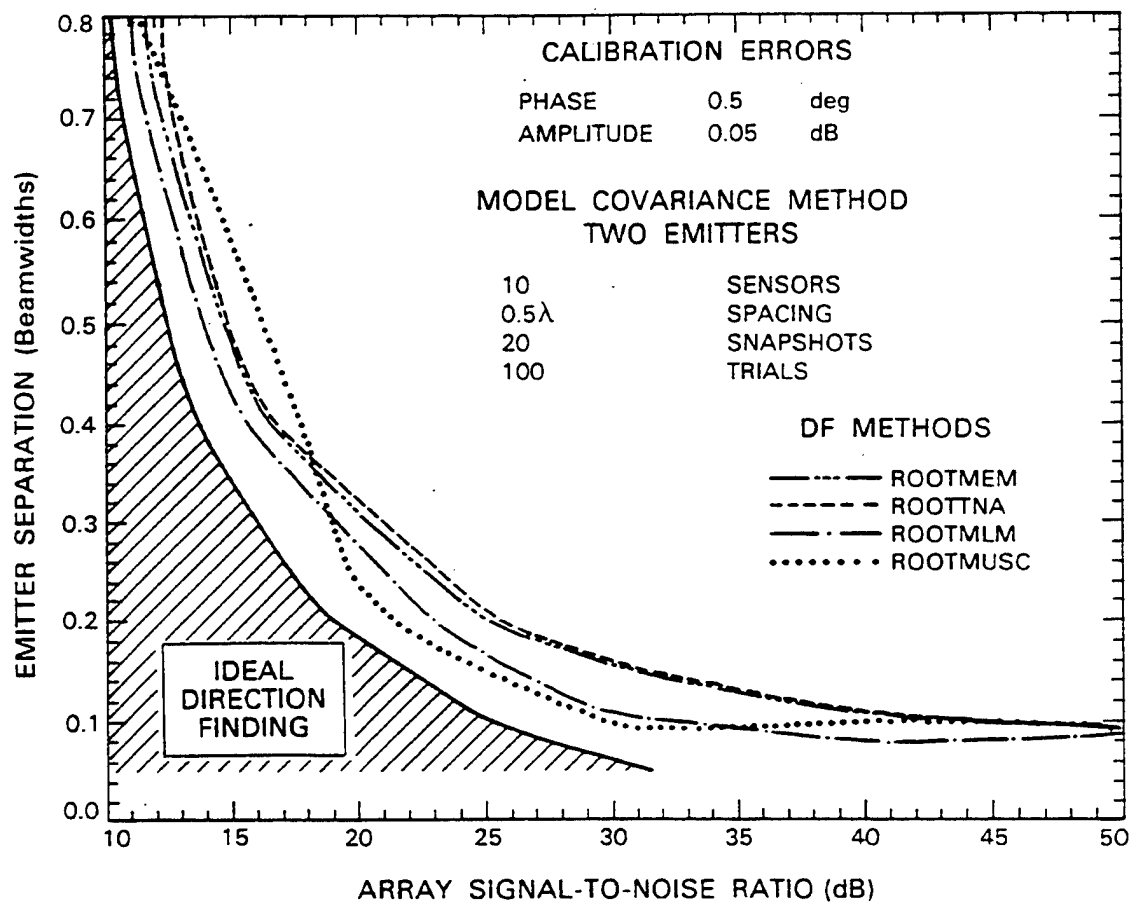


Fig. G.8.

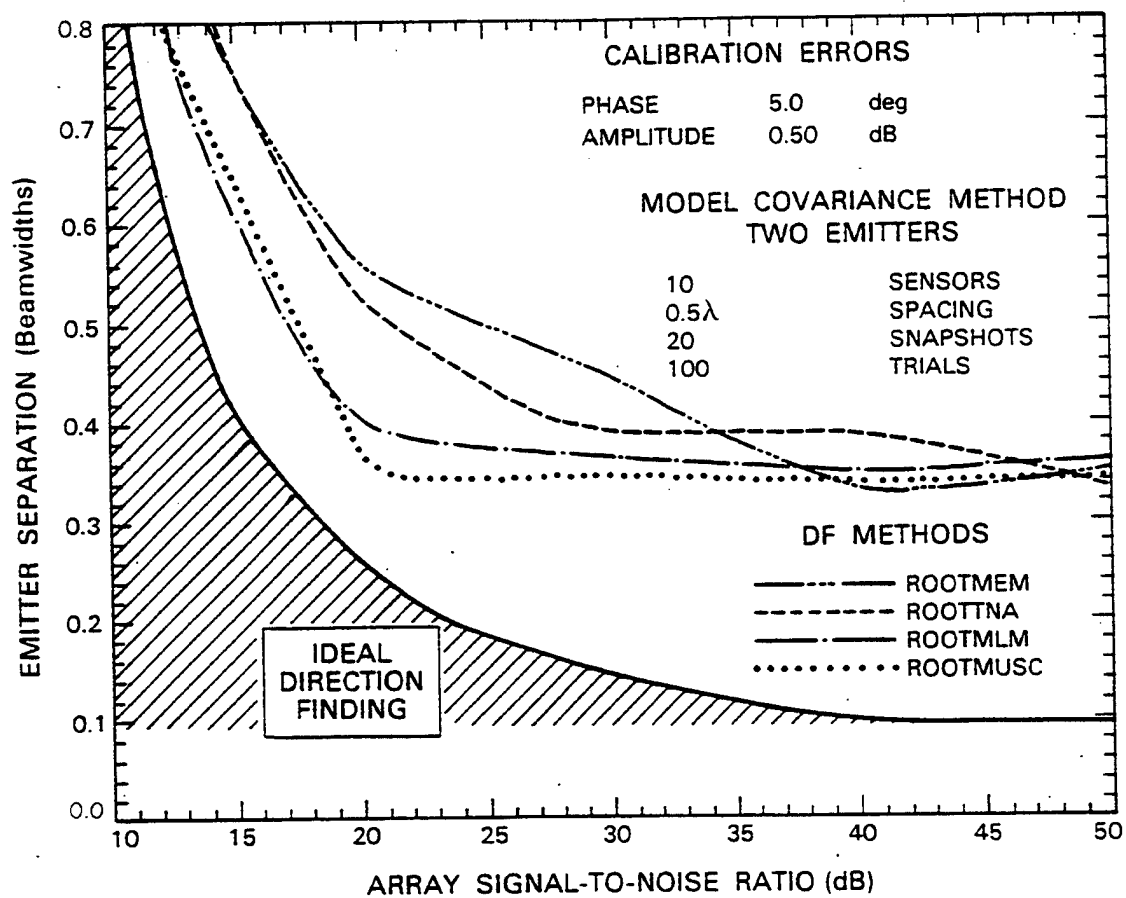


Fig. G.9.

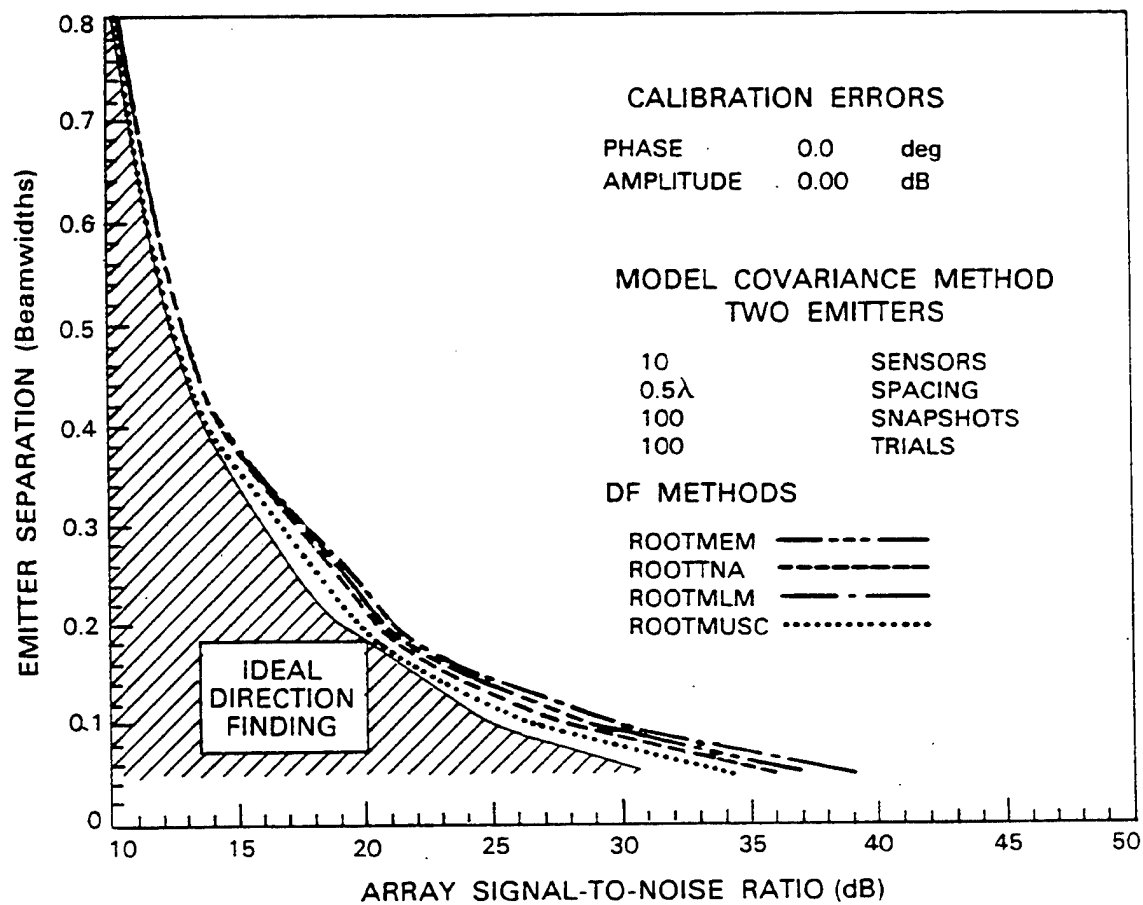


Fig. G.10.

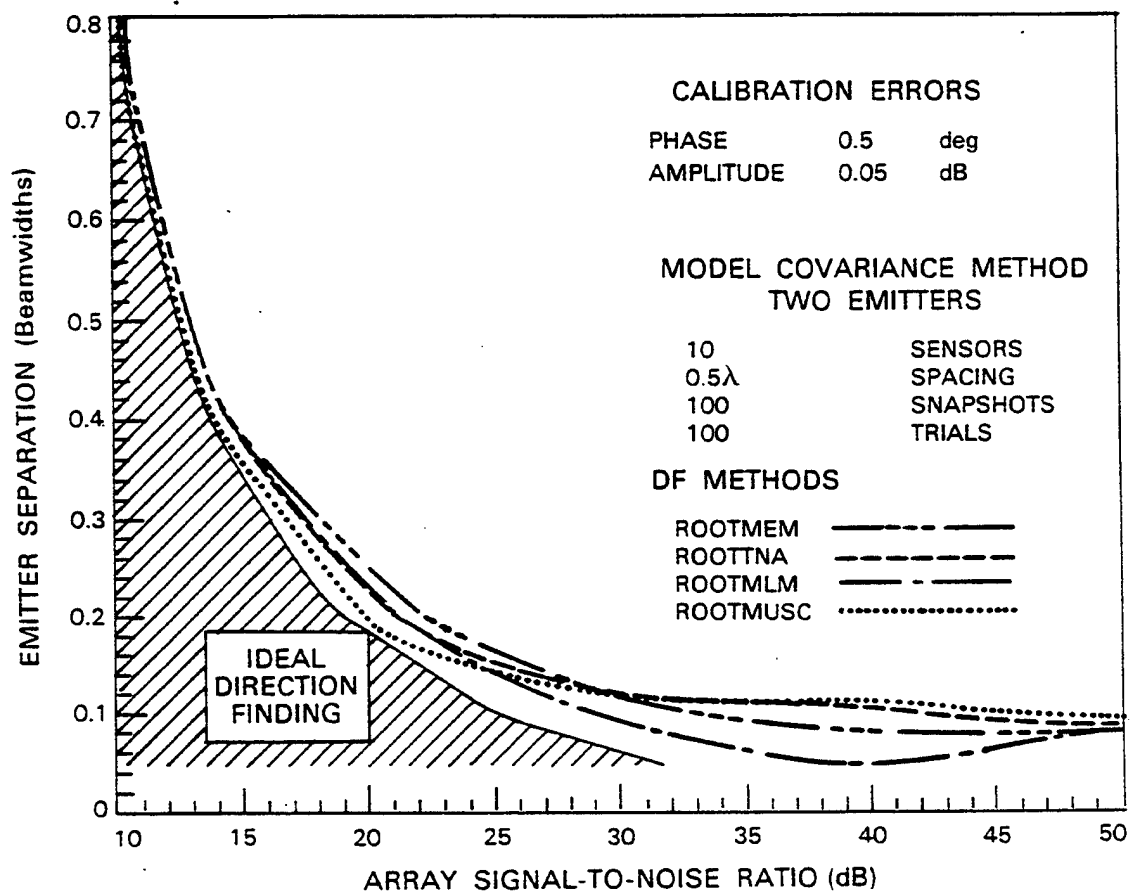


Fig. G.11.

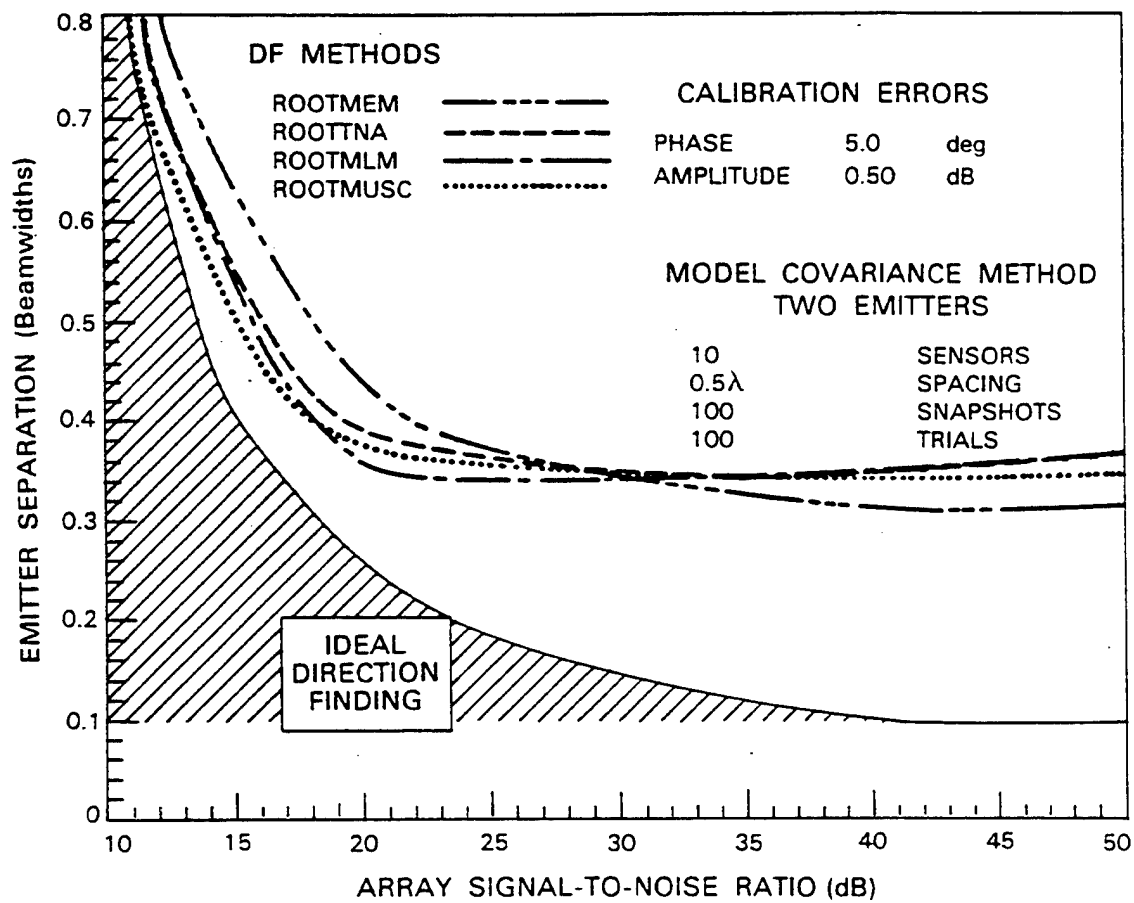


Fig. G.12.

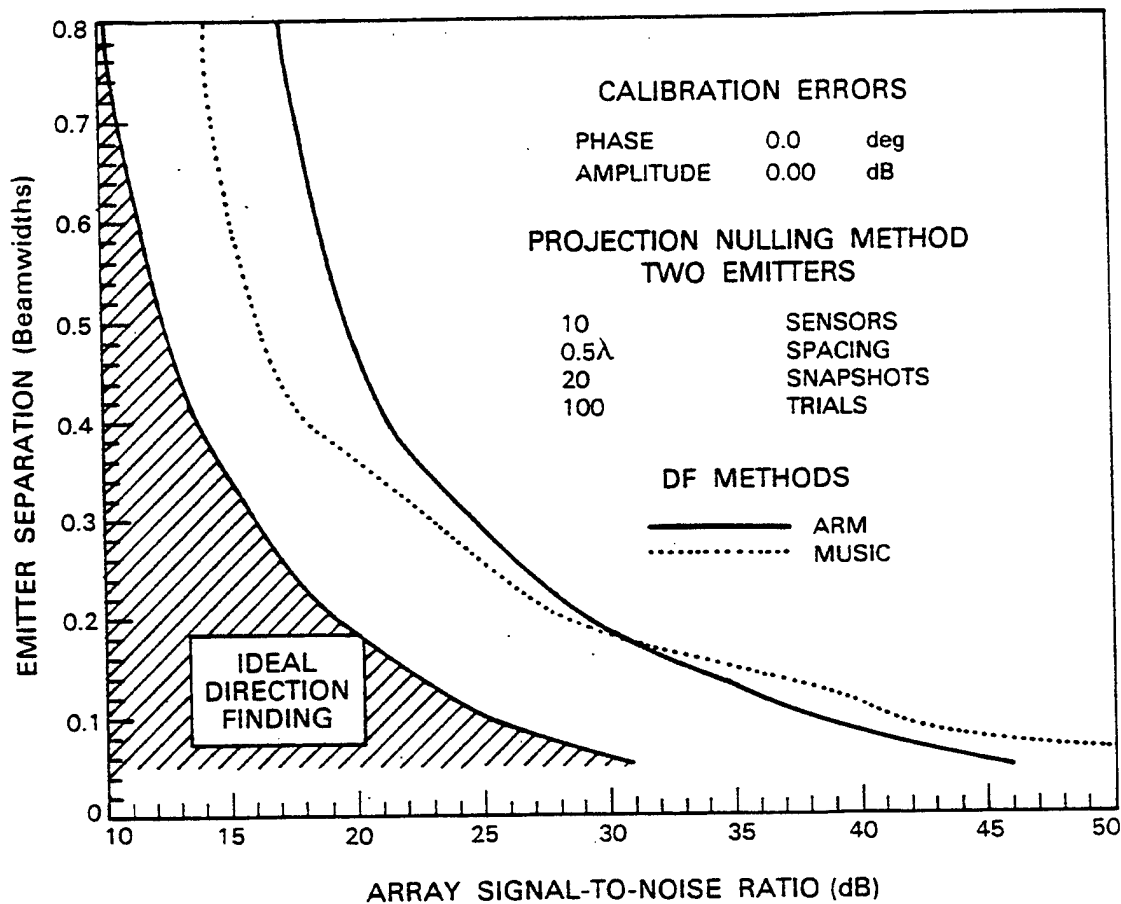


Fig. G.13.

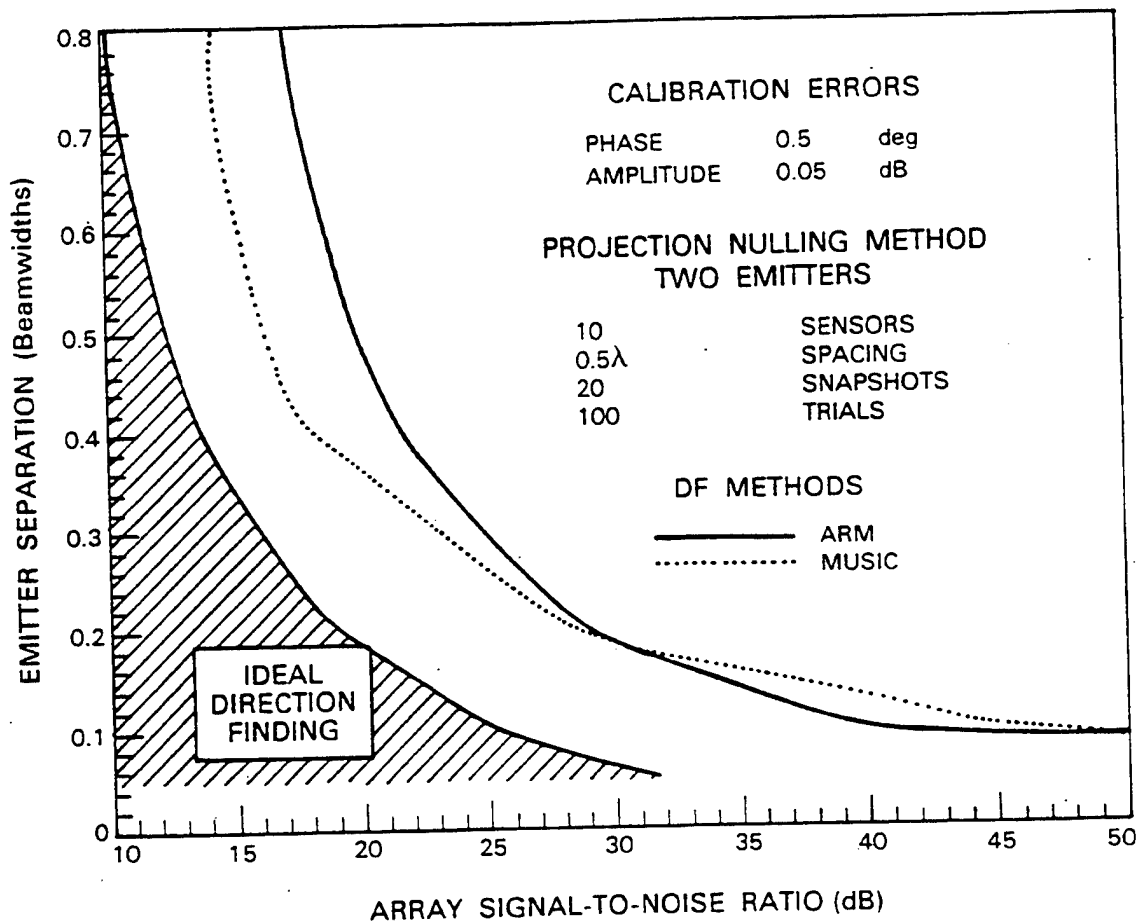


Fig. G.14.

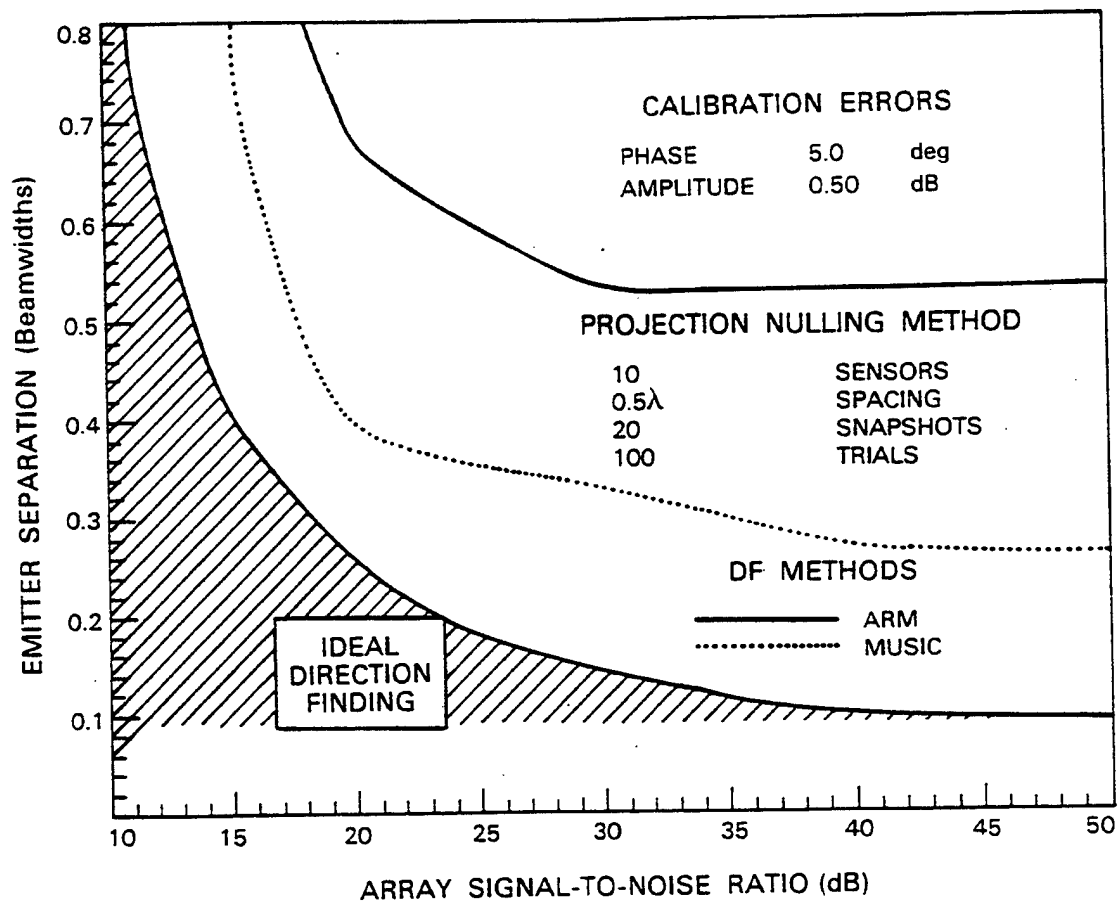


Fig. G.15.

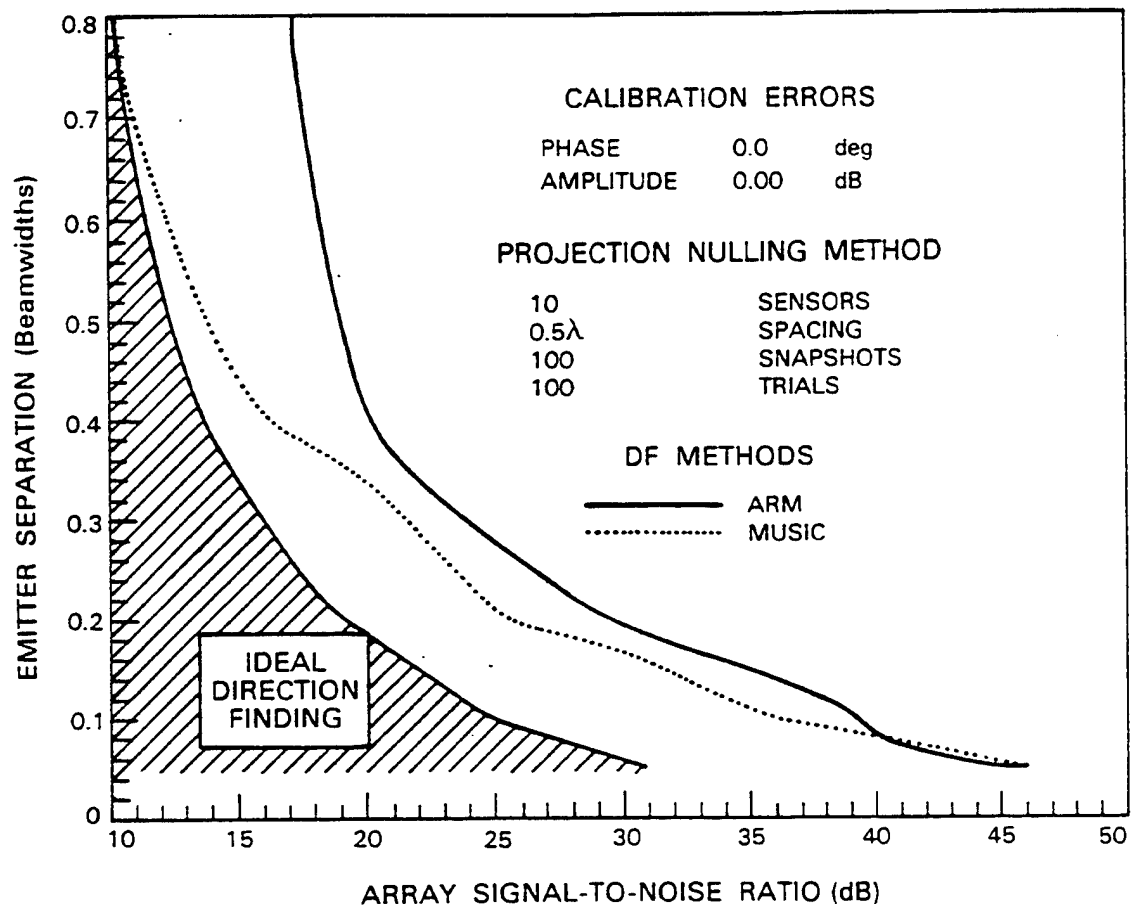


Fig. G.16.

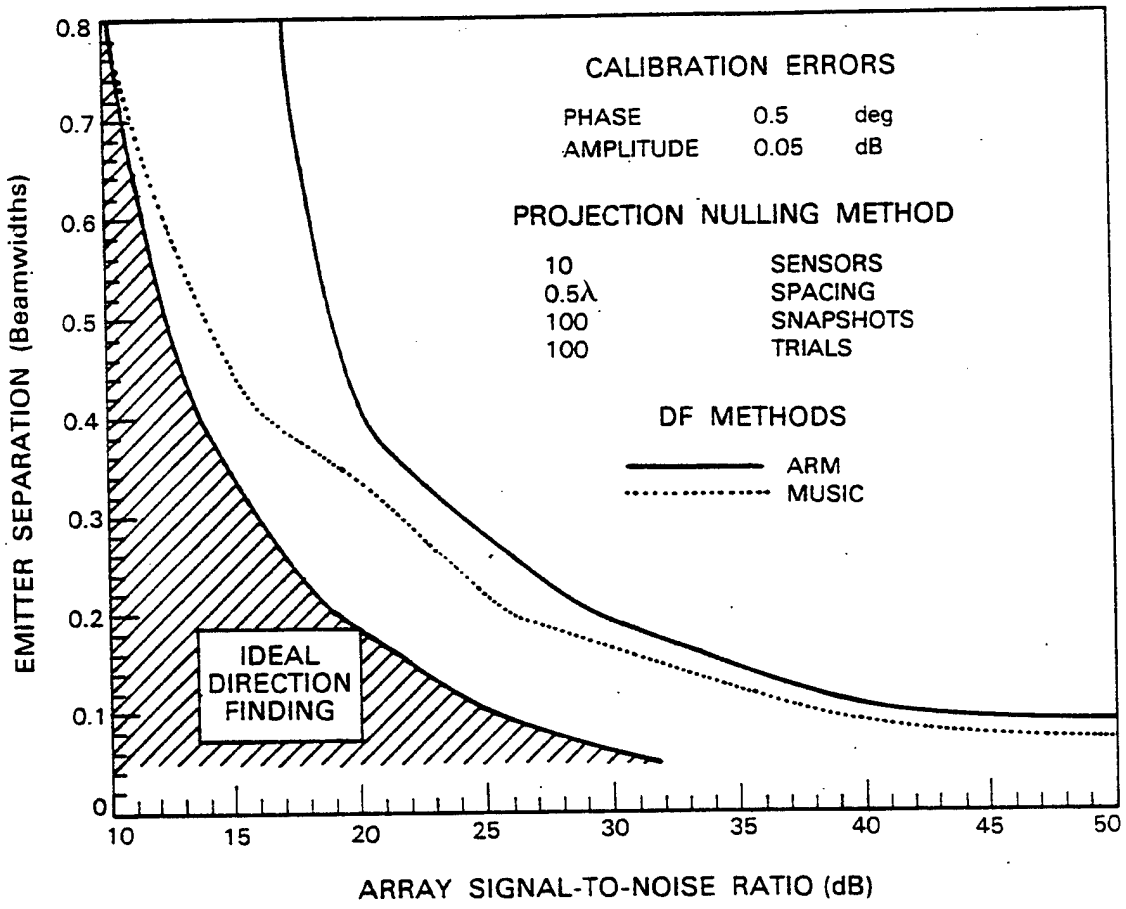
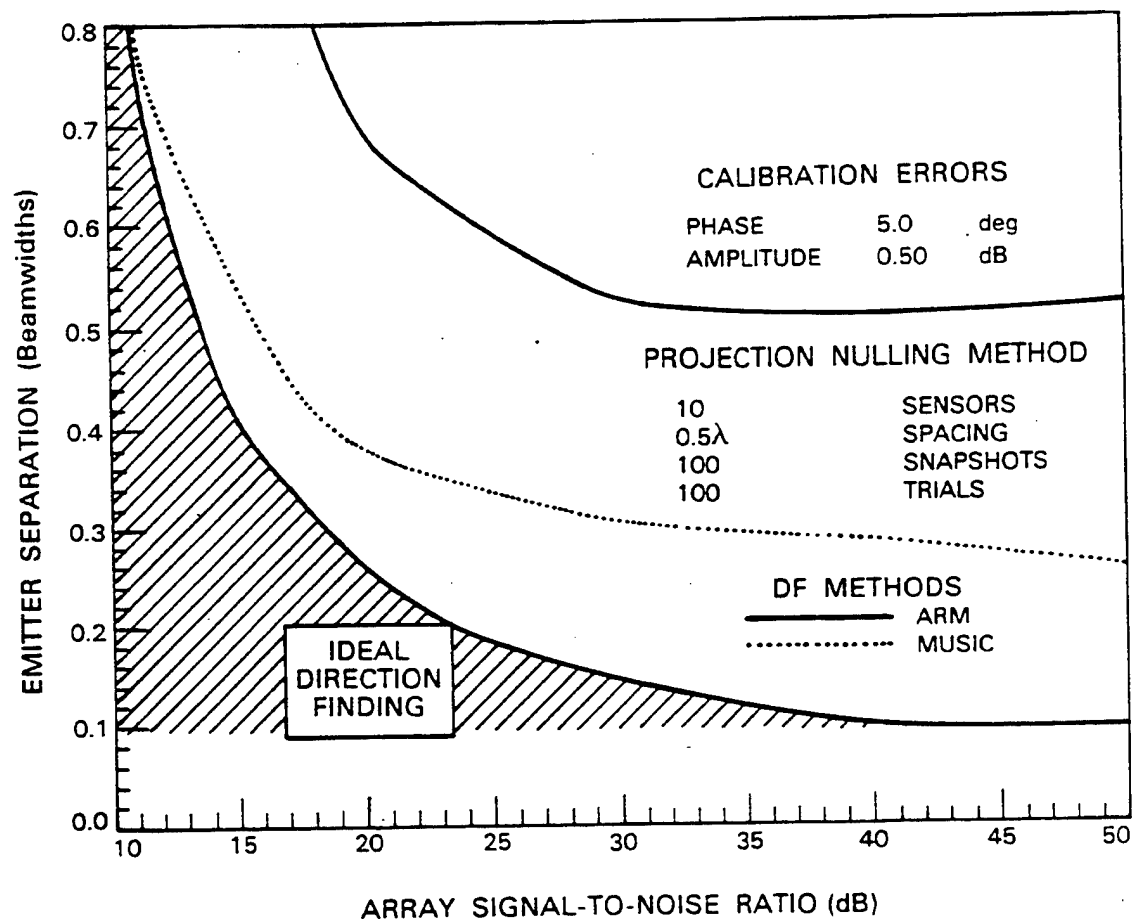


Fig. G.17.



13 3995-R

Fig. G.18.

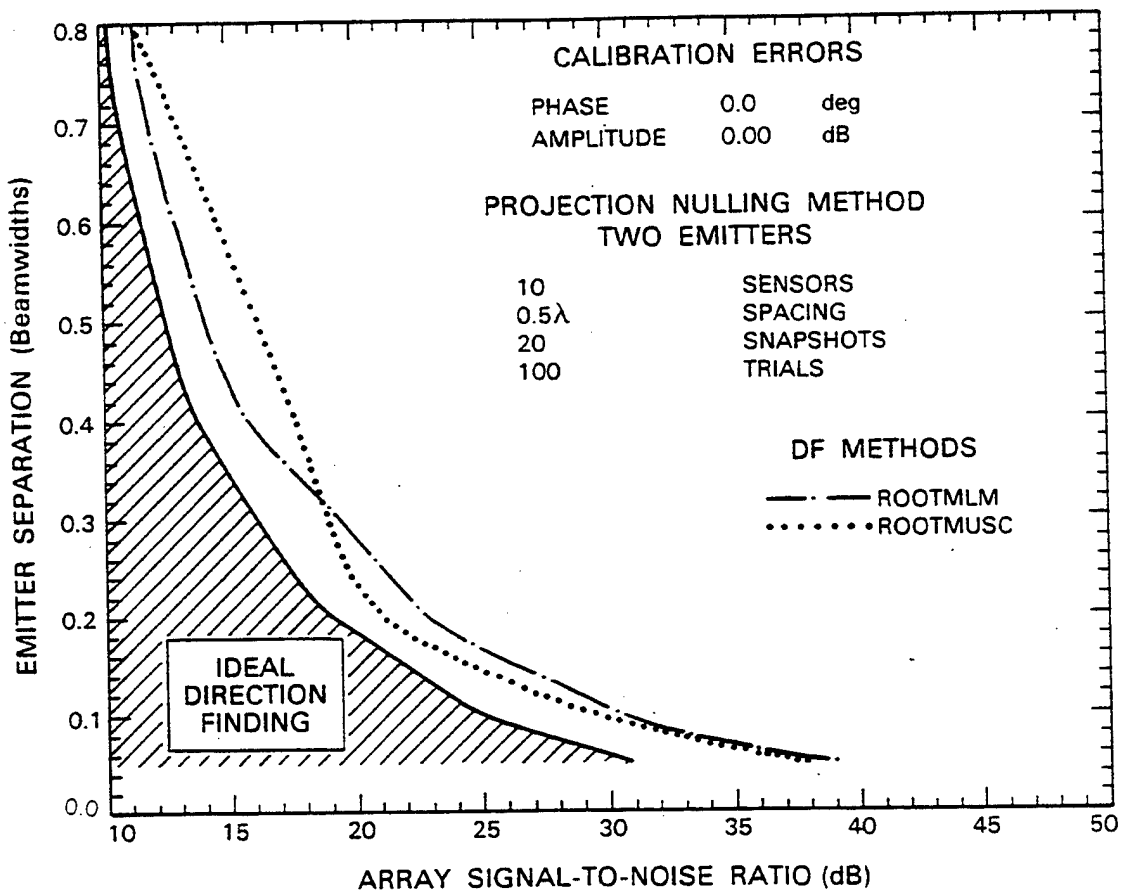


Fig. G.19.

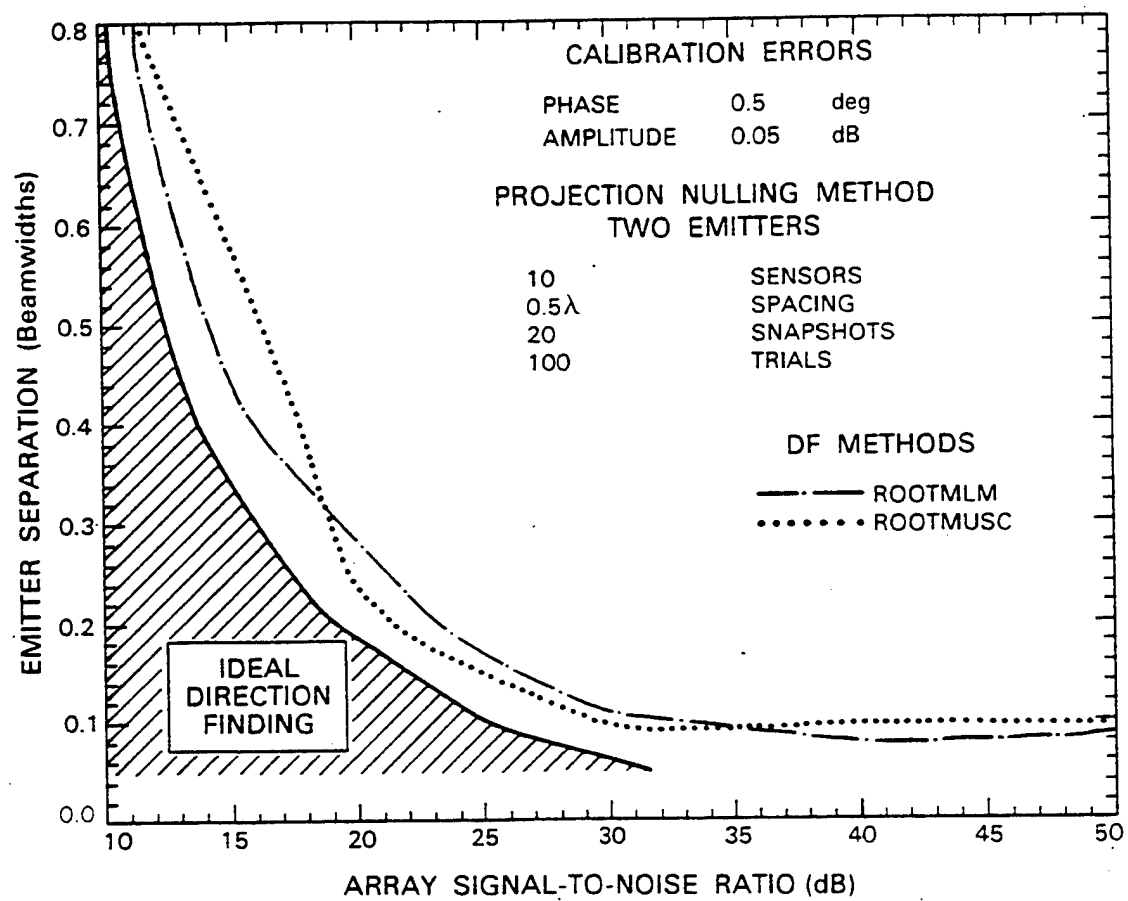


Fig. G.20.

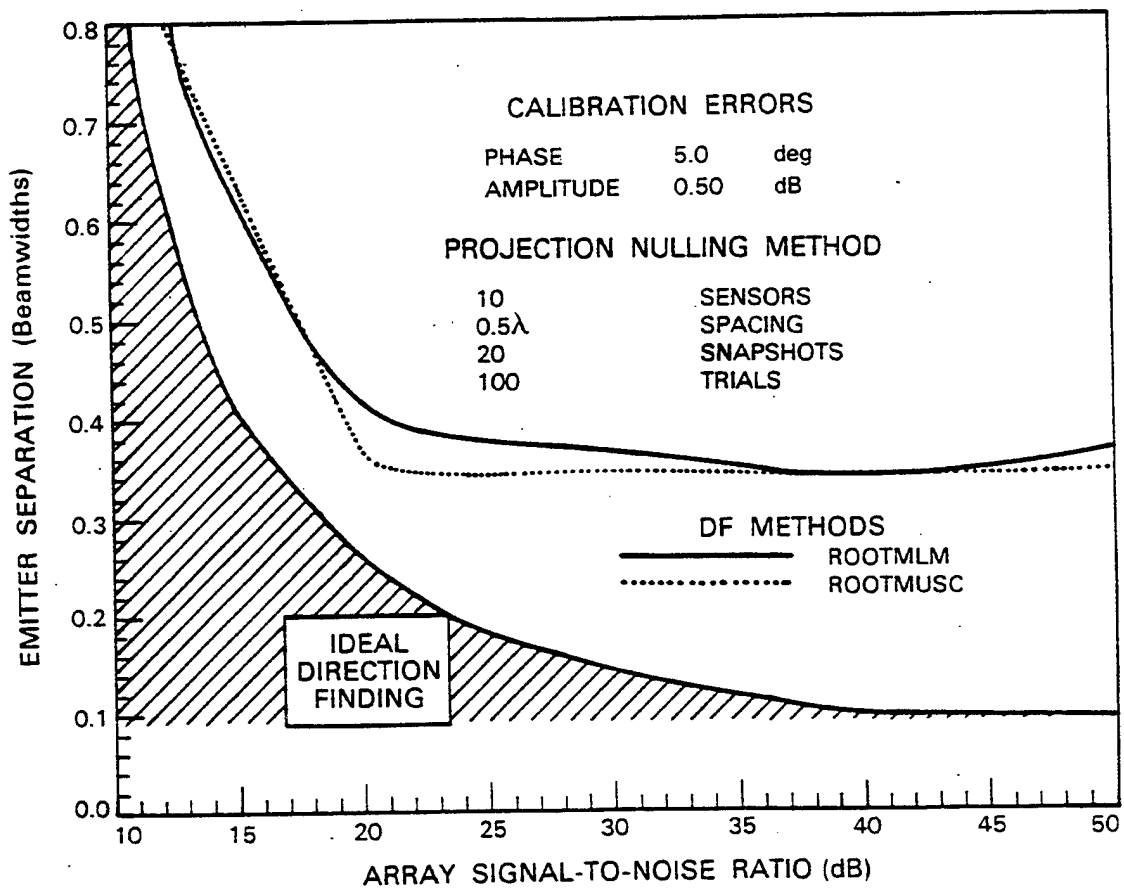


Fig. G.21.

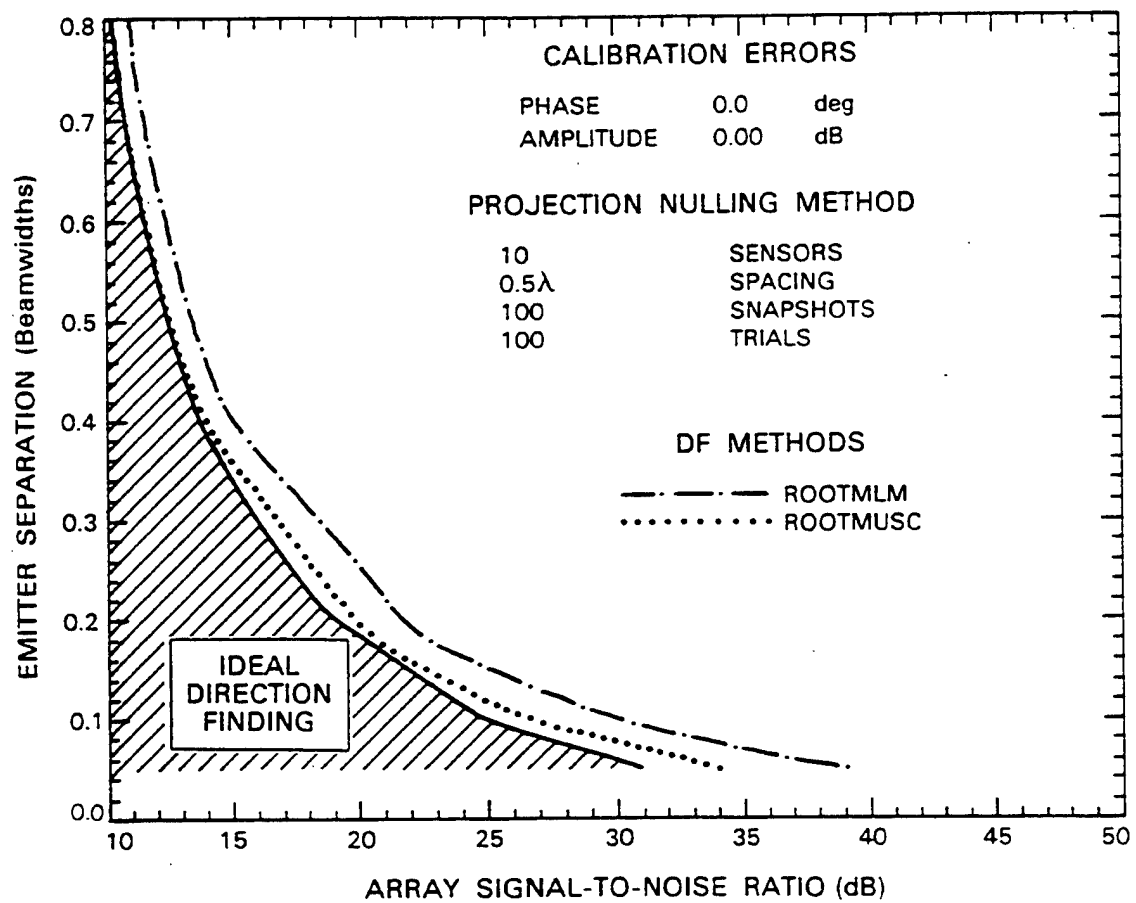


Fig. G.22.

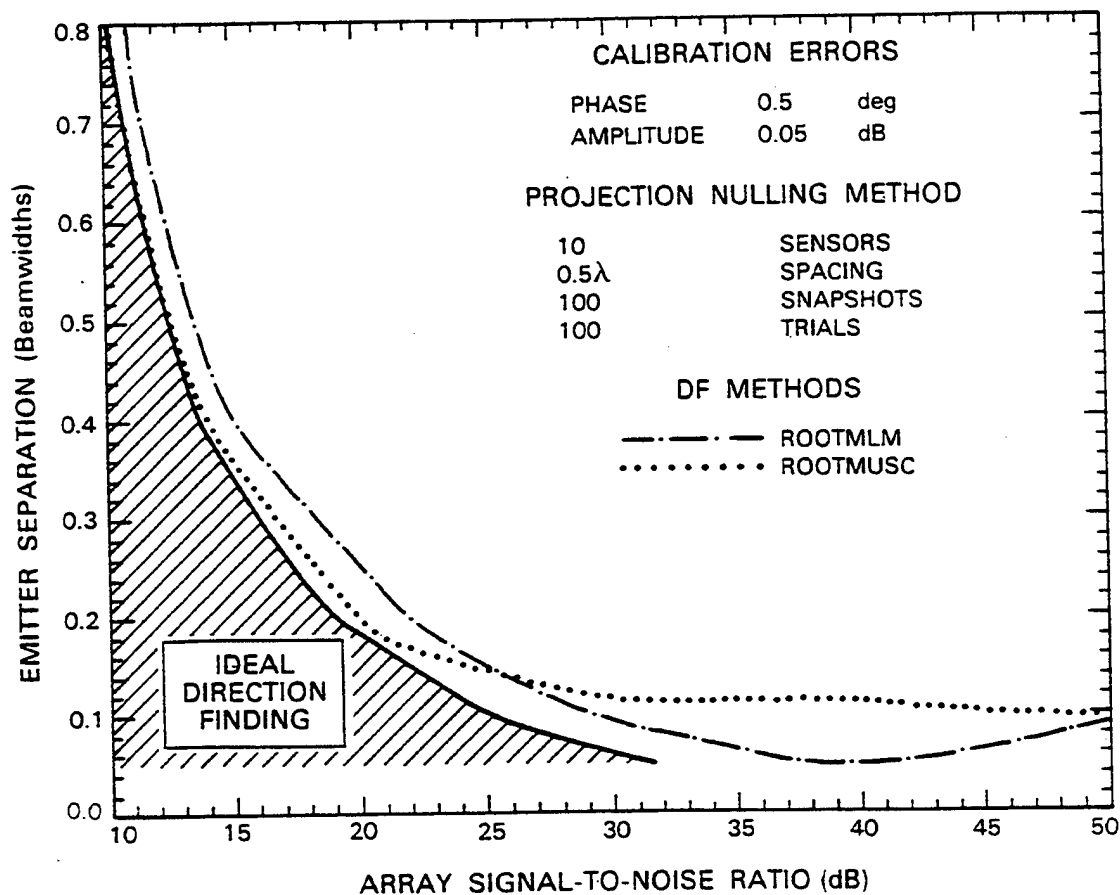


Fig. G.23.

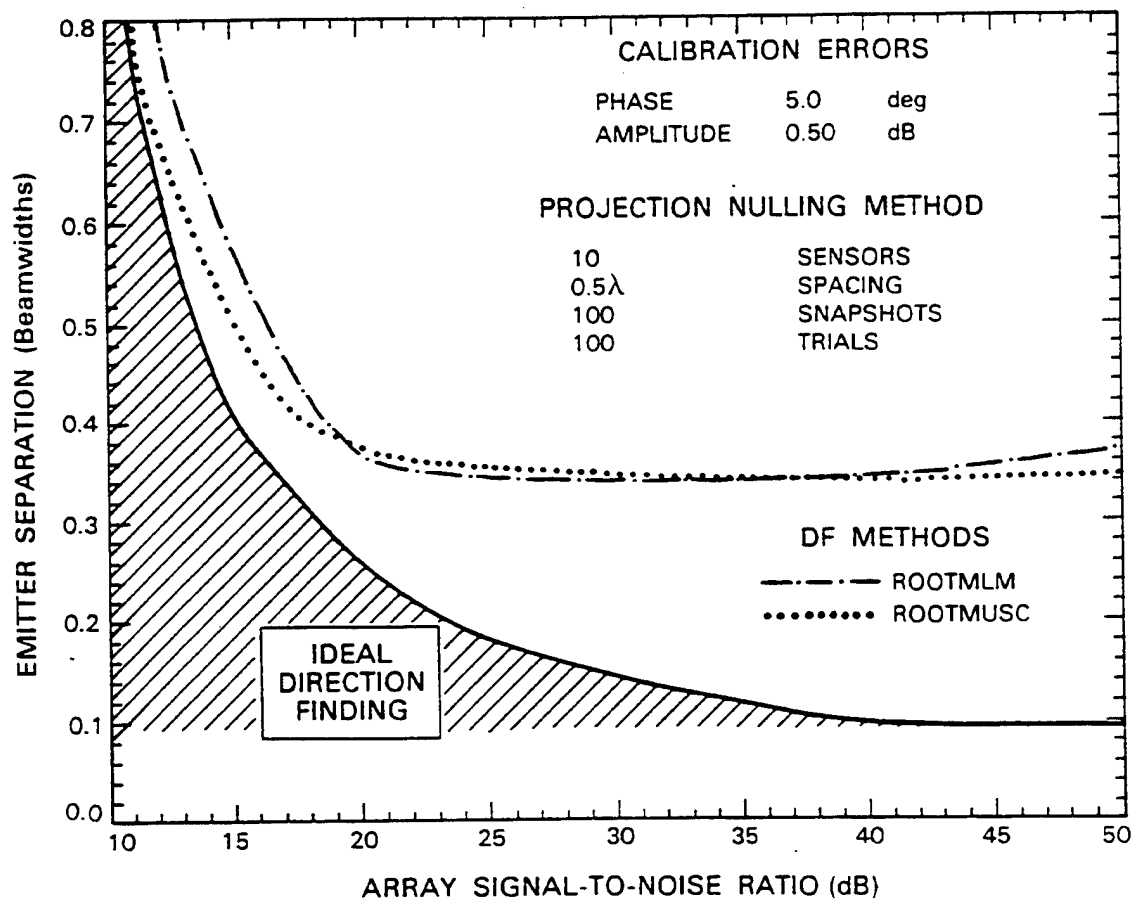


Fig. G.24.

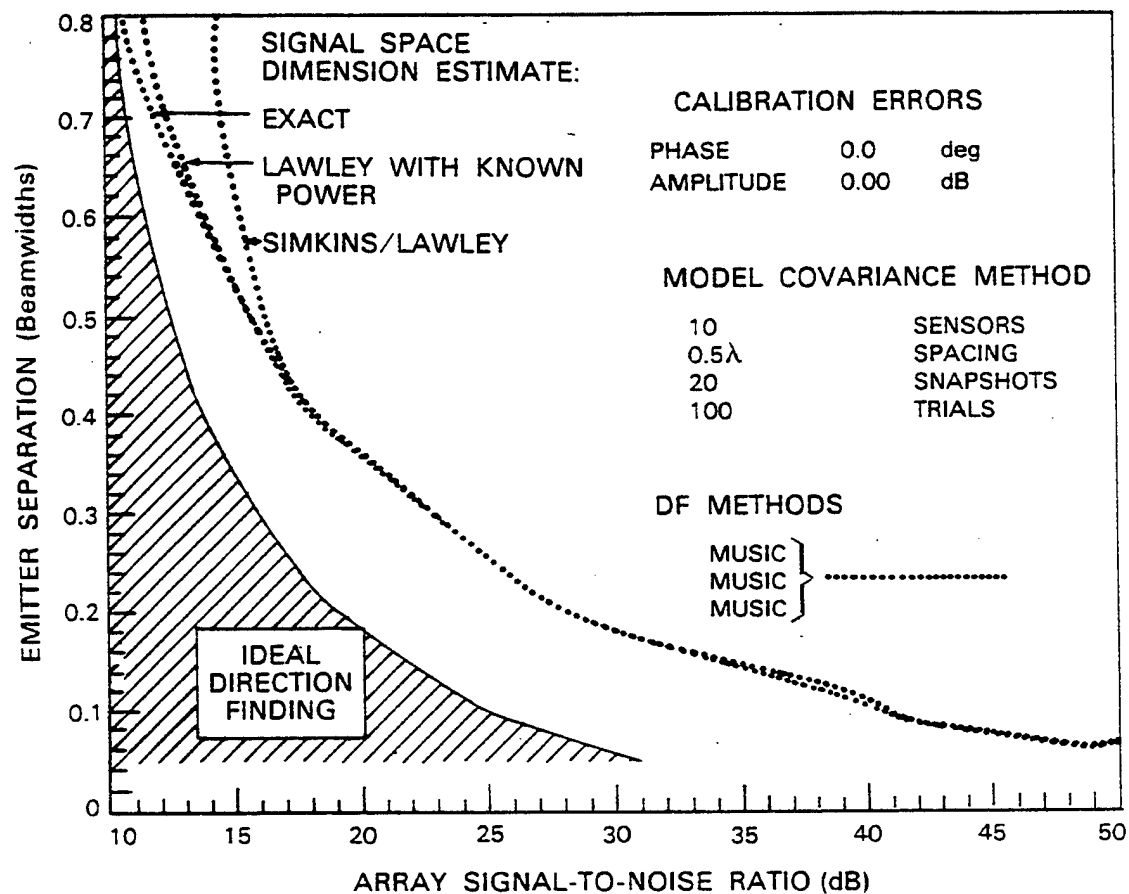


Fig. G.25.

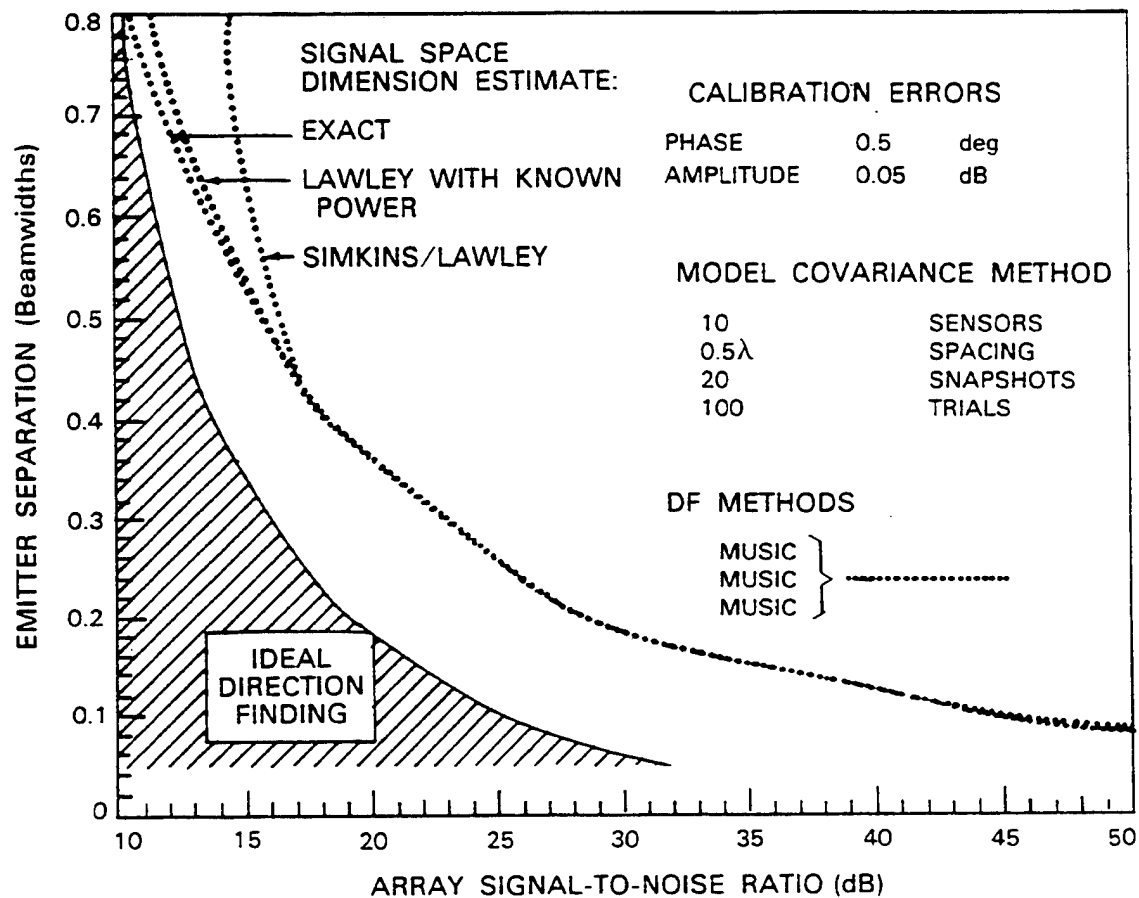


Fig. G.26.

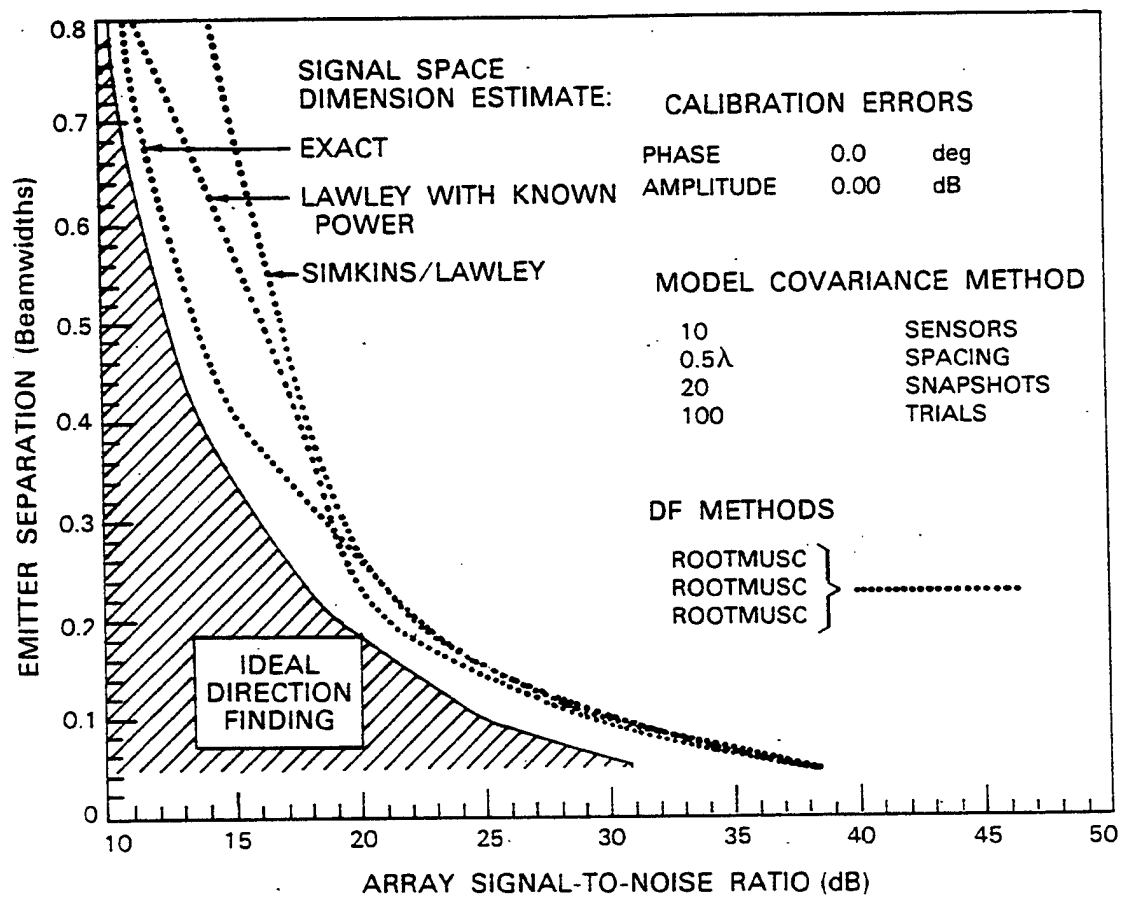


Fig. G.27.

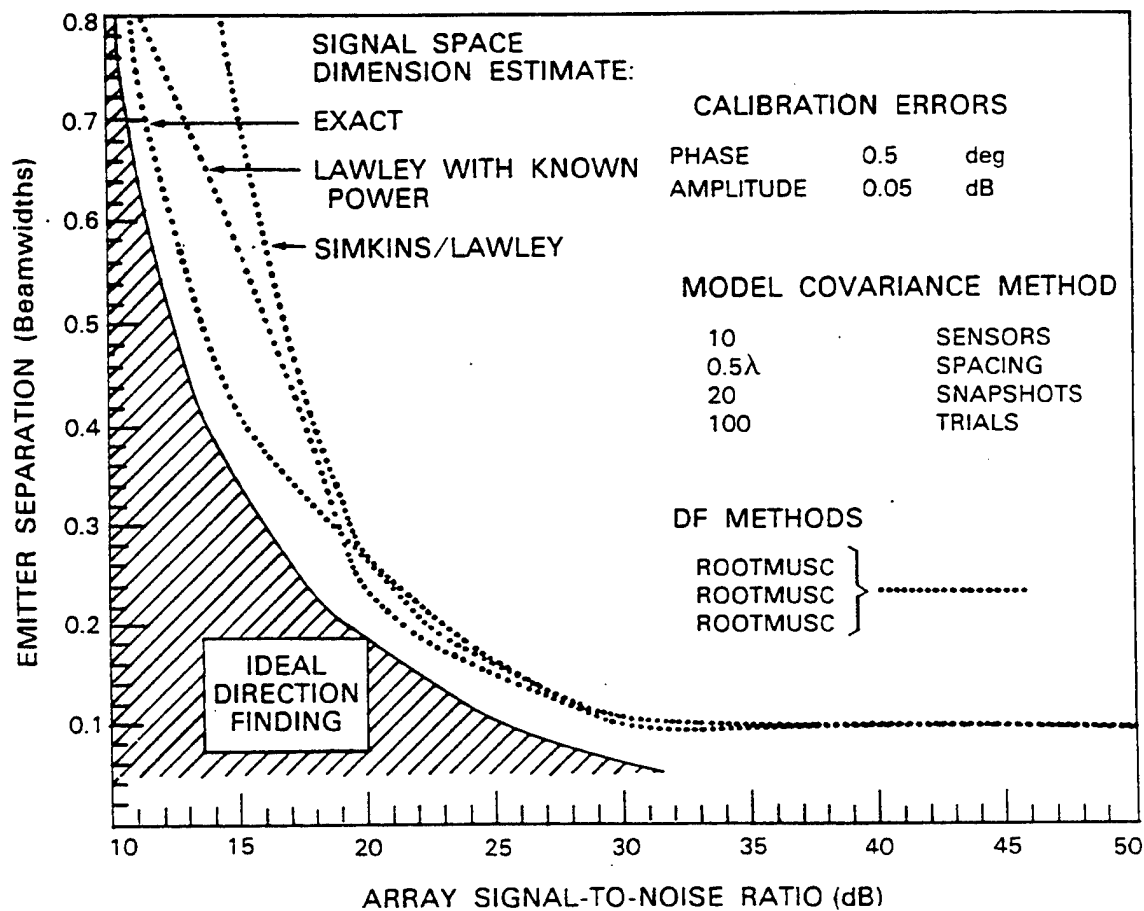


Fig. G.28.

ACKNOWLEDGEMENTS

The authors could not have contemplated such a monumental undertaking without the diligent and understanding support of many people. Assisting in the development of the Monte Carlo simulation facility were M. A. Lippert, P. Linder, and F. M. White. Monitoring the generation of computer graphics were D. Gerber, K. Bronson, P. Linder, and K. R. Eastburn. Finally, for patience without relief during preparation of the manuscript, our thanks go to D. M. Young and K. R. Eastburn.

REPORT DOCUMENTATION PAGE

Form Approved
OMB No. 0704-0188

Public reporting burden for this collection of information is estimated to average 1 hour per response, including the time for reviewing instructions, searching existing data sources, gathering and maintaining the data needed, and completing and reviewing the collection of information. Send comments regarding this burden estimate or any other aspect of this collection of information, including suggestions for reducing this burden, to Washington Headquarters Services, Directorate for Information Operations and Reports, 1215 Jefferson Davis Highway, Suite 1204, Arlington, VA 22202-4302, and to the Office of Management and Budget, Paperwork Reduction Project (0704-0188), Washington, DC 20503.

1. AGENCY USE ONLY (Leave blank)	2. REPORT DATE Revised 15 June 1998	3. REPORT TYPE AND DATES COVERED Project Report	
4. TITLE AND SUBTITLE Performance Comparison of Superresolution Array Processing Algorithms		5. FUNDING NUMBERS C — F19628-95-C-0002	
6. AUTHOR(S) A.J. Barabell, J. Capon, D.F. DeLong, J.R. Johnson, K.D. Senne			
7. PERFORMING ORGANIZATION NAME(S) AND ADDRESS(ES) Lincoln Laboratory, MIT 244 Wood Street Lexington, MA 02420-9108		8. PERFORMING ORGANIZATION REPORT NUMBER	
9. SPONSORING/MONITORING AGENCY NAME(S) AND ADDRESS(ES) HQ Air Force Materiel Command AFMC/STSC Wright-Patterson AFB, OH 45433-5001		10. SPONSORING/MONITORING AGENCY REPORT NUMBER ESC-TR-97-121	
11. SUPPLEMENTARY NOTES None			
12a. DISTRIBUTION/AVAILABILITY STATEMENT Approved for public release; distribution is unlimited.		12b. DISTRIBUTION CODE	
13. ABSTRACT (Maximum 200 words) This report summarizes the results of the initial phase of a comprehensive simulation study of alternative signal processing algorithms for data adaptive superresolution direction finding and spatial nulling to support signal copy in the presence of strong cochannel interference. The need for such a study arises because, although most of the techniques evaluated have been documented in the literature, no systematic comparison has heretofore been undertaken. The general approach of the current study is to simulate a sequence of increasingly more general, i.e., realistic, signaling environments, and to expose each of the more promising algorithms to all of the "standardized" experiments, in turn. For the initial phase of the inquiry, we have selected an ideal environment characterized by a uniform, linear array of identical isotropic elements and perfect receivers. In addition, partial results are obtained for the case when the array steering vectors are in error by a small amount which might be caused by residual calibration errors, unmodeled multipath distortions, near-field emitters, etc.			
14. SUBJECT TERMS			15. NUMBER OF PAGES 202
			16. PRICE CODE
17. SECURITY CLASSIFICATION OF REPORT Unclassified	18. SECURITY CLASSIFICATION OF THIS PAGE Same as report	19. SECURITY CLASSIFICATION OF ABSTRACT Same as report	20. LIMITATION OF ABSTRACT Same as report